UNIVERSITY OF CAPE TOWN

DEPARTMENT OF MECHANICAL ENGINEERING

DETERMINATION OF MATERIAL PROPERTIES OF MILD STEEL AT DIFFERENT TEMPERATURES AND STRAIN RATES

Amit Rashiklal Vara

Dissertation presented in partial fulfilment of the requirements for the degree of Master of Science in Mechanical Engineering

December 2007

PLAGIARISM DECLARATION

1. I know that plagiarism is wrong. Plagiarism is to use another's work and pretend that it is one's own.
2. I have used the scientific convention for citation and referencing. Each significant contribution to, and quotation in this dissertation from the works of other people has been attributed, and has been cited and referenced.
3. This project is my own work.
4. I have not allowed, and will not allow anyone to copy my work with the intention of passing it off as his or her own work.

Signature: Signed by candidate

Name: Amit. R. Vara

Date: December 2007

ACKNOWLEDGEMENTS

I would like to extend my heartfelt thanks to the following people:

- Prof. Nurick for his supervision and guidance during the course of this project and for accepting me into BISRU
- Prof. Tait for his guidance on the basic use of the ESH 100kN Universal Tester in the Centre for Materials Engineering at UCT
- Associate Prof. Knutsen for his insight into various material science aspects
- Mr. Andrew Cousins, whose initial help will always be appreciated
- Members of BISRU for being excellent colleagues to work with and also being a wellspring of useful information
- Mr. Glen Newins, Mr. Len Watkins, Mr. Hubert Tomlinson, Mr. Willie Slaverse and the rest of the workshop staff for their invaluable assistance
- Mrs. Penny Park-Ross and Ms. Leizl Matthews for their help with the microstructure specimen preparation and Ms. Sarah George for her instruction on how to use the research microscope in the Centre for Materials Engineering at UCT
- Ms. Yvonne Chi for her enthusiastic help with the photographs
- Finally, my family for their boundless love, support and confidence in me

ABSTRACT

Quantification of material properties through physical experiments is of significant importance. Test data from such experiments aid in the understanding of the material behaviour when exposed to a variety of loading conditions. Such data also help in the formulation of empirical and constitutive relations that can be applied in numerical simulations.

This project dealt with the determination of the variation of the yield stress of mild steel with temperature and strain rate. This was achieved by carrying out high temperature tensile tests at different strain rates on mild steel specimens. These experiments also helped set a methodology for carrying out high temperature tensile tests using a servohydraulic universal tester. Results from the tests indicated that increases in temperature tended to decrease the yield stress, whereas increases in strain rate had the opposite effect. This was found to be consistent with data found in literature. It was also noted that the temperature effect was more dominant than the strain rate effect over quasi-static strain rates.

The test results were also compared with existing material models, and it was noted that while there were regions where the predictions of the material models coincided with the experimental data, the predictions did not hold over the entire range of temperatures investigated. Therefore, an alternative empirical model for the variation of the yield stress of mild steel with temperature was proposed based on the tensile test results:

$$\sigma_{yn} = 1 - 2.67 \times 10^{-3}(T - 25) \qquad 25°C < T \leq 100°C$$
$$\sigma_{yn} = 0.8 - 4 \times 10^{-4}(T - 100) \qquad 100°C < T \leq 450°C$$
$$\sigma_{yn} = 0.66 - 1.7 \times 10^{-3}(T - 450) \qquad 450°C < T \leq 600°C$$

Where σ_{yn} is the normalised yield stress of mild steel as a function of temperature (T)

TABLE OF CONTENTS

LIST OF FIGURES

1. INTRODUCTION

Material properties determine the behaviour of a material under various circumstances. Therefore, determining these properties is of paramount importance when it comes to evaluating the usefulness of the material in terms of a design viewpoint. Moreover, for numerical modelling of structures, a suitable material model is necessary to model the behaviour of the structure under various loading conditions. As such, the material model needs to accurately simulate how the material will behave when exposed to different scenarios. These material models are assembled after extensive tests have been carried out on the material itself. Therefore, experiments to determine material properties are an essential and integral part of formulating suitable material models that can be used for numerical simulations.

1.1. Purposes of the Study

This project intended to investigate the effects of temperature and strain rate on the yield stress of mild steel. To achieve this, tensile tests were carried out at various temperatures and strain rates. Moreover, the tests have been used to set up a methodology for high temperature tensile testing.

Furthermore, the tested specimens were analysed on a micro-structural level to see the effect that the test temperatures and strain rates had on the deformation of the grains of the material.

Finally, it was desired to develop an empirical model describing the yielding behaviour of mild steel at elevated temperatures.

1.2. Limitations

Mild steel is the only material tested in this project, primarily as the material has wide spread use, is readily available and relatively cheaper than other materials. Secondly, as the core of the experiments are tensile tests, the strain rates employed were limited to the quasi-static region, that is $10^{-4}s^{-1} \sim 10^{-1}s^{-1}$. As such, these tests will not be able to determine the properties at very high strain rates.

1.3. Plan of Development

The report is set out with a review of relevant subject matter; thereafter the implemented testing procedure is described. The test results are then presented and analysed. Based on these, conclusions are drawn and recommendations made.

2. LITERATURE REVIEW

Material properties determine the behaviour of a material when exposed to different circumstances. Given this straightforward fact, determination of material properties takes on paramount importance. The implications of such studies have far and wide uses, with the results being applied in various aspects of design engineering. Applications involving the determination of material properties can be found in the design of turbine blades and turbine casings, design of vehicle chassis, as well as the structural integrity and safety parameter calculations for buildings. Various techniques have been devised and employed over the years to determine material properties. Table 2.1 outlines testing techniques based on the applied strain rate.

Table 2.1 – Classification of Testing Techniques based on Strain Rate

Test Type	**Strain Rate Range (s^{-1})**	**Testing Apparatus**
Creep	$10^{-8} \sim 10^{-5}$	Constant Load Machines
Quasi-static Strain Rates	$10^{-5} \sim 10^{-1}$	Electromechanical or Servohydraulic Machines
Intermediate Strain Rates	$10^{-1} \sim 10^{2}$	Special Servohydraulic Machines
High Strain Rates	$10^{2} \sim 10^{4}$	Split-Hopkinson Pressure Bar
Very High Strain Rates	$\geq 10^{4}$	Blast Loading

The tests presented in this project fall into the quasi-static strain range. Some of these testing techniques are discussed next.

2.1. Experimental Techniques

Tensile testing is one of the oldest and basic methods of establishing material properties. Commercial tensile testing equipment has been available since the late 1800s. Tinius Olsen was a pioneer on this front, being granted a patent in 1880 on his 180kN testing machine that was operated via a hand crank. He was also the first to develop an autographic machine capable of producing a stress-strain diagram in 1891 [1]. Tensile testing still forms the basis of material property determination, being the preferred choice to determine the yield stress. Additionally, results from tensile tests can be applied to predict the behaviour of a material in loading cases other than uniaxial tension [2].

Tensile tests are mostly performed on electromechanical or servohydraulic machines. Electromechanical or screw driven machines apply the load via drive screws and drive nuts that move a crosshead. The crosshead is fixed to a grip, which holds one end of the specimen, and the other specimen end is held by a grip fixed to the base. The rate at which the drive screws can be turned is variable, thus allowing tensile tests to be performed at different speeds [3]. Servohydraulic testers, on the other hand, apply the load to the specimen via hydraulic pressure through an actuator. An advantage of these systems is their greater flexibility over electromechanical testers. Greater speeds and forces are possible, and there is also more control over how the load is applied. This enables such machines to carry out other tests such as fatigue and fracture mechanics tests. Another benefit is the fast response time of servohydraulic systems, which allows the system to adapt in real time to changes in material properties such as specimen yielding [4]. Environmental chambers have also been used in conjunction with tensile testers to induce various conditions such as high or low temperatures as the test is carried out. Thus the effect on the material properties of the environmental conditions used can be studied. Tensile specimens themselves may vary according to the specific requirements of the test and no single standard tensile piece is specified due to the variety of forms and dimensions [5].

The premise behind tensile tests is the straining of a specimen, usually until failure, and simultaneously recording the applied load and corresponding elongation of the specimen. This data along with the specimen dimensions can then be used to obtain stress – strain curves from which the yield and ultimate tensile stresses can be determined. Equations 2.1.1 – 2.1.2 outline this process:

$$\sigma_e = \frac{F}{A_0} \qquad \text{(Equation 2.1.1)}$$

Where σ_e is the engineering stress, F is the applied load and A_0 is the original cross-sectional area of the gauge section of the specimen.

$$\varepsilon_e = \frac{L_t - L_0}{L_0} = \frac{\Delta L}{L_0} \qquad \text{(Equation 2.1.2)}$$

Where ε_e is the engineering strain, L_t is the length of the gauge section at any point in time after the load has been applied and L_0 is the original gauge length of the specimen.

The true stress can be derived by assuming the gauge section of the specimen to have a constant volume and a homogeneous distribution of strain.

$$V_{const} = A_0 L_0 = A_t L_t \qquad \text{(Equation 2.1.3)}$$

Where V_{const} is the volume of the gauge section, assumed to be constant, and A_t is the cross sectional area of the gauge section at any point in time after the load has been applied. Therefore, the true stress, σ_t, can be expressed as:

$$\sigma_t = \frac{F}{A_t} = \frac{FL_t}{A_0 L_0} = \frac{F}{A_0}\left(\frac{L_t}{L_0}\right) = \frac{F}{A_0}\left(\frac{\Delta L + L_0}{L_0}\right) \qquad \text{(Equation 2.1.4a)}$$

$$\therefore \sigma_t = \sigma_e(\varepsilon_e + 1) \qquad \text{(Equation 2.1.4b)}$$

It should be noted that due to the assumptions in its derivation, equation 2.1.4b is only valid until the onset of necking [6].

The true strain, ε_t, can be derived by considering the incremental change in length dl divided by the original length l of the specimen to be the incremental true strain $d\varepsilon_t$ and integrating as shown in equations 2.1.5a – 2.1.5b:

$$\int_0^{\varepsilon_t} d\varepsilon_t = \int_{L_0}^{L_t} \frac{dl}{l} \Rightarrow \varepsilon_t = \ln\left(\frac{L_t}{L_0}\right) = \ln\left(\frac{L_0 + \Delta L}{L_0}\right) \qquad \text{(Equation 2.1.5a)}$$

$$\therefore \varepsilon_t = \ln(1 + \varepsilon_e) \qquad \text{(Equation 2.1.5b)}$$

Once necking begins, the stress state in the specimen is no longer that of uniaxial tension. The extension of the specimen in the axial direction of the applied load causes the material to contract laterally setting up a triaxial stress state. The Bridgman correction factor as reported by Scheider et al [7] is an analytical solution that relates the true stress to the measured load once necking has begun in circular cross-section specimens. Equation 2.1.6 gives the form of the correction factor.

$$F_{Bridgman} = \left[\left(\frac{1+2\rho}{R}\right)\left(\ln\left(1+\frac{R}{2\rho}\right)\right)\right]^{-1} \qquad \text{(Equation 2.1.6)}$$

Where $F_{Bridgman}$ is the Bridgman correction factor, R is the radius of the circular cross-section specimen and ρ is the radius of the neck.

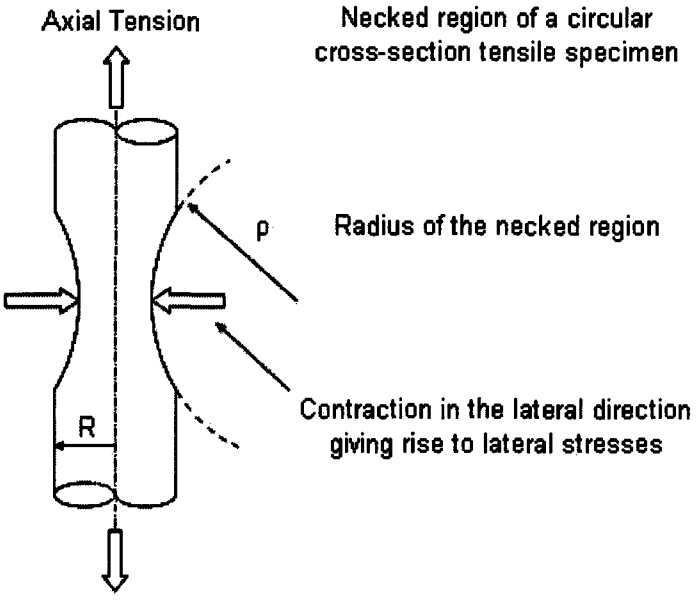

Figure 2.1.1 – Necked Region of a Round Tensile Specimen

Figure 2.1.1 depicts the necked section of a round tensile specimen. To be able to apply the Bridgman correction factor, the reduction of diameter and the neck radius need to be measured continuously as the tensile test is carried out. Scheider et al [7] have also extended the concept of the Bridgman correction to apply to rectangular cross-section specimens. This was achieved with the aid of optical techniques applied to physical tests of specimens and finite element analyses.

It should be noted that determining the true stress becomes even more difficult after continuous necking due to internal fracture by the development and coalescence of micro voids in the specimen. At this point the load is not supported by the entire cross-section; therefore the stress determined through any physical measurement after severe necking has occurred is not a true indication of the actual stress.

Tensile tests have usually been limited to quasi-static strain rates due to the limitations on the testing speeds possible by the tensile testers. Therefore, other methods needed to be devised to study the effect of higher strain rates on the properties of a material.

In 1949, Kolsky [8] published his method for determining the stress – strain relation of materials when stresses are applied for durations of the order of 20μs. His apparatus consisted of a modified Hopkinson pressure bar and was used to test rubbers, plastics and metals (copper and lead). Figure 2.1.2 depicts the split – Hopkinson apparatus invented by Kolsky.

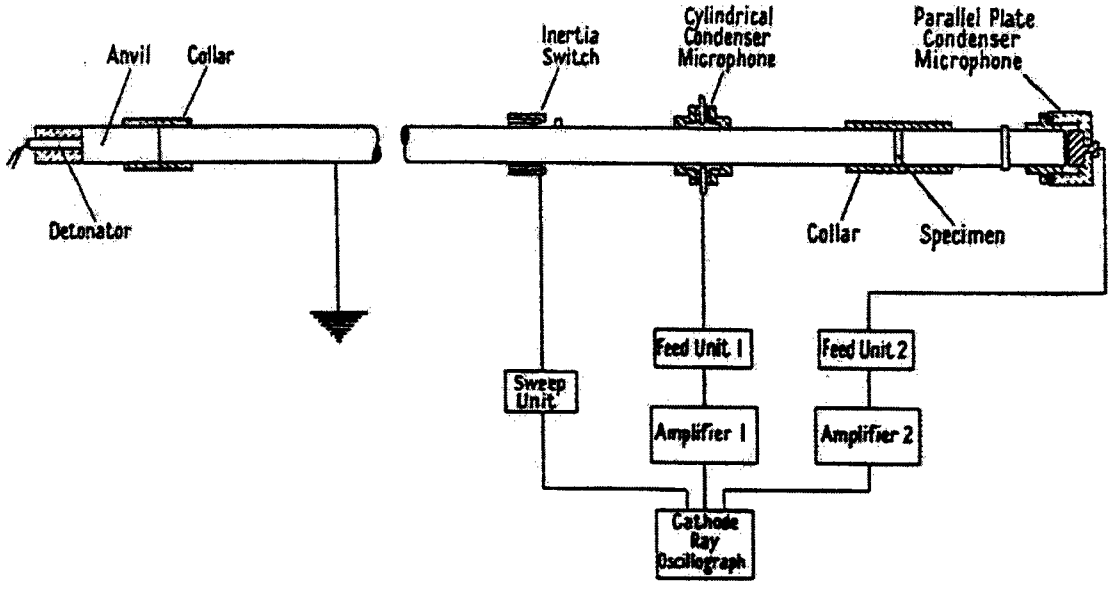

Figure 2.1.2 – Modified Hopkinson bar apparatus used by Kolsky [8]

Generally, split – Hopkinson bar testing involves placing a test specimen between an input and output bar and propagating a stress wave through the input bar. Measurements of the stress wave propagation in the bars and one dimensional wave theory are then used to deduce the stress and strain time histories through the specimen. Thus the stress –strain response of the material can be determined at a high strain rate.

More details on the use of the split – Hopkinson pressure bar can be found in reference [9].

Experiments to determine temperature effects on material properties have also been carried out. Krafft et al [10] studied the effect of loading and temperature on the yield stress of iron and mild steel. Compressive static and dynamic tests were carried out at temperatures ranging from 195°C to 100°C. The static tests were carried out in a special apparatus, depicted in figure 2.1.3, whereby the specimen was compressed in a chamber where different liquids were circulated to give different temperatures; liquid nitrogen was used to obtain a temperature of –195°C, alcohol and solid carbon dioxide gave –75°C and boiling water for 100°C. Intermediate temperatures were obtained by cooling the specimen to a lower temperature, applying loads lesser than the yield, and allowing the temperature to rise slowly and recording the temperature at yield. Loading was carried out hydraulically and the movement of the platens in the apparatus served as an approximate measurement of the strain of the specimens.

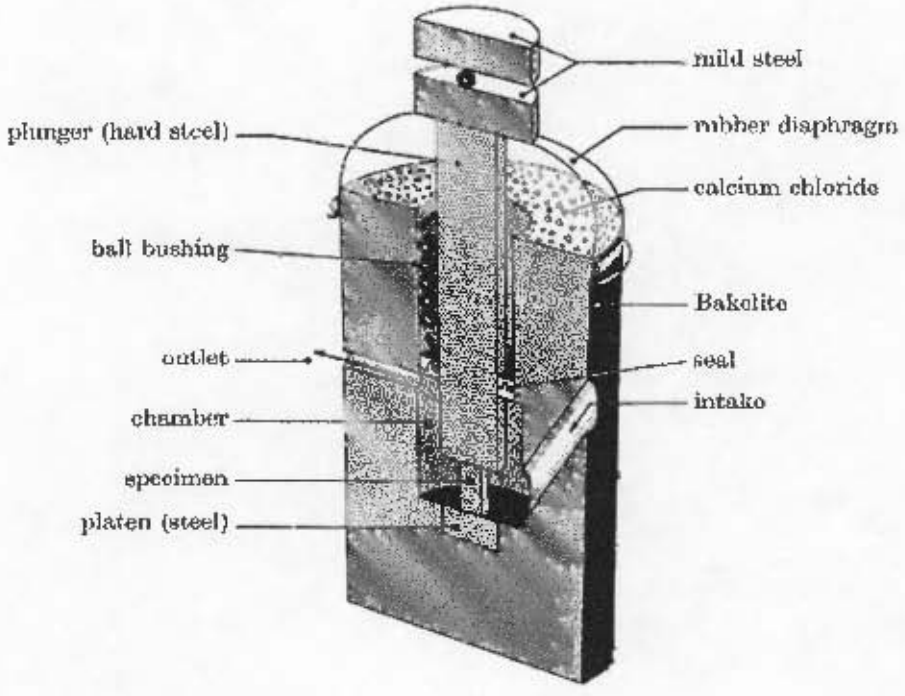

Figure 2.1.3 – Static Compression Test Apparatus with an Environmental Chamber [10]

Dynamic tests were carried out on a Hopkinson bar setup as shown in figure 2.1.4. The temperature control utilised was similar to that used in the static tests.

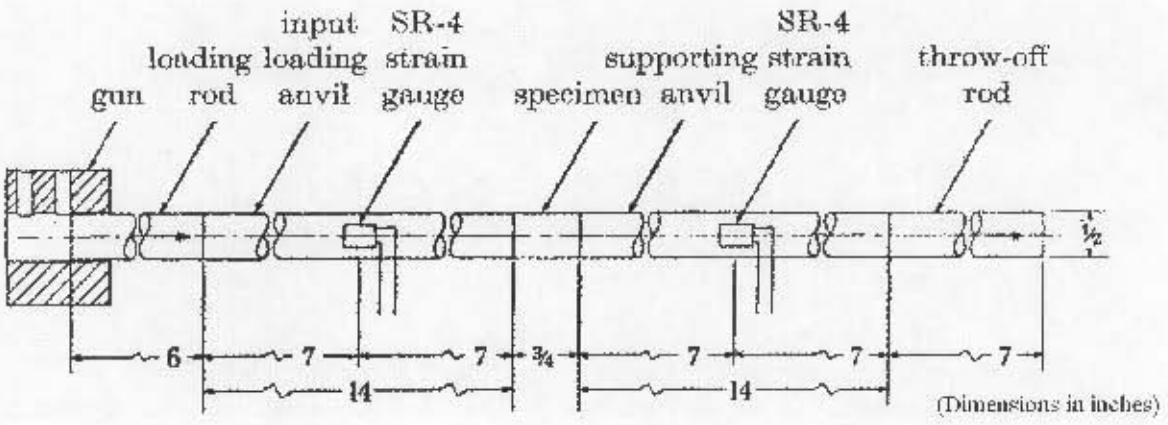

Figure 2.1.4 – Dynamic Compression Test Apparatus [10]

Testing methods involving the coupling of temperature and strain rate effects have also been investigated by Lennon and Ramesh [11]. Their experimental technique enables high temperature experiments to be carried out at high strain rates on a split-Hopkinson pressure bar. The apparatus used, depicted in figure 2.1.5, consists of an air cooled infrared spot heater that is used to heat the specimen before the input and output bars are brought into contact with the specimen. Temperature measurement is carried out via a K – type thermocouple and the heating system is able to achieve the desired temperature in less than 60s with a maximum temperature of 800°C. The strain rate range of the apparatus is $10^2 \sim 8\times10^3\ s^{-1}$.

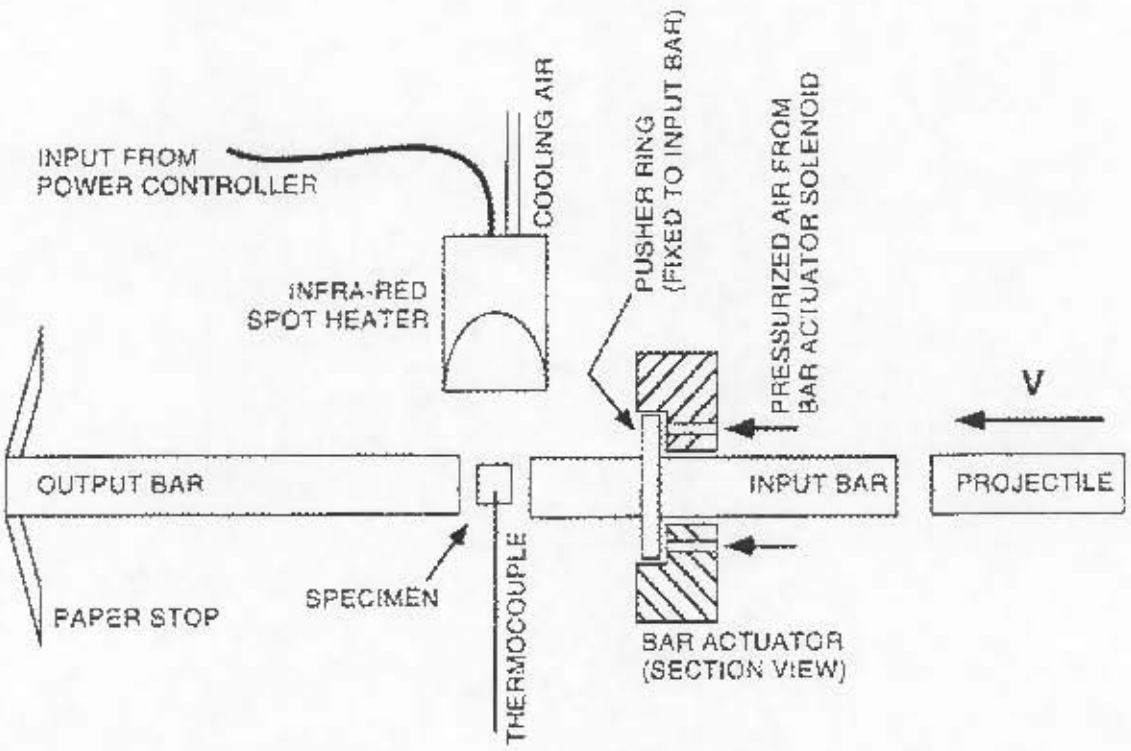

Figure 2.1.5 – Schematic of the High Temperature Split-Hopkinson Pressure Bar [11]

The design is based on the concept of heating the specimen prior to bringing the bars in contact with the specimen. Thus problems such as developing temperature gradients in the bars, which would affect the stress wave velocities, can be avoided making readings more accurate. This method also prevents the cyclic heating of the bars during repeated tests and ensures that the material properties of the bars are not altered due to temperature.

A similar method has been devised by Macdougall [12] for use on the tensile split-Hopkinson bar. It also makes use of infrared heaters and is capable of heating the specimen up to 800°C in 10s.

2.2. Results of Experimental Work on Steel

As described in the preceding section, experimental works investigating the effects of temperature and strain rate on material properties have been carried out. In certain cases only the temperature effect or the strain rate effect has been studied and in others the two have been studied together. This section reviews some of the experimental data generated through such investigations with a focus on steel. However, prior to presenting these experimental results, a brief background of steel in terms of a material science viewpoint is necessary.

2.2.1. Material Science Background of Steel

Reasons for the variation of the material properties under different environmental and loading conditions may be attributed to their material composition and microstructure. The properties of steel depend very much on the carbon content present. Figure 2.2.1.1 gives the Iron – Carbon equilibrium phase diagram.

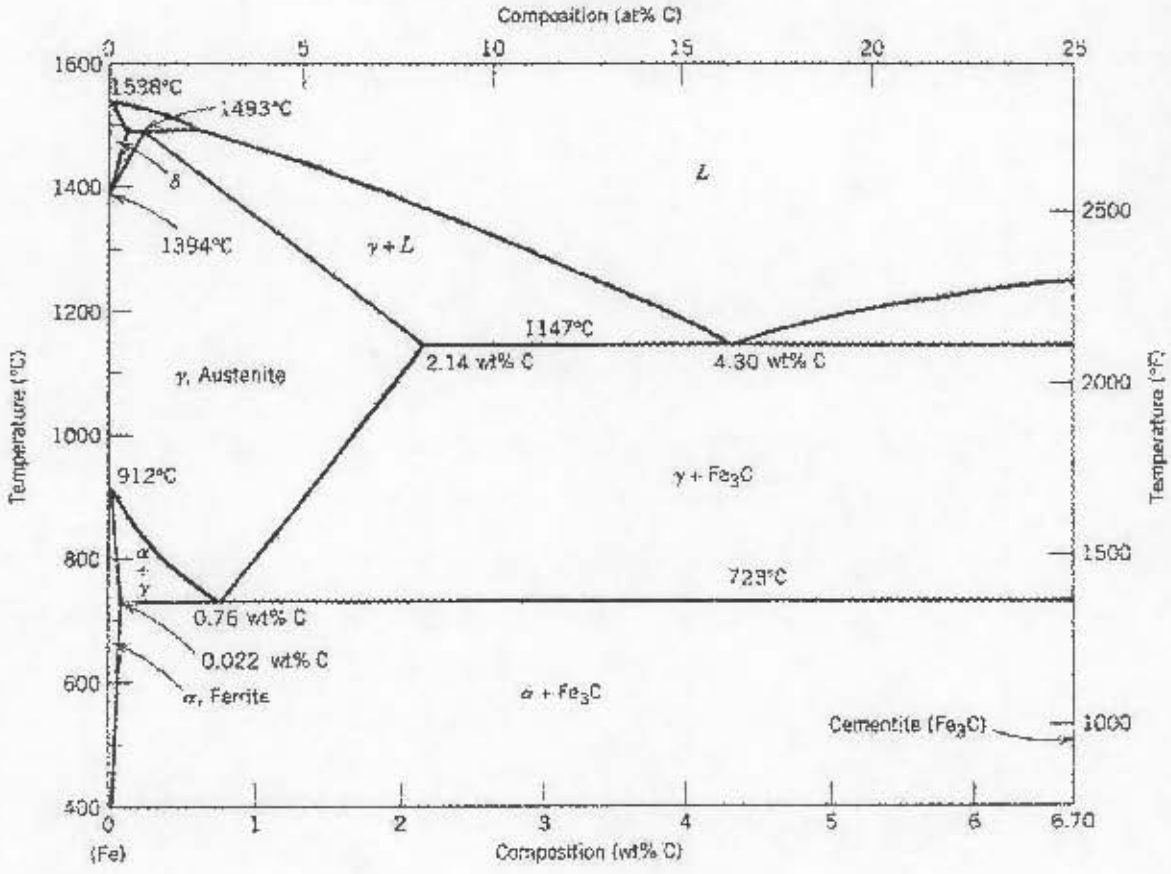

Figure 2.2.1.1 – Iron – Carbon Equilibrium Phase Diagram

The areas bounded by lines represent the equilibrium phases and the lines demarcate where the phase changes will occur. L refers to the liquid state; γ refers to the austenite phase and α refers to the ferrite phase. The crystal structure of austenite is face centred cubic (FCC) while that of ferrite is body centred cubic (BCC). Martensite is another phase of steel; however it is not an equilibrium phase and thus does not appear in figure 2.2.1.1. Martensite has a body centred tetragonal (BCT) crystal structure. The microstructure of steel is stable below 723°C as a mixture of ferrite and iron carbide (Fe_3C).

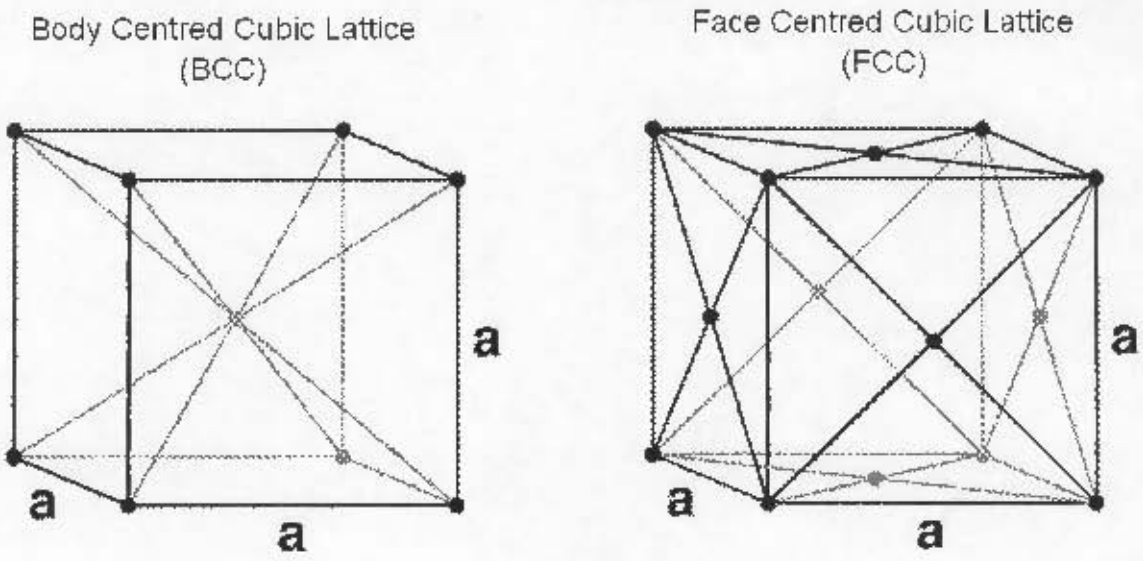

Figure 2.2.1.2 – BCC and FCC Crystal Lattices [13]

Steels are generally considered to have ≤2.11% by weight of carbon present. Beyond this point the material is considered a cast iron. Table 2.2.1.1 presents a general classification of plain carbon steels according to their carbon content.

Table 2.2.1.1 Classification of Plain Carbon Steels

Steel Type	Carbon Content (wt %)
Ultra Low Carbon Steel	0.03 (Max)
Low Carbon Steel	0.04 ~ 0.15
Mild Steel	0.15 ~ 0.30
Medium Carbon Steel	0.30 ~ 0.60
High Carbon Steels	0.60 ~ 2.11

Itabashi and Kawata [14] investigated the effect of carbon content on the material properties of different carbon steels with carbon contents ranging from 0.14 – 0.54 wt %. Tensile tests were carried out at four different strain rates ($1\times10^{-3}\,s^{-1}$,

$1\times10^{-2}s^{-1}$, $1\times10^{-1}s^{-1}$ and $1\times10^{3}s^{-1}$). The quasi-static tests were carried out with a conventional screw driven machine and the high strain rate tests were carried out by a special sling shot type high velocity loading machine. The tests were used to determine the upper and lower yield stresses, tensile strength, failure strains as well as energy absorbed per unit volume. From the results they obtained, they noticed the following:

- The lower yield stress and tensile strengths increased with increasing strain rates.
- The lower yield stress and tensile strengths increased with increasing carbon content.
- Ductility of the steels reduced with increasing carbon content.
- The presence of Manganese (Mn) in the chemical composition also affected the lower yield stress and tensile strengths, especially when coupled with higher concentrations of Carbon. The lower yield stress was found to generally increase with a rise in Manganese content over the quasi-static and high strain rates. The tensile strength was found to increase at quasi-static strain rates but at higher strain rates, the effect was reversed and increasing the Manganese content caused a slight decrease in the tensile strength.

The work presented by Itabashi and Kawata [14] supports what is accepted as fact in material science concerning steels. This is because the carbon atoms present as a solid solution in the crystal lattice of iron provide obstacles to dislocation movements during deformations. Therefore as the carbon content increases, more obstacles are provided to dislocation movements, hence strengthening the steel. The presence of these interstitial carbon atoms also gives rise to yielding phenomena such as dynamic strain ageing. This occurs when interstitial carbon atoms diffuse towards dislocations that are temporarily pinned, thus increasing the stress required to move these dislocations. This manifests itself macroscopically as a serrated stress – strain curve. It also gives rise to strain hardening, lowers the ductility of the material and negative strain rate sensitivity is displayed. Zeghib and Klepackzo [15]

report that this phenomenon occurs for mild steel approximately between 77°C and 327°C.

Generally all phenomena that affect the microstructure of the material, such as cold working or heat treating, contribute to the overall properties that the material will display. The following section presents the macroscopic observations of experiments carried out on various types of steel.

2.2.2. Experimental Results

Various experiments have been performed on steel over the years to glean their material properties. Manjoine [16] carried out extensive work on determining the effect of strain rate and temperature on the yield stress of mild steel. He tested a commercial low-carbon open-hearth steel at temperatures ranging from room temperature to 600°C. The strain rates employed in carrying out the tensile tests ranged from $10^{-6}s^{-1}$ to $10^{3}s^{-1}$. Figures 2.2.2.1 – 2.2.2.4 show the results of his tests.

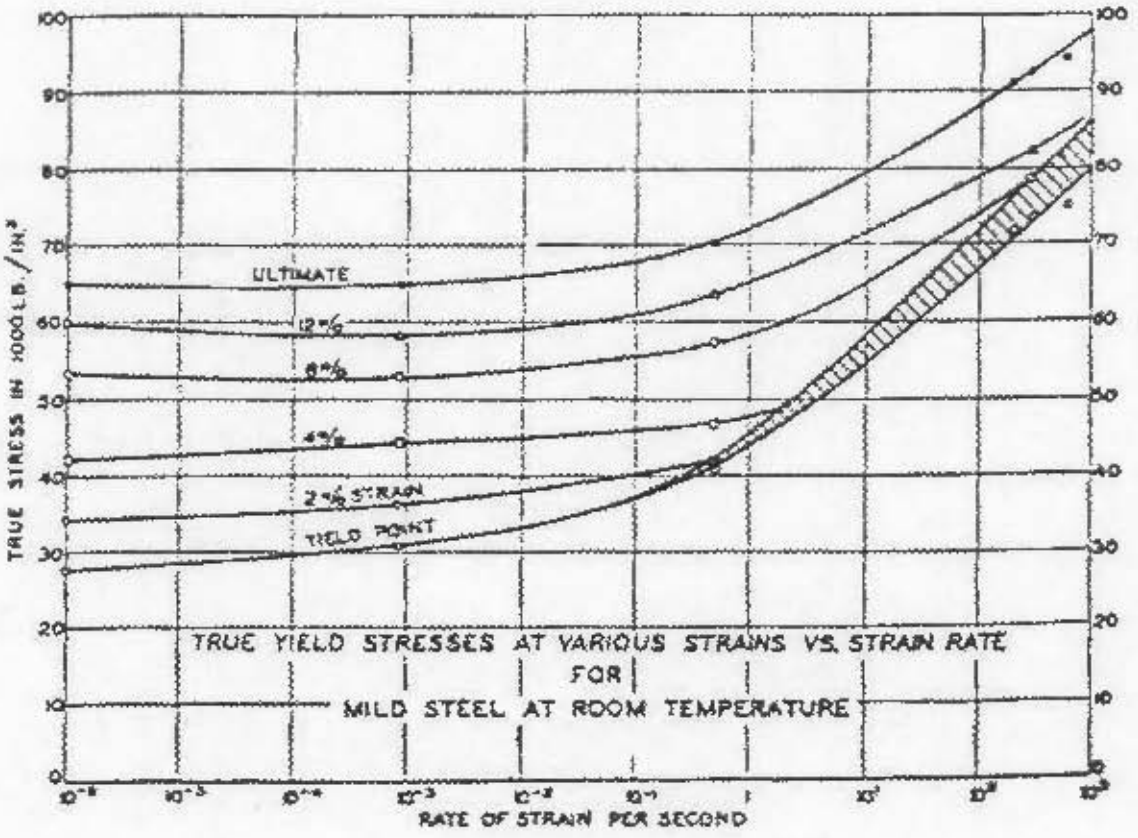

Figure 2.2.2.1 – Variation of Yield Stress for Mild Steel with Strain Rate at 25°C [16]

At room temperature, the yield stresses increased as the applied strain rate increased. However, at the higher strains, the effect of dynamic strain ageing was noticed. This is exhibited in the regions where the recorded stresses decreased with an increase in strain rate as seen in the curves depicting the stresses at 8% and 12% strains over the region of lower strain rates.

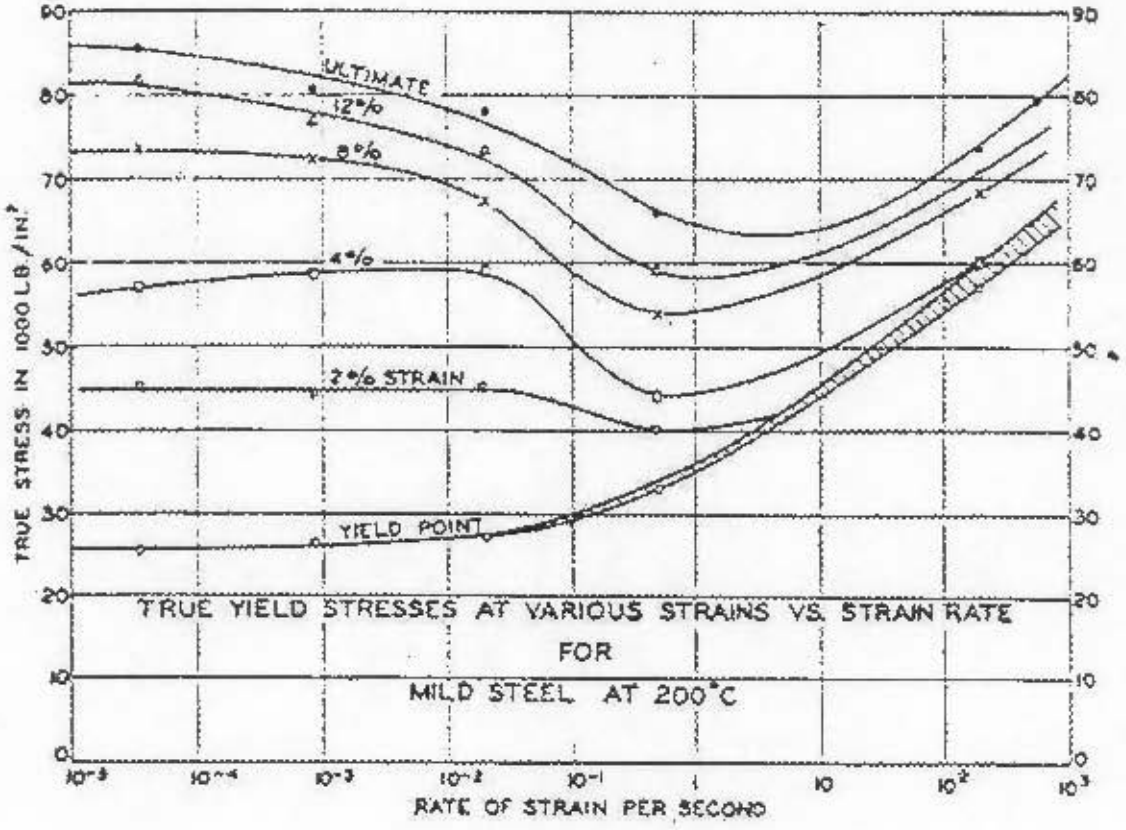

Figure 2.2.2.2 – Variation of Yield Stress for Mild Steel with Strain Rate at 200°C [16]

At 200°C, the yield point increased with an increase in the applied strain rate. However, at this temperature, the effect of dynamic strain ageing was significant and noticed for all strains above the yield. The ultimate tensile stress and stresses recorded at 8% and 12% strains showed considerable regions of negative strain rate sensitivity.

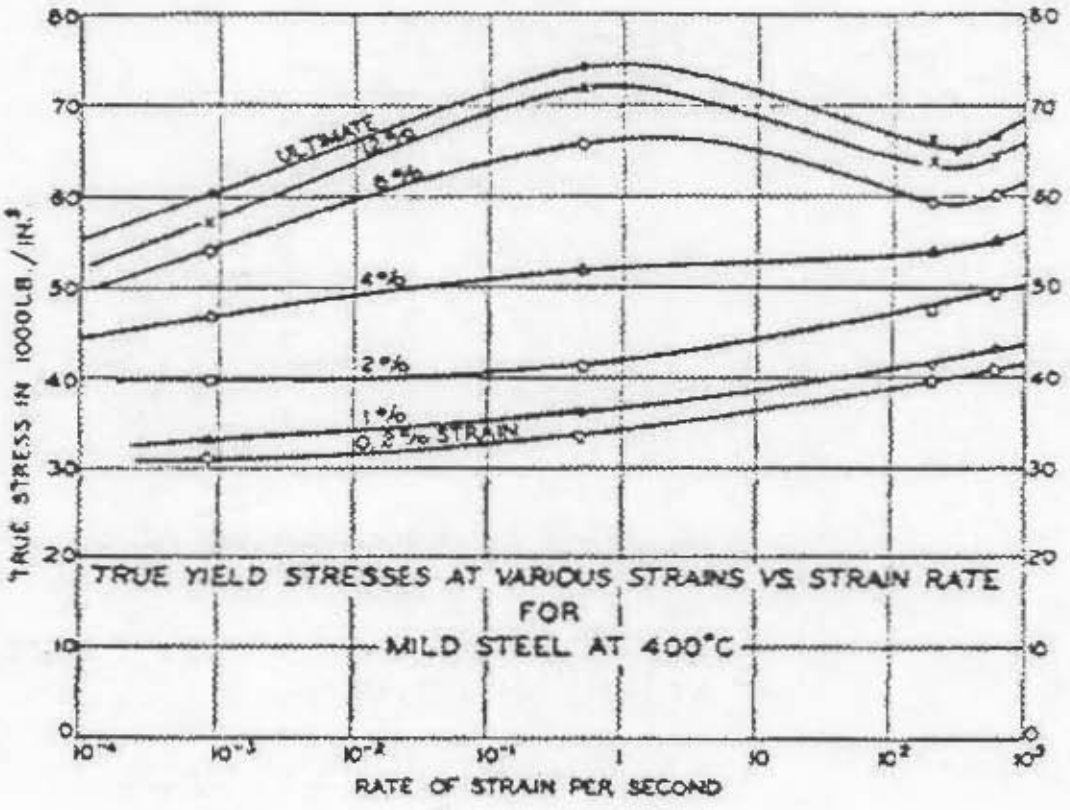

Figure 2.2.2.3 – Variation of Yield Stress for Mild Steel with Strain Rate at 400°C [16]

The effect of dynamic strain ageing was less pronounced at 400°C than at 200°C. The stresses recorded at strains below 4% increased with strain rate over the entire range. At the higher strains (8%, 12% and ultimate) and lower strain rates, the material is kept at temperature over a longer period of time. This allows the effects of dynamic strain ageing to be overcome by over-ageing which weakens the material. Thus the stresses increase with strain rate up to approximately $1s^{-1}$. At this point, the tests occur over a shorter time duration minimising the possibility of over-ageing, thus negative strain rate sensitivity is once again exhibited.

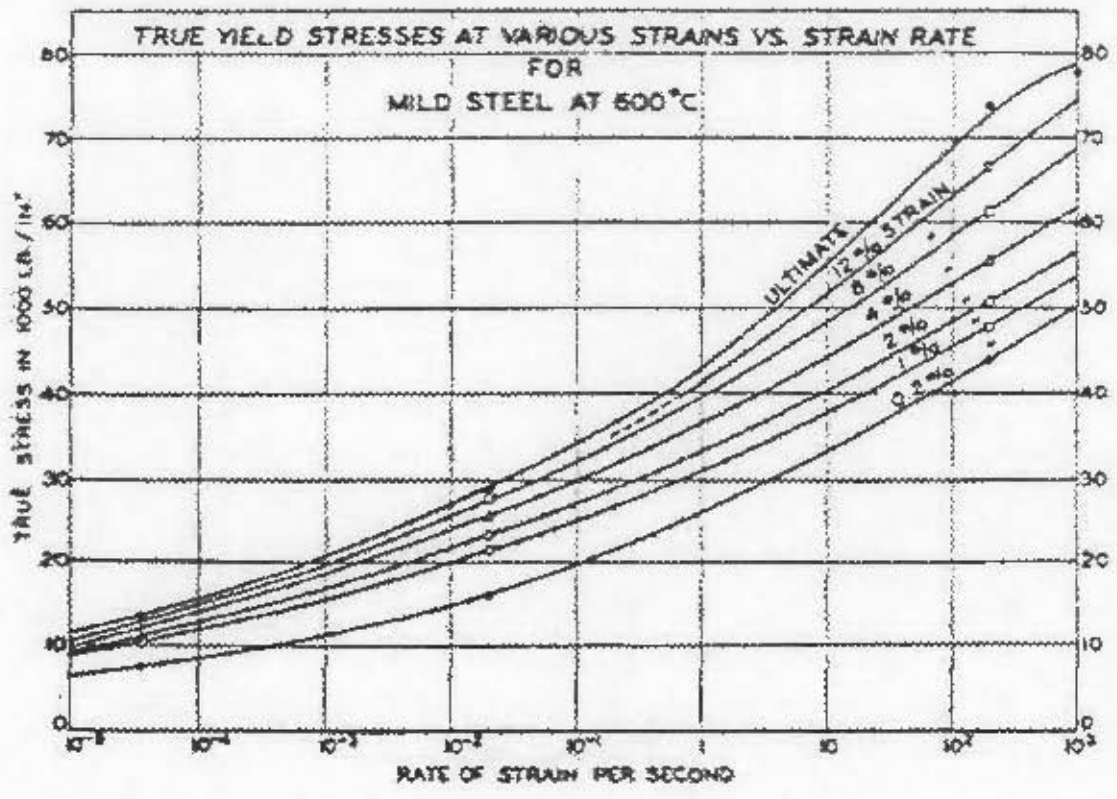

Figure 2.2.2.4 – Variation of Yield Stress for Mild Steel with Strain Rate at 600°C [16]

At 600°C, the strain rate effect is dominant. The stresses recorded at all the strains increase with applied strain rate over the entire range of strain rates investigated.

Similar trends have been observed by Steichen [17] on AISI 304 Stainless Steel. He carried out tensile tests ranging from $3\times10^{-5}\,s^{-1}$ to $1\times10^{2}\,s^{-1}$ at temperatures between 316°C (600°F) and 871°C (1600°F). The yield stress of AISI 304 Stainless Steel was found to increase with strain rate over all the temperatures investigated as shown in figure 2.2.2.5. The ultimate stress was prone to dynamic strain ageing at the lower strain rates for temperatures ranging from 316°C (600°F) to 538°C (1000°F). This is depicted in figure 2.2.2.6.

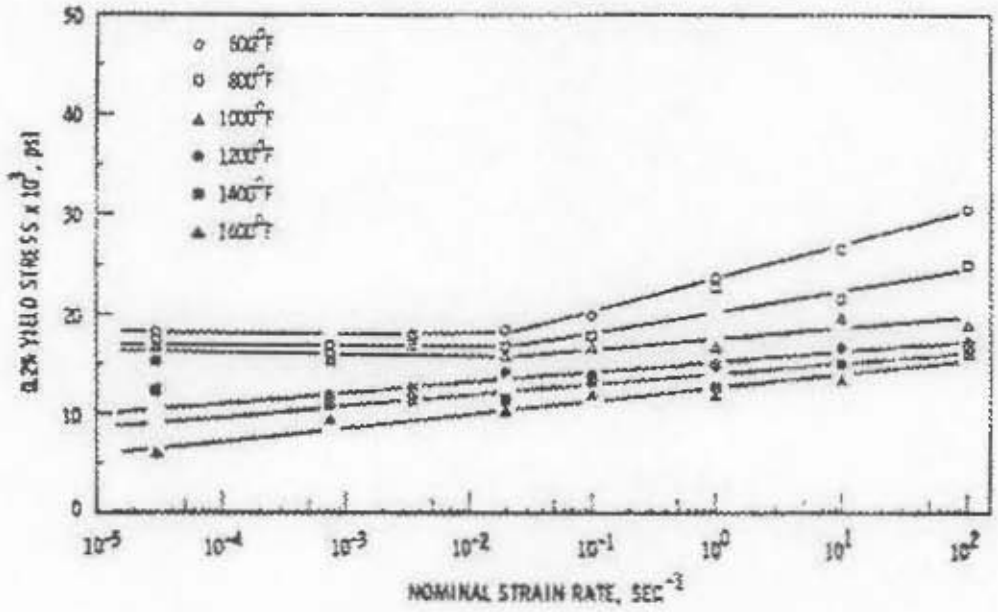

Figure 2.2.2.5 – Temperature Effect on the Yield Stress of AISI 304 [17]

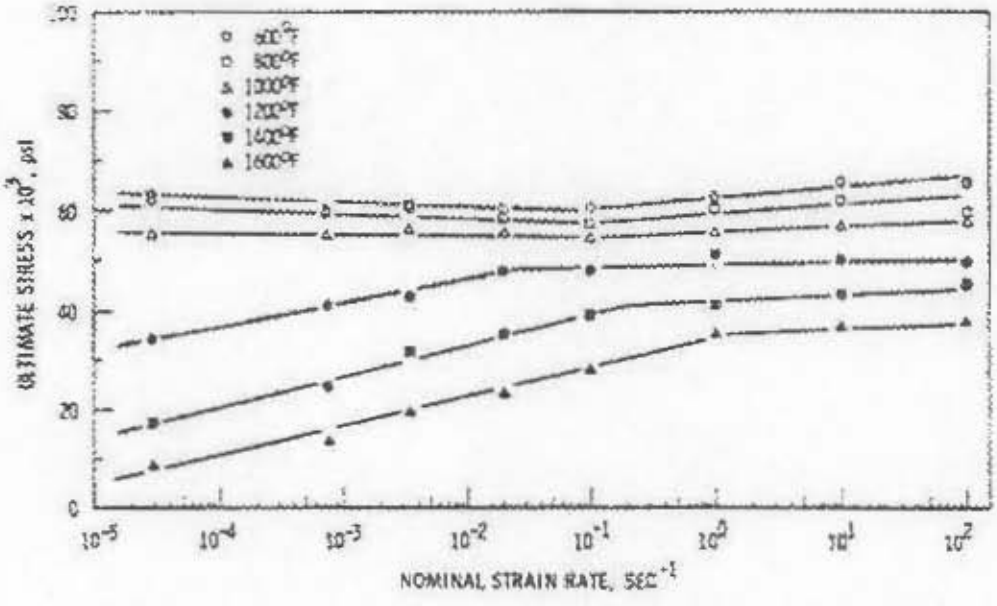

Figure 2.2.2.6 – Temperature Effect on the Ultimate Stress of AISI 304 [17]

Davies and Magee [18] investigated the effect of strain rate on a number of engineering materials, mostly comprised of steels, to aid in evaluating and improving the crashworthiness of vehicle chassis. Tensile tests were carried out over strain rates from $1\times10^{-3}s^{-1}$ to $1\times10^{4}s^{-1}$. They reported the yield stress to be more sensitively dependent on the strain rate than the flow stresses at higher strains. Generally for the steels, they noted the yield stresses and ultimate tensile strengths increased with strain rate. However, the strain rate was found to have little effect on the tensile elongations of the materials. Figure 2.2.2.7 depicts the strain rate effect on the ultimate tensile strengths of hot rolled steels with carbon contents varying from 0.1 wt% to 0.82 wt%. For the hot rolled steels, the ultimate tensile strength increased with an increase in both carbon content and applied strain rate.

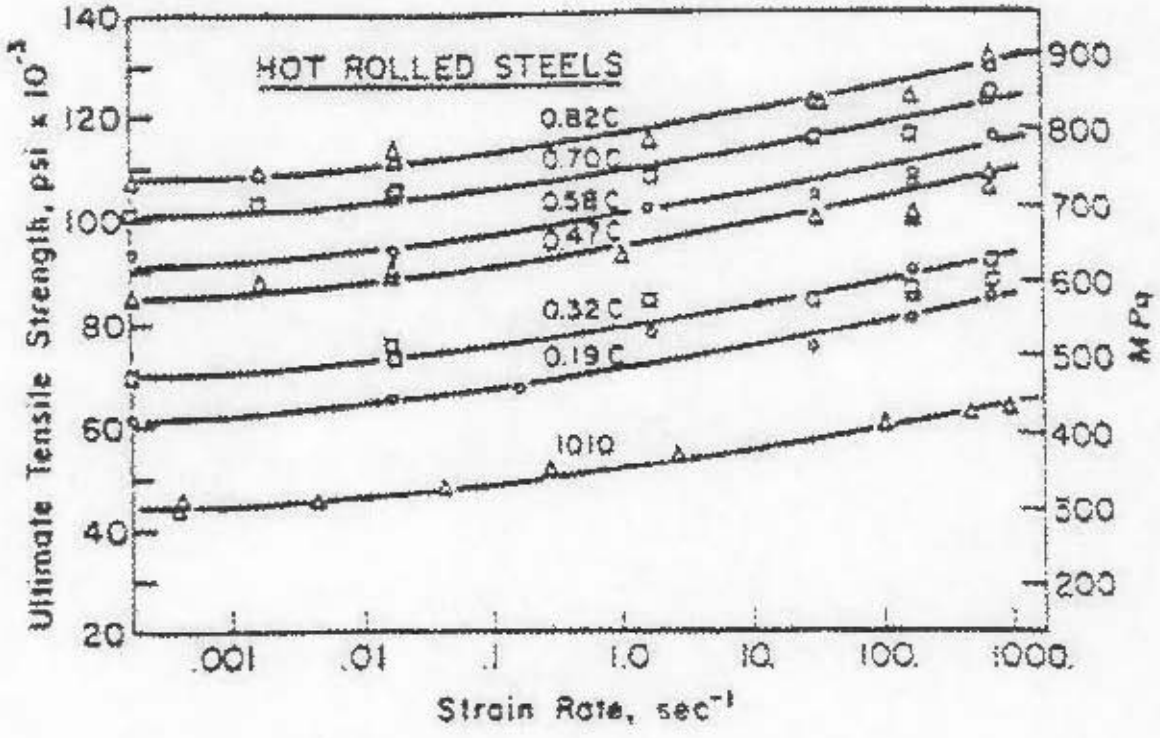

Figure 2.2.2.7 – Strain Rate Effect on the Ultimate Tensile Strengths of Hot Rolled Steels [18]

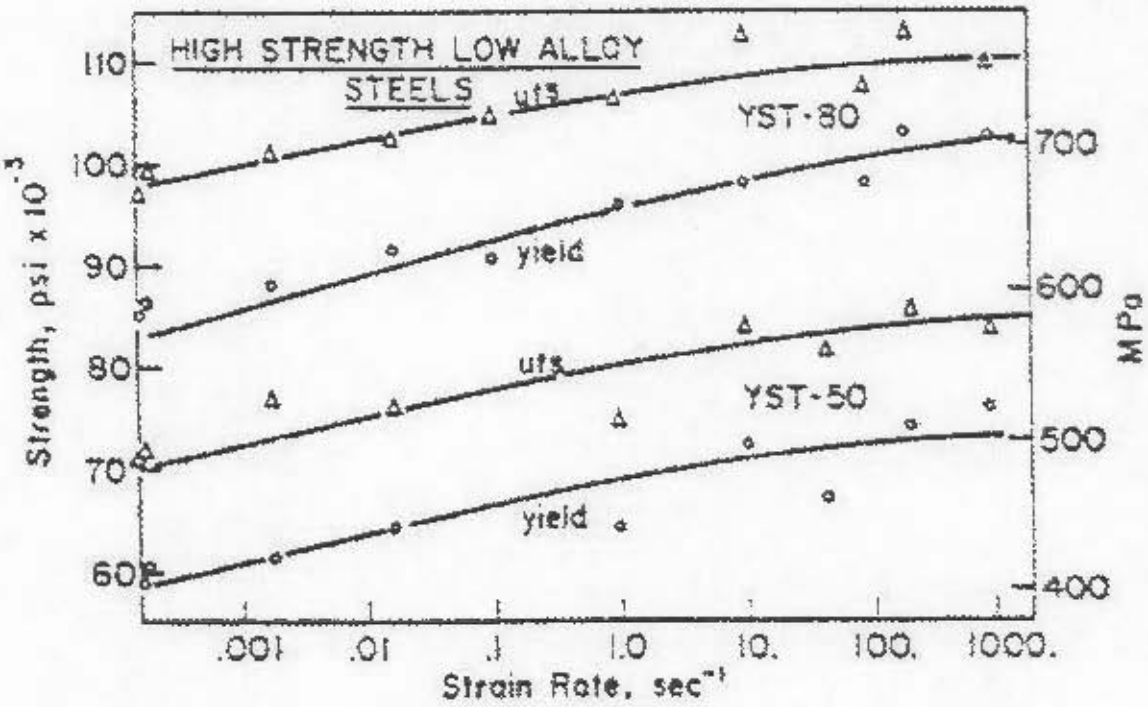

Figure 2.2.2.8 – Strain Rate Effect on the Properties of YST 50 and YST 80 [18]

Figure 2.2.2.8, also extracted from reference [18], shows the effect of the applied strain rate on two high strength low alloy steels (YST 50 and YST 80). The yield and ultimate tensile strengths for both materials increase as strain rate increases. A similar trend is noticed in figure 2.2.2.9 where the yield strengths of two types of stainless steel (AISI 302 and AISI 310) are shown to increase with applied strain rate. The ultimate tensile strength of the AISI 302 Stainless Steel remains invariant with the applied strain rate though that of the AISI 310 Stainless Steel increases with strain rate.

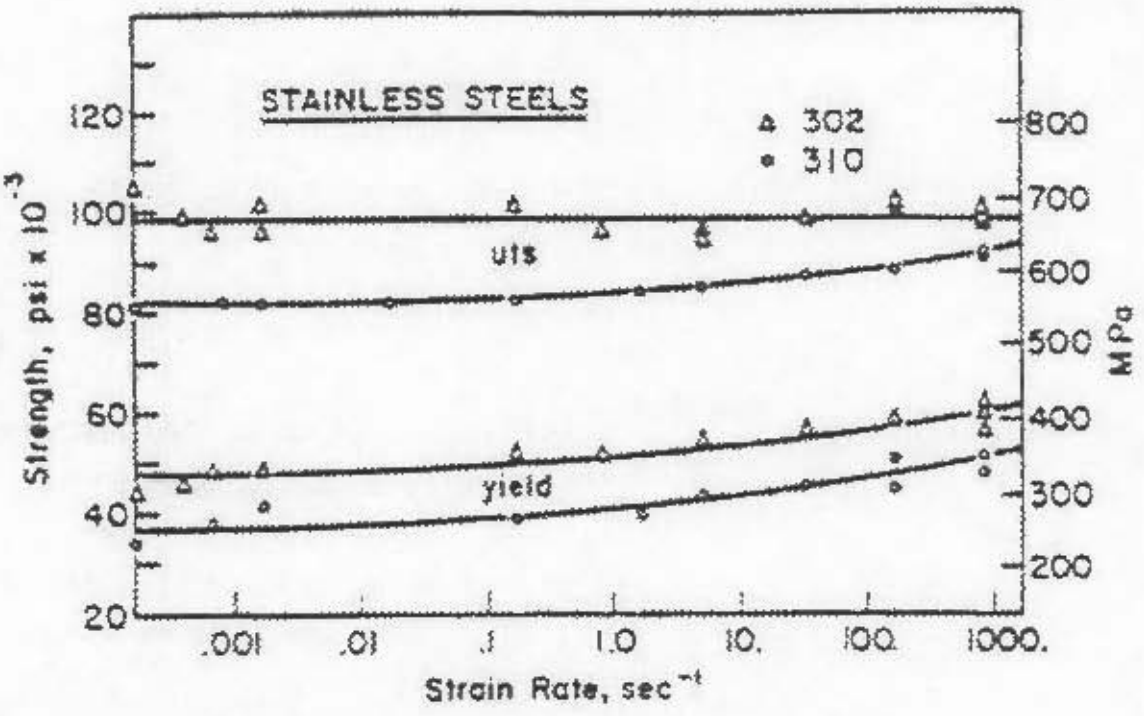

Figure 2.2.2.9 – Strain Rate Effect on the Properties of AISI 302 and AISI 310 [18]

Such test data has also proved insightful in nuclear plant design. Albertini and Montagnani [19] carried out high temperature tests on three different austenitic stainless steels (AISI 304L, AISI 316L and AISI 321) with strain rates between $3\times10^{-3}s^{-1}$ and $5\times10^{2}s^{-1}$. The work was done to aid in the study of loading conditions experienced in the event of explosive accidents in fast breeder containment structures. Tensile tests were carried out at 20°C, 400°C, 550°C, 750°C and 950°C. Figures 2.2.2.10 – 2.2.2.12 show the strain rate effect on the ultimate tensile stress of the three materials at different temperatures. The data points used to plot figures 2.2.2.10 – 2.2.2.12 were extracted from the engineering stress – strain curves presented in reference [19]. The effect of the strain rate on the yield points was not considered as the yield points were not clearly discernible from these engineering stress – strain curves.

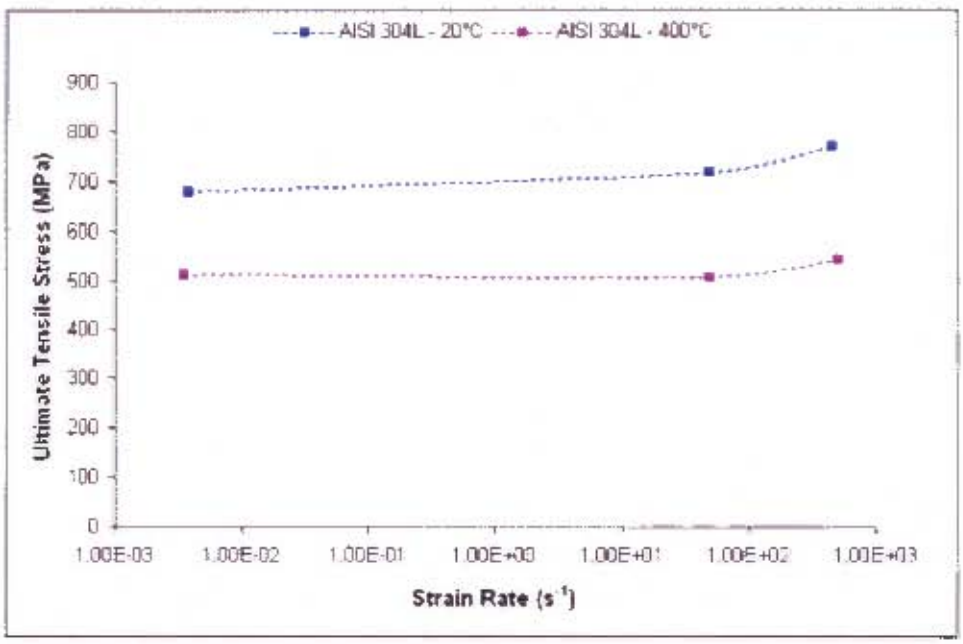

Figure 2.2.2.10 – Strain Rate Effect on the Ultimate Tensile Stress of AISI 304L

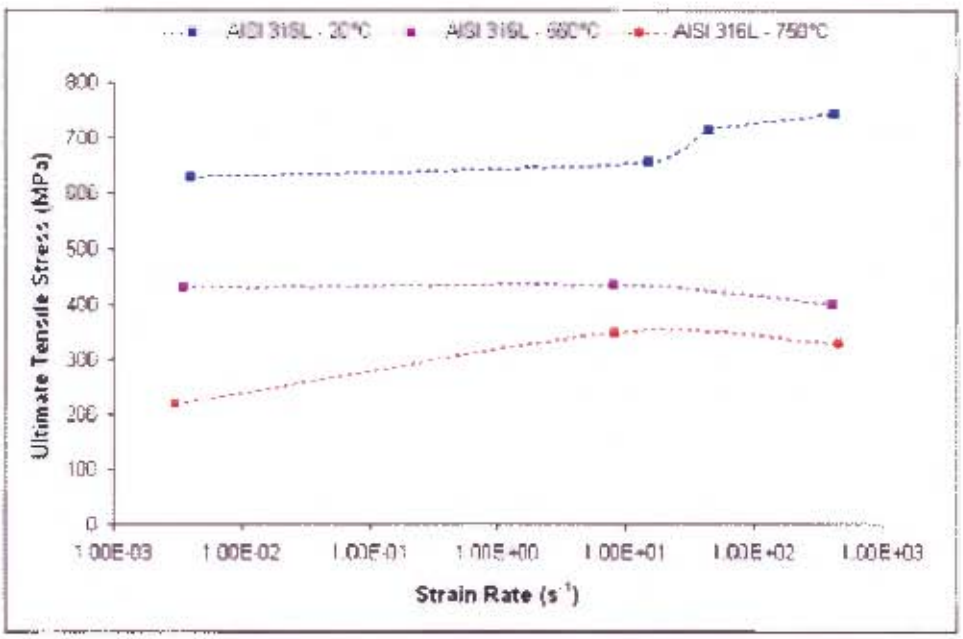

Figure 2.2.2.11 – Strain Rate Effect on the Ultimate Tensile Stress of AISI 316L

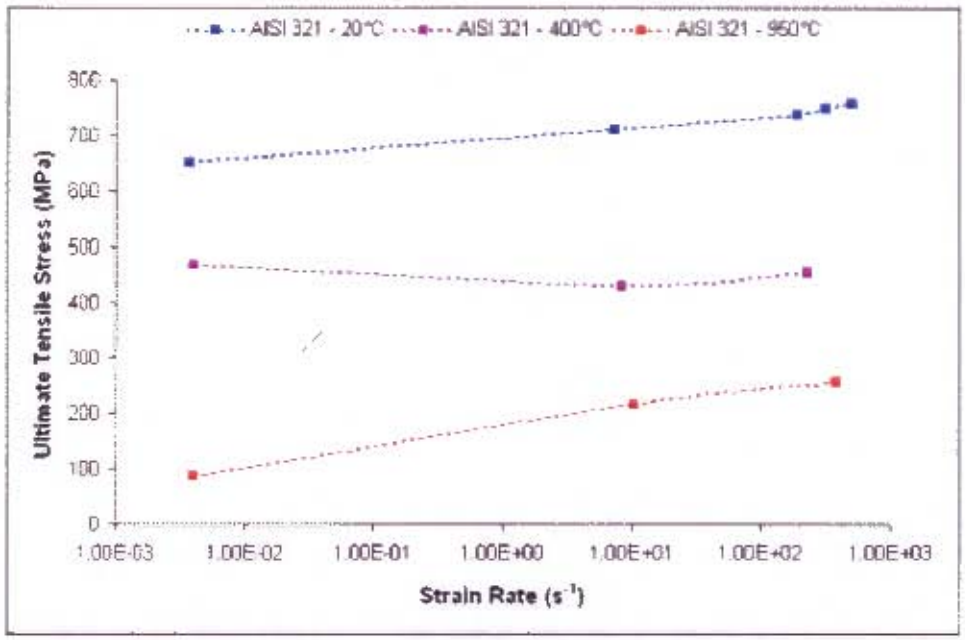

Figure 2.2.2.12 – Strain Rate Effect on the Ultimate Tensile Stress of AISI 321

For all three materials, at room temperature the flow stresses were found to increase with increasing strain rate. At 550°C and 750°C for AISI 316L and 400°C for AISI 321, regions of negative strain rate sensitivity were exhibited, where the ultimate tensile stresses decreased with increasing strain rate. From figures 2.2.2.10 – 2.2.2.12, it is evident that the test temperature has a larger impact on the ultimate tensile stresses than the applied strain rates for the three materials. It should be noted that austenitic steels generally have good properties at elevated temperatures, thus they are able to maintain their strength when exposed to high temperatures over longer durations.

Masui et al [20] presented an empirical relationship for the variation of the yield stress of steel based on the results of high temperature tensile tests carried out on a 5 ton Instron Tester. Equations 2.2.2.1a – 2.2.2.1c present their temperature model.

$$\frac{\sigma_y}{\sigma_0} = 1 \qquad T \leq 200°C \qquad \text{(Equation 2.2.2.1a)}$$

$$\frac{\sigma_y}{\sigma_0} = 1 - 0.00178(T - 200) \qquad 200°C < T \leq 700°C \qquad \text{(Equation 2.2.2.1b)}$$

$$\frac{\sigma_y}{\sigma_0} = 0.133 - 0.000388(T - 700) \qquad 700°C < T \leq 1000°C \qquad \text{(Equation 2.2.2.1c)}$$

Where σ_y is the yield stress at the given temperature whereas σ_0 refers to the uniaxial yield stress at room temperature.

Masui et al [20] also reported the Young's Modulus (E) for steel as a function of temperature:

$$E = \left(210 \times 10^9 - 58.34 \times 10^6 T\right) Pa \qquad \text{(Equation 2.2.2.2a)}$$

For $T \leq 600°C$

$$E = \left(3.1 \times 10^5 (T - 1100)^2 + 97 \times 10^9\right) Pa \qquad \text{(Equation 2.2.2.2.b)}$$

For $600°C < T \leq 1100°C$

Figure 2.2.2.13 depicts a plot of the temperature model for steel proposed by Masui et al [20].

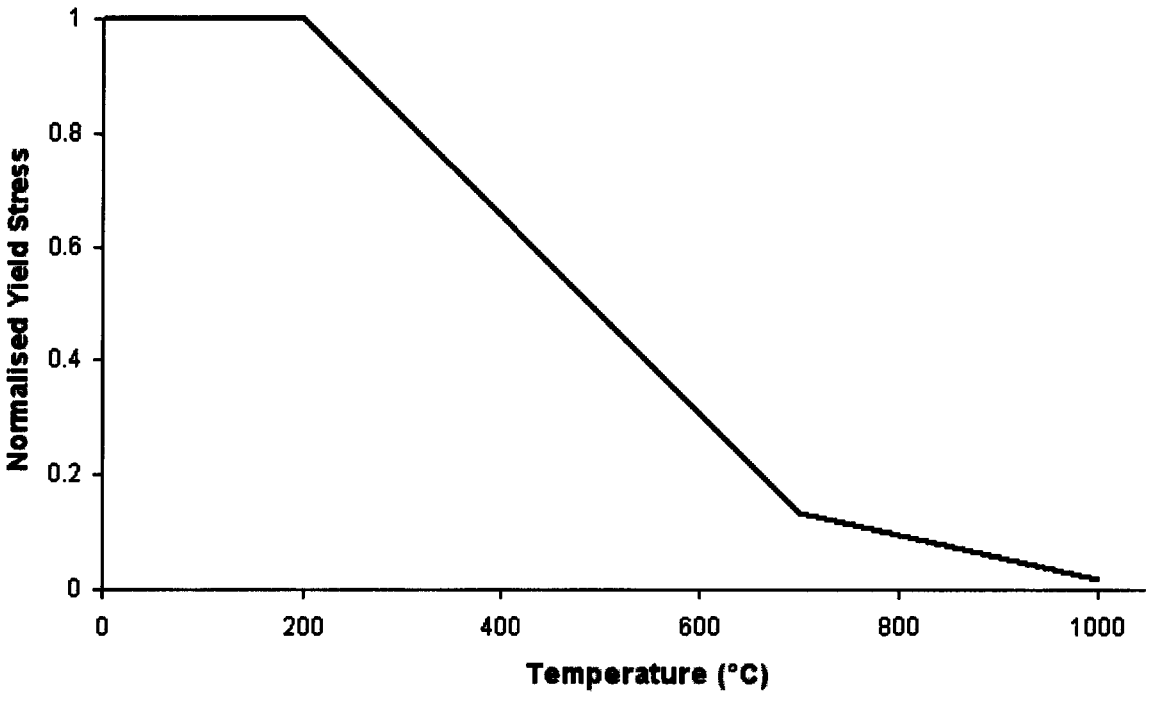

Figure 2.2.2.13 – Temperature Model for Steel by Masui et al [20]

More recent work investigating the temperature and strain rate effects on steel have been carried out by Gilat and Wu [21]. Their work investigated the effects of dynamic strain ageing on 1020 steel and they endeavoured to formulate a constitutive equation that would adequately model this behaviour. They carried out torsion tests on thin walled tubes of hot-rolled 1020 steel at temperatures of 25°C, 200°C, 400°C and 600°C, and strain rates of $5 \times 10^{-4} s^{-1}$, $2s^{-1}$, and $1000s^{-1}$. Figures 2.2.2.14 – 2.2.2.20 extracted from reference [21] depict the results they obtained.

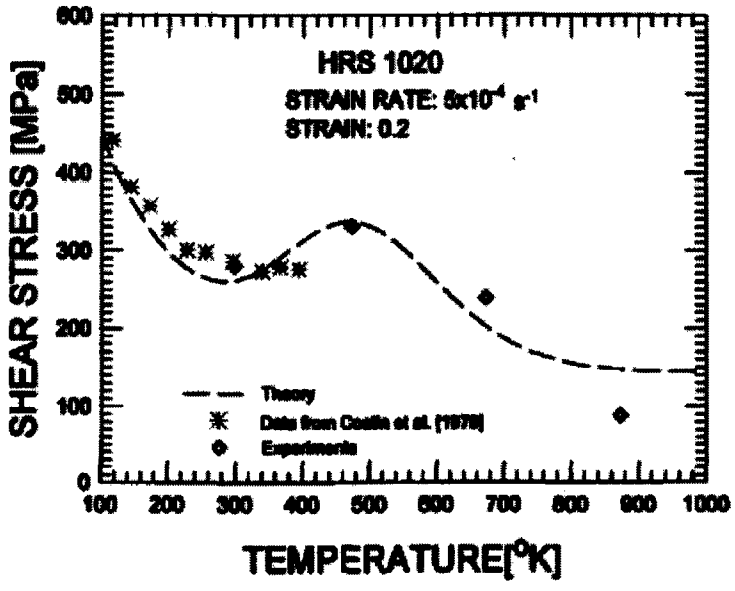

Figure 2.2.2.14 – Variation of shear stress with temperature (strain rate: 5 x $10^{-4}s^{-1}$) [21]

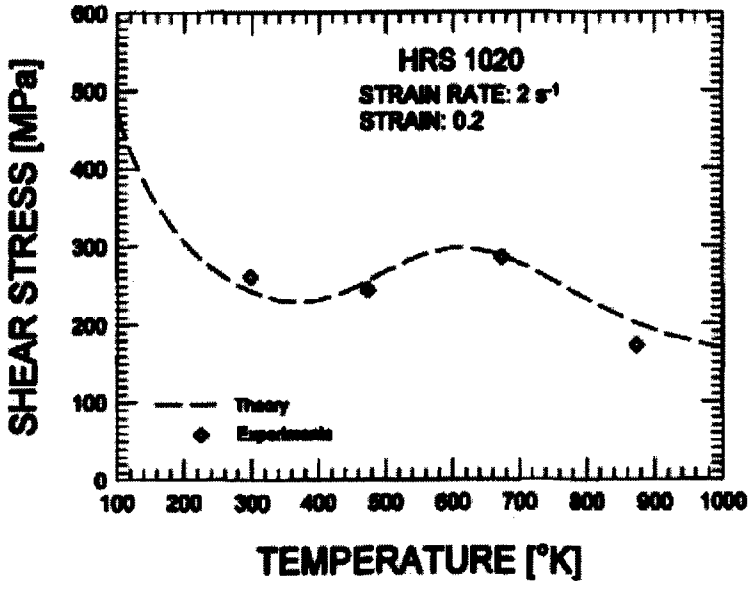

Figure 2.2.2.15 – Variation of shear stress with temperature (strain rate: $2s^{-1}$) [21]

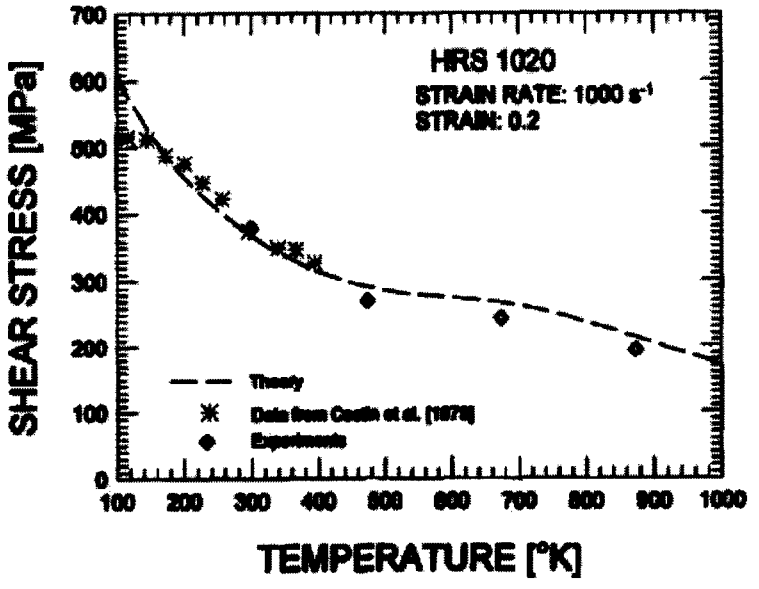

Figure 2.2.2.16 – Variation of shear stress with temperature (strain rate: $1000s^{-1}$) [21]

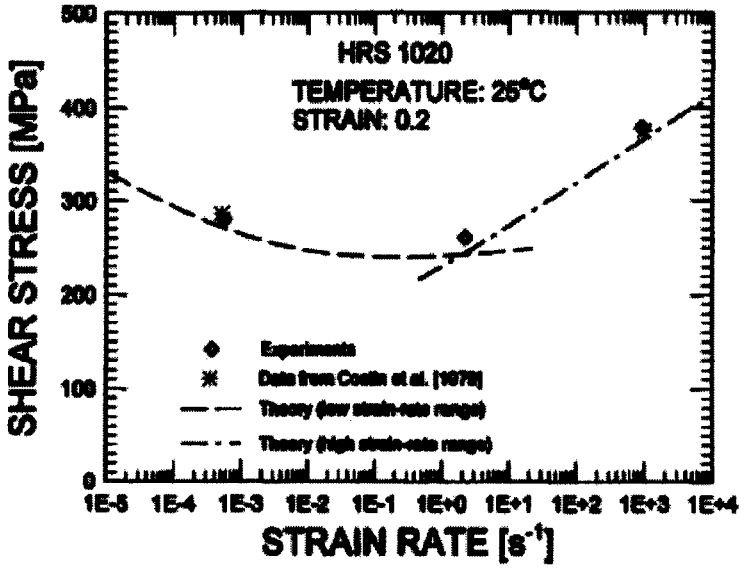

Figure 2.2.2.17 – Variation of shear stress with strain rate (temperature: 25°C) [21]

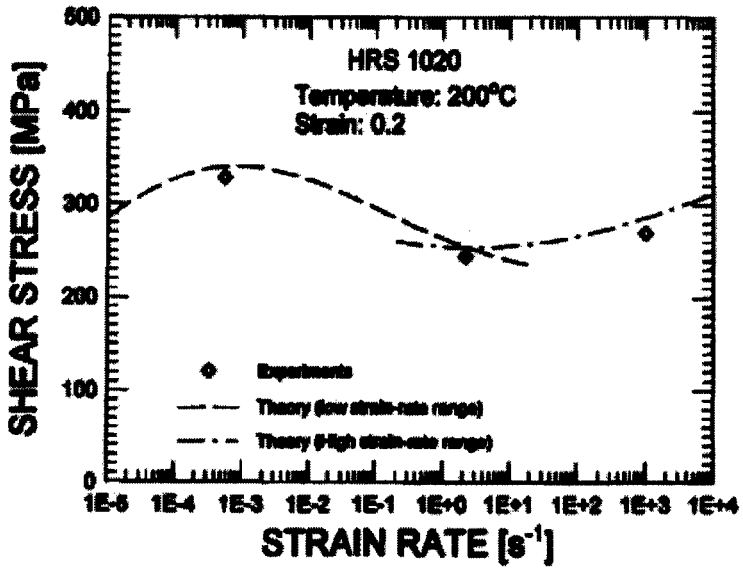

Figure 2.2.2.18 – Variation of shear stress with strain rate (temperature: 200°C) [21]

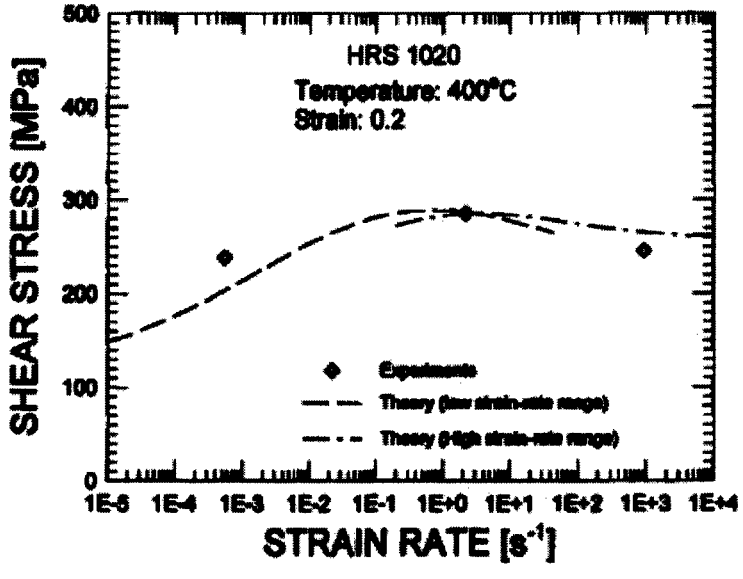

Figure 2.2.2.19 – Variation of shear stress with strain rate (temperature: 400°C) [21]

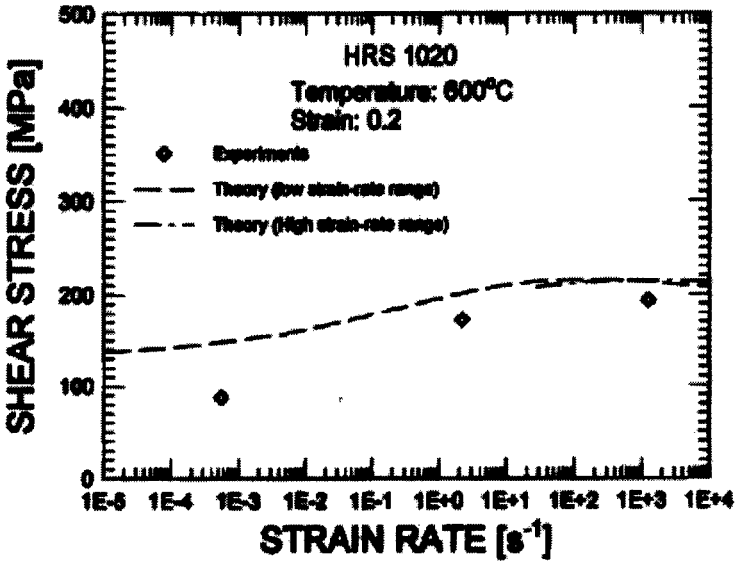

Figure 2.2.2.20 – Variation of shear stress with strain rate (temperature: 600°C) [21]

Note the curves presented with dashed lines in figures 2.2.2.14 – 2.2.2.20 are the results of predictions made with constitutive relations and theory presented in reference [21]. Figures 2.2.2.17 – 2.2.2.20 show the strain rate effect on 1020 steel and regions of negative strain rate sensitivity are observed at temperatures of 25°C, 200°C and 400°C. However, at 600°C the shear stress was found to increase with applied strain rate over the entire range of strain rates.

Figures 2.2.2.14 – 2.2.2.16 are summarised in figure 2.2.2.21 to show the regions of dynamic strain ageing where the shear stress increases with increasing temperature.

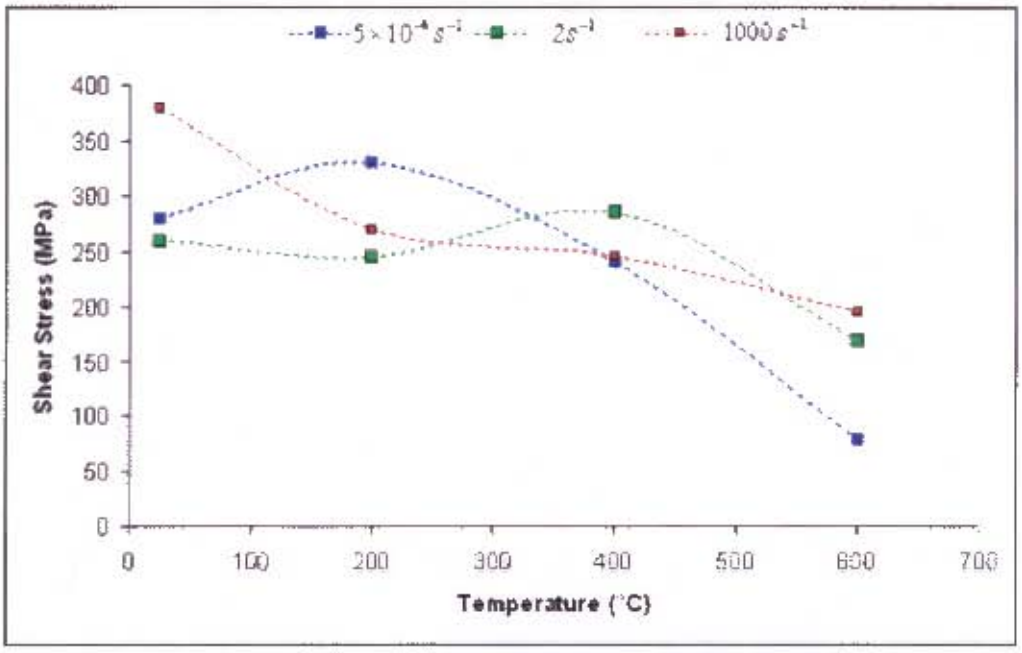

Figure 2.2.2.21 – Temperature Effect on the Shear Stress of 1020 Steel

For tests carried out at $5\times10^{-4}\,s^{-1}$, as shown in figure 2.2.2.21, the stress increases from 25°C to 200°C. At a strain rate of $2s^{-1}$, dynamic strain ageing occurs at higher temperatures (between 200°C and 400°C). Conversely, at a strain rate of $1000s^{-1}$ the effects of dynamic strain ageing are small, with the shear stress decreasing with increasing temperature over the range of temperatures investigated by Gilat and Wu [21].

These results show that temperature and strain rate significantly affect the material response. Moreover, these results demonstrate that there exist different combinations of temperature and strain rate where the effects of dynamic strain ageing are significant, thus proving plastic deformation to be a complex process. Gilat and Wu [21] noted the difficulty involved in modelling such plastic deformation over a wide range of temperatures and strain rates through constitutive relations. They also noted that material characteristics were better represented when data from a wide range of loading conditions was available. However, as the range

of loading conditions increased, so too did the difficulty in developing constitutive relations that could model the results of these loading conditions. The next section presents a brief overview of some of the constitutive relations used in numerical modelling.

2.3. Constitutive Models

Based on the need to come up with computationally effective ways of simulating structural behaviour of various components without the need of expensive experimental tests has prompted the development of constitutive material models. These constitutive models can then be applied to finite element codes to simulate the behaviour of components when subjected to different loading conditions at different temperatures. Some of the more prominent and wide spread models are discussed here.

2.3.1. Cowper – Symonds Constitutive Equation

The Cowper – Symonds constitutive equation [22] accounts for the effect of strain rate on material properties.

$$\frac{\sigma_0'}{\sigma_0} = 1 + \left(\frac{\dot{\varepsilon}}{D}\right)^{\frac{1}{q}} \qquad \text{(Equation 2.3.1.1)}$$

Where: σ_0' is the dynamic flow stress at a uniaxial plastic strain rate $\dot{\varepsilon}$

σ_0 is the associated static flow stress

D and q are constants for a particular material

Values for the constants for different materials [23] are presented in table 2.3.1.1.

Table 2.3.1.1 – Material Constants for the Cowper – Symonds Equation

Material	D (s^{-1})	q
Mild Steel	40.4	5
Aluminium Alloy	6500	4
Aluminium 6061-T6	1288000	4
α-Titanium (Ti 50A)	120	9
Stainless Steel 304	100	10

Alternative material constants for mild steel have been proposed in literature with Abramowicz and Jones [24] defining $D = 802s^{-1}$ and $q = 3.585$ and Marais et al [25] defining $D = 844s^{-1}$ and $q = 2.207$. Figure 2.3.1.1 extracted from reference [26] shows the Cowper – Symonds equation plotted against a compilation of mild steel test results carried out over a span of 30 years. The constants used to plot the curve were $D = 40.4s^{-1}$ and $q = 5$.

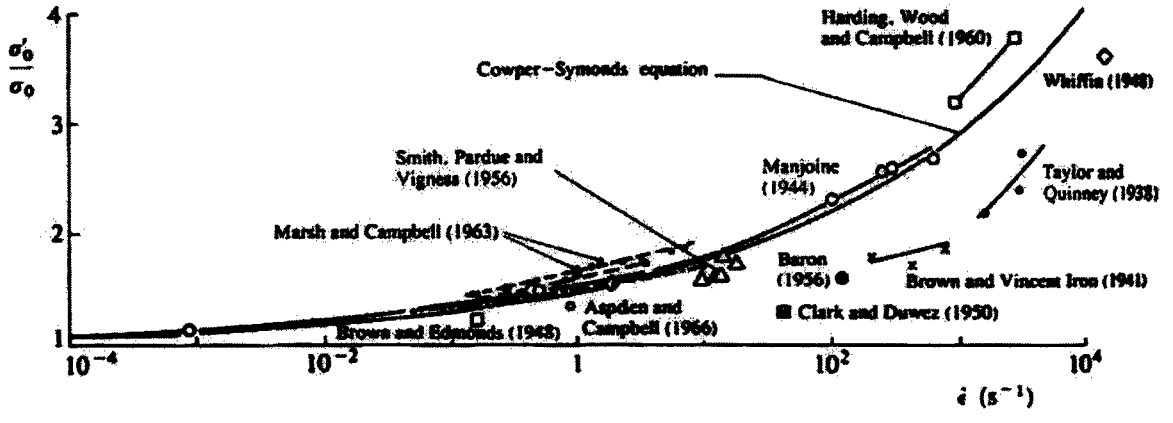

Figure 2.3.1.1 – Cowper – Symonds equation plotted with experimental results [26]

The Cowper – Symonds equation does not account for the effect of temperature changes which occur at high strain rates due to adiabatic heating. However, this equation has been used in conjunction with the temperature model for steel

proposed by Masui et al [20] to form an effective constitutive model that accounts for both temperature and strain rate effects on the material properties [27-28]. The model was used in numerical simulations to successfully predict the deformation and tearing of quadrangular stiffened plates of mild steel subjected to blast loading. The form of this model is given in equation 2.3.1.2:

$$\sigma(\dot{\varepsilon},T)=\sigma_0\left[1+\left(\frac{\dot{\varepsilon}}{D}\right)^{\frac{1}{q}}\right]f(T) \qquad \text{(Equation 2.3.1.2)}$$

$$f(T)=1 \qquad T\le 200°C$$
$$f(T)=[1-0.00178(T-200)] \qquad 200°C<T\le 700°C$$
$$f(T)=[0.133-0.000388(T-700)] \qquad 700°C<T\le 1000°C$$

Where $\sigma(\dot{\varepsilon},T)$ is the flow stress as a function of strain rate and temperature and $f(T)$ is the temperature model proposed by Masui et al [20].

2.3.2. Bodner – Partom Model

Bodner and Partom [29] formulated a set of constitutive equations to represent elastic-viscoplastic strain-hardening material behaviour for large deformations and arbitrary loading histories. An important feature of their formulation is that the total deformation rate is considered to be separable into elastic and inelastic components which are functions of state variables at all stages of loading and unloading. Therefore, the formulation is independent of any yield criteria or loading and unloading conditions. The deformation rate components are determinable from the current state which allows an incremental formulation of problems. Strain hardening is considered in the equations by introducing plastic work as the representative state variable. It should be noted that the formulation assumes isotropy and isothermal conditions even though strain hardening induces anisotropy.

The general formulation is based upon separation of the total deformation rate d_{ij} into elastic (reversible) and plastic (irreversible) components at all stages of deformation:

$$d_{ij} = d_{ij}^{e} + d_{ij}^{p} \qquad \text{(Equation 2.3.2.1)}$$

Where d_{ij} is the symmetric part of the velocity gradient:

$$d_{ij} = \frac{1}{2}\left(v_{ij} + v_{ji}\right) \qquad \text{(Equation 2.3.2.2)}$$

The elastic deformation rate, d_{ij}^{e}, can be related to the stress rate through a strain energy function. Liang and Khan [30] reported this relationship as a generalised form of Hooke's Law:

$$d_{ij}^{e} = \frac{\dot{t}_{ij}}{G} - \frac{\gamma \dot{t}_{kk}\delta_{ij}}{2G(3\gamma + 2G)} \qquad \text{(Equation 2.3.2.3)}$$

Where: $\dot{t}_{ij}$ is the stress rate tensor

δ_{ij} is the Kronecker delta

γ is an elastic Lamé constant

G is the elastic shear modulus

The plastic deformation rate, d_{ij}^{p}, is assumed to be related to the stress though the flow rule of classical plasticity. The flow rule is expressed as:

$$d_{ij}^{p} = \underline{d}_{ij}^{p} = \lambda \underline{\sigma}_{ij} \qquad \text{(Equation 2.3.2.4)}$$

Where: $\underline{d}_{ij}^{p}$ is the plastic deformation rate deviator (the bar symbol indicates the deviator)

$\underline{\sigma}_{ij}$ is the stress deviator

λ is a proportional factor

Squaring equation 2.3.2.4 gives:

$$\lambda^2 = \frac{D_2^p}{J_2} \qquad \text{(Equation 2.3.2.5)}$$

Where: D_2^p is the second invariant of the plastic deformation rate deviator

J_2 is the second invariant of the stress deviator

$$D_2^p = \frac{1}{2}\underline{d}_{ij}^{p}\,\underline{d}_{ji}^{p} \qquad \text{(Equation 2.3.2.6)}$$

$$J_2 = \frac{1}{2}\underline{\sigma}_{ij}\,\underline{\sigma}_{ji} \qquad \text{(Equation 2.3.2.7)}$$

Viscoplastic theory considers D_2^p as a function of J_2, that is:

$$D_2^p = f(J_2) \qquad \text{(Equation 2.3.2.8)}$$

Bodner and Partom [29] suggest that equation 2.3.2.8 can be expressed as:

$$D_2^p = D_0^2 \exp\left[-\left(\frac{n+1}{n}\right)\left(\frac{Z^2}{3J_2}\right)^n\right] \qquad \text{(Equation 2.3.2.9)}$$

Where: D_0^2 is a material constant influencing the strain rate sensitivity; Liang and Khan [30] report D_0 as the limiting or maximum strain rate

n is a material constant governing the strain rate sensitivity

Z is a loading history dependent internal variable

The internal variable, Z, in equation 2.3.2.9 is assumed to be a function of the plastic work (W_p) and is expressed as:

$$Z = Z_1 + (Z_0 - Z_1)\exp\left(\frac{-mW_p}{Z_0}\right) \qquad \text{(Equation 2.3.2.10)}$$

Where Z_0 and Z_1 are initial and saturation values of Z, and m is another material constant.

Bodner and Partom [29] stated that the preferred functional form for equation 2.3.2.8 for a particular material would be essentially empirically based and any monotonically increasing function of D_2^p with J_2 was allowable.

2.3.3. Johnson – Cook Constitutive Model

Johnson and Cook [31] developed and presented in 1983, a constitutive model for the flow stress, σ, of a material. The model was primarily intended for computational purposes. It was developed from a series of experiments ranging from torsion tests over a wide range of strain rates to dynamic Hopkinson bar tensile tests over a range of temperatures. Static tensile test data also contributed to the development of the model. The final equation took the form:

$$\sigma = \left[A + B\varepsilon^{n}\right]\left[1 + C\ln\dot{\varepsilon}^{*}\right]\left[1 - T^{*m}\right] \qquad \text{(Equation 2.3.3.1)}$$

Where: σ is the von Mises flow stress;

ε is the equivalent plastic strain;

$\dot{\varepsilon}^{*} = \frac{\dot{\varepsilon}}{\dot{\varepsilon}_0} =$ dimensionless plastic strain rate for $\dot{\varepsilon}_0 = 1.0s^{-1}$;

T^{*} is the homologous temperature and is given by $T^{*} = \frac{T - T_{ROOM}}{T_{MELT} - T_{ROOM}}$

The material constants are represented by A, B, n, C and m where:

A is the yield stress;
B and n represent the effects of strain hardening;
C is the strain rate constant and;
m is the thermal softening fraction.

Equation 2.3.3.1 is set up such that the first set of brackets gives the stress as a function of strain while the second and third sets of brackets represent the effects of strain rate and temperature respectively. It should be noted that to use the model effectively for any given material, the material constants need to be determined experimentally or obtained from literature. Some of the material constants are

presented in table 2.3.3.1. The constants were extracted from reference [31] with the exception of mild steel where the constants were assembled from references [32-33].

Table 2.3.3.1 – Material Constants for the Johnson – Cook Constitutive Model

Material	Constitutive Constants				
	A (MPa)	B (MPa)	n	C	m
OFHC Copper	90	292	0.31	0.025	1.09
Cartridge Brass	112	505	0.42	0.009	1.68
Nickel 200	163	648	0.33	0.006	1.44
Armco Iron	175	380	0.32	0.060	0.55
Carpenter Electrical Iron	290	339	0.40	0.055	0.55
1006 Steel	350	275	0.36	0.022	1.00
2024-T351 Aluminium	265	426	0.34	0.015	1.00
7039 Aluminium	337	343	0.41	0.010	1.00
4340 Steel	792	510	0.26	0.014	1.03
S-7 Tool Steel	1539	477	0.18	0.012	1.00
Tungsten Alloy (0.07Ni, 0.03Fe)	1506	177	0.12	0.016	1.00
DU – 0.75Ti	1079	1120	0.25	0.007	1.00
Mild Steel	250	275	0.36	0.079	0.55

Liang and Khan [30] noted that one of the characteristics of the Johnson – Cook equation is that for two different strain rates (where $\dot{\varepsilon}_2 > \dot{\varepsilon}_1$), when the strain increases, the magnitude of the change in flow stress always increases ($\Delta\sigma_2 > \Delta\sigma_1$). This is depicted in figure 2.3.3.1:

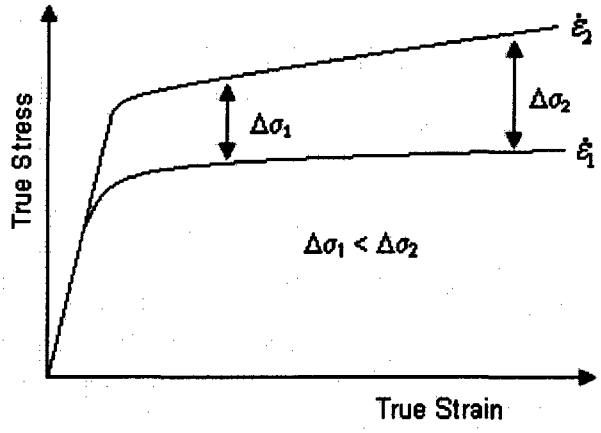

Figure 2.3.3.1 – Hardening Characteristic of the Johnson – Cook Equation

Thus it is appropriate for modelling the hardening behaviour of metals such as OFHC (oxygen free high conductivity) copper and nickel where the general trend is an increase in the change in flow stress ($\Delta\sigma$) with increasing strain rates. However, it is inappropriate for modelling metals such as tantalum whereby the hardening decreases ($\Delta\sigma_2 < \Delta\sigma_1$) with an increase in strain rate.

2.3.4. Zerilli – Armstrong Constitutive Models

Zerilli and Armstrong [34] noted that the crystal structure of a material (i.e. body centred cubic – BCC or face centred cubic – FCC) determined the type of constitutive behaviour the material would experience based on the dislocation characteristics for that particular structure. Thus, they proposed two constitutive models, one for BCC materials and the other for FCC materials.

The BCC material constitutive equation is given by:

$$\sigma = c_0 + B_0 e^{-\beta T} + K\varepsilon^n \qquad \text{(Equation 2.3.4.1)}$$

The FCC material constitutive equation is given by:

$$\sigma = c_0 + B_1 \varepsilon^{1/2} e^{-\beta T} \qquad \text{(Equation 2.3.4.2)}$$

Where $\beta = \beta_0 - \beta_1 \ln \dot{\varepsilon}$ and $c_0 = \sigma_G + kl^{-1/2}$

For these constitutive relations,

σ is the equivalent von Mises stress
ε is the equivalent strain
$\dot{\varepsilon}$ is the strain rate
T is the absolute temperature
l is the average grain diameter
σ_G is the athermal stress attributed to the initial dislocation density and the effect of solutes in the microstructure
The parameters $B_0, B_1, \beta_0, \beta_1, K, k, n$ and σ_G are considered to be constant for a given material.

The Zerilli – Armstrong model for BCC metals presumes that the work hardening rate is independent of the temperature and strain rate [30]. However, this is not the case for most metals as the work hardening rate does depend to some extent on the temperature and strain rate. Thus the Zerilli – Armstrong model for BCC materials is not appropriate for modelling the work hardening behaviour of materials such as mild steel which have strong temperature and strain rate dependencies.

2.4. Concluding Remarks

The background information presented in this chapter highlights several important aspects of material behaviour when subjected to different loading conditions. Results are presented on various experiments that have been carried out and empirical and constitutive models developed are discussed. The complexities in developing such constitutive material models are also highlighted. Furthermore, the importance of the knowledge of relationships between the microstructure and chemical composition and material behaviour is acknowledged. Simplified empirical models vastly aid in numerical modelling of tests where physical experiments are not feasible. And with the need of quantifying the material response of mild steel at elevated temperatures and differing strain rates, it is necessary to carry out physical experiments.

The following chapters describe the processes used to measure the material response of mild steel at elevated temperatures and different strain rates in the quasi-static range. This is done with the aim of developing an empirical relationship of the yield stress of mild steel with temperature.

3. PROCEDURE AND DEVELOPMENT

The objective of this project was to determine the variation of the material properties of mild steel, with specific regard to its yield stress, when exposed to differing temperatures and strain rates. To achieve that end, high temperature tensile tests were carried out at different strain rates using the ESH 100kN Universal Tester pictured in figure 3.1. The tester is located in the Centre for Materials Engineering at UCT.

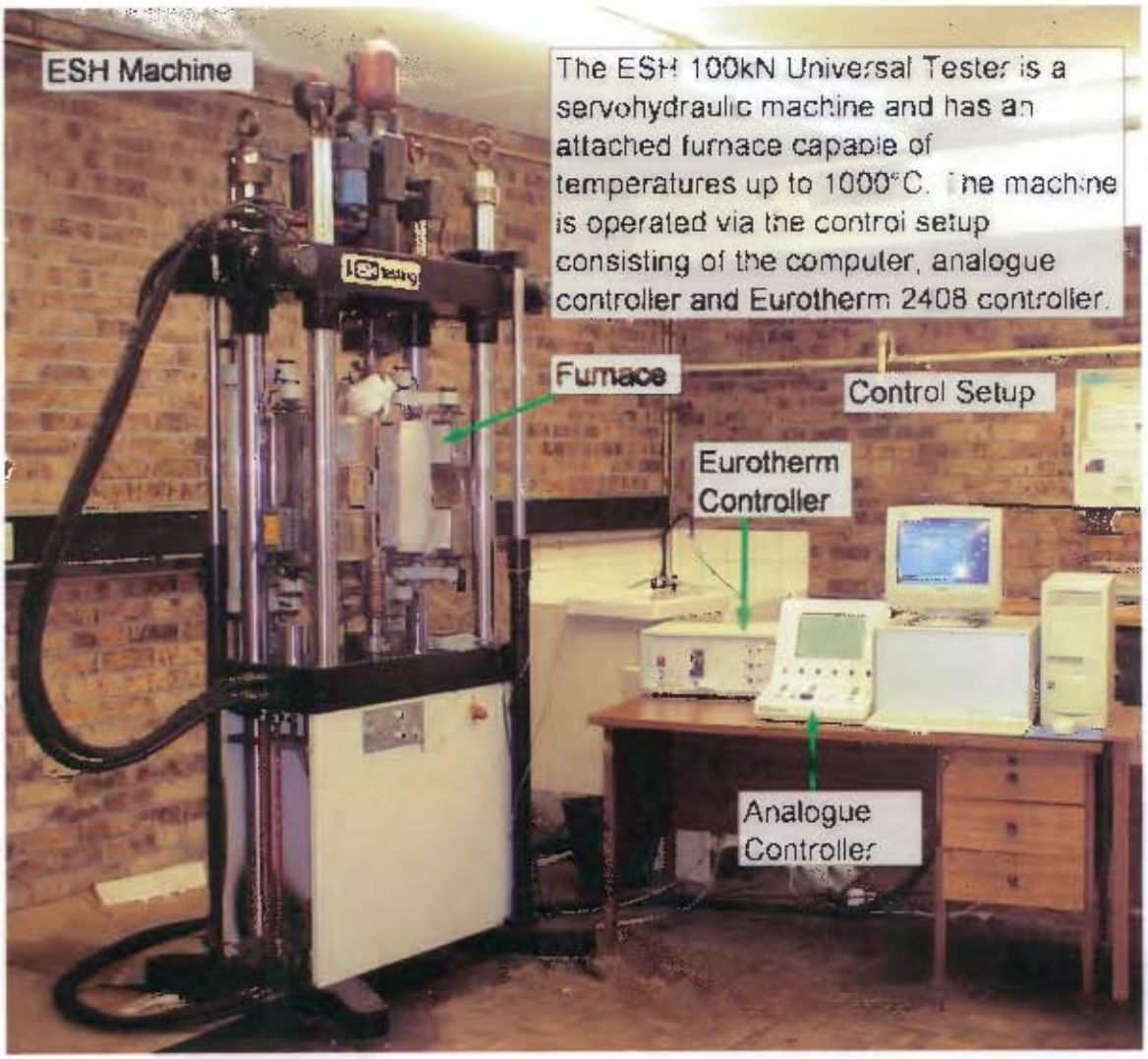

Figure 3.1 – ESH 100kN Universal Tester

Dog bone specimens of mild steel were used and tested at temperatures ranging from room temperature to a maximum of 600°C. The specimens had a gauge length of 60mm and figure 3.2 depicts a specimen and its dimensions.

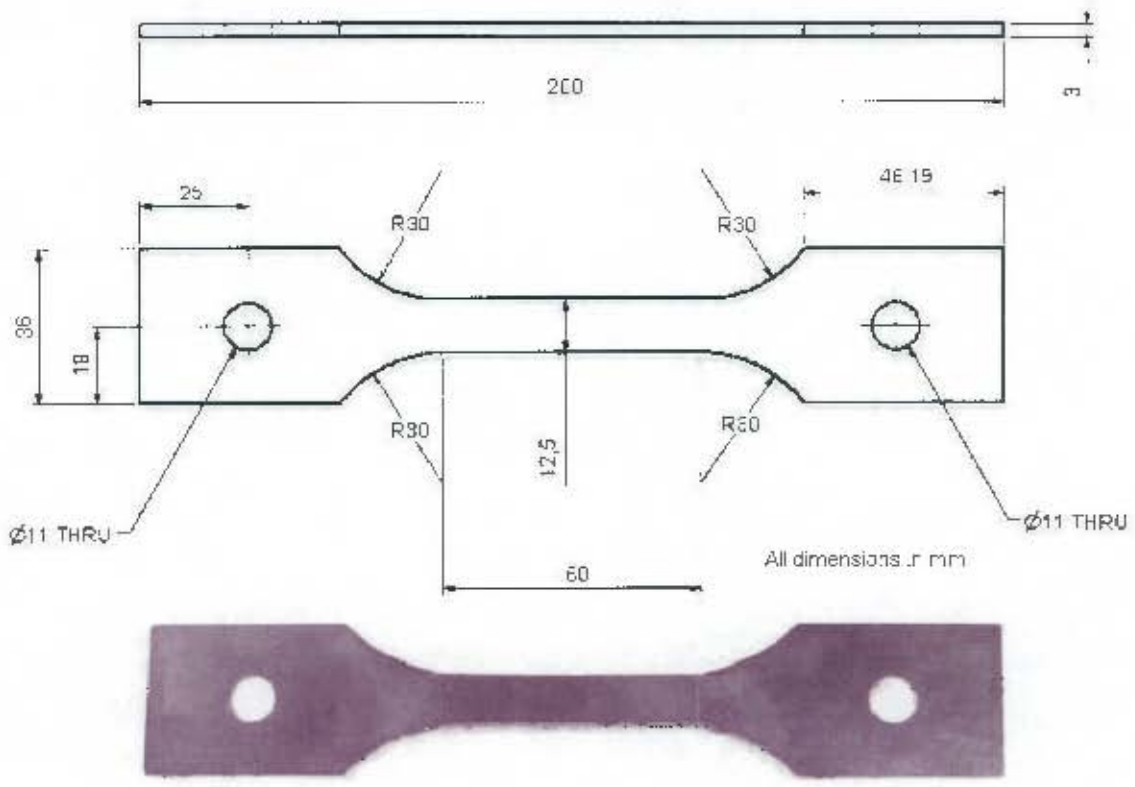

Figure 3.2 – Dog Bone Specimen Dimensions

The specific chemical composition of the specimens is presented in table 3.1. This shows that the specimens are a low carbon content mild steel. The analysis report for the chemical composition of the specimens is presented in Appendix A3.

Table 3.1 – Chemical Composition of Mild Steel Tensile Specimens

Chemical	Carbon (C)	Manganese (Mn)	Silicon (Si)	Phosphorous (P)	Sulphur (S)
%m/m	0.06 ~ 0.07	0.14 ~ 0.15	<0.05	0.005 ~ 0.006	0.002

[Note: The balance of the composition is made up of Iron (Fe)]

Specific details pertaining to the adaptation of the ESH 100kN Universal Tester to carry out high temperature tensile tests may be found in Appendix A1. It should be noted that Appendix A1 is written as an informal manual to use the ESH machine to carry out high temperature tensile tests. This is done to present a methodology for carrying out such tests. Furthermore, no specific manuals were present for the machine with respect to high temperature tensile testing: therefore Appendix A1 serves as a detailed source of information on the particulars of how the high temperature tensile tests were carried out. A brief overview of the experimental procedure is presented next.

3.1. Experimental Procedure

Due to the versatility of the tests possible with the ESH 100kN Tester, it had to be specifically adapted to carry out the high temperature tensile tests required for this project. This involved the use of special grips designed expressly for use within the furnace as well as programming the ESH machine to carry out tensile tests at specified rates based on the velocity of the hydraulic actuator. Details pertaining to the grips used and the programming of the ESH machine can be found in Appendix A1.

Four different programs were used to carry out tensile tests at different strain rates based on regulating the velocity of the hydraulic actuator. The velocities selected were $0.025mms^{-1}$, $0.2mms^{-1}$, $1mms^{-1}$ and $10mms^{-1}$ as they provided a sufficient range of strain rates within the quasi-static region. However, tests attempted at $10mms^{-1}$ were

inconclusive as the test data was not being captured accurately at that velocity. Therefore an upper limit of the hydraulic actuator velocities, where the test data could be captured with reasonable repeatability and accuracy, needed to be determined. This velocity was found to be 6mms^{-1} and was then used in place of the 10mms^{-1} tests.

Tests were carried out at six different temperatures (room temperature, 100°C, 200°C, 300°C, 450°C and 600°C) at the following strain rates:

- $4.17\times10^{-4}s^{-1}$ corresponding to a hydraulic actuator velocity of 0.025mms^{-1}
- $3.33\times10^{-3}s^{-1}$ corresponding to a hydraulic actuator velocity of 0.2mms^{-1}
- $1.67\times10^{-2}s^{-1}$ corresponding to a hydraulic actuator velocity of 1mms^{-1}
- $1\times10^{-1}s^{-1}$ corresponding to a hydraulic actuator velocity of 6mms^{-1}

3.1.1. Executing the Tensile Tests

Firstly, the appropriate program was selected to carry out the tensile test depending on what the required strain rate was. The specimen was then mounted onto the high temperature grips with a K-Type thermocouple attached to its midpoint.

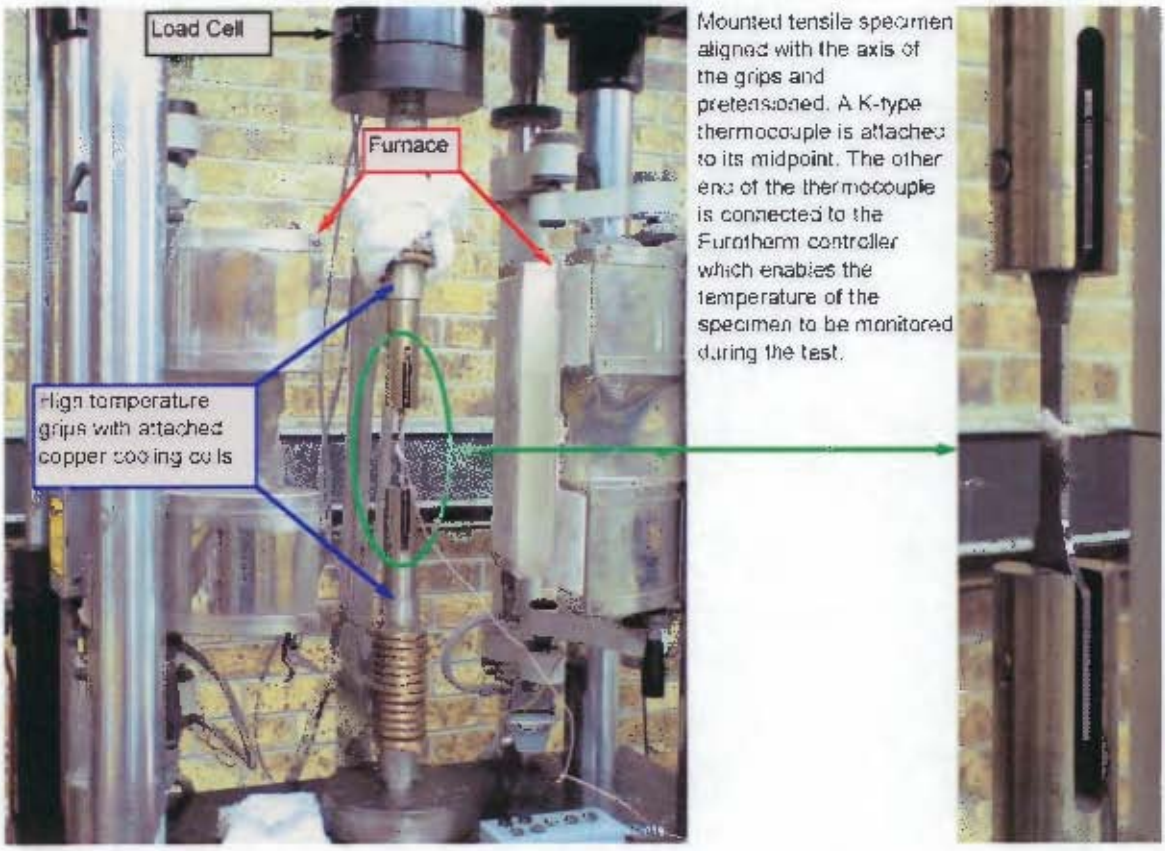

Figure 3.1.1.1 – Mounted Tensile Specimen with attached Thermocouple

After the specimen had been aligned vertically with the axis of the grips and pre-tensioned slightly, the furnace was enclosed over it. Then the furnace was insulated to prevent any heat damage to the load cell and cooling water was supplied to cooling coils attached to the high temperature grips.

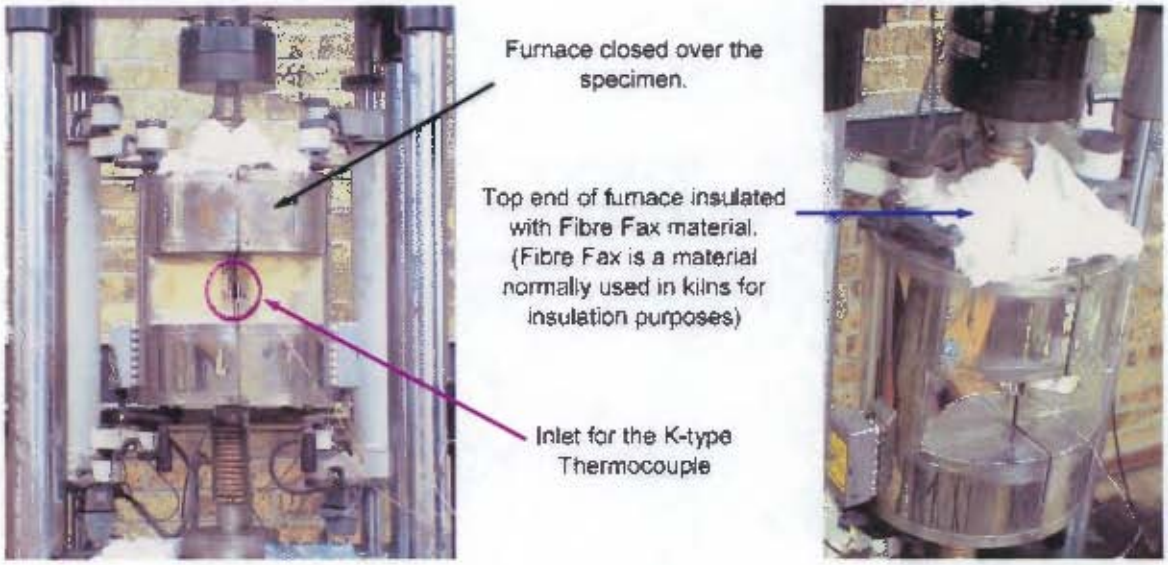

Figure 3.1.1.2 – Specimen Enclosed in the Furnace

Thereafter, the furnace temperature was set and heated up while the temperature of the specimen was monitored via the K-type thermocouple and the Eurotherm© 2408 controller. Figure 3.1.1.3 depicts the furnace temperature set at 300°C. The specimen temperature, as measured by the K-type thermocouple, is at 156°C and rising to the set temperature of 300°C.

Once the specimen reached the required temperature, that is the measured temperature via the K-type thermocouple coincided with the set furnace temperature, the test was carried out. Room temperature tests were carried out in a similar manner, except without using the furnace.

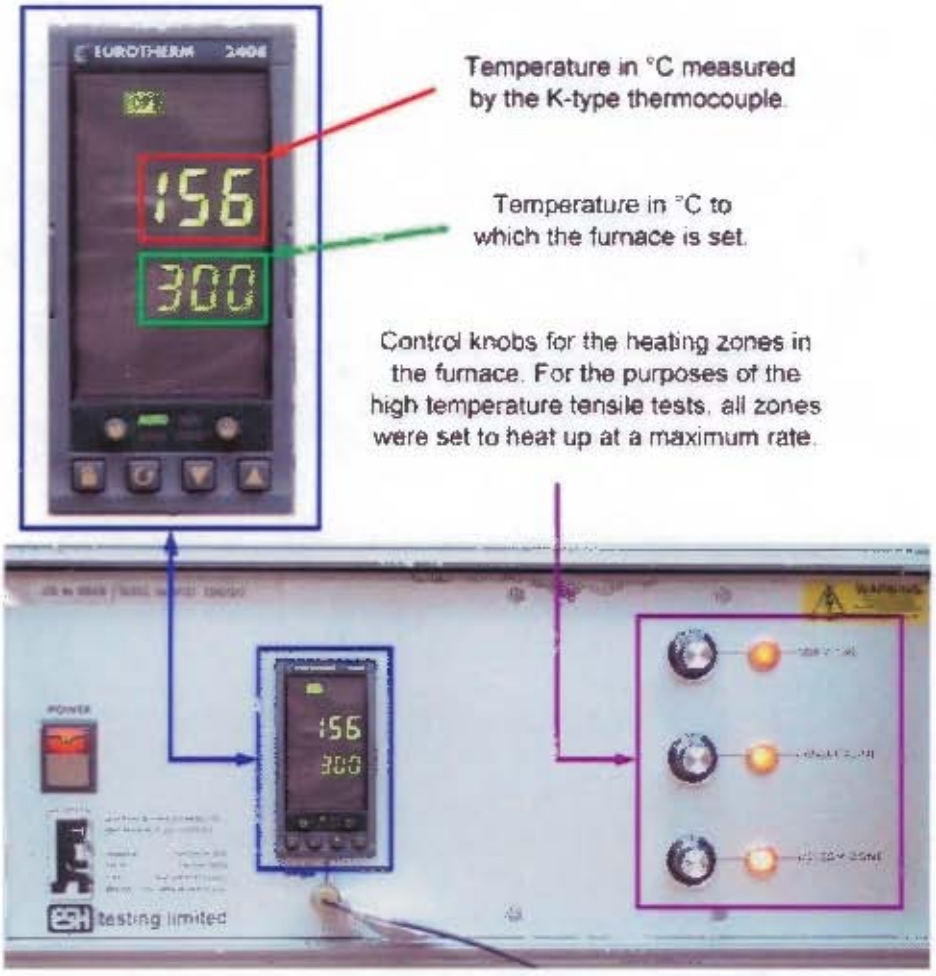

Figure 3.1.1.3 – Furnace Temperature Control (Eurotherm© 2408 Controller)

The force measured by the load cell and the stroke of the hydraulic actuator, which corresponds to the extension of the specimen, was logged in a result file for each test. This file was then imported into a spreadsheet program for the test results to be processed. This is discussed in more detail in chapter 4. Additional information about the results file and explicit details pertaining to the testing procedure may be found in Appendix A1. The following section indicates the tensile tests done for this project.

3.2. Tests Carried Out

A total of 71 effective tests were carried out and table 3.2.1 indicates the distribution of the test specimens. The specimen names consist of random letter-number combinations and no specific nomenclature was applied. In every instance a specimen name is used in this report, the test conditions (i.e. the temperature and strain rate at which the specimen was tested) are also supplied for clarity. The results of these tests are presented in chapter 4, and the individual test results are provided in Appendix A2.

Table 3.2.1 – Specimens and Test Conditions

Specimen Names	Temperature (°C)	Strain Rate (/s)
(18 Specimens)		
A1, A2, S1	Room	4.17×10^{-4}
NA1, NA2, NA3	100	4.17×10^{-4}
B1NEW, B2, S2	200	4.17×10^{-4}
C1, C2, S3	300	4.17×10^{-4}
D1, S4, T1	450	4.17×10^{-4}
U1, U2, U3	600	4.17×10^{-4}
(19 Specimens)		
F1, F2, MN1	Room	3.33×10^{-3}
NB1, NB2, NB3	100	3.33×10^{-3}
G1, G1NEW, G2, MN2	200	3.33×10^{-3}
H1, H2, MN3	300	3.33×10^{-3}
V1, V2, V3	450	3.33×10^{-3}
W1, W2, W3	600	3.33×10^{-3}
(19 Specimens)		
K1, K2, XZ1	Room	1.67×10^{-2}
NC1, NC2, NC3	100	1.67×10^{-2}
L1, L1NEW, L2, FN2	200	1.67×10^{-2}
M1, M2, FN3	300	1.67×10^{-2}
X1, X2, X3	450	1.67×10^{-2}
Y1, Y2, Y3	600	1.67×10^{-2}
(15 Specimens)		
SA2, SA6	Room	1×10^{-1}
SB2, XE2, FD3	100	1×10^{-1}
SC1, SC2, SC3	200	1×10^{-1}
SD2, XB2	300	1×10^{-1}
SE1, XC1, XC2	450	1×10^{-1}
SF3, XD2	600	1×10^{-1}

3.3. Analysis of the Microstructure

From the tensile specimens tested, 24 were selected as samples for examination under an optical microscope. This was done so as to observe the deformation where the specimen failed on a microscopic scale. Each selected specimen had been tested at a unique temperature and strain rate combination. An additional sample was selected from an untested specimen, giving a total of 25 samples. Table 3.3.1 indicates the selected specimens.

Table 3.3.1 Microstructure Analysis Samples

Specimens	Test Temperatures and Strain Rate
Untested	N/A
A1, NA1, B1NEW, C1, D1 and U2	25°C to 600°C respectively; $4.17\times10^{-4}\,s^{-1}$
F1, NB3, G1, H2, V2 and W2	25°C to 600°C respectively; $3.33\times10^{-3}\,s^{-1}$
K2, NC3, L2, M1, X2 and Y1	25°C to 600°C respectively; $1.67\times10^{-2}\,s^{-1}$
SA2, SB2, SC1, XB2, SE1 and SF3	25°C to 600°C respectively; $1\times10^{-1}\,s^{-1}$

For each of the tested specimens, one end was selected and cut as indicated in figure 3.3.1. The untested specimen was first cut in half then pieces were cut from the gauge section in a similar manner to that of the tested specimens.

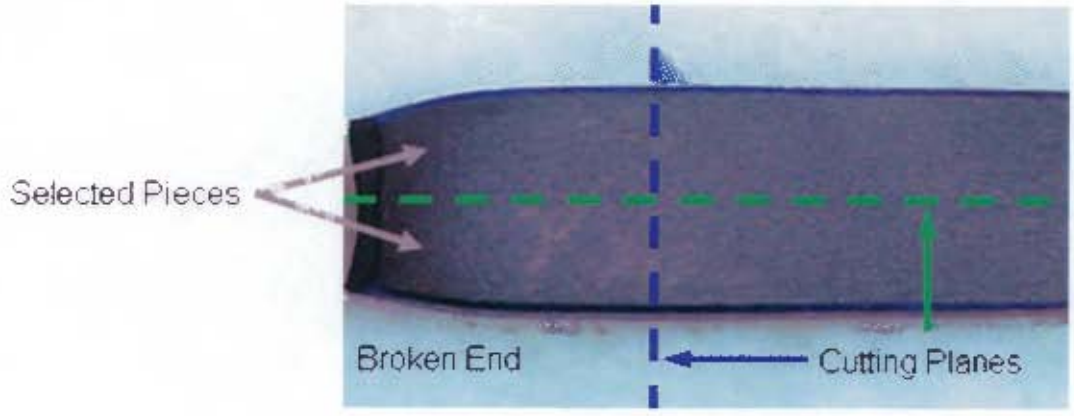

Figure 3.3.1 – Selected Pieces for Microstructure Analysis

The selected pieces were then cold mounted in a polymer resin. Figure 3.3.2 depicts a sketch of the top view of the orientation of the cut pieces as they were mounted per sample. This enabled the study of the microstructure from two different planes, one through the middle of the gauge length and the other along the flat portion of the gauge length.

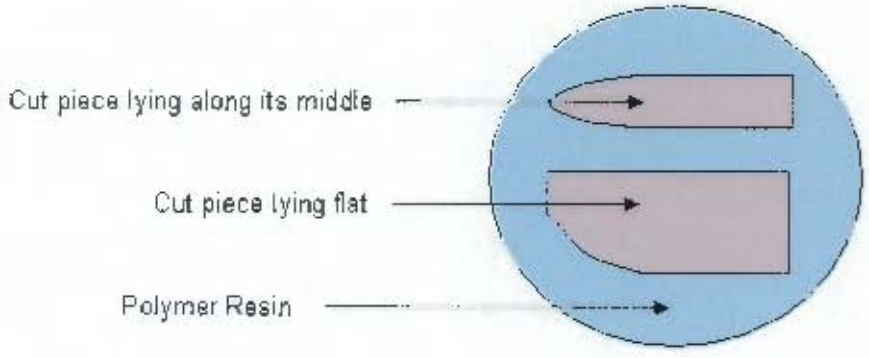

Figure 3.3.2 – Orientation of Mounted Pieces in a Typical Sample

The samples were then ground using 500, 800 and 1200 grit paper. Thereafter, they were polished to 3μm and then 1μm using a slurry of diamond paste on polishing pads. Once this was accomplished, the specimens were etched in a 3% nital solution (nitric acid dissolved in ethanol) for approximately 25 seconds. The specimens were then

viewed under an optical microscope and photographs were taken at 500 times magnification. Four photographs were taken for each sample from the tested specimens, with the regions of interest depicted in figure 3.3.3. Only two photographs were required from the untested specimen, one from the piece lying along its middle and the other from the piece lying flat.

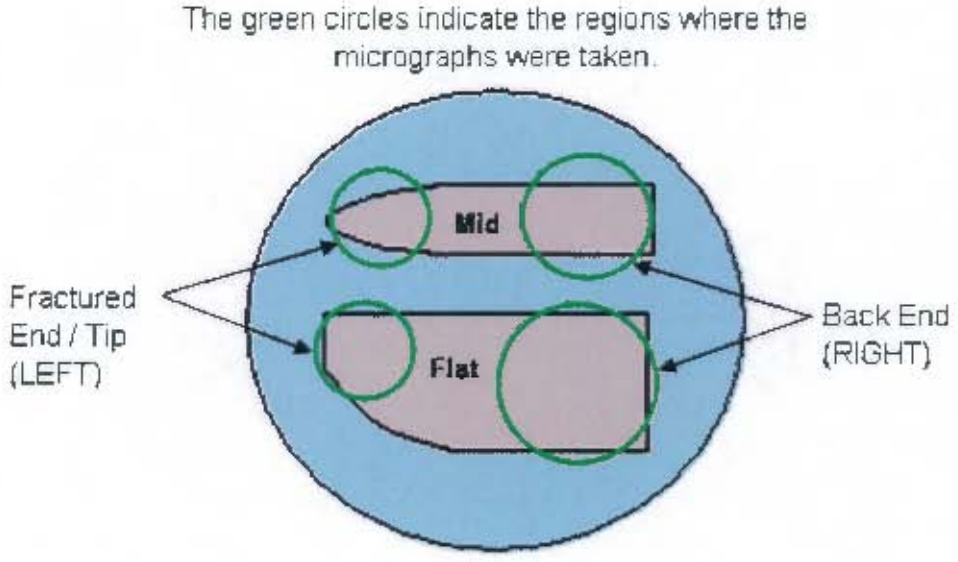

Figure 3.3.3 – General Micrograph Regions

The micrographs are provided in Appendix A4. Observations from the micrographs are presented in chapter 4.

4. EXPERIMENTAL RESULTS

This section outlines the results obtained from the tensile tests carried out. For each test carried out, a result file was created that logged the load measured by the load cell of the ESH machine and the corresponding stroke of the hydraulic actuator. The extension of the specimen was taken to be this measured stroke value. These result files were then imported into a spreadsheet program, in this case Microsoft Excel®, and the graphs of the engineering stress verses the engineering strain were plotted based on the recorded load and stroke values. Equations 4.1 and 4.2 were used to achieve this:

$$\sigma_e = \frac{F}{A_0} \qquad \text{(Equation 4.1)}$$

Where σ_e = engineering stress; F = measured load; A_0 = initial cross-sectional area of the gauge length of the specimen.

$$\varepsilon_e = \frac{L_i - L_0}{L_0} \qquad \text{(Equation 4.2)}$$

Where ε_e = engineering strain; L_i = length of the gauge section at any point in time after the load has been applied; L_0 = original gauge length of the specimen.

The 0.2% offset yield was then obtained from the engineering stress vs. engineering strain graphs. A least squares fit was used to generate a line from the linear elastic portion of the engineering stress – strain curve. Thereafter, this line was offset parallel to the elastic region by a strain of 0.002 and interpolation was used to determine where it crossed the original stress – strain curve to obtain the yield point.

An example is shown in figure 4.1, which depicts the results of a test carried out at room temperature and a strain rate of $4.17 \times 10^{-4} s^{-1}$. The detailed results of each individual test may be found in Appendix A2.

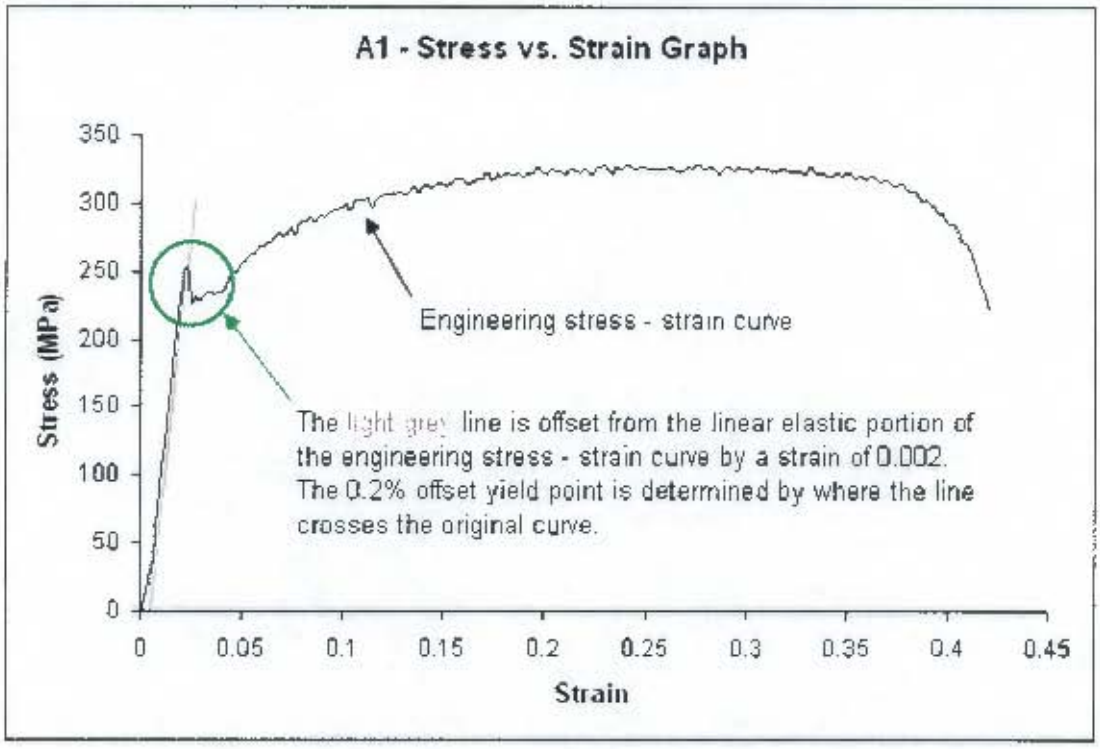

Figure 4.1 – Obtaining the Yield Point

The 0.2% offset method of determining the yield point was applied consistently for all the test results. This was especially necessary for tests at elevated temperatures where the change from the elastic to plastic region was not easily discernible through a specific point. This is depicted in figure 4.2, where the engineering stress – strain curve of a test carried out at a temperature of 450°C and a strain rate of $3.33 \times 10^{-3} s^{-1}$ is shown. The test results are presented in the section following figure 4.2.

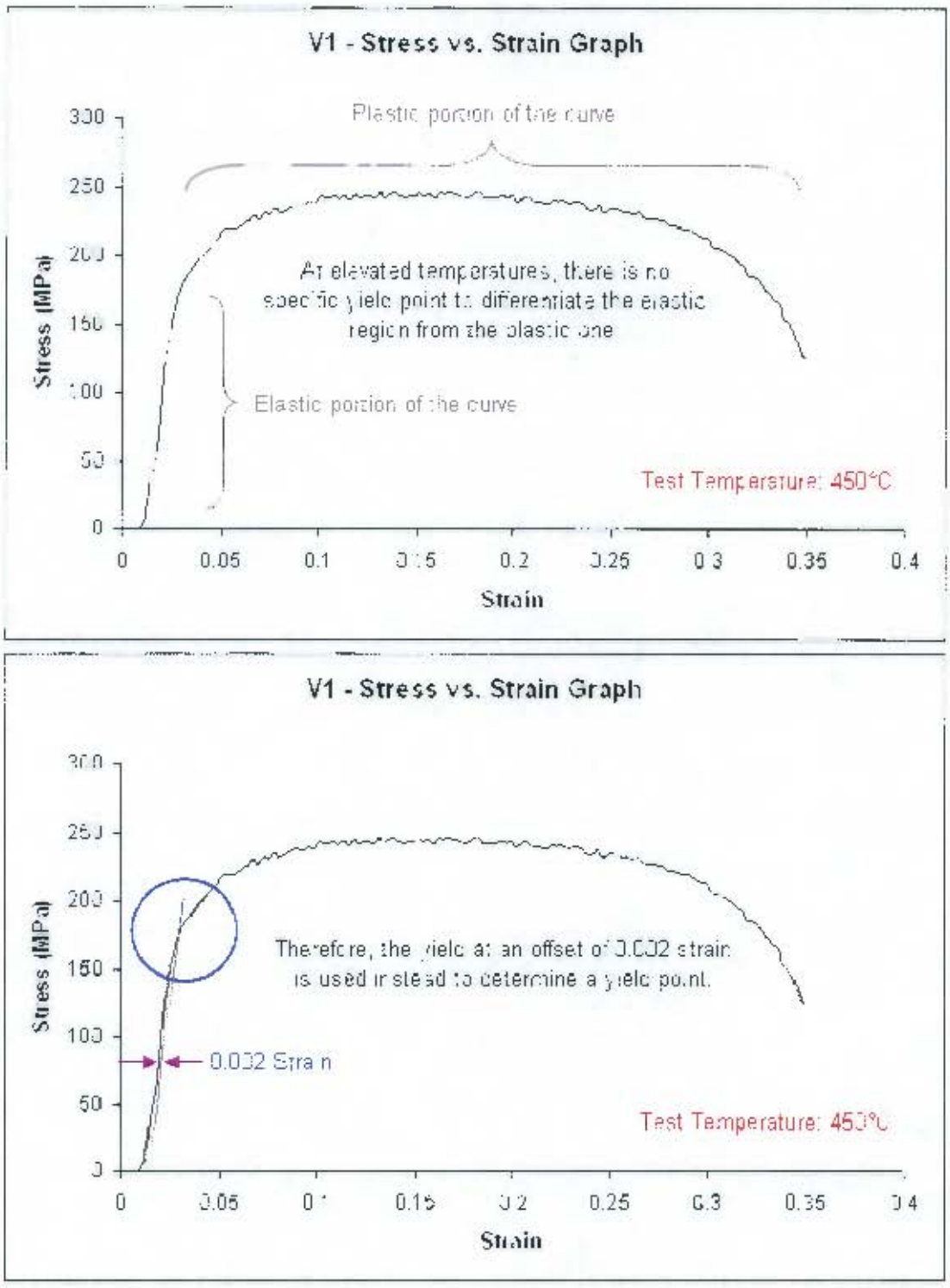

Figure 4.2 – Determining the Yield Point for Elevated Temperature Tests

4.1. Tables of Results

Tables 4.1.1 – 4.1.4 present a summary of the results of the tests carried out at the four different strain rates. The yield stress, ultimate tensile stress and strain at failure are reported. The ultimate tensile stress refers to the maximum stress recorded on the engineering stress – strain curve.

Table 4.1.1 – Test Results at a Strain Rate of $4.17 \times 10^{-4} s^{-1}$

Specimen	Temperature (°C)	Yield Stress (MPa)	Ultimate Tensile Stress (MPa)	Strain at Failure (%)
A1	25	247.89	328.08	38.33
A2	25	243.47	327.24	40.67
S1	25	261.16	336.09	36.33
NA1	100	208.90	319.42	23.00
NA2	100	204.16	306.32	20.83
NA3	100	190.93	305.29	24.17
B1NEW	200	206.61	388.58	18.50
B2	200	207.86	395.41	19.17
S2	200	208.73	401.69	17.83
C1	300	190.81	361.51	27.00
C2	300	190.30	362.69	28.50
S3	300	183.10	334.41	25.67
D1	450	164.82	229.32	32.67
S4	450	159.29	216.96	29.67
T1	450	163.10	217.78	30.50
U1	600	93.90	103.90	32.00
U2	600	76.80	94.28	35.33
U3	600	90.06	99.65	34.33

Table 4.1.2 – Test Results at a Strain Rate of $3.33 \times 10^{-3} s^{-1}$

Specimen	Temperature (°C)	Yield Stress (MPa)	Ultimate Tensile Stress (MPa)	Strain at Failure (%)
F1	25	266.92	335.23	35.50
F2	25	275.62	348.32	36.17
MN1	25	260.12	323.63	36.33
NB1	100	199.23	282.72	29.00
NB2	100	214.19	299.13	30.67
NB3	100	213.74	292.97	28.50
G1	200	213.90	375.49	18.17
G1NEW	200	200.99	388.51	17.83
G2	200	213.19	385.35	19.33
MN2	200	213.81	391.59	16.67
H1	300	188.33	370.01	25.33
H2	300	186.08	371.32	25.17
MN3	300	195.19	371.58	24.17
V1	450	172.59	246.05	32.83
V2	450	170.96	249.97	33.50
V3	450	168.97	246.42	32.33
W1	600	102.62	123.09	33.00
W2	600	101.38	123.59	34.67
W3	600	96.35	121.75	33.17

Table 4.1.3 – Test Results at a Strain Rate of $1.67 \times 10^{-2} s^{-1}$

Specimen	Temperature (°C)	Yield Stress (MPa)	Ultimate Tensile Stress (MPa)	Strain at Failure (%)
K1	25	272.99	338.91	33.67
K2	25	276.71	343.29	35.50
XZ1	25	279.11	319.54	34.67
NC1	100	216.20	292.84	29.17
NC2	100	208.04	293.53	32.50
NC3	100	209.69	284.59	30.50
L1	200	210.72	348.65	16.83
L1NEW	200	205.46	361.14	18.67
L2	200	210.94	348.09	16.33
FN2	200	201.74	322.84	14.00
M1	300	186.97	379.23	22.50
M2	300	189.90	384.91	25.83
FN3	300	194.39	383.07	22.33
X1	450	174.36	272.75	31.33
X2	450	173.55	278.17	31.67
X3	450	174.16	270.53	33.00
Y1	600	112.15	136.89	35.83
Y2	600	115.87	142.94	36.67
Y3	600	114.00	140.72	36.17

Table 4.1.4 – Test Results at a Strain Rate of $1 \times 10^{-1} s^{-1}$

Specimen	Temperature (°C)	Yield Stress (MPa)	Ultimate Tensile Stress (MPa)	Strain at Failure (%)
SA2	25	282.26	315.27	38.83
SA6	25	283.62	324.47	38.50
SB2	100	248.64	306.69	32.83
XE2	100	227.63	300.71	32.17
FD3	100	221.63	299.68	33.33
SC1	200	216.66	314.45	21.33
SC2	200	211.32	317.62	17.33
SC3	200	206.00	333.54	21.50
SD2	300	191.83	371.32	19.67
XB2	300	202.97	367.80	22.83
SE1	450	195.07	307.17	33.00
XC1	450	192.11	296.77	32.67
XC2	450	188.62	310.94	33.17
SF3	600	144.85	175.00	39.67
XD2	600	141.04	161.91	39.33

4.2. Graphs of Results

Figures 4.2.1 – 4.2.4 depict the distribution of the yield stresses with respect to temperature at the four different strain rates.

Figure 4.2.5, which is a combined plot of figures 4.2.1 – 4.2.4 on the same set of axes, displays the overall effect of temperature on the yield stress of mild steel over the range of strain rates utilised.

The effect of strain rate on the yield stress is shown in figure 4.2.6.

Figure 4.2.7 displays the strains recorded at failure for each test and the temperatures at which they occurred.

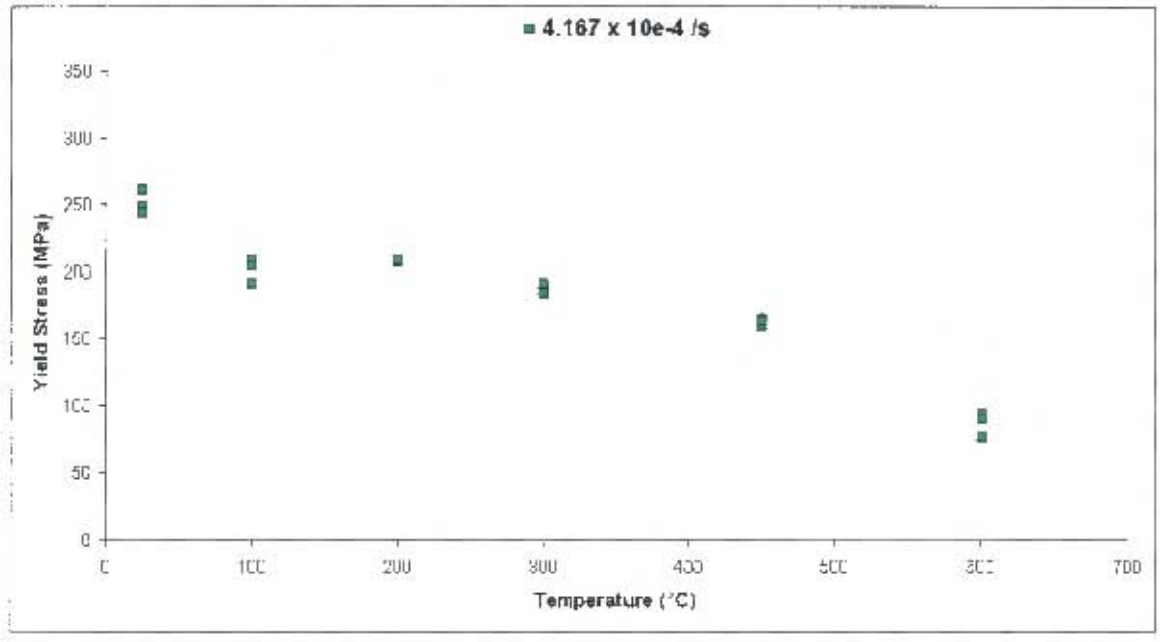

Figure 4.2.1 – Variation of Yield Stress with Temperature (Strain Rate: 4.17 x 10^{-4} s^{-1})

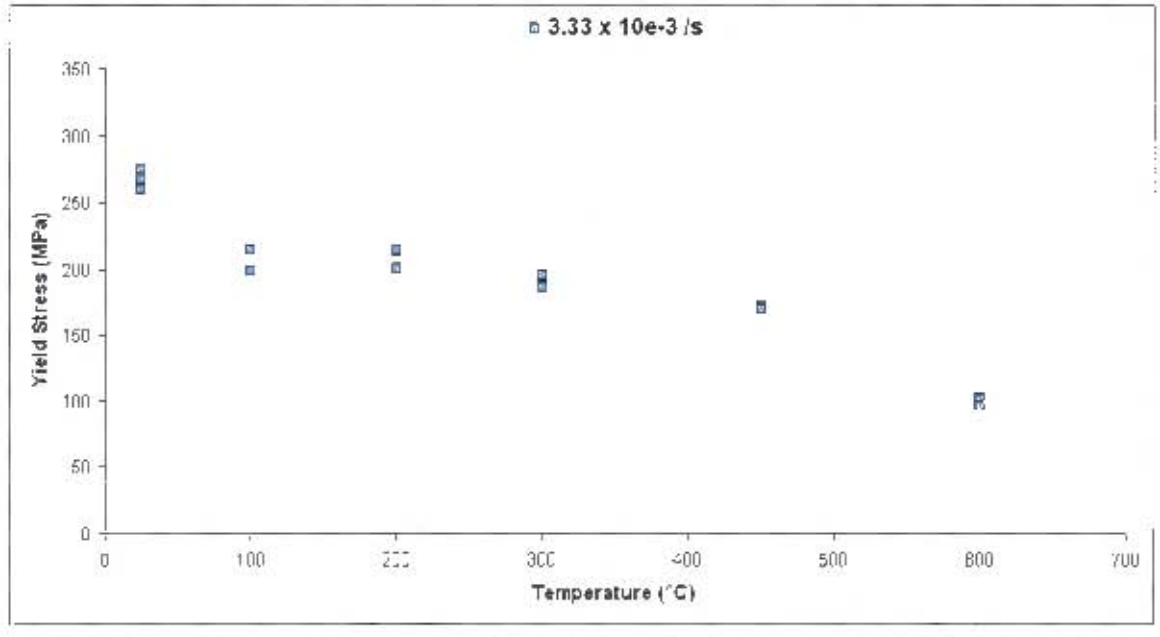

Figure 4.2.2 – Variation of Yield Stress with Temperature (Strain Rate: 3.33 x $10^{-3}$$s^{-1}$)

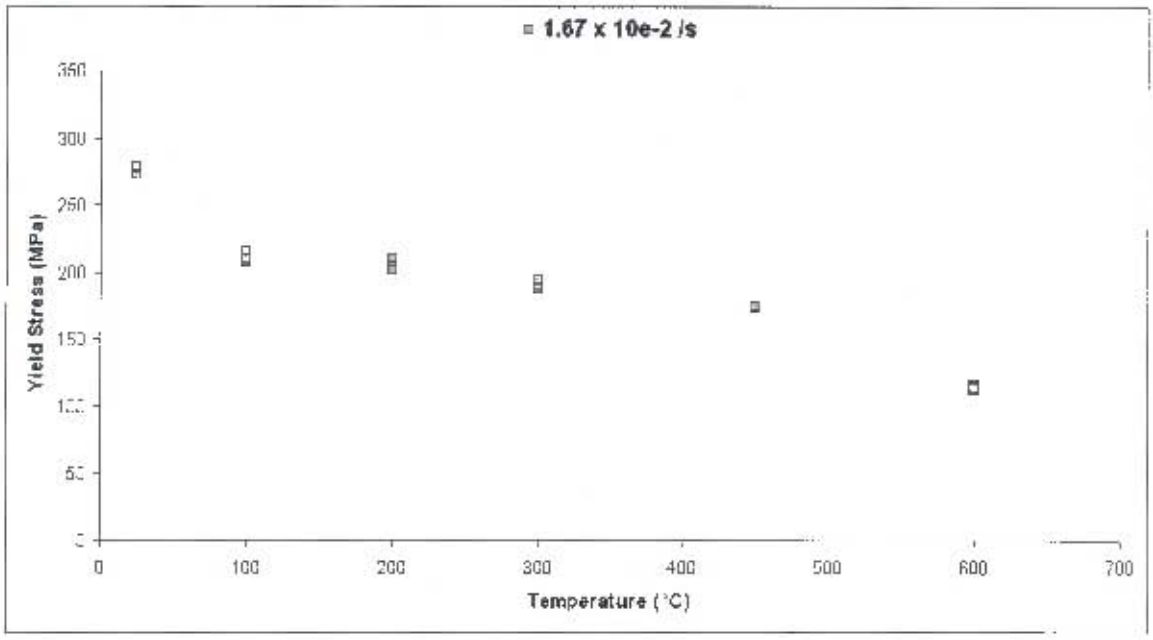

Figure 4.2.3 – Variation of Yield Stress with Temperature (Strain Rate: 1.67 x $10^{-2}s^{-1}$)

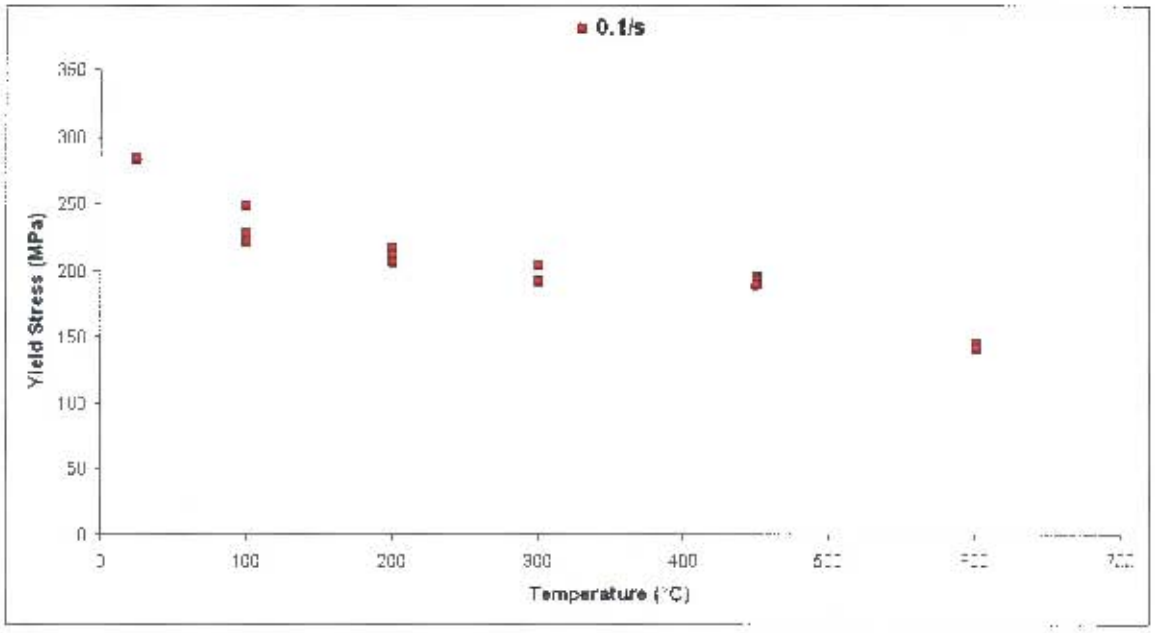

Figure 4.2.4 – Variation of Yield Stress with Temperature (Strain Rate: 1 x $10^{-1}s^{-1}$)

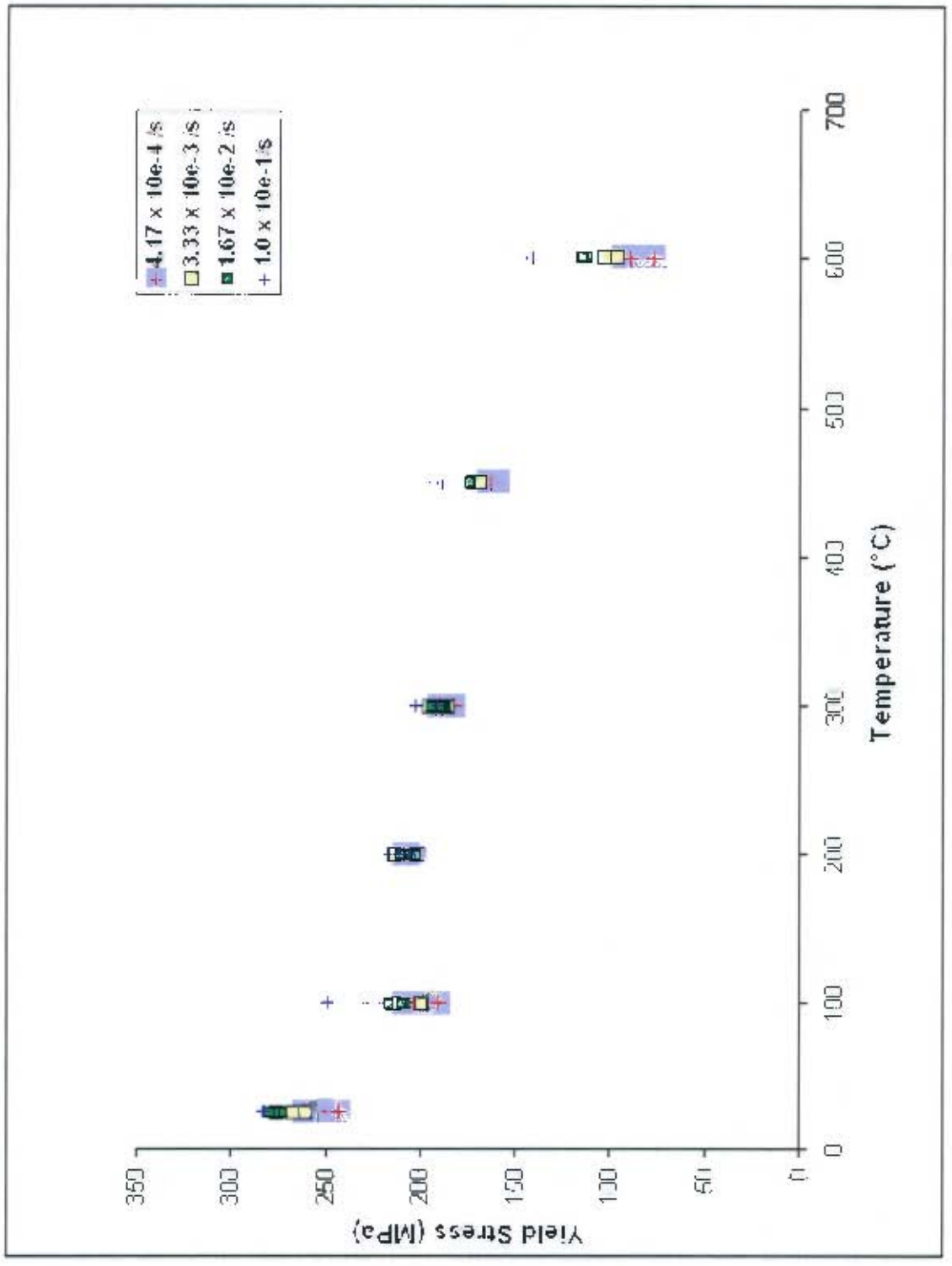

Figure 4.2.5 - Variation of Yield Stress with Temperature

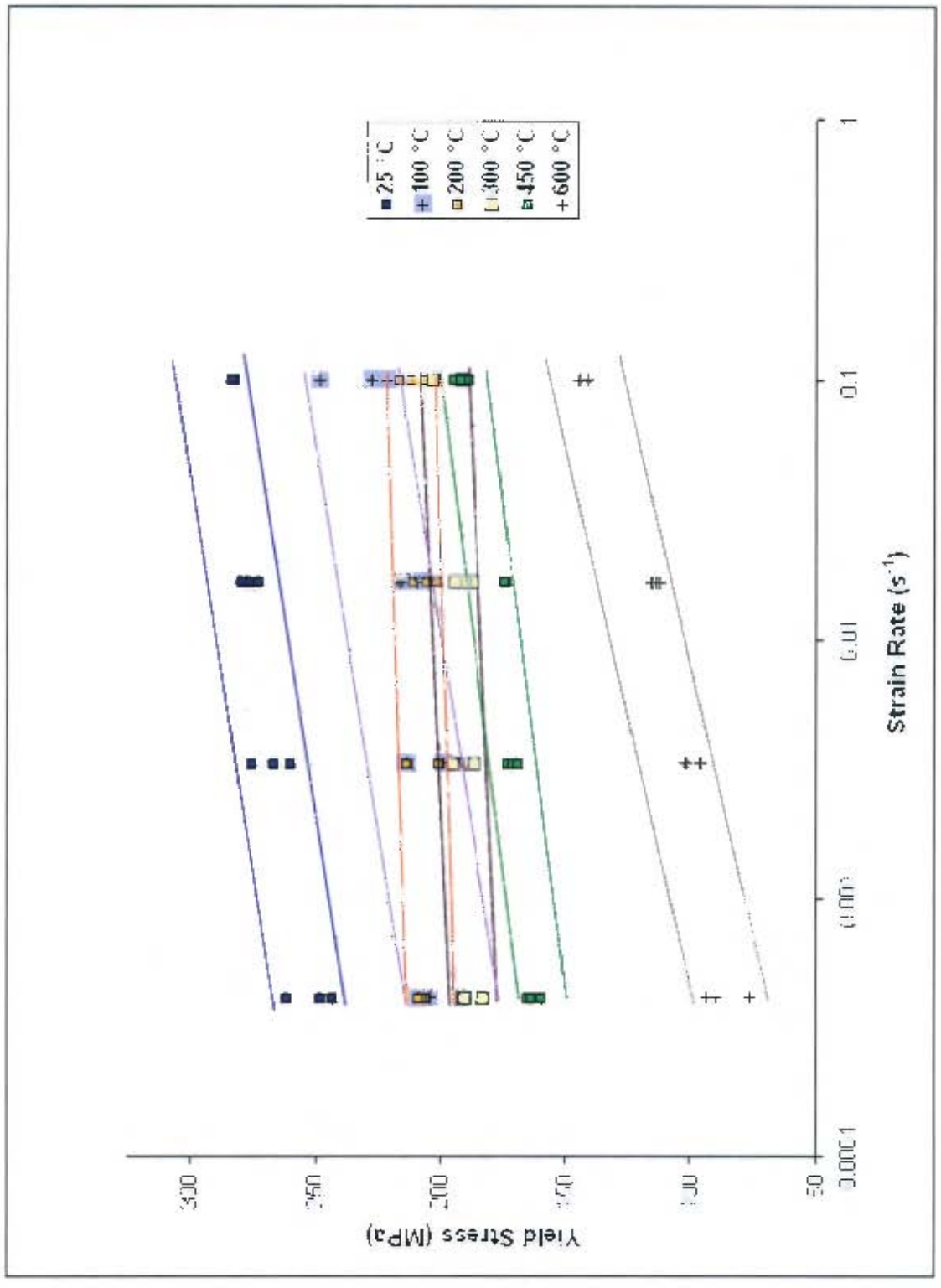

Figure 4.2.6 – Variation of Yield Stress with Strain Rate

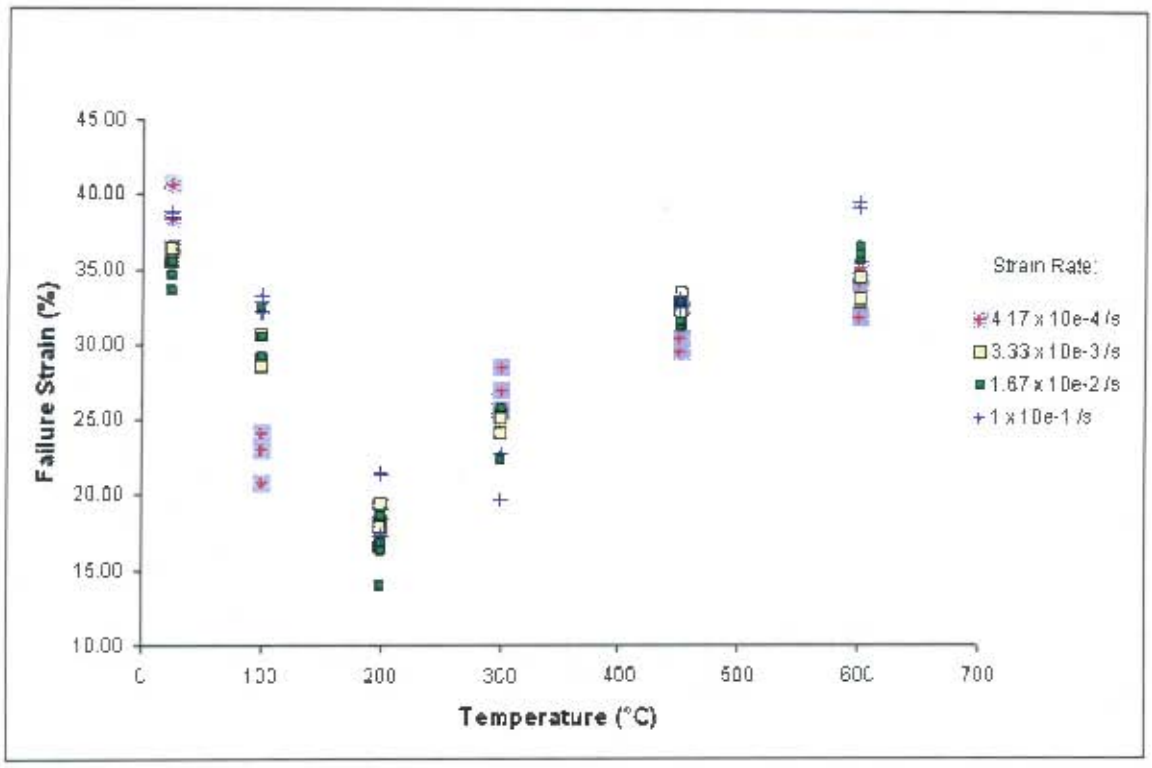

Figure 4.2.7 – Distribution of Failure Strains with Temperature

4.3. General Observations from the Test Results

Brief observations from the test results are presented next. Further analysis of the results is carried out in chapter 5.

- The measured yield points all decreased with increasing temperature. The amount by which the yield points decreased was found to be lowest between temperatures of 100°C and 450°C.
- Increasing the strain rate generally caused an increase in the recorded yield stress; however the effect was not as substantial as that of temperature over the range of strain rates employed. Furthermore, the strain rate effect on the yield point was observed to be negligible at 200°C and 300°C.
- The strain rate had no noticeable effect on the elongations experienced by the specimens and the lowest failure strains generally occurred at 200°C. A possible reason for this observation is the onset of dynamic strain ageing at this temperature. From the test results of mild steel at 200°C by Manjoine [16], it is evident that dynamic strain ageing is significant at this temperature. Therefore, the loss of ductility as a result of dynamic strain ageing can be attributed to the low strains at failure experienced at this temperature. Once the temperatures increased beyond 200°C, the failure strains increased in magnitude.

4.4. Observations from Micrographs

All the micrographs are presented in Appendix A4. Micrographs taken from the mid tip regions displayed the highest magnitudes of deformation on the granular level.

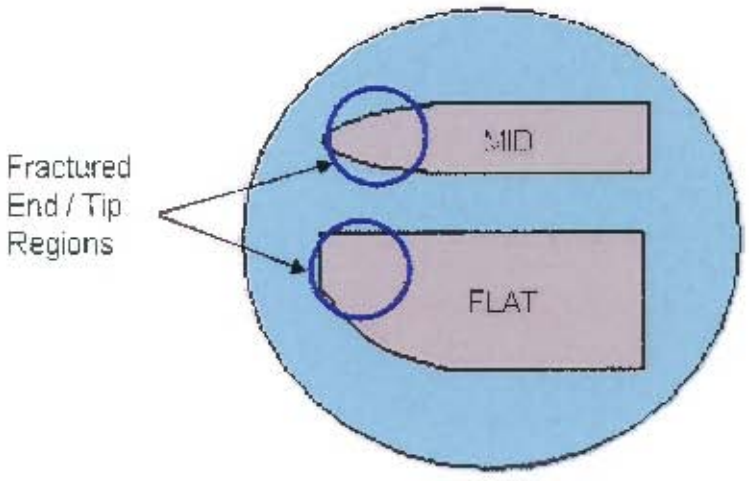

Figure 4.4.1 – 'Mid Tip' and 'Mid Flat' Regions on the Microstructure Samples

The strain rate did not appear to impact upon the amount of deformation experienced, however the temperature was observed to do so significantly. Moreover, the trend in the failure strains was reflected in the trend observed for the granular deformation. That is, the grain elongation in the direction of the applied stress appeared to decrease from room temperature to 200°C. Thereafter, the amount of deformation increased with temperature. This is highlighted in figures 4.4.2 – 4.4.5.

Figure 4.4.2 is a micrograph of an untested specimen along the mid region showing the undeformed grains.

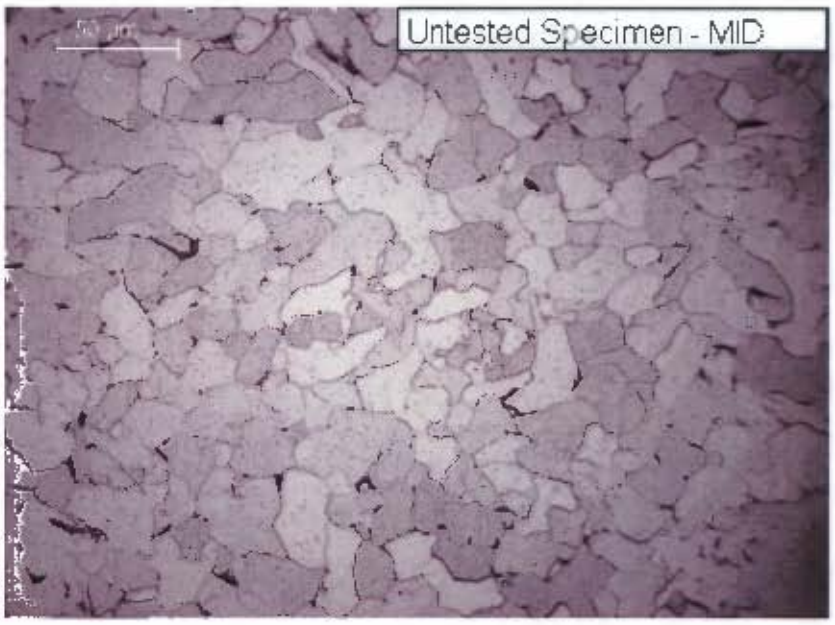

Figure 4.4.2 – Micrograph of an Untested Specimen along the Mid Region

Figures 4.4.3 – 4.4.5 are micrographs taken at the mid tip regions of specimens which were tested at the same strain rate ($4.17 \times 10^{-4} s^{-1}$). The amount of granular deformation at failure is less in the specimen tested at 200°C (figure 4.4.4) than it is in the one tested at room temperature (figure 4.4.3). This is consistent with the observations made with the failure strains where the elongation of the specimens at failure decreased from room temperature to 200°C, regardless of the strain rates employed (figure 4.2.7). Furthermore, the grains appeared to become less angular in form as the temperature increased.

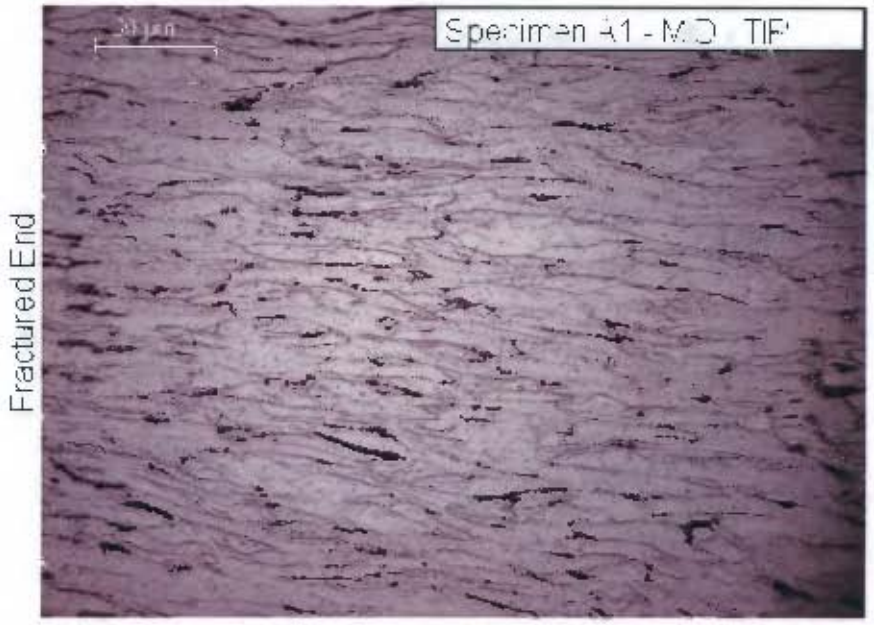

Figure 4.4.3 – Micrograph of Specimen A1 (Tested at 25°C and 4.17 x $10^{-1}s^{-1}$)

Figure 4.4.4 – Micrograph of Specimen B1NEW (Tested at 200°C and 4.17 x $10^{-1}s^{-1}$)

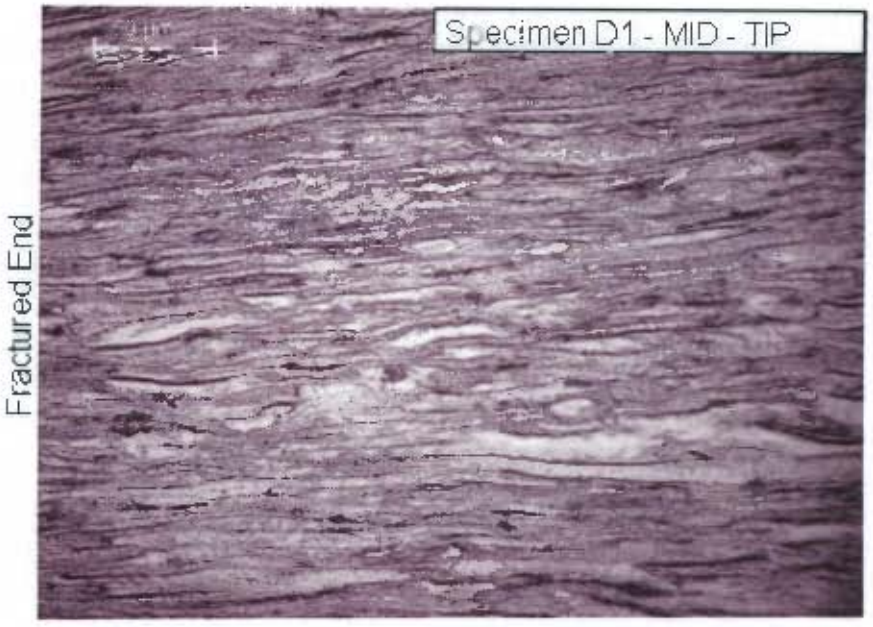

Figure 4.4.5 – Micrograph of Specimen D1 (Tested at 450°C and 4.17 x $10^{-4}s^{-1}$)

At temperatures beyond 200°C, the amount of deformation increases significantly. For temperatures of 450°C and 600°C the magnitude of granular deformation was such that the grains appeared as elongated bands in the direction of the applied stress (figure 4.4.5).

5. ANALYSIS OF EXPERIMENTAL RESULTS

Chapter 4 presented the results from the tensile tests carried out. This chapter attempts to draw meaningful information out of these results through further examination. Moreover, comparisons are made with published results and predicted results through the use of constitutive equations.

The results are summarised as a 3 – dimensional plot of the yield stress of mild steel as a function of temperature and strain rate in figure 5.1. The average values of the yield stresses at each strain rate and temperature combination were used as data points and plotted using MATLAB®.

Every point on the surface presented in figure 5.1 effectively describes the yield stress of mild steel for a unique combination of temperature and strain rate within the following ranges:

- Temperature: $25°C \leq T \leq 600°C$
- Strain Rate: $4.17 \times 10^{-4} s^{-1} \leq \dot{\varepsilon} \leq 10^{-1} s^{-1}$

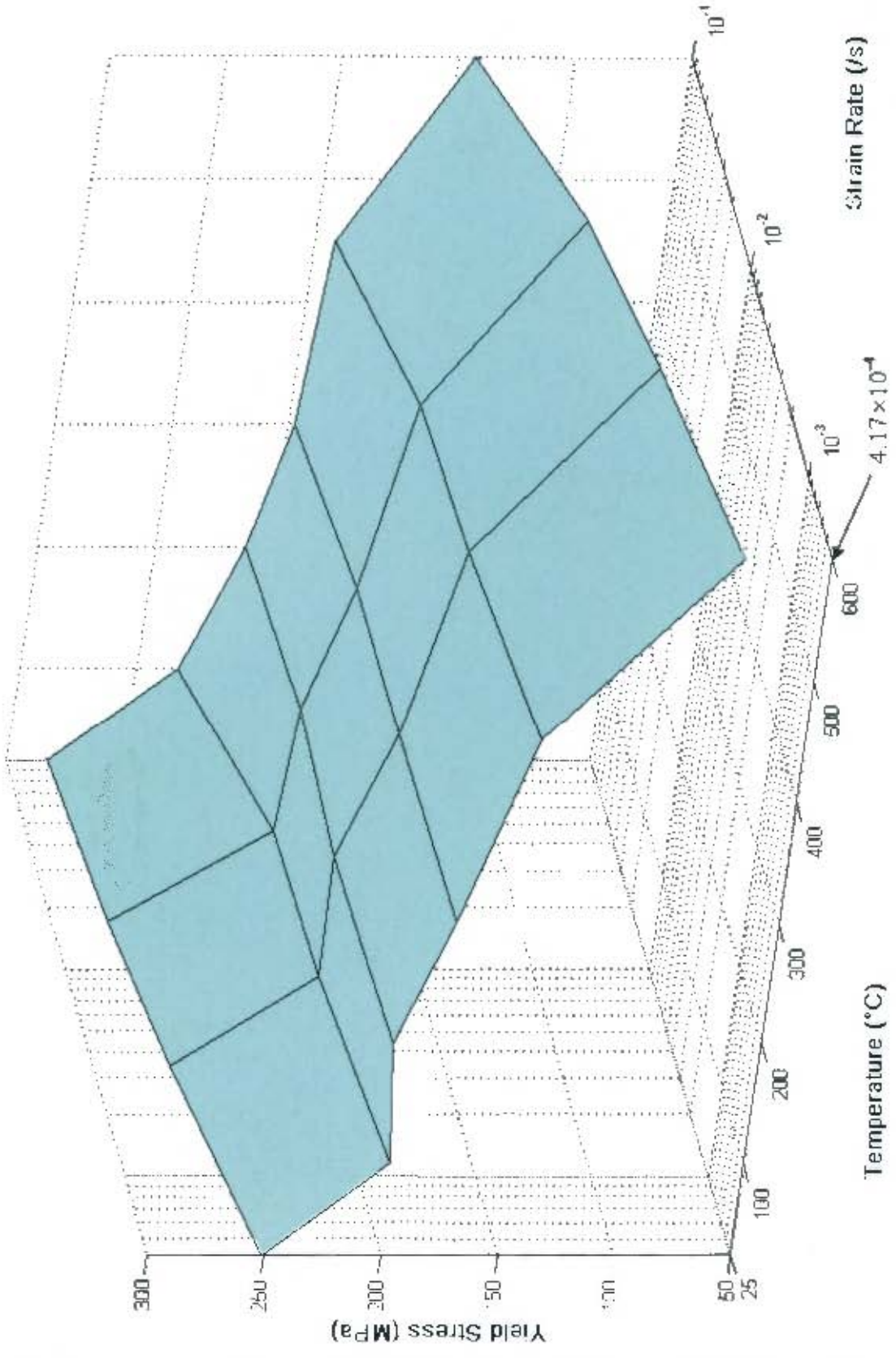

Figure 5.1 Variation of the Yield Stress of Mild Steel with Temperature and Strain Rate

Between temperatures of 100°C and 450°C, the surface in figure 5.1 appears almost level indicating that the strain rate effect is minimal in this temperature range. However, the strain rate effects are more pronounced at room temperature and at 600°C where the yield stresses increase more significantly with applied strain rate than at the other temperatures.

From figure 5.1, it is also evident that the temperature effect is more dominant that the strain rate effect on the yield stress over quasi-static strain rates. Significant drops in the yield stress occur between room temperature and 100°C as well as between 450°C and 600°C. The amount by which the yield stress decreases with increasing temperature is observed to be lowest between 100°C and 450°C, regardless of the applied strain rate.

The following section looks at comparisons of the test results with the published results of Manjoine [16].

5.1. Comparison of Test Results with Published Results

A comparison of the test results with those reported by Manjoine [16] is presented in this section and is used as a verification of the observations presented thus far. The test results were converted to the same scale used by Manjoine [16] and superimposed over his results. Figures 5.1.1 – 5.1.4 depict these comparisons.

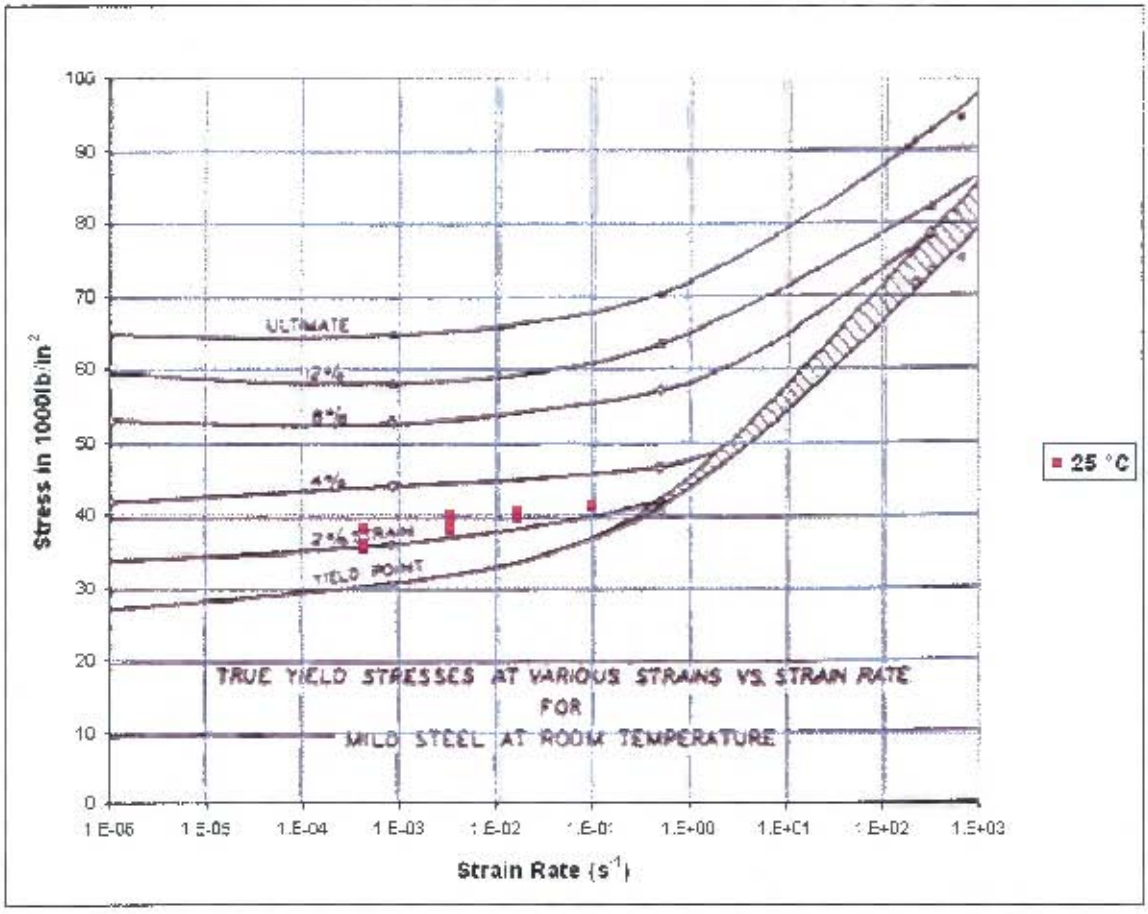

Figure 5.1.1 – Comparison of Test Results at Room Temperature

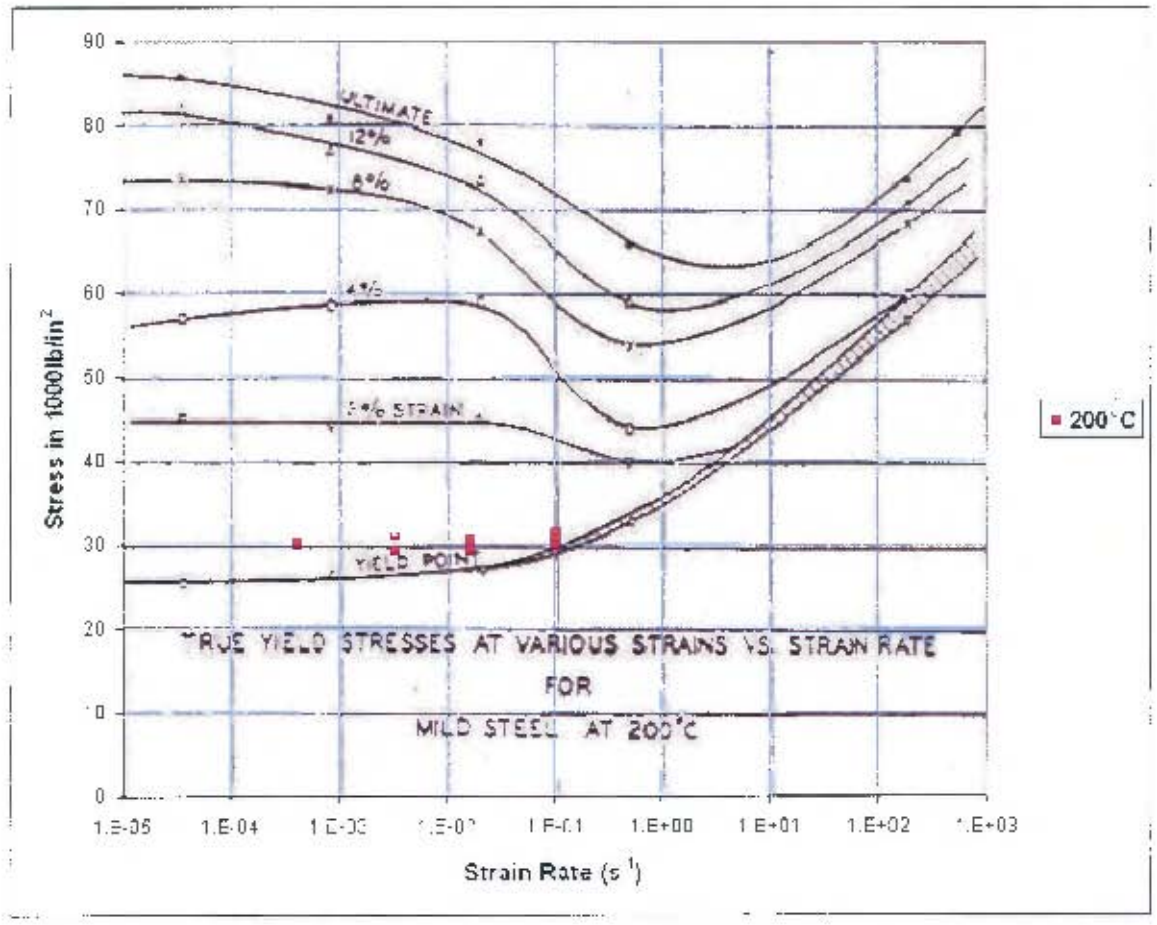

Figure 5.1.2 – Comparison of Test Results at 200°C

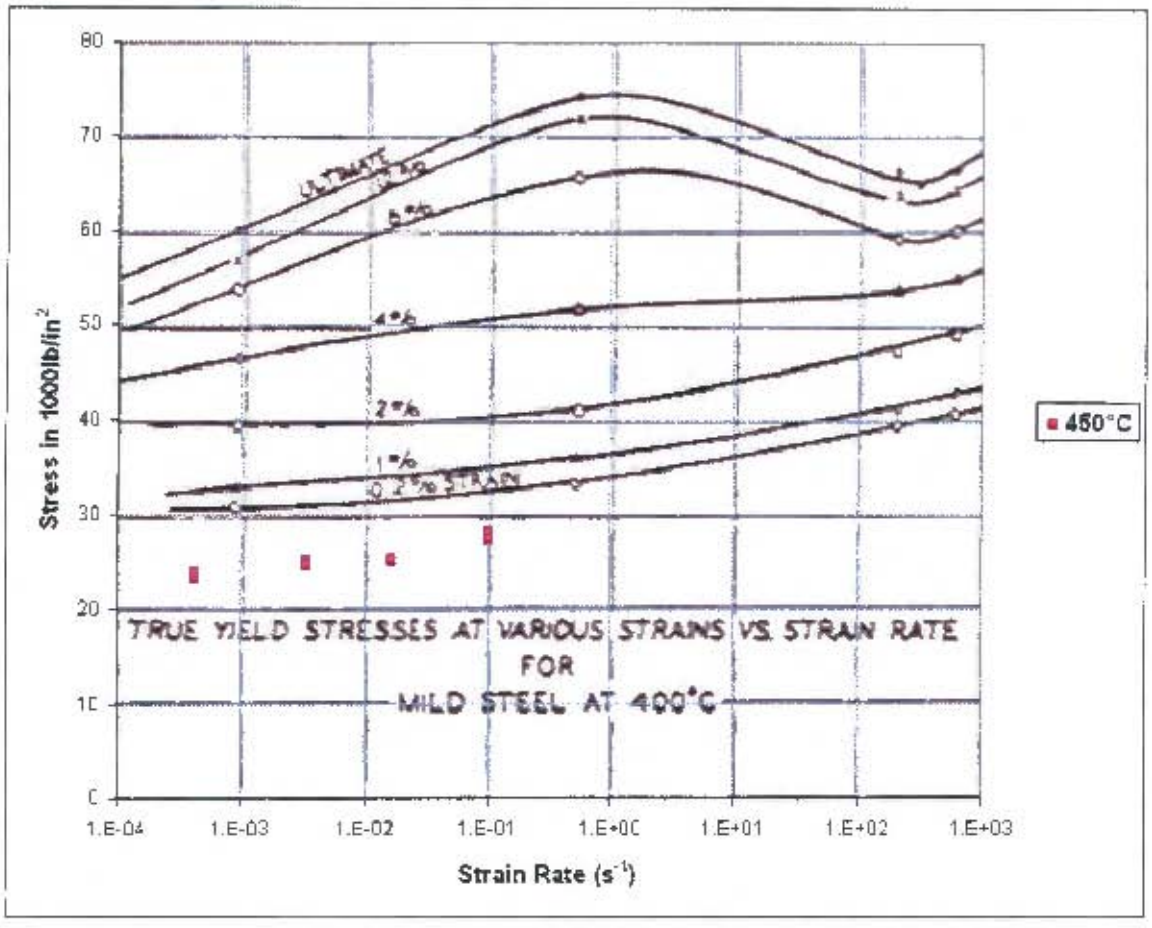

Figure 5.1.3 – Comparison of Test Results at 400°C and 450°C

Note that in figure 5.1.3, the results indicated with the red data points were of tests carried out at a temperature of 450°C whereas the tests by Manjoine [16] were carried out at 400°C.

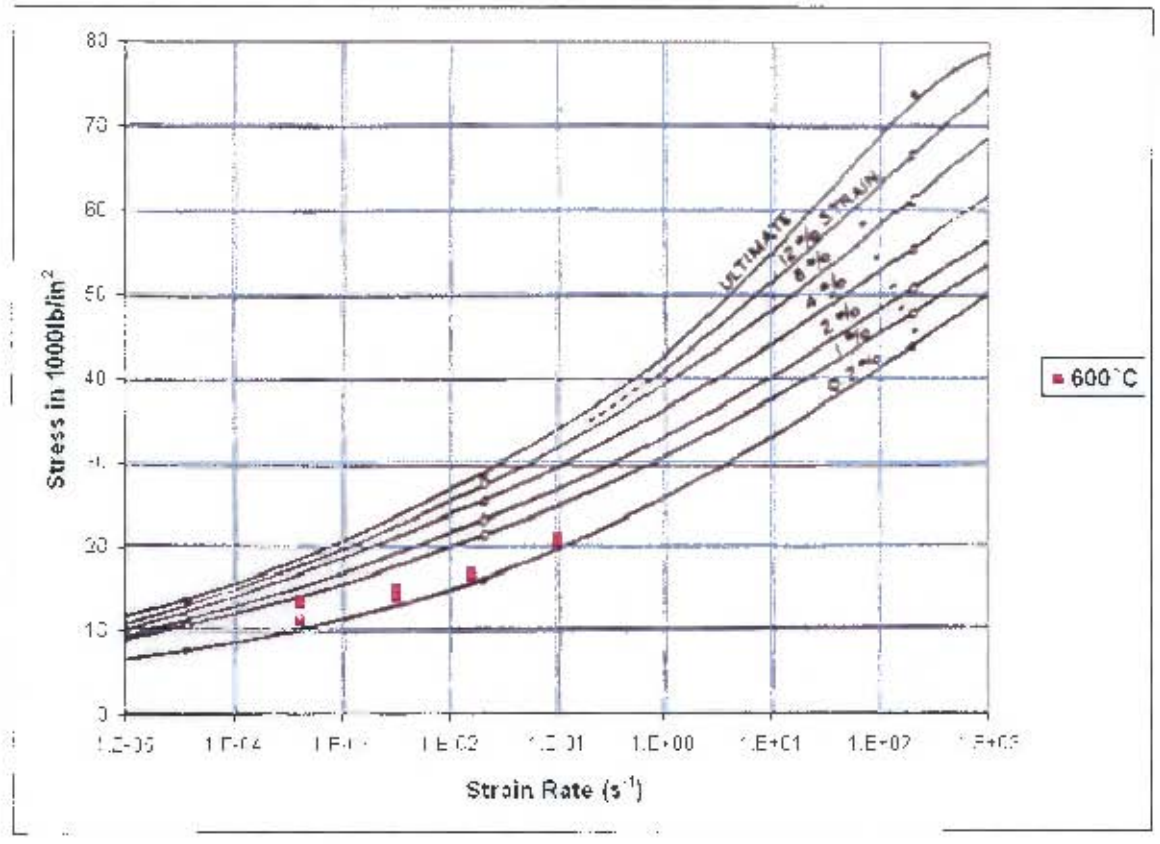

Figure 5.1.4 – Comparison of Test Results at 600°C

From figures 5.1.1 – 5.1.4, there is a good correlation with the results reported by Manjoine [16]. At all temperatures, the trends in the variation of the yield point stresses are similar in both cases. The minor variations in the values can be attributed to the different types of mild steel tested. It should be noted that the yield stresses reported by Manjoine [16] at 400°C are similar in value to those he reported at room temperature. This was not the case with the results obtained in this project. However, despite the large difference in values observed in the comparison at 400°C and 450°C temperatures (figure 5.1.3), the trends of the yield point stresses increasing with strain rate are alike.

The next section compares the results obtained in this project with predictions made with the temperature term of the Johnson – Cook constitutive equation [31] and with the temperature model for steel proposed by Masui et al [20].

5.2. Comparison of Results with Material Models

The temperature term of the Johnson – Cook equation [31] is given by equation 5.2.1.

$$\sigma_n = 1 - \left(\frac{T - T_{ROOM}}{T_{MELT} - T_{ROOM}} \right)^m \qquad \text{(Equation 5.2.1)}$$

Where σ_n is the normalised flow stress, m is the thermal softening fraction, T is the temperature (in Kelvin) at which the flow stress needs to be determined. T_{ROOM} and T_{MELT} are the room temperature and melting temperature of the material respectively.

The variation of the normalised yield stress of steel with temperature as proposed by Masui et al [20] for steel is given by equations 5.2.2a – 5.2.2c.

$$\frac{\sigma_y}{\sigma_0} = 1 \qquad T \le 200°C \qquad \text{(Equation 5.2.2a)}$$

$$\frac{\sigma_y}{\sigma_0} = 1 - 0.00178(T - 200) \qquad 200°C < T \le 700°C \qquad \text{(Equation 5.2.2b)}$$

$$\frac{\sigma_y}{\sigma_0} = 0.133 - 0.000388(T - 700) \qquad 700°C < T \le 1000°C \qquad \text{(Equation 5.2.2c)}$$

To enable a comparison with these material models, the test results at each strain rate were normalised using the average yield stress at ambient temperature for that particular strain rate. Figure 5.2.1 presents the comparison. Three different values of m were used for the Johnson – Cook model in an attempt to encompass all the test data points. The values selected were 0.55, 0.70 and 0.85 respectively.

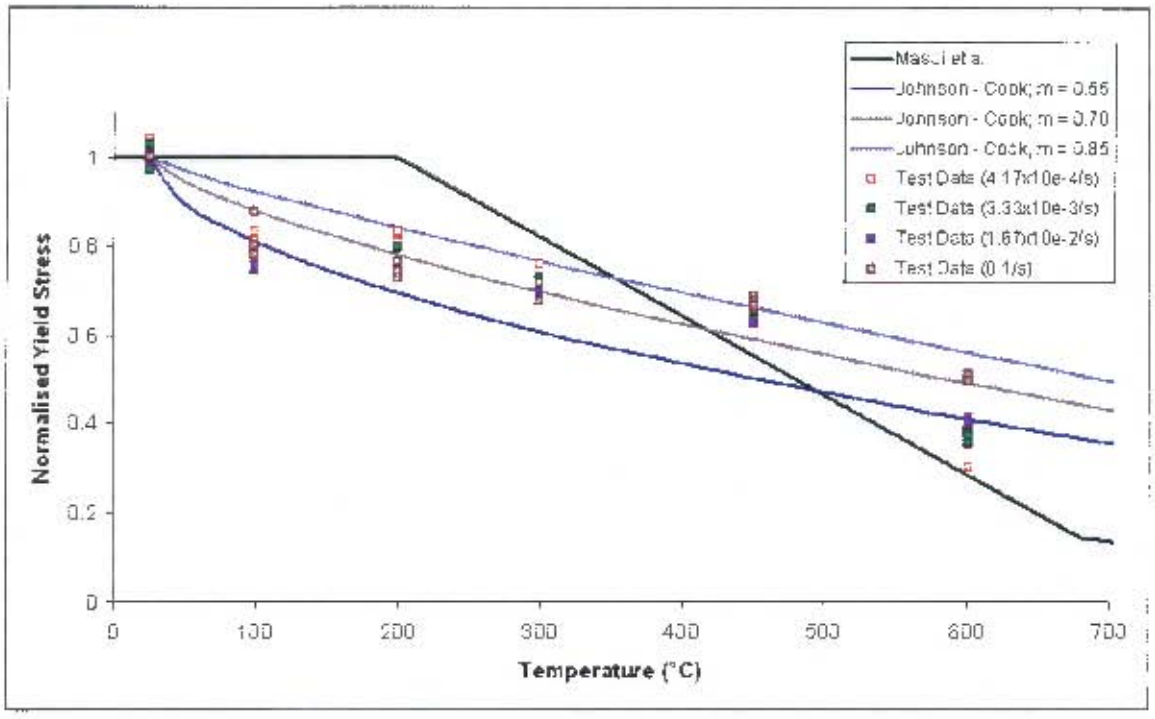

Figure 5.2.1 – Comparison of Test Results with Material Models

From figure 5.2.1, the prediction given by the temperature term of the Johnson – Cook equation [31] matches closely with a majority of the test data points when the thermal softening fraction, m, has value in the neighbourhood of 0.7. However at temperatures close to 600°C, the prediction begins to deviate from the test results. The temperature model proposed by Masui et al [20] shows a poor correlation with the test results for temperatures ranging from room temperature to 300°C. A closer match with the test results is achieved between 450°C to 600°C. The comparison makes it apparent that neither the prediction of the temperature effect given by the Johnson – Cook equation [31] nor the model proposed by Masui et al [20] adequately models the yield stress of mild steel over the entire range of temperatures. Therefore an alternative to these models is desired that sufficiently matches the test results over the 25°C to 600°C temperature range. The next section deals with this matter.

5.3. Formulation of an Empirical Temperature Model

The flow stress (σ) of a material can be considered to be a function of strain (ε), strain rate ($\dot{\varepsilon}$) and temperature (T). Therefore,

$$\sigma = \sigma(\varepsilon, \dot{\varepsilon}, T) \qquad \text{(Equation 5.3.1)}$$

Assume this stress function is of the form:

$$\sigma(\varepsilon, \dot{\varepsilon}, T) = \sigma_0 \cdot f(\varepsilon) \cdot g(\dot{\varepsilon}) \cdot h(T) \qquad \text{(Equation 5.3.2)}$$

This assumption is consistent with the postulation used for the form of the Johnson – Cook constitutive equation [31]. The symbols used in equation 5.3.2 are defined below:

σ_0 is an assumed static flow stress

$f(\varepsilon)$ is a strain effect modification function

$g(\dot{\varepsilon})$ is a strain rate effect modification function

$h(T)$ is a temperature effect modification function

At constant strains, the flow stress can be assumed to depend on the applied strain rate and temperature only. Therefore, equation 5.3.2 can be rewritten as:

$$\sigma = \sigma(\dot{\varepsilon}, T) = \sigma_0 \cdot g(\dot{\varepsilon}) \cdot h(T) \qquad (\varepsilon \text{ constant}) \qquad \text{(Equation 5.3.3)}$$

The form of equation 5.3.3 is consistent with the material model used in references [27-28] where the Cowper – Symonds equation [22] is used in conjunction with the equations for the temperature effect on the yield stress of steel proposed by Masui et al [20].

Thus the strain rate effect modification function, $g(\dot{\varepsilon})$, can be taken as the Cowper – Symonds equation [22] and equation 5.3.3 can be rewritten as:

$$\sigma(\dot{\varepsilon},T)=\sigma_0\cdot\left[1+\left(\frac{\dot{\varepsilon}}{D}\right)^{\frac{1}{q}}\right]\cdot h(T) \qquad \text{(Equation 5.3.4)}$$

Where: $\sigma(\dot{\varepsilon},T)$ is the flow stress at a given strain rate and temperature (with ε constant)

σ_0 is the associated static flow stress

D and q are material constants

From the Cowper – Symonds equation [22],

$$\sigma_0'=\sigma_0\cdot\left[1+\left(\frac{\dot{\varepsilon}}{D}\right)^{\frac{1}{q}}\right] \qquad \text{(Equation 5.3.5)}$$

Where: σ_0' is the dynamic flow stress at room temperature

Thus, the temperature modification function, $h(T)$, can be obtained by equation 5.3.6, given test data of the flow stress at elevated temperatures.

$$h(T)=\frac{\sigma(\dot{\varepsilon},T)}{\sigma_0'} \qquad \text{(Equation 5.3.6)}$$

Hence, the temperature modification function is derived from the test results by first normalising the test data. That is, for each strain rate used, the average yield stress at room temperature is calculated. The test results for a given strain rate are then divided

by the average yield stress at room temperature for that strain rate to obtain the normalised yield stresses. This is done for the different strain rates used and is depicted in figure 5.3.1.

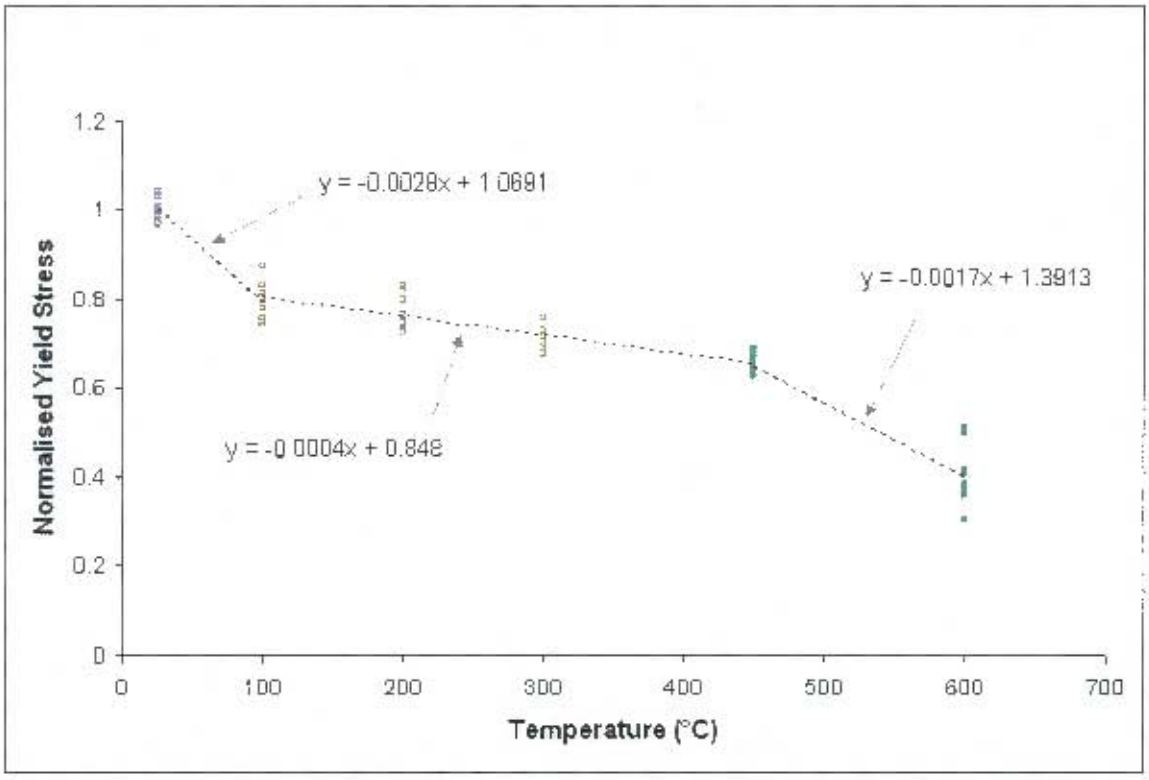

Figure 5.3.1 – Normalised Yield Stresses

From figure 5.3.1, it is possible to fit linear functions between the temperature ranges of 25°C to 100°C, 100°C to 450°C, and 450°C to 600°C. The least squares fit for linear equations in the three regions are indicated in figure 5.3.1. These equations were then manipulated algebraically to ensure that the values at the boundaries of the three temperature regions coincided and that the value of the equation at room temperature corresponded to 1. The forms of these adjusted equations were determined to be:

$y = 1.05 - 0.0025x$ (25°C to 100°C) (Equation 5.3.7a)

$y = 0.84 - 0.0004x$ (100°C to 450°C) (Equation 5.3.7b)

$y = 1.425 \quad 0.0017y$ (450°C to 600°C) (Equation 5.3.7c)

Consequently, these modified equations (equations 5.3.7a – 5.3.7c) represent the temperature modification function $h(T)$, and can be expressed as:

$\sigma_{yn} = 1 - 2.67 \times 10^{-3}(T - 25)$ $25°C < T \leq 100°C$ (Equation 5.3.8a)

$\sigma_{yn} = 0.8 - 4 \times 10^{-4}(T - 100)$ $100°C < T \leq 450°C$ (Equation 5.3.8b)

$\sigma_{yn} = 0.66 - 1.7 \times 10^{-3}(T - 450)$ $450°C < T \leq 600°C$ (Equation 5.3.8c)

Where: σ_{yn} is the normalised yield stress as a function of temperature only

T is the temperature in °C

Figure 5.3.2 portrays a plot of equations 5.3.8a – 5.3.8c over the normalised yield stress data points.

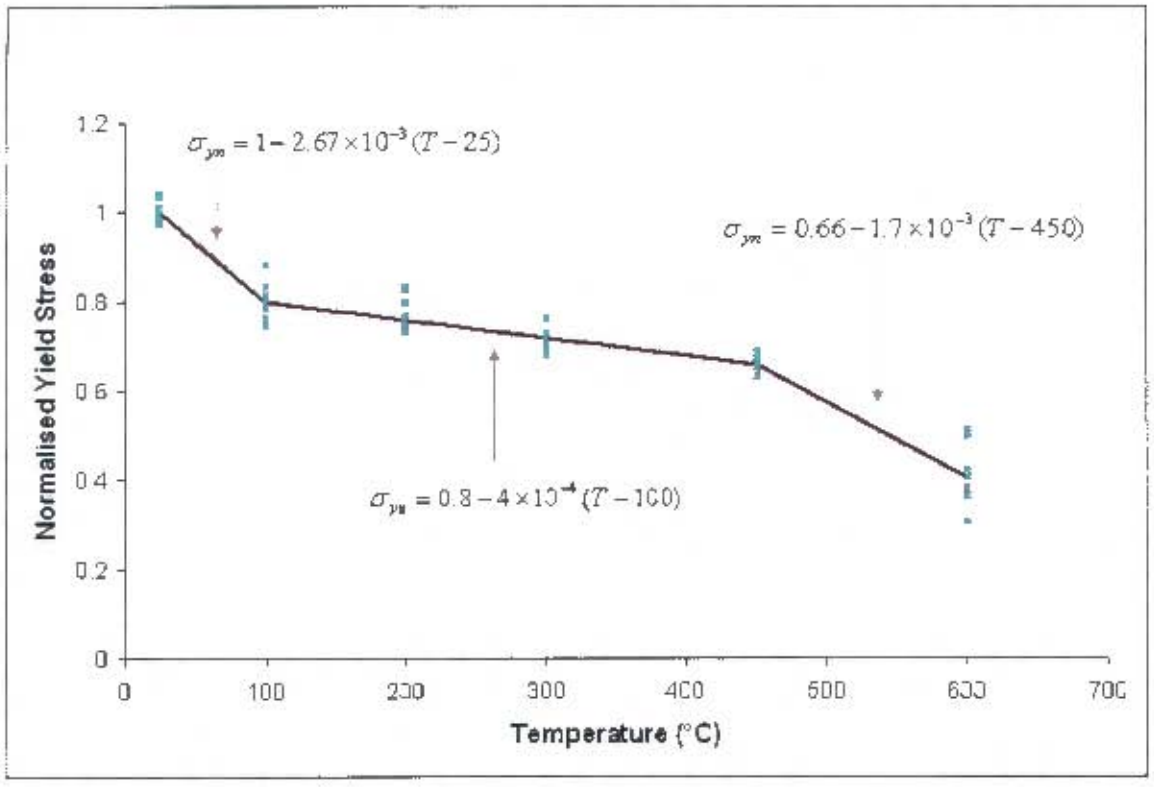

Figure 5.3.2 – Empirical Temperature Model for Mild Steel

6. CONCLUSIONS

The results of tensile tests carried out on mild steel specimens have been presented. In carrying out these tests, a testing methodology was set up for carrying out high temperature tensile tests at customisable strain rates using the ESH 100kN Universal Tester. This process has been detailed in Appendix A1. Conclusions drawn from these tests are presented next.

The material response of mild steel loaded over quasi-static strain rates ($4.17\times10^{-4}s^{-1}$, $3.33\times10^{-3}s^{-1}$, $1.67\times10^{-2}s^{-2}$ and $1\times10^{-1}s^{-1}$) at temperatures ranging from 25°C to 600°C was determined. **A major observation made was that the temperature effect on the yield stress was more dominant than the strain rate effect over the range of strain rates investigated.** However, from figure 4.2.6, there were variations observed in the yield stress due to the strain rate at room temperature, 100°C, 450°C and 600°C. In these instances, the yield stresses were found to increase when the applied strain rate increased. The strain rate effect was found to be minimal at 200°C and 300°C. Furthermore, the applied strain rate was found to have no effect on the tensile elongations and the effect of dynamic strain ageing was noticed on the failure strains at 200°C. As expected from literature, the yield stresses were found to decrease in magnitude with increasing temperature.

Samples were selected from the tested specimens for a micro-structural analysis. This was done to observe the deformation of the grains at the fractured end of the specimens due to the test conditions. The strain rate did not appear to impact upon the granular deformation over the range of quasi-static strain rates used. However, the temperature was observed to affect the granular deformation significantly. It was also observed that the trend of granular deformation in close proximity to the fractured end was similar to the trend of the global strains at failure. At higher temperatures (≥ 450°C), the overall

granular deformation was observed to be substantial, with the grains appearing as elongated bands in the direction of the applied stress.

The results of the tensile tests were then compared to published work and found to be consistent with similar work done on mild steel by Manjoine [16]. These results were also compared to predictions given by the empirical temperature model for steel by Masui et al [20] and the Johnson – Cook constitutive equation [31]. It was found that both these material models showed a good correlation with the test results over certain regions only. A thermal softening fraction (m) value of 0.7 for the Johnson – Cook equation [31] was found to give an acceptable match with the test results for temperatures up to 450°C, whereas the temperature model given by Masui et al [20] corresponded better with the test results at higher temperatures (450°C to 600°C).

Finally, an empirical temperature model for the variation of the yield stress of mild steel with temperature was formulated using the test results. This was done using assumptions consistent in literature and a temperature model similar in manner to that proposed by Masui et al [20] was presented.

7. RECOMMENDATIONS

The following recommendations are made based on the work carried out in this project:

- The displacement transducer on the hydraulic actuator of the ESH 100kN Universal Tester was used to obtain the extension of the tensile specimen as the tests were carried out. For more accurate strain measurements, the use of extensometers attached directly to the specimen is advised. High temperature alloys are recommended for the extensometer parts that will have to be placed within the furnace when elevated temperature tensile tests are being carried out. The design of such extensometers will also have to account for the limited space available within the closed furnace.
- The test temperatures were limited to a maximum of 600°C for this project as the grips used for the tensile tests were manufactured from stainless steel 316. In order to investigate the material properties at higher temperatures, it is recommended that the grips be designed from high temperature alloys (for example, the Haynes® 230® Alloy).
- Tensile testing is adequate for covering the quasi-static strain rate ranges. However, to obtain a better representation of the material characteristics, tests at elevated temperatures should be carried out over the intermediate to high strain rate range (i.e. strain rates of the order $10^0 s^{-1}$ ~ $10^4 s^{-1}$). Testing methods coupling high temperatures with high strain rates have been investigated by Lennon and Ramesh [11] and Macdougall [12]. These methods, which involve the use of the split-Hopkinson pressure bar, can be implemented to achieve results at higher strain rates than those possible by tensile testing.
- The empirical model formulated in this project for the variation of the yield stress of mild steel with temperature should be utilised in numerical models of experiments where physical test data is available for comparison. The results obtained from the numerical simulation can then be compared to the physical test

results and the proposed temperature model can be validated as a useful tool in numerical simulations involving mild steel.

8. REFERENCES

[1] Han P., ed, Tensile Testing, ASM International, 1999, pp. 25-26

[2] Han P., ed, Tensile Testing, ASM International, 1999, p1

[3] Han P., ed, Tensile Testing, ASM International, 1999, p27

[4] Han P., ed, Tensile Testing, ASM International, 1999, p29

[5] British Standard Method for Tensile Testing of Metals (including aerospace materials) BS 18: 1987, p5

[6] http://www.key-to-steel.com/ViewArticle.asp?ID=42 (Accessed online – 03/08/2006)

[7] SCHEIDER, I, BROCKS, W, and CORNEC, A. "Procedure for the Determination of True Stress-Strain Curves From Tensile Tests With Rectangular Cross-Section Specimens." Journal of Engineering Materials and Technology, Vol. 126, No. 1, Jan 2004, pp. 70-76

[8] KOLSKY, H. "An investigation of the mechanical properties of materials at very high rates of loading." Proceedings of the Physical Society, B62, 1949, pp 676-700

[9] ZHAO, H, and GARY, G. "On the use of SHPB techniques to determine the dynamic behaviour of materials in the range of small strains." Int. J. Solids Structures, Volume 33, No. 23, 1996, pp. 3363-3375

[10] KRAFFT, JM, SULLIVAN, AM and TIPPER, CF. "The effect of static and dynamic loading and temperature on the yield strength of iron and mild steel in compression." Proceedings of the Royal Society of London. Series A, Mathematical and Physical Sciences, Volume 221, No. 1144, 7th Jan. 1954, pp. 114-127

[11] LENNON, AM, and RAMESH, KT. "A technique for measuring the dynamic behaviour of materials at high temperatures." International Journal of Plasticity, Volume 14, No. 12, 1998, pp 1279-1292

[12] MACDOUGALL, D. "A radiant heating method for performing high-temperature high-strain-rate tests." Measurement and Science Technology, Volume 9, No. 10, 1998, pp. 1657-1662

[13] http://en.wikipedia.org/wiki/Face-centered_cubic (Accessed online - 16/10/2007)

[14] ITABASHI, M. and KAWATA, K. "Carbon content effect on high-strain-rate tensile properties for carbon steels." International Journal of Impact Engineering, Volume 24, 2004, pp 117-131

[15] ZEGHIB, NE. and KLEPACKZO. JR. "Work hardening of mild steel within dynamic strain ageing temperatures." Journal of Materials Science, Vol. 31, 1996, pp. 6085-6088

[16] MANJOINE, MJ. "Influence of rate of strain and temperature on yield stresses of mild steel." J. Appl. Mech. 1944;11, pp. A-211 – A-218

[17] STEICHEN, JM. "High Strain Rate Tensile Properties of AISI Type 304 Stainless Steel." Journal of Engineering Materials and Technology, Volume 95, No. 3, July 1973, pp. 182-185

[18] DAVIES, RG. and MAGEE, CL. "The Effect of Strain-Rate Upon the Tensile Deformation of Materials." Journal of Engineering Materials and Technology, Volume 97, No. 2, April 1975, pp151-155

[19] ALBERTINI, C. and MONTAGNANI, M. "Dynamic uniaxial and biaxial stress-strain relationships for austenitic stainless steels." Nuclear Engineering and Design 57, 1980, pp 107-123

[20] MASUI, T. NUNOKAWA, T. and HIRAMATSU, T. "Shape correction of hot-rolled sheet steel using an on-line leveller." Journal of Japan Society for Technology of Plasticity, Volume 28, No. 312, 1987, pp. 81-87

[21] GILAT, A. and WU, X. "Plastic Deformation of 1020 Steel Over a Wide Range of Strain Rates and Temperatures." International Journal of Plasticity, Vol. 13, Nos. 6-7, 1997, pp. 611-632

[22] JONES, N., Structural Impact, Cambridge University Press, 1989, p348

[23] JONES, N., Structural Impact, Cambridge University Press, 1989, pp.349-350

[24] ABRAMOWICZ, W. and JONES, N. "Dynamic progressive buckling of circular and square tubes." International Journal of Impact Engineering, Volume 4, No. 4, 1986, pp. 243-270

[25] MARAIS, ST, TAIT, RB, CLOETE, TJ, and NURICK, GN. "Material testing at high strain rate using the split Hopkinson pressure bar." Latin American Journal of Solids and Structures, 2004, pp. 319-339

[26] JONES, N., Structural Impact, Cambridge University Press, 1989, p340

[27] CHUNG KIM YUEN, S and NURICK, GN. "Experimental and numerical studies on the response of quadrangular stiffened plates - Part I: uniform blast loading", International Journal of Impact Engineering, Volume 31, Issue 1, 2005, pp 55-83

[28] LANGDON, GS, CHUNG KIM YUEN, S and NURICK, GN. "Experimental and numerical studies on the response of quadrangular stiffened plates – Part II: localised blast loading", International Journal of Impact Engineering, Volume 31, Issue 1, 2005, pp 85-111

[29] BODNER, SR, and PARTOM, Y. "Constitutive equations for elastic-viscoplastic strain-hardening materials." Journal of Applied Mechanics, June 1975, pp. 385-389

[30] LIANG, R, and KHAN, AS. "A critical review of experimental results and constitutive models for BCC and FCC metals over a wide range of strain rates and temperatures." International Journal of Plasticity, Volume 15, 1999, pp. 963-980

[31] JOHNSON, GR, and COOK, WH. "A constitutive model and data for metals subjected to large strains, high strain rates and high temperatures." Proceedings of the Seventh Symposium on Ballistics, The Hague, Netherlands, 1983, pp. 541-547

[32] TANIMURA, S, MINURA, K, and UMEDA, T. "New testing techniques to obtain tensile stress-strain curves for a wide range of strain rates." Journal de Physique IV France, 2003; 110: pp385-390

[33] BALDEN, VH, and NURICK, GN. "Numerical simulation of the post-failure motion of steel plates subjected to blast loading." International Journal of Impact Engineering, Volume 32, 2005, pp. 14-34

[34] ZERILLI, FJ, and ARMSTRONG, RW. "Dislocation-mechanics-based constitutive relations for material dynamics calculations." Journal of Applied Physics, Volume 61 (5), 1987, pp 1816-1825

APPENDICES

A1. USING THE ESH MACHINE FOR TENSILE TESTS

The ESH 100kN Universal Tester used to carry out the tensile tests for this project is a servo-hydraulic machine capable of a wide range of tests such as fatigue and fracture mechanics tests. FigureA1.1 shows the machine with its control setup:

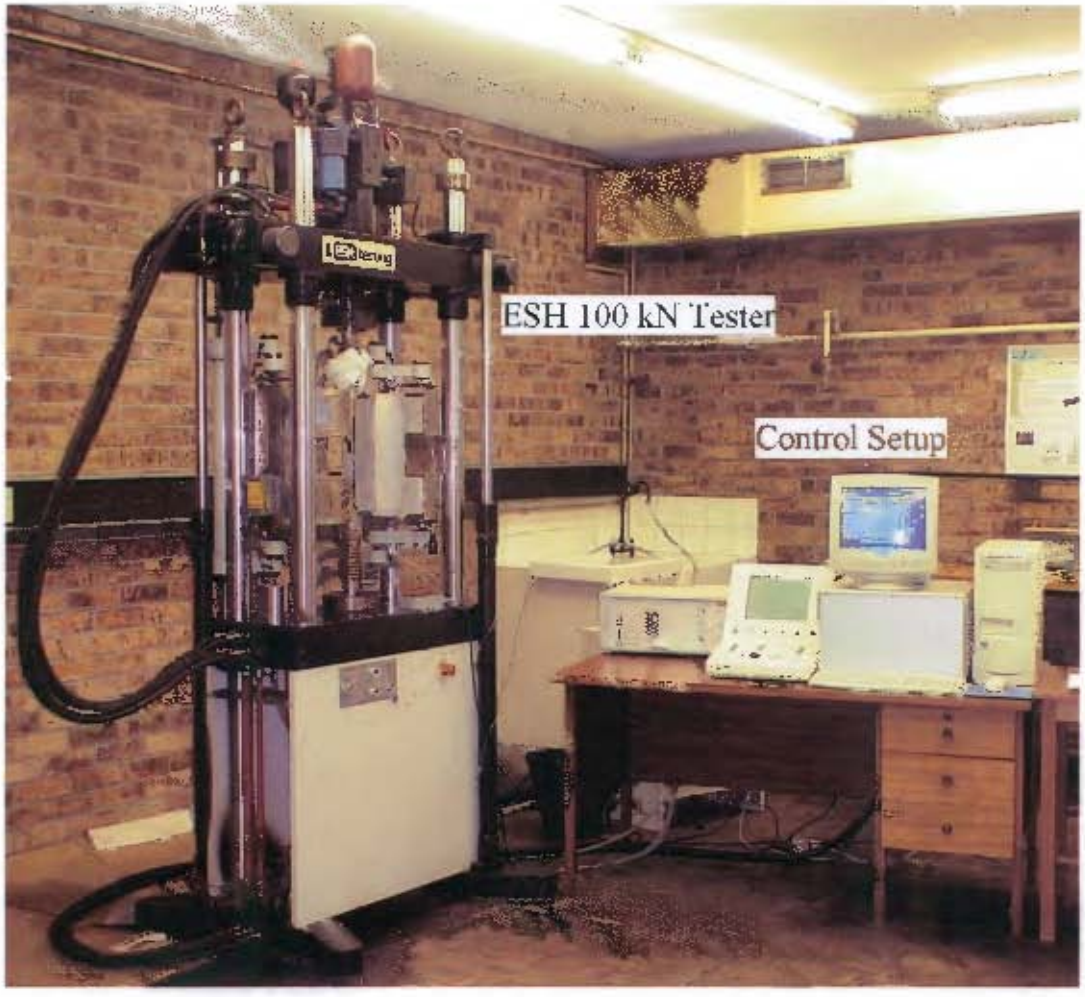

Figure A1.1 – ESH 100kN Universal Tester and Control Setup

This appendix describes how the machine was adapted to carry out high temperature tensile tests.

A1.1. Grips for High Temperature Tensile Tests

As the high temperature tensile tests involve heating the specimen with the attached furnace, a set of grips was specifically designed to withstand the high temperatures and protect the ESH machine. The grips are briefly described below:

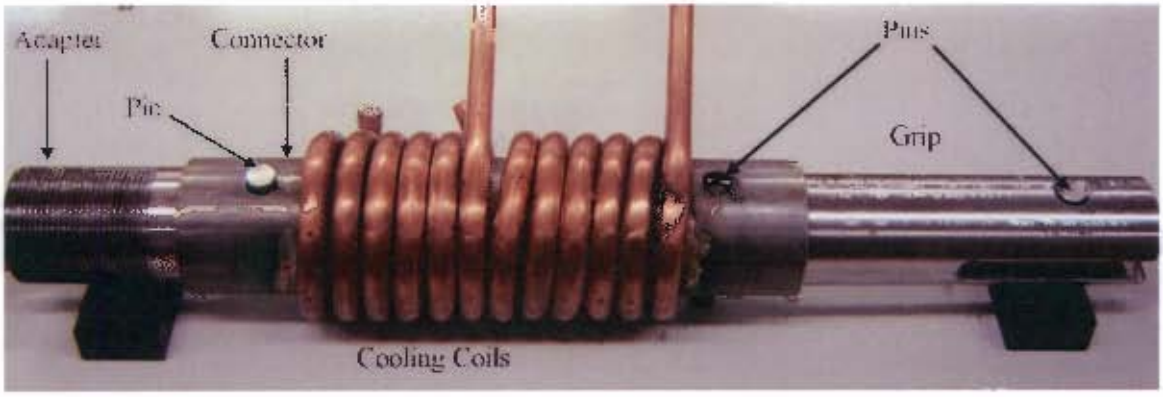

Figure A1.1.1 – High Temperature Grip Assembly

The grips, one of which is shown in figure A1.1.1, consist of three separate pieces interconnected with pins to form the grip assembly. The first piece is the adapter which screws into the ESH machine; the connector is the second piece and has two copper coils brazed onto it for cooling purposes and finally the grip itself. All components of the grip assembly, with the exception of the coils, were made from stainless steel 316. Details pertaining to the design of the grips may be found in reference [1]. The grips hold dog bone specimens of mild steel with a gauge length of 60mm. The other dimensions are depicted in figure A1.1.2:

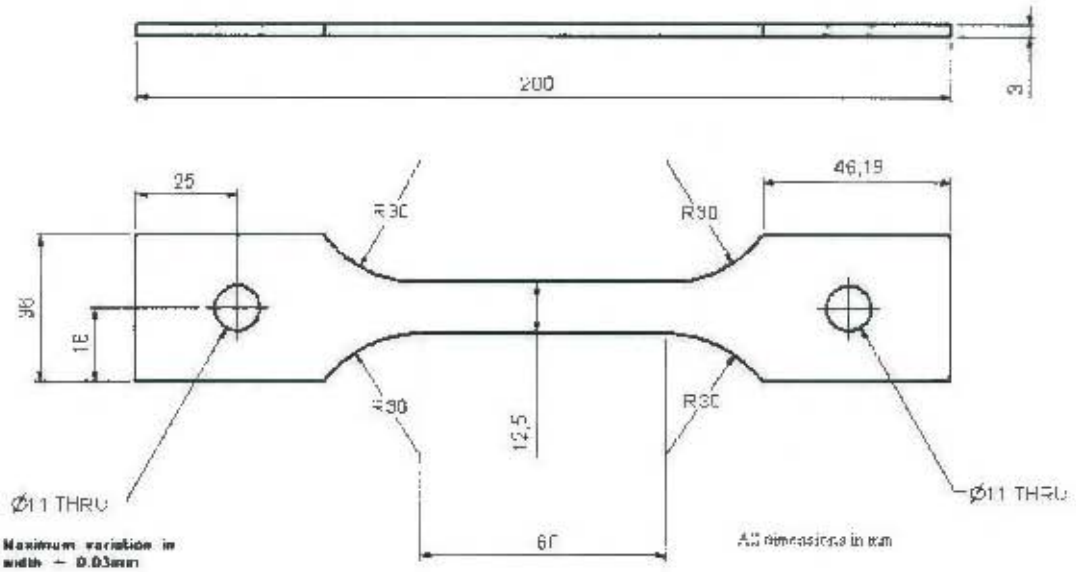

Figure A1.1.2 – Tensile Test Specimen Dimensions

A1.2. Setting Up a Custom Tensile Test

This section outlines how to set up a customised tensile test. A Block Program for the tensile tests is created using the ESH software loaded on the control setup computer, as shown below:

- From the Start menu select Programs → ESH Programs → Block and LCF Editor
- The window shown in figure A1.2.1 will then pop up:

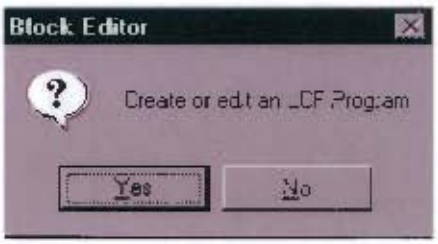

Figure A1.2.1 – Creating a Block Program

- Select 'No' to proceed to the Block Editor as depicted in figure A1.2.2:

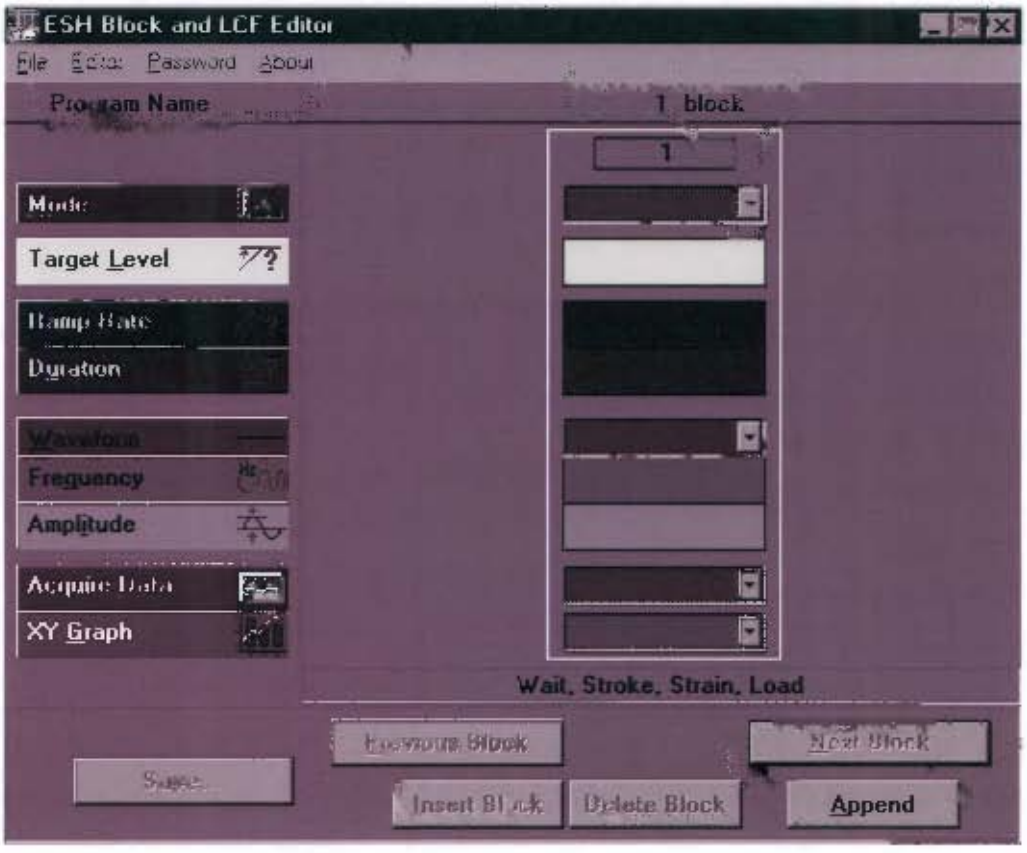

Figure A1.2.2 – The Block Editor

- To set up the customised tensile test, select the following options from the Block Editor screen:
  - Set Mode to → Stroke
  - Set Target Level to → (distance in mm either relative to the position of the crosshead i.e. REL; or from the 0 position i.e. ABS). This sets the distance the hydraulic actuator will move in total from its reference position.
  - Set Ramp Rate to → (any value between 0.0025 to 400 mm/s, mm/m or mm/h). This sets the rate at which the hydraulic actuator will move for the tensile test.

- Set Acquire Data to → Yes
- Set XY Graph to → LvS
- Leave the other options blank

- Certain points need to be noted about the selection of the options above. Firstly, the target level is dependent on the dimensions of the grips used, the position of the crosshead and the distance required to strain a specimen to failure. Therefore care must be taken to choose a suitable value here. Secondly, the units will need to be specified when selecting the ramp rate. Figure A1.2.3 depicts the values used to carry out the 1mm/s tensile tests using the grips described in §A1.1:

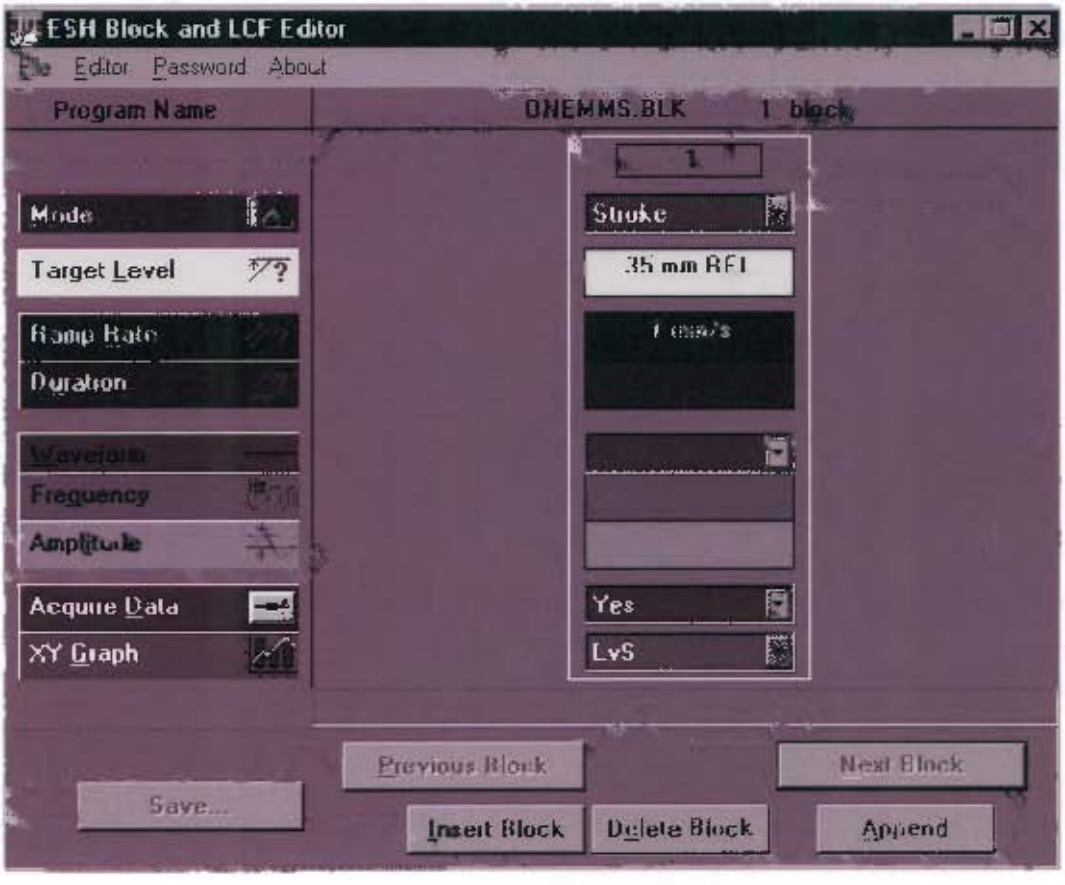

Figure A1.2.3 – Block Program for carrying out 1mms^{-1} Tensile Tests

- A password is required before the program can be saved. Select the Password option from the main menu and enter **ESH** as the password.

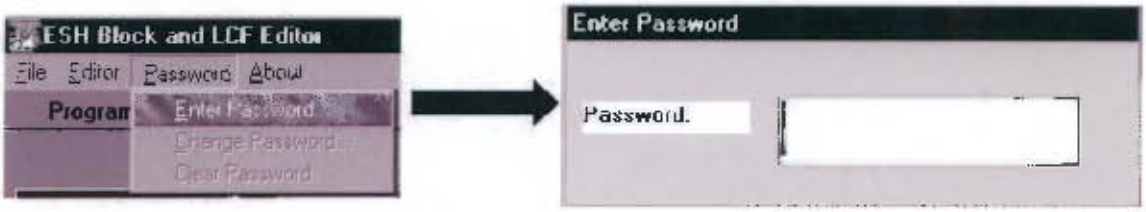

Figure A1.2.4 – Entering the Password

- Then select File → Save Program from the main menu to save the program into a suitable directory. The Block Program will then be retrieved from this directory when carrying out the tensile test.

Figure A1.2.5 – Saving the Block Program

A1.3. Executing the Tensile Test

Once the custom tensile test is set up as shown in the previous section, the ESH 100kN Universal Tester can be used to carry out the tensile tests. The following steps outline the process:

- Ensure that the tester and all the components of the control setup (i.e. the Eurotherm© 2408 controller, the analogue controller and the computer) are switched on and the interlocks have been cleared. It is assumed at this point that the crosshead of the tester has been suitably positioned to ensure that the grips are accommodated and the furnace can freely move to enclose the specimen when in place. Note that the position of the crosshead is controlled by the valve and the 'Raise' and 'Lower' buttons found on the front panel of the tester itself and furthermore, once the crosshead has been positioned, no further adjustments are required using the front panel.
- Switch the analogue controller to remote (turn the key at the back of the controller to remote).

Figure A1.3.1 – Control Setup for the ESH© 100kN Universal Tester

- From the Start menu select Programs → ESH Programs → Virtual Control Panel. Once the connection with the computer is established, the screen in figure A1.3.2 should appear:

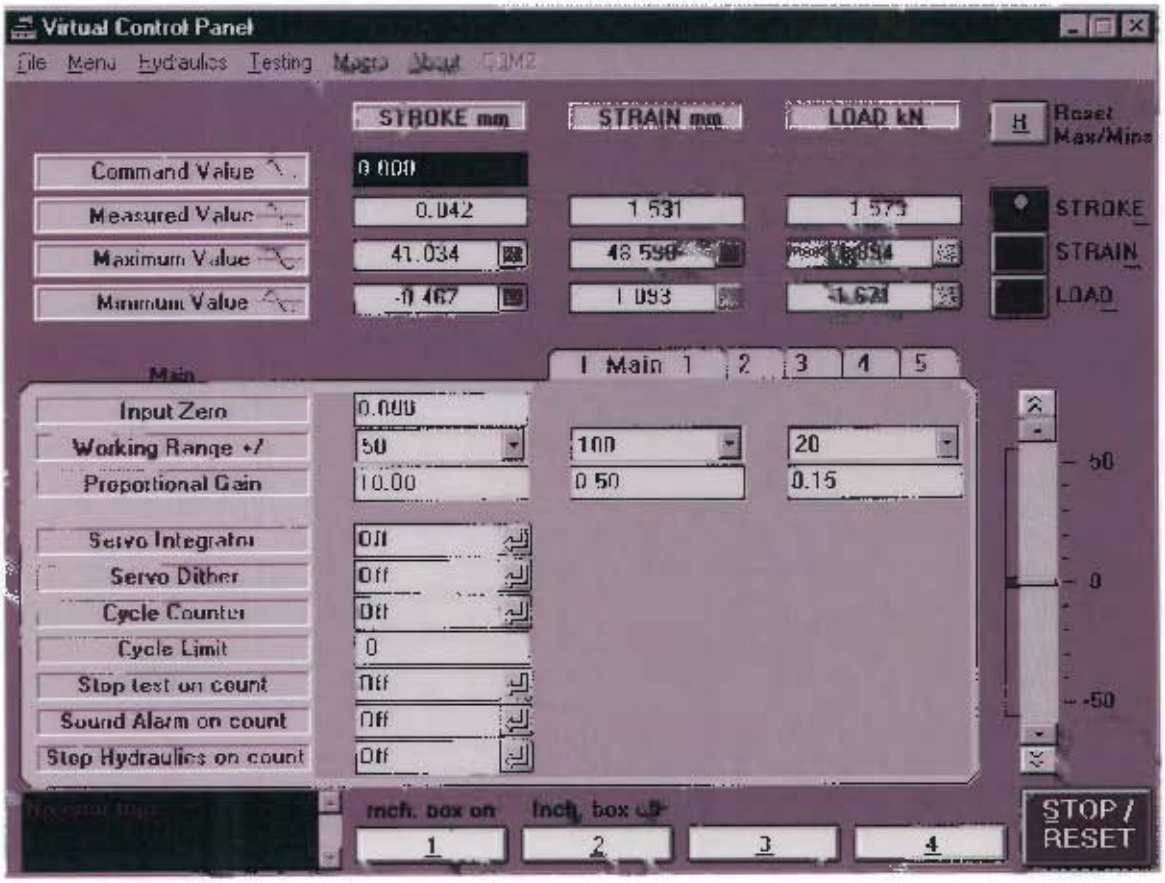

Figure A1.3.2 – The Virtual Control Panel

- Note: with the set of grips described in §A1.1, the optimal position of the crosshead is such that when the stroke command value is set to zero, the specimen can be positioned in the grips with minimal adjustment and the furnace can enclose the specimen centrally. As the customised tensile tests are all set up with a target level that moves relative to the initial position of the crosshead, it is necessary to ensure that the stroke command value is set to zero prior to each and every test.

- Once the Virtual Control Panel has successfully started up, the Block Run Program can be initiated. From the Start menu select Programs → ESH Programs → Block Run Program, and the screen in figure A1.3.3 should pop up:

Figure A1.3.3 – The Block Run Program

- With reference to the Block Program screen as shown in figure A1.3.3, select the following options:
    - In the Machine Settings block, select the appropriate stroke, strain and load ranges. For the purposes of the tensile tests described here, the ranges selected were 50mm for the stroke, 100mm for the strain and 20kN for the load.
    - In the Program Settings block, click the 'Retrieve Program 1' button and select the customised block program from the directory it was saved in. It is

also possible to name the specimen being tested by filling out the 'Part No' option.

- In the Results block, select an appropriate file name for the test being carried out. The result file will be stored in the default directory (c:\esh\results); however the file can be stored elsewhere by selecting the 'Change File Path' button.
- In the Specimen Details block, fill in either the diameter in mm for circular cross-section specimens or the width and depth in mm for rectangular cross-section specimens.

- Once all the relevant details have been filled out, the test can be started by clicking the 'Run Test' button. The screen in figure A1.3.4 should appear once the button has been clicked:

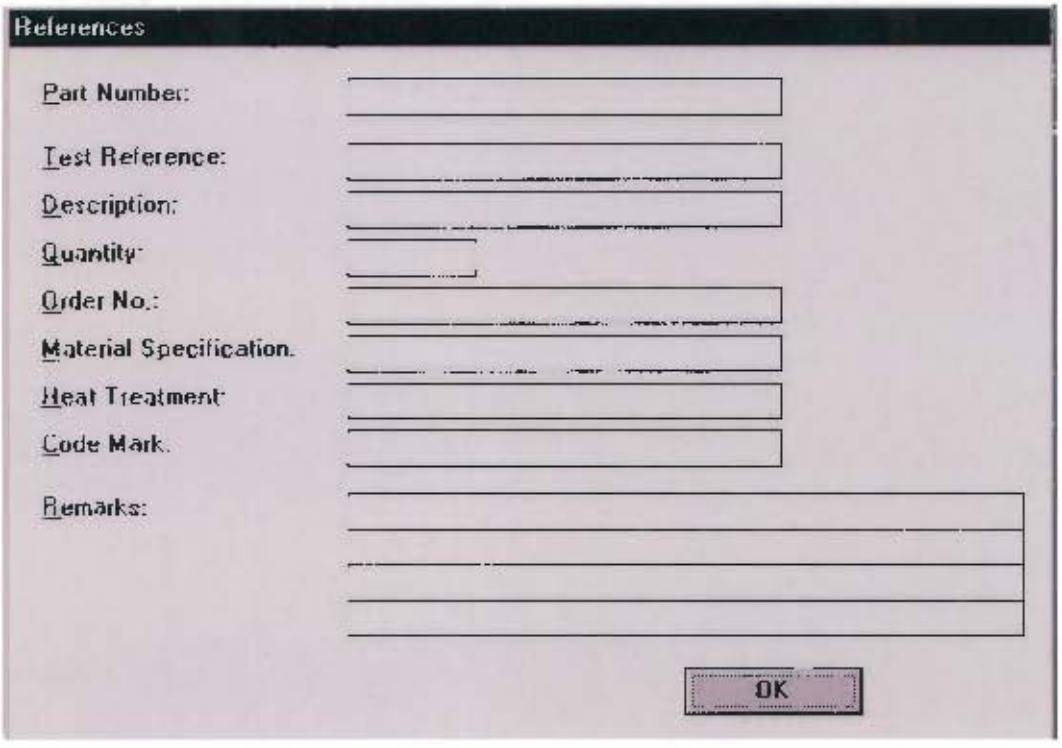

Figure A1.3.4 – References Screen

- Filling out the details on the References screen is optional, though recommended as the information will be stored in the results file. To continue with the test click the 'OK' button. The Specimen Setup screen should appear then, as shown in figure A1.3.5:

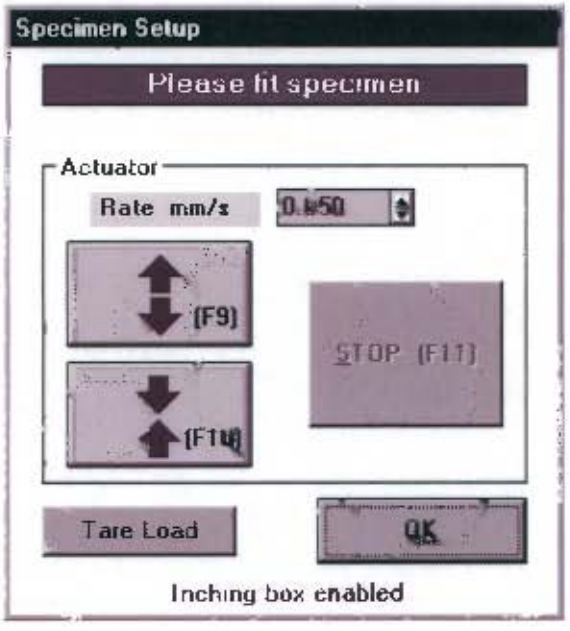

Figure A1.3.5 – Specimen Setup Screen

- While the specimen setup screen is displayed, fit the specimen into the grips and use the Inching Box, depicted in figure A1.3.6, to pretension the specimen slightly prior to commencing the test. If carrying out a high temperature test, please refer to §A1.4 before continuing.

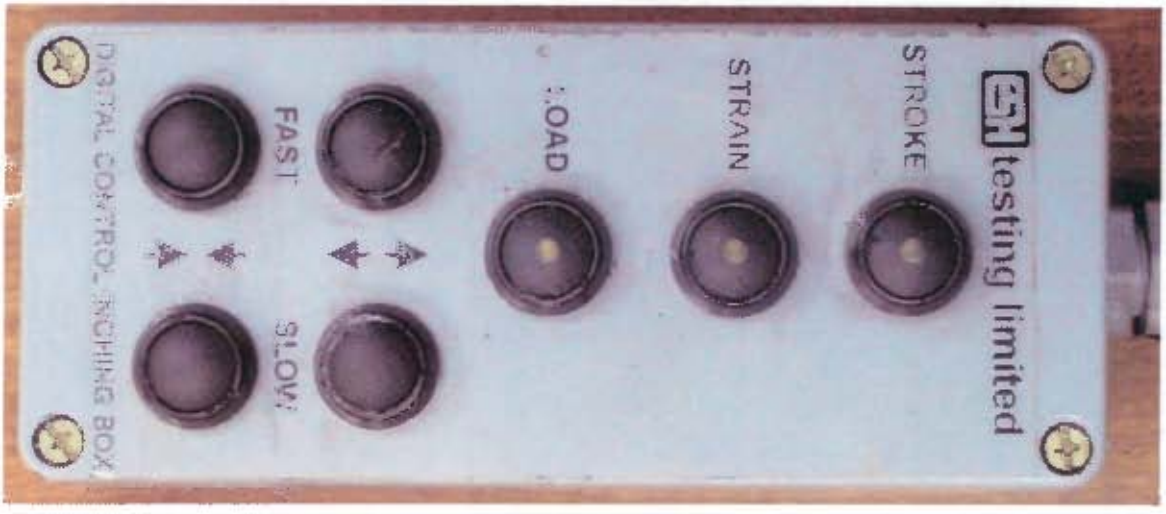

Figure A1.3.6 – Inching Box

- Once the specimen is in place, click the 'Tare Load' button, which effectively brings the load on the specimen as close to zero as possible. Then click the 'OK' button to continue. The Ready screen should then appear accompanied with the Feedbacks window, as shown in figure A1.3.7:

Figure A1.3.7 – Ready Screen and Feedbacks Window

- The Feedbacks window gives the absolute position of the hydraulic actuator, the measured strain, applied load and temperature. To commence the test, click on the 'Start Test' button. Once this is done, the test will begin and the progress of the test will be depicted as shown in figure A1.3.8:

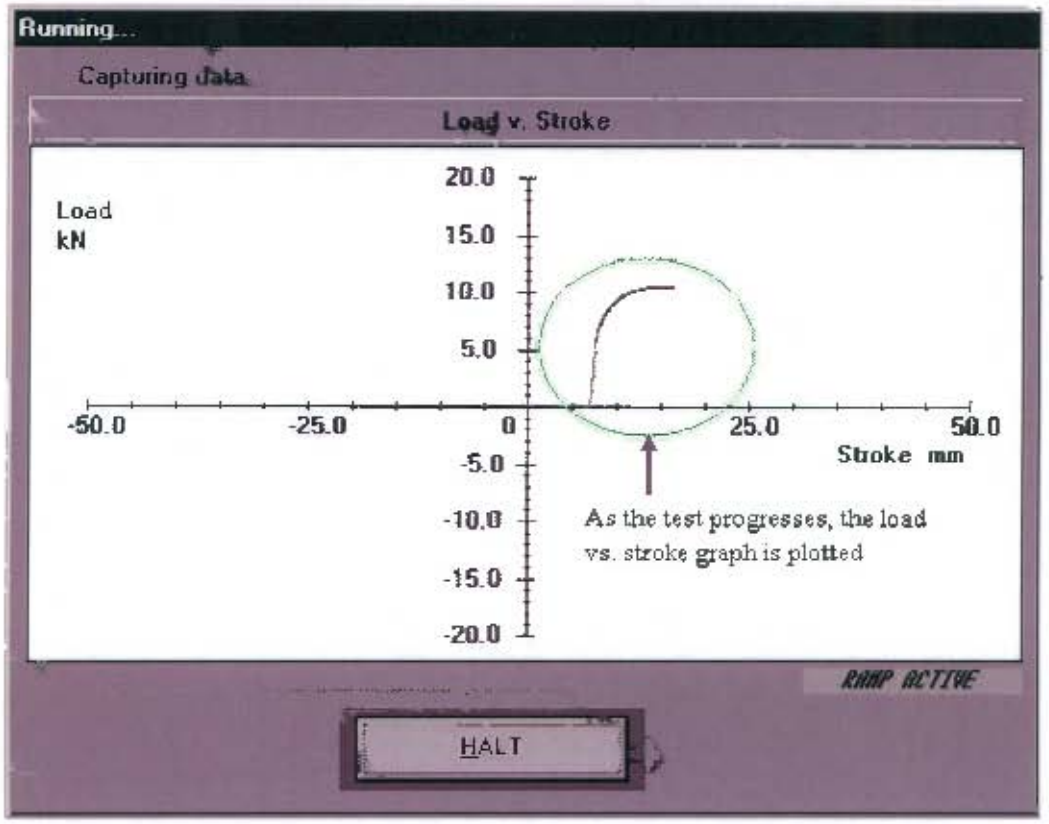

Figure A1.3.8 – Tensile Test in Progress

- Once the specimen breaks, the final graph can be zoomed and viewed and thereafter an option is available to print the graph to an attached printer if any is present. The specimen can then be removed and the process repeated to carry out another test.

A1.4. Using the Furnace

This section outlines using the furnace when carrying out high temperature tensile tests. As per §A1.3, once the Specimen Setup screen depicted in figure A1.3.5 is reached, the following should be done:

- A K-type thermocouple should be attached to the midpoint of the test specimen. The thermocouple should also be attached to the Eurotherm® 2408 controller.

- Fit the specimen into the grips and use the inching box to pretension the specimen.
- Ensure that the specimen is aligned vertically with the axis of the grips. Once the specimen is aligned and pre-tensioned, tare the load using the Specimen Setup screen (figure A1.3.5). Figure A1.4.1 shows the specimen positioned in place:

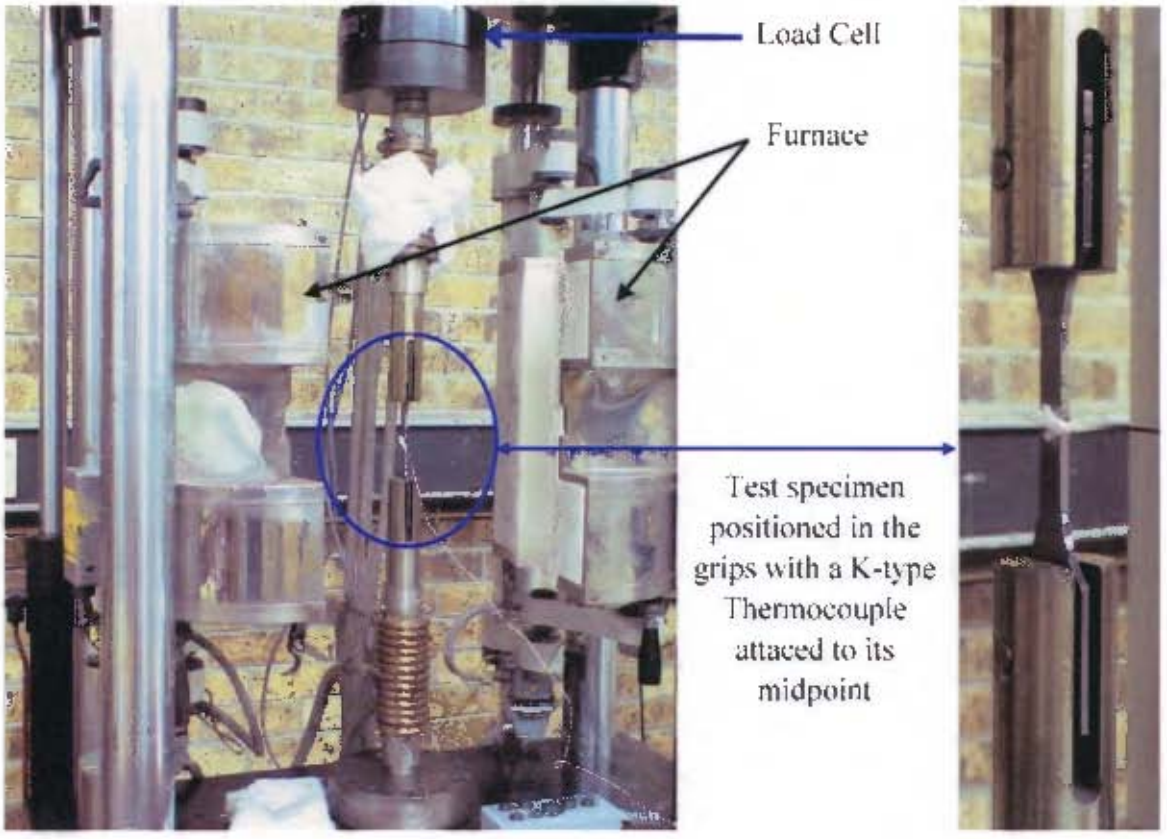

Figure A1.4.1 – Positioned Tensile Specimen

- Close the furnace over the specimen and insulate the top end of the furnace with Fibre Fax. Note: Fibre Fax is a material normally used in kilns for insulation purposes. This step is essential to protect the load cell of the ESH machine.

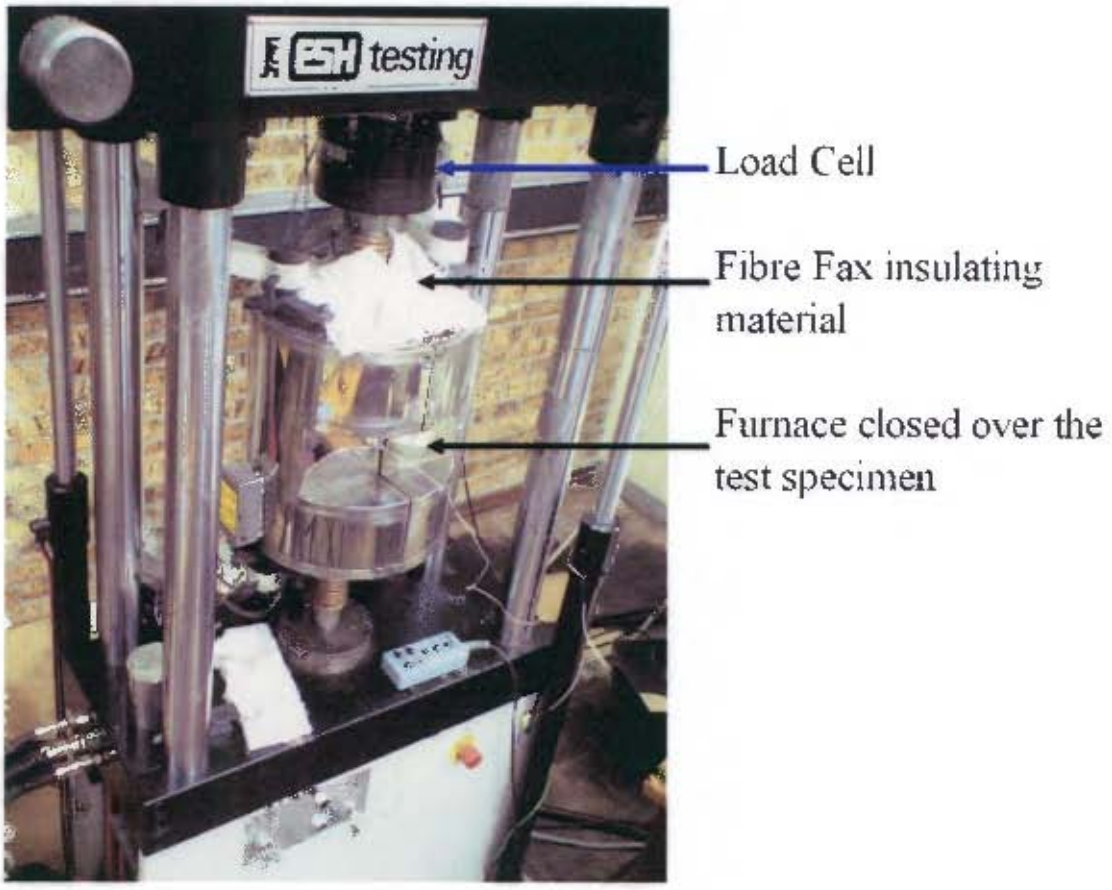

Figure A1.4.2 – Furnace Insulated with Fibre Fax

- Ensure that the cooling water is running prior to starting the furnace.
- Once the cooling water is running through the coils, use the Eurotherm© 2408 controller to set the desired temperature to which the specimen must be heated. Figure A1.4.3. shows the measured temperature at 18°C and the test temperature set at 300°C:

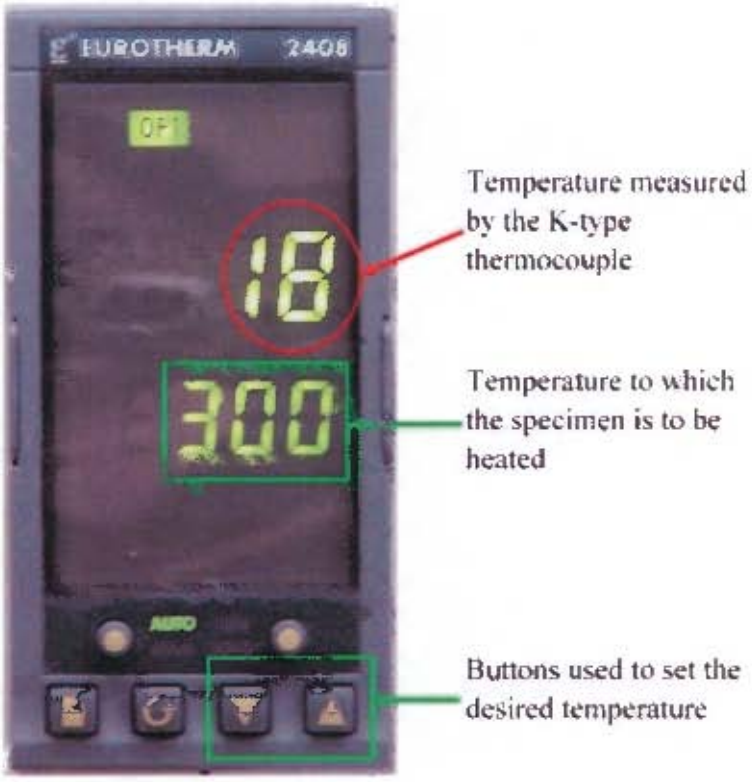

Figure A1.4.3 – Setting the Test Temperature

- Once the desired temperature has been set, use the control knobs (as shown in figure A1.4.4) to start the heating process. Heating in the furnace is divided into three zones namely top, centre and bottom and each is controlled with a separate control knob. For the purposes of the high temperature tensile tests, all control knobs should be turned up to maximum.

Figure A1.4.4 – Furnace Temperature Controls

- Wait till the specimen reaches the desired temperature (i.e. the measured temperature value coincides with the set temperature value). Once the specimen is at temperature, click the 'OK' button on the Specimen Setup screen (figure A1.3.5). If necessary, tare the load once more prior to clicking the 'OK' button. Thereafter, click the 'Start Test' button on the Ready screen (figure A1.3.7) to commence the test.
- Once the test is completed, care should be taken when handling the specimen as it will still be very hot.
- When the high temperature tests are concluded, wait till the grips cool down to at least 50°C before turning the cooling water off. (Use the K-type thermocouple and Eurotherm© 2408 controller to monitor the grip temperature during the cooling down process)

A2. TEST RESULTS

Tensile tests were carried out at temperatures ranging from room temperature to 600°C using the following strain rates:

- $4.17\times10^{-4}s^{-1}$
- $3.33\times10^{-3}s^{-1}$
- $1.67\times10^{-2}s^{-1}$
- $1\times10^{-1}s^{-1}$

This appendix presents the tensile test results in the form of engineering stress verses engineering strain curves. The curves were obtained via processing the result files in a spreadsheet program. In this case, Microsoft Excel® was used. The engineering stress verses engineering strain curves are presented as depicted in figure A2.1:

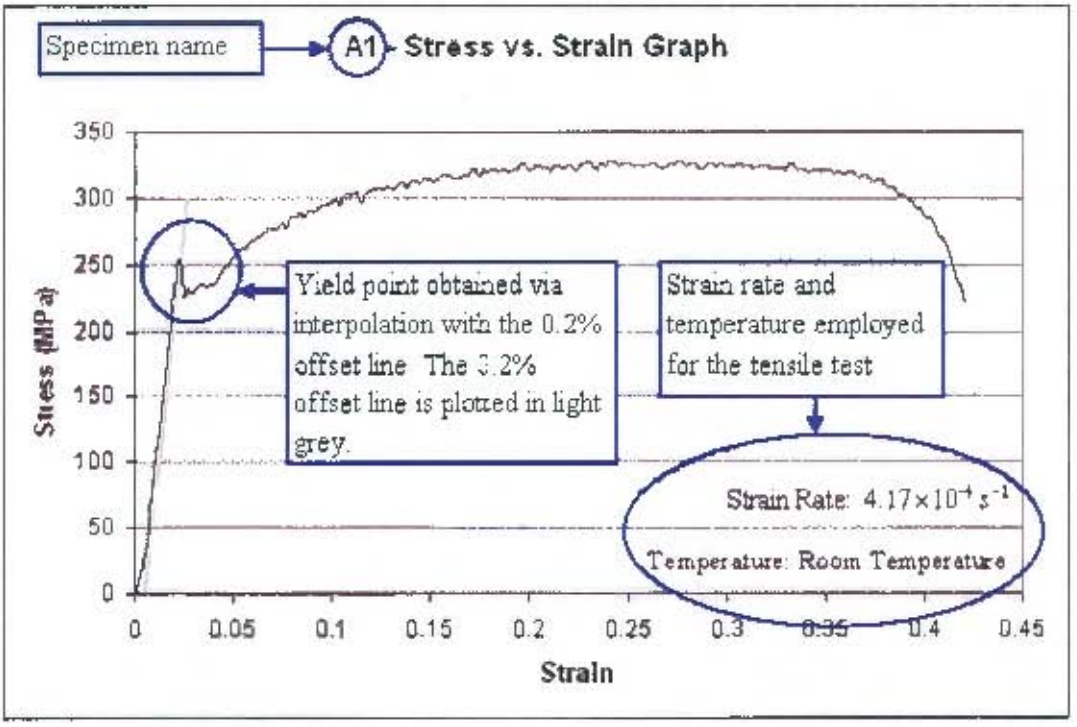

Figure A2.1 – Generic Test Result

A2.1. Test Results at a Strain Rate of: 4.17 x $10^{-4}s^{-1}$

A total of 18 tests were carried out at a strain rate of $4.17\times10^{-4}s^{-1}$. Table A2.1.1 outlines the tests carried out and the graphed results follow the table.

Table A2.1.1 – Tensile Tests Carried Out at $4.17\times10^{-4}s^{-1}$

Specimen Name	Cross Section Details of Gauge Length			Temperature (°C)
	Width (mm)	Thickness (mm)	Area (mm^2)	
A1	12.56	3.00	37.68	25
A2	12.70	3.00	38.10	25
S1	12.58	3.00	37.74	25
NA1	12.72	3.00	38.16	100
NA2	12.66	3.00	37.98	100
NA3	12.22	3.00	36.66	100
BINEW	12.40	3.00	37.20	200
B2	12.56	3.00	37.68	200
S2	12.64	3.00	37.92	200
C1	12.66	3.00	37.98	300
C2	12.56	3.00	37.68	300
S3	12.68	3.00	38.04	300
D1	12.70	3.00	38.10	450
S4	12.68	3.00	38.04	450
T1	12.54	3.00	37.62	450
U1	12.38	3.00	37.14	600
U2	12.58	3.00	37.74	600
U3	12.56	3.00	37.68	600

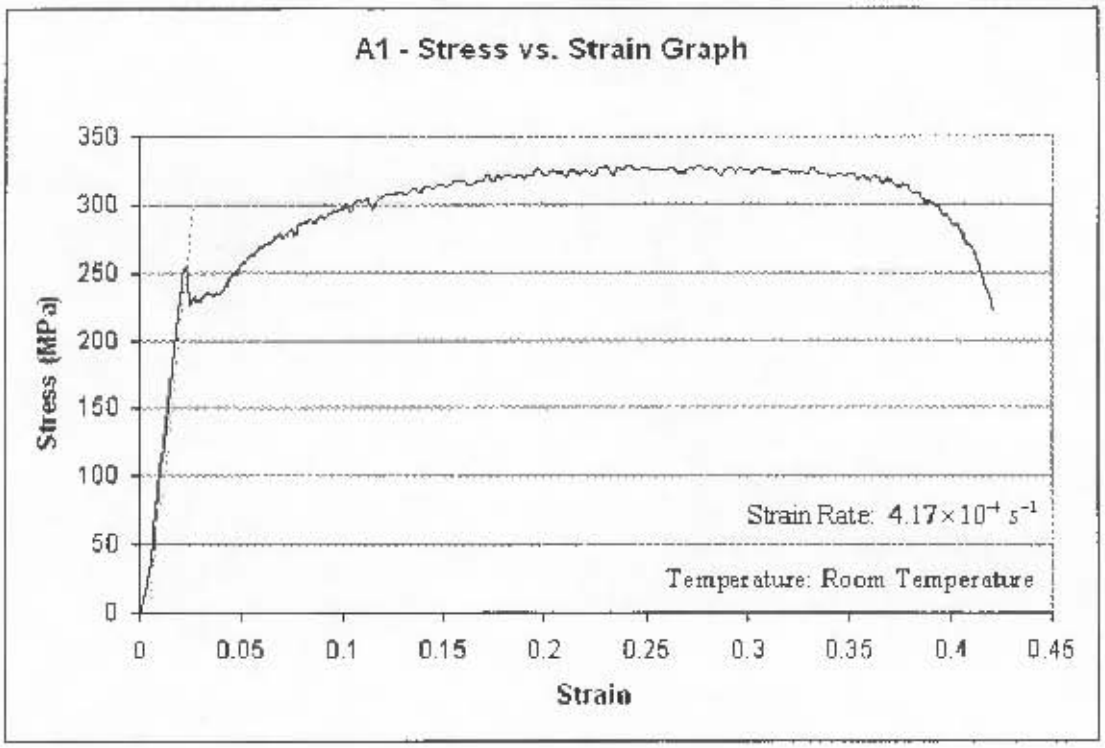

Figure A2.1.1 – Test Result for Specimen A1

Table A2.1.1 – Yield Stress and Failure Strain for Specimen A1

Yield Stress (MPa)	247.89
Ultimate Tensile Stress (MPa)	328.08
Gauge Length at Failure (mm)	83.0
Elongation of Gauge Length at Failure (mm)	23.0
Strain at failure (%)	38.33

Note: The ultimate tensile stress reported here refers to the maximum stress recorded as per the engineering stress vs. engineering strain graph. It does not refer to the true stress experienced at failure. This applies to all the test results at a strain rate of $4.17\times10^{-4}s^{-1}$.

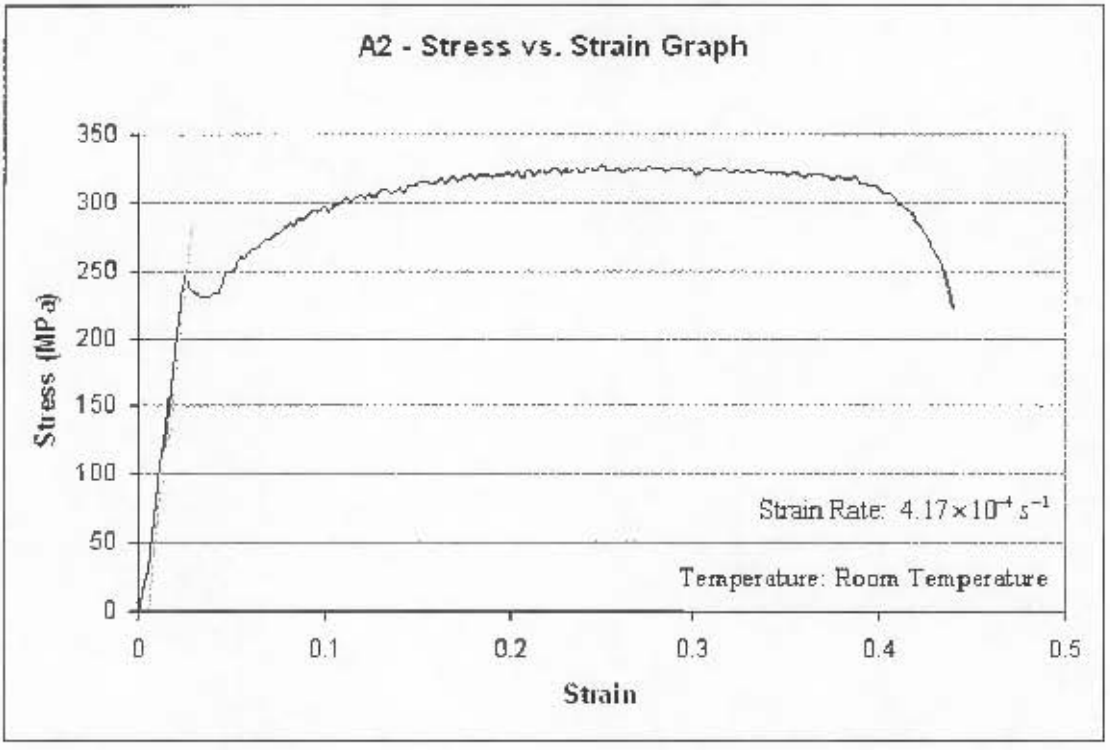

Figure A2.1.2 – Test Result for Specimen A2

Table A2.1.2 – Yield Stress and Failure Strain for Specimen A2

Yield Stress (MPa)	243.47
Ultimate Tensile Stress (MPa)	327.24
Gauge Length at Failure (mm)	84.4
Elongation of Gauge Length at Failure (mm)	24.4
Strain at failure (%)	40.67

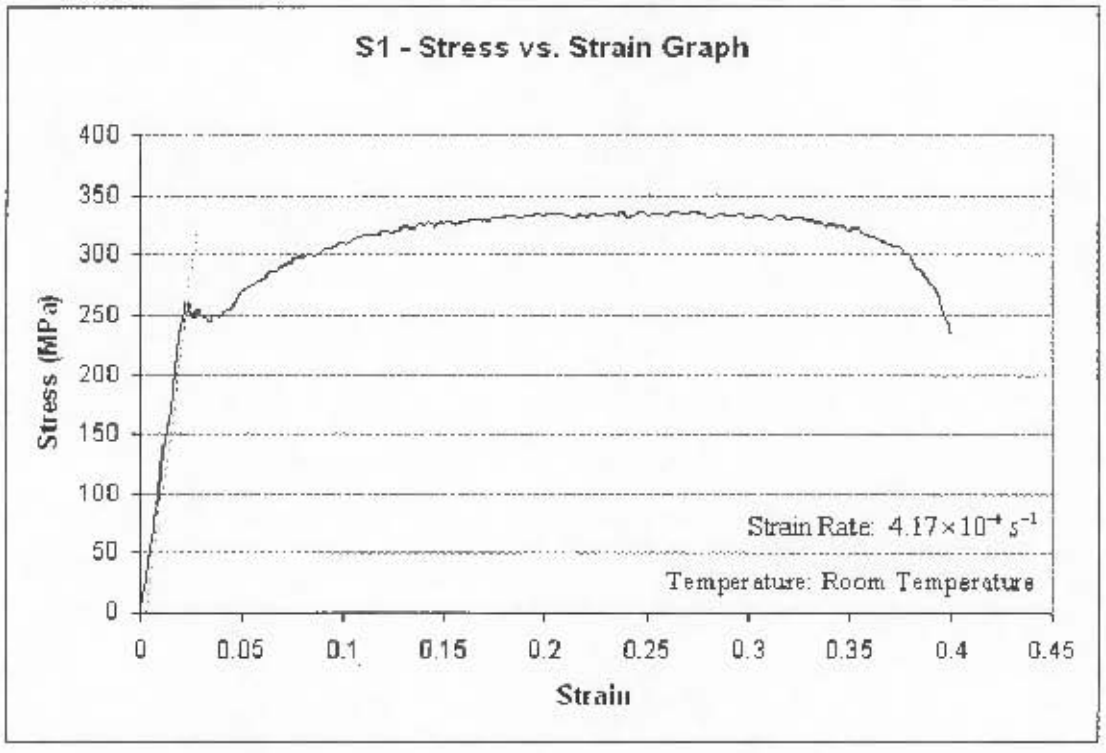

Figure A2.1.3 – Test Result for Specimen S1

Table A2.1.3 – Yield Stress and Failure Strain for Specimen S1

Yield Stress (MPa)	261.16
Ultimate Tensile Stress (MPa)	336.09
Gauge Length at Failure (mm)	81.8
Elongation of Gauge Length at Failure (mm)	21.8
Strain at failure (%)	36.33

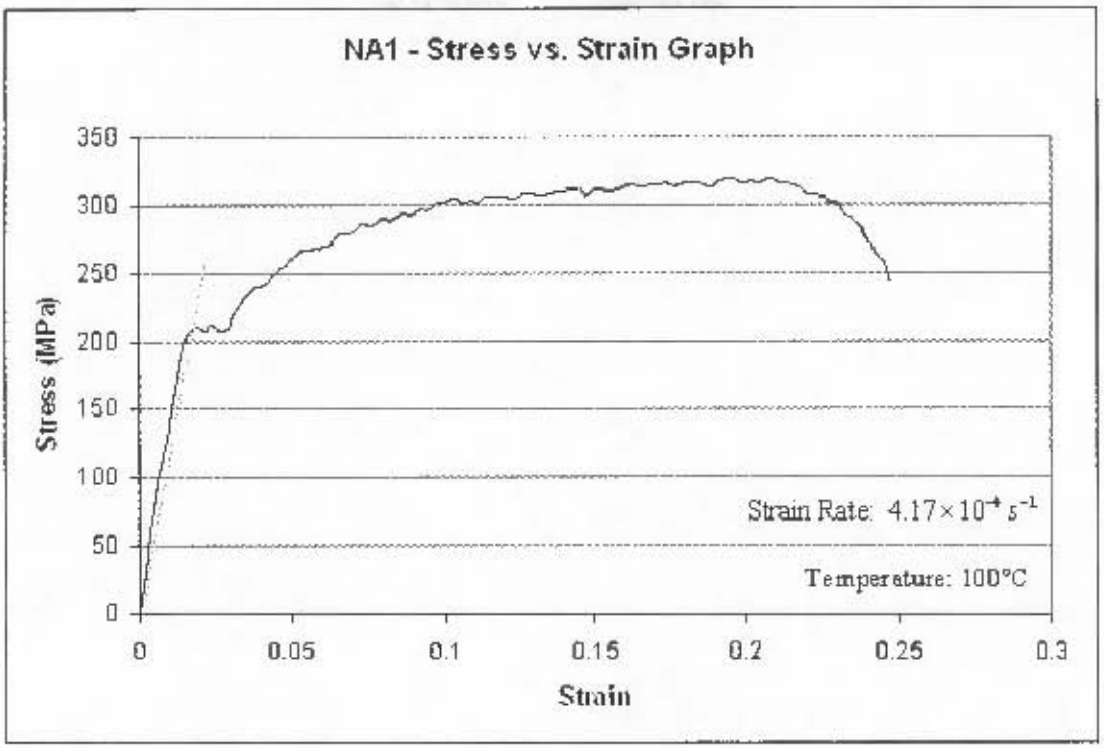

Figure A2.1.4 – Test Result for Specimen NA1

Table A2.1.4 Yield Stress and Failure Strain for Specimen NA1

Yield Stress (MPa)	208.90
Ultimate Tensile Stress (MPa)	319.42
Gauge Length at Failure (mm)	73.8
Elongation of Gauge Length at Failure (mm)	13.8
Strain at failure (%)	23.00

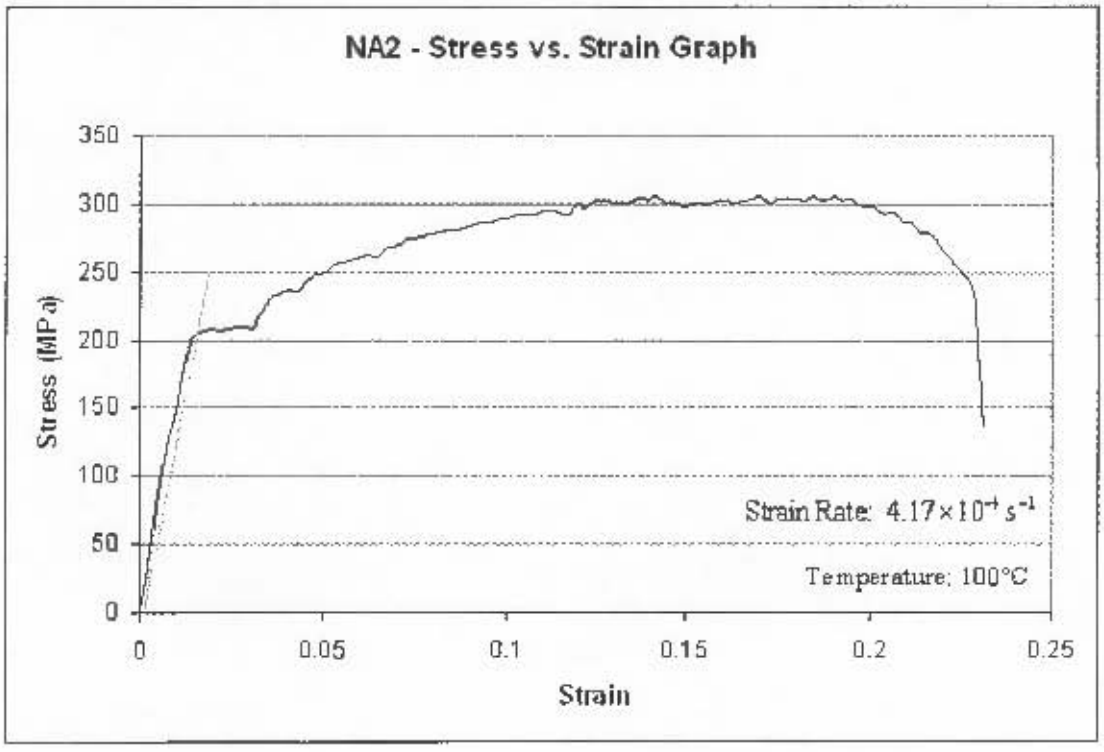

Figure A2.1.5 – Test Result for Specimen NA2

Table A2.1.5 – Yield Stress and Failure Strain for Specimen NA2

Yield Stress (MPa)	204.16
Ultimate Tensile Stress (MPa)	306.32
Gauge Length at Failure (mm)	72.5
Elongation of Gauge Length at Failure (mm)	12.5
Strain at failure (%)	20.83

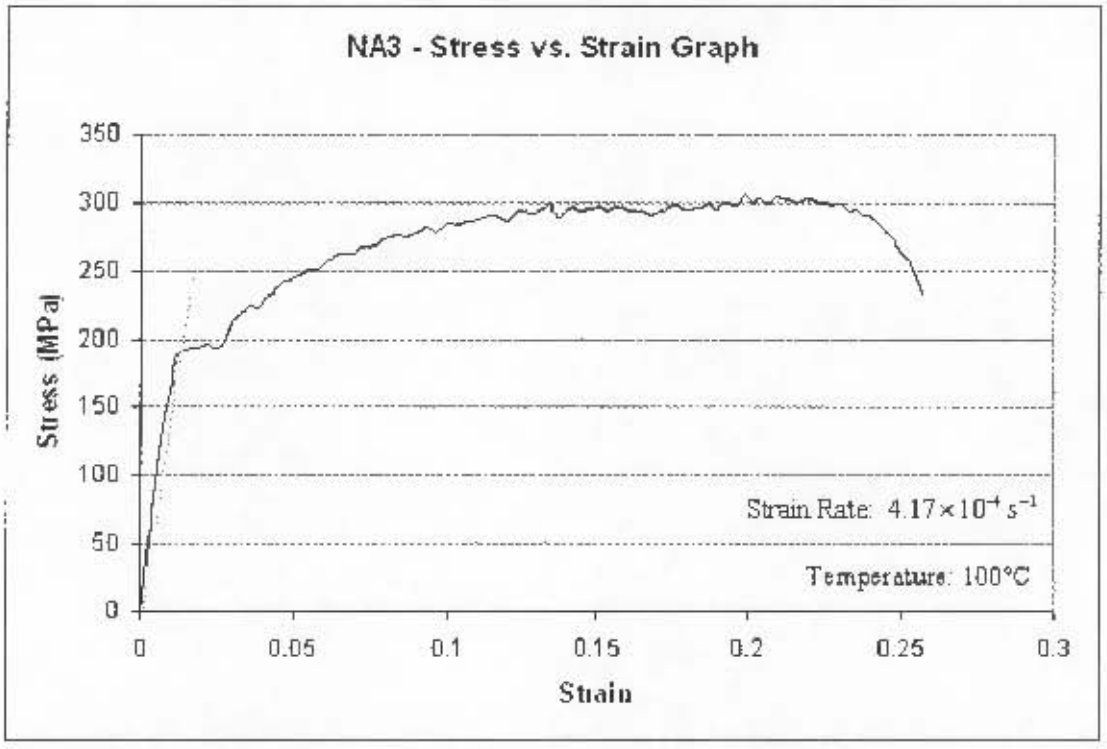

Figure A2.1.6 – Test Result for Specimen NA3

Table A2.1.6 – Yield Stress and Failure Strain for Specimen NA3

Yield Stress (MPa)	190.93
Ultimate Tensile Stress (MPa)	305.29
Gauge Length at Failure (mm)	74.5
Elongation of Gauge Length at Failure (mm)	14.5
Strain at failure (%)	24.17

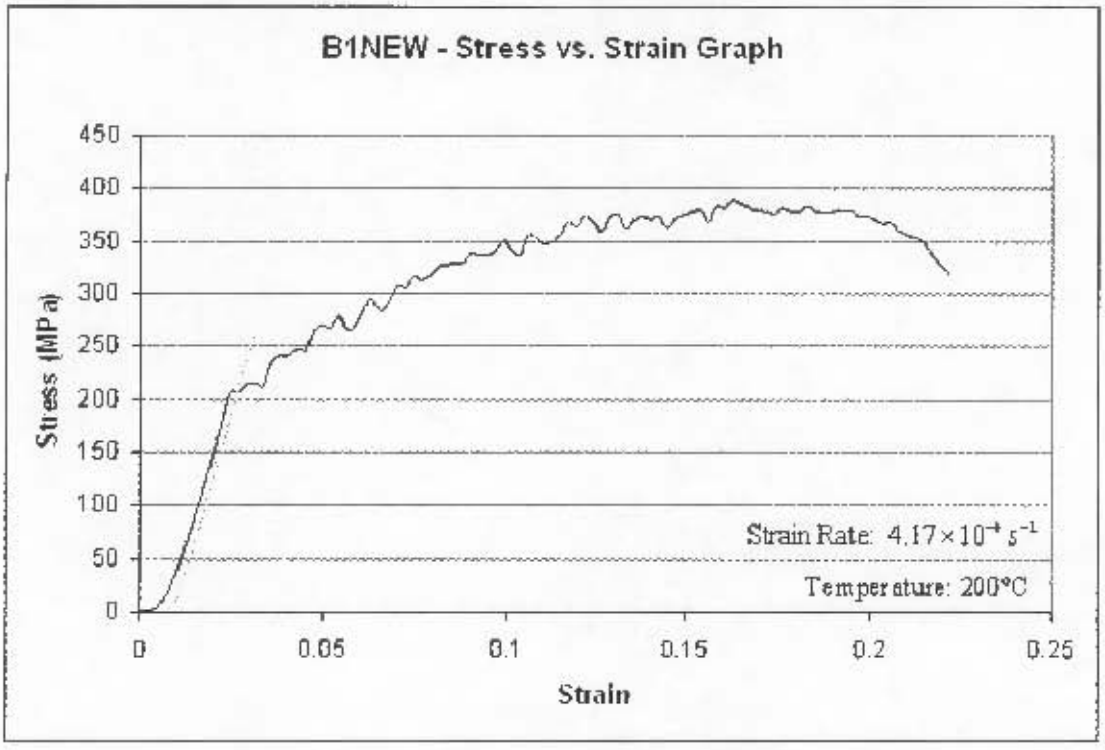

Figure A2.1.7 – Test Result for Specimen B1NEW

Table A2.1.7 – Yield Stress and Failure Strain for Specimen B1NEW

Yield Stress (MPa)	206.61
Ultimate Tensile Stress (MPa)	388.58
Gauge Length at Failure (mm)	71.1
Elongation of Gauge Length at Failure (mm)	11.1
Strain at failure (%)	18.50

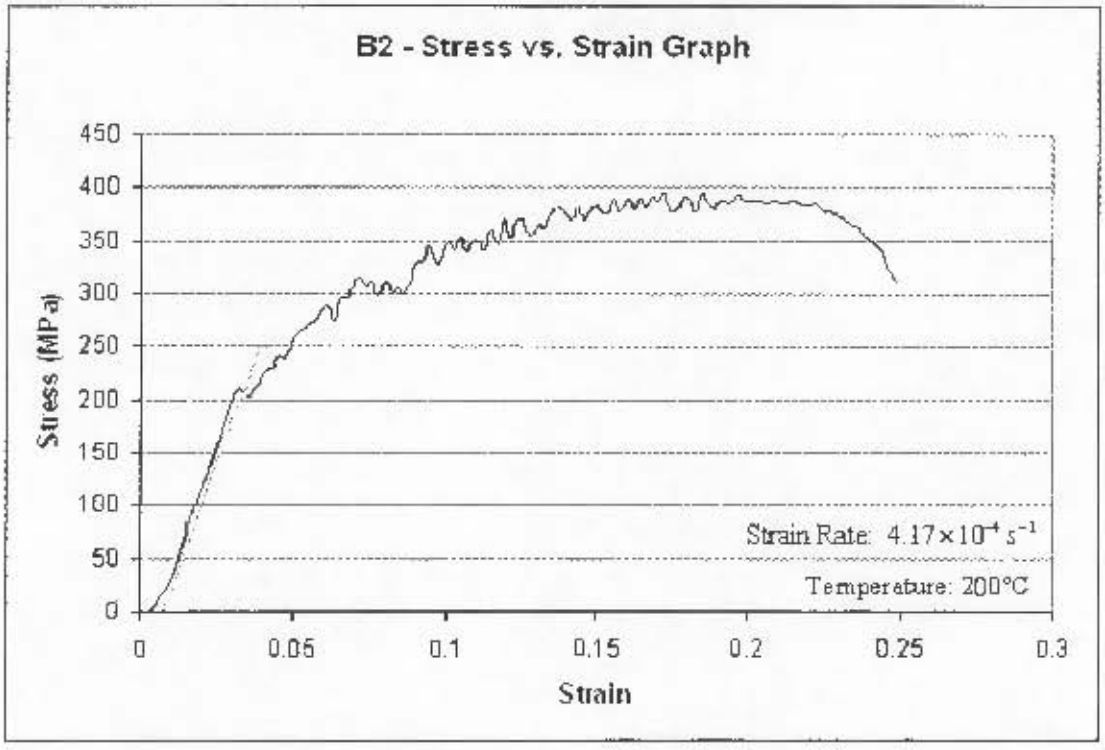

Figure A2.1.8 – Test Result for Specimen B2

Table A2.1.8 – Yield Stress and Failure Strain for Specimen B2

Yield Stress (MPa)	207.86
Ultimate Tensile Stress (MPa)	395.41
Gauge Length at Failure (mm)	71.5
Elongation of Gauge Length at Failure (mm)	11.5
Strain at failure (%)	19.17

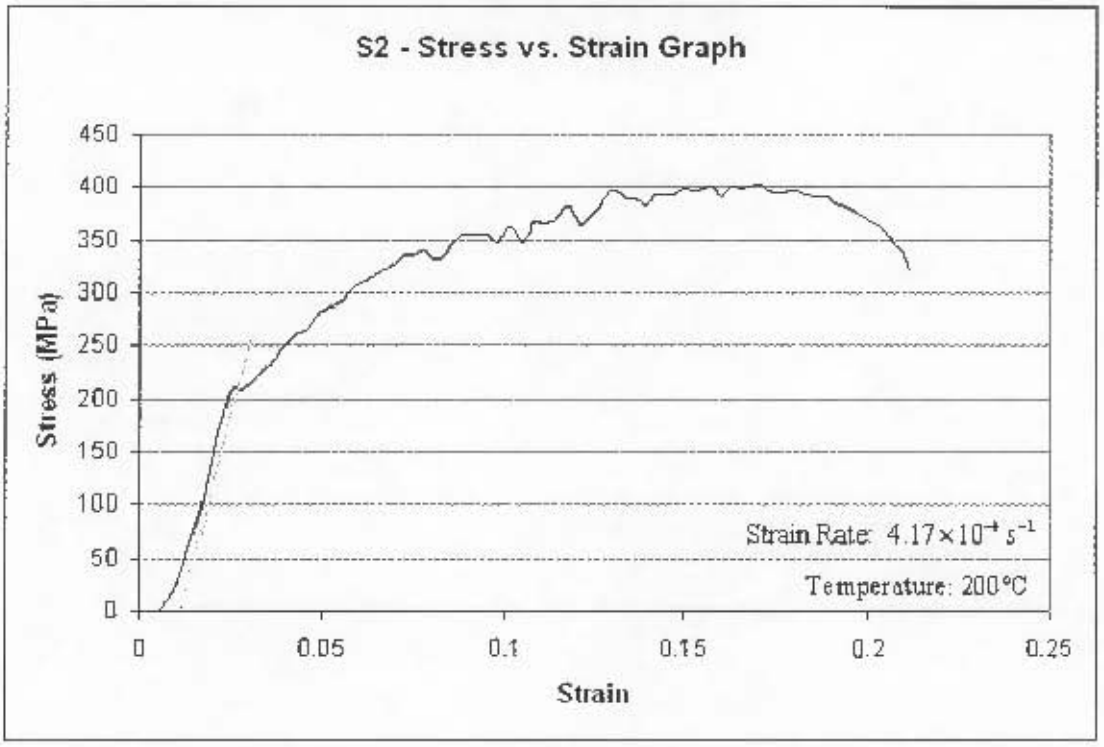

Figure A2.1.9 – Test Result for Specimen S2

Table A2.1.9 – Yield Stress and Failure Strain for Specimen S2

Yield Stress (MPa)	208.73
Ultimate Tensile Stress (MPa)	401.69
Gauge Length at Failure (mm)	70.7
Elongation of Gauge Length at Failure (mm)	10.7
Strain at failure (%)	17.83

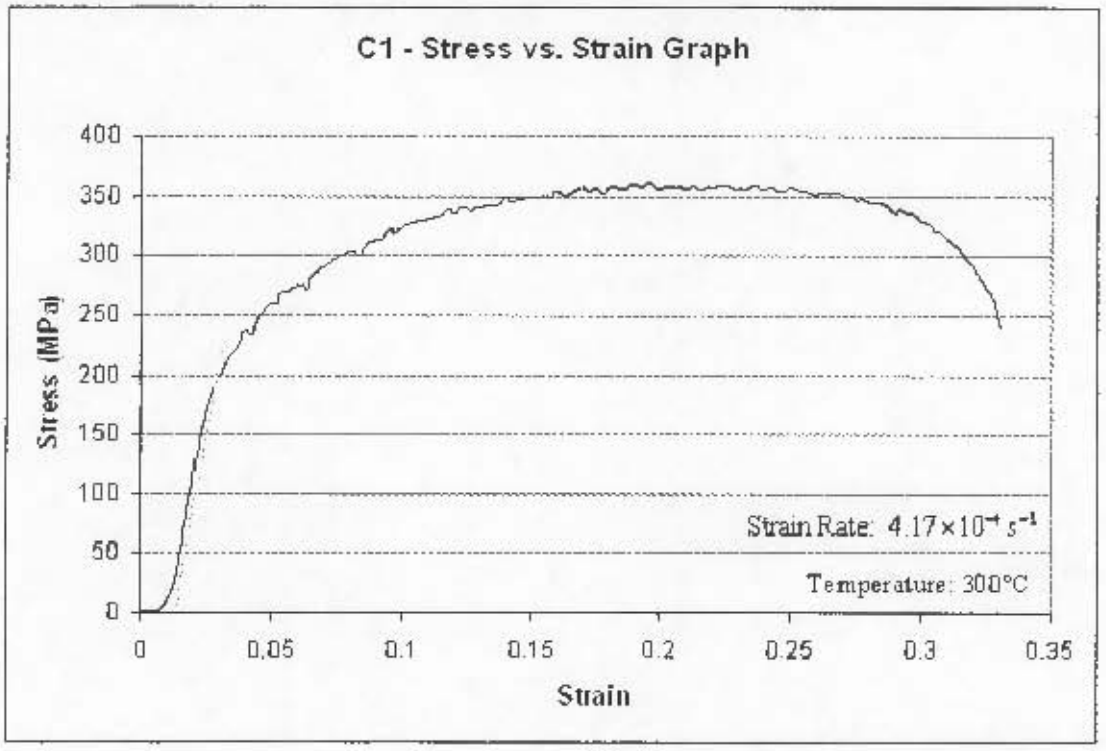

Figure A2.1.10 – Test Result for Specimen C1

Table A2.1.10 – Yield Stress and Failure Strain for Specimen C1

Yield Stress (MPa)	190.81
Ultimate Tensile Stress (MPa)	361.51
Gauge Length at Failure (mm)	76.2
Elongation of Gauge Length at Failure (mm)	16.2
Strain at failure (%)	27.00

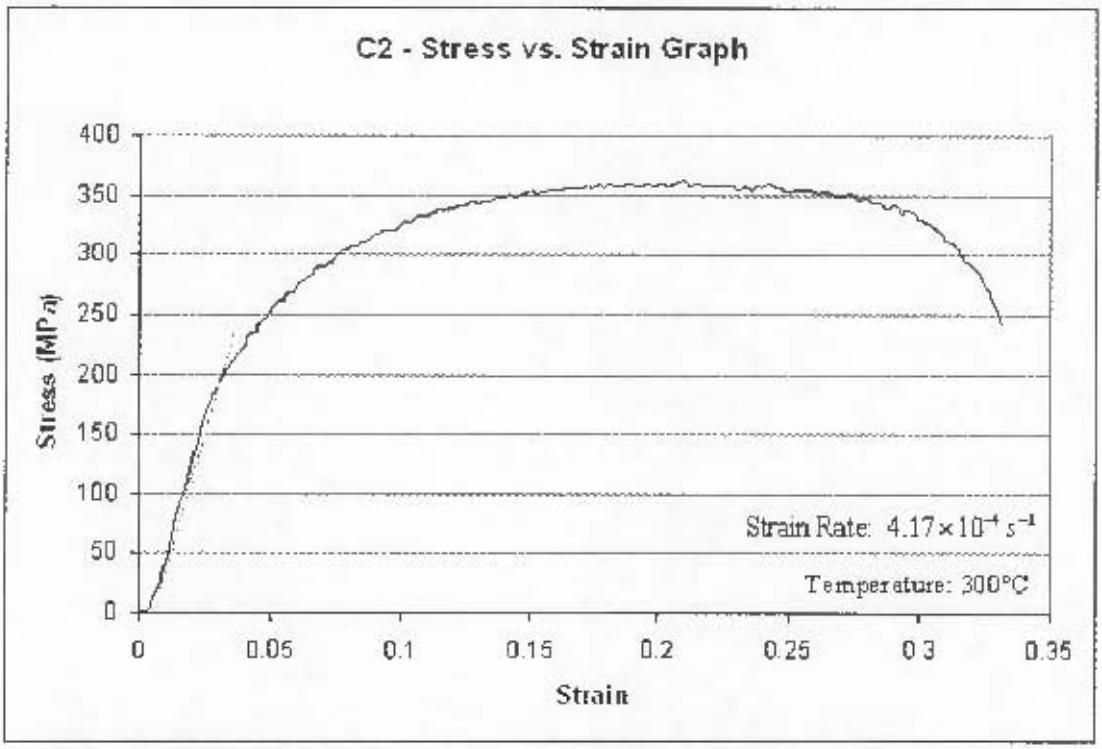

Figure A2.1.11 – Test Result for Specimen C2

Table A2.1.11 – Yield Stress and Failure Strain for Specimen C2

Yield Stress (MPa)	190.30
Ultimate Tensile Stress (MPa)	362.69
Gauge Length at Failure (mm)	77.1
Elongation of Gauge Length at Failure (mm)	17.1
Strain at failure (%)	28.50

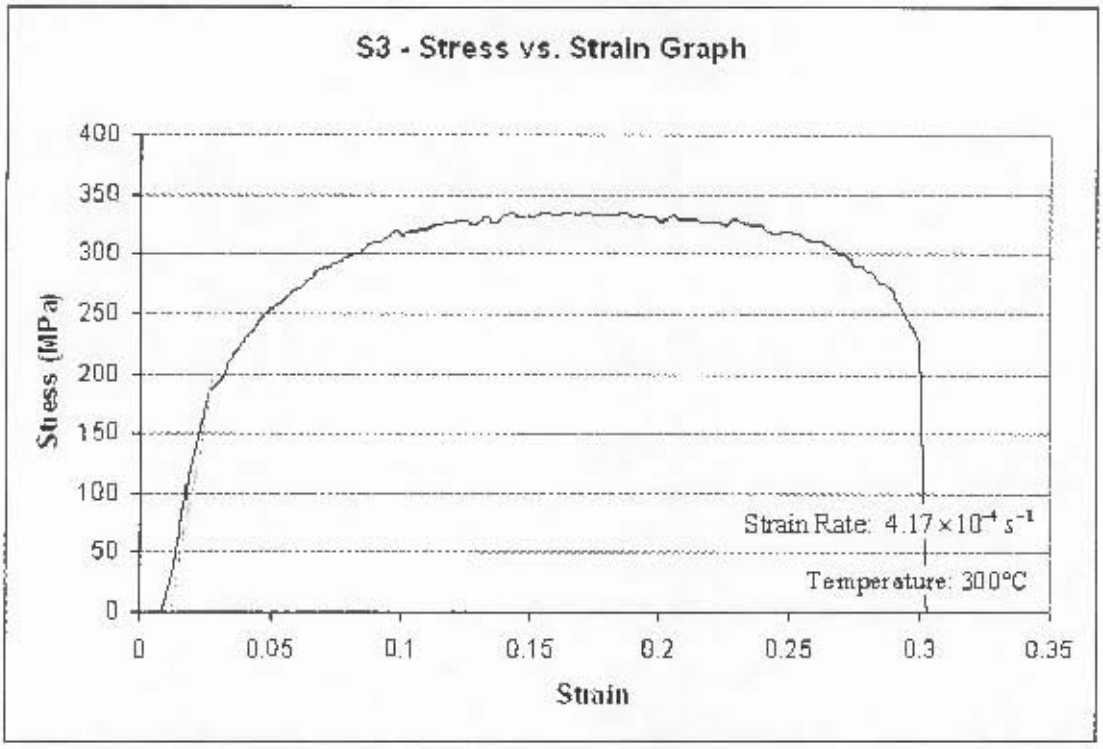

Figure A2.1.12 – Test Result for Specimen S3

Table A2.1.12 Yield Stress and Failure Strain for Specimen S3

Yield Stress (MPa)	183.10
Ultimate Tensile Stress (MPa)	334.41
Gauge Length at Failure (mm)	75.4
Elongation of Gauge Length at Failure (mm)	15.4
Strain at failure (%)	25.67

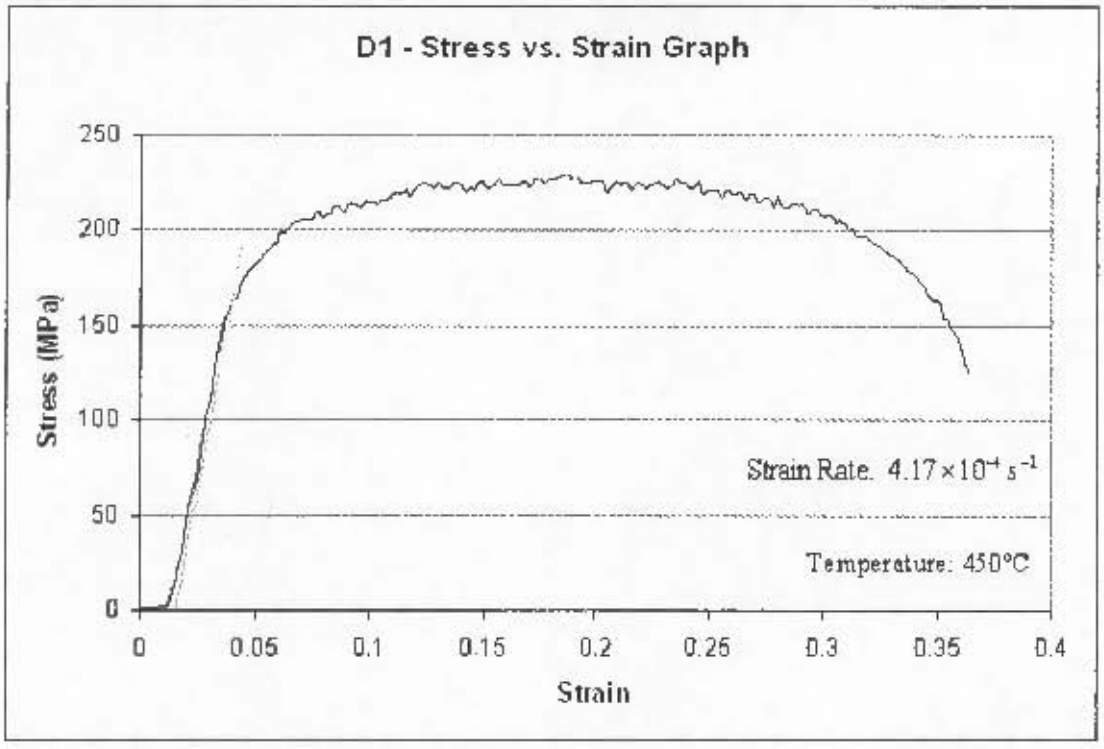

Figure A2.1.13 – Test Result for Specimen D1

Table A2.1.13 – Yield Stress and Failure Strain for Specimen D1

Yield Stress (MPa)	164.82
Ultimate Tensile Stress (MPa)	229.32
Gauge Length at Failure (mm)	79.6
Elongation of Gauge Length at Failure (mm)	19.6
Strain at failure (%)	32.67

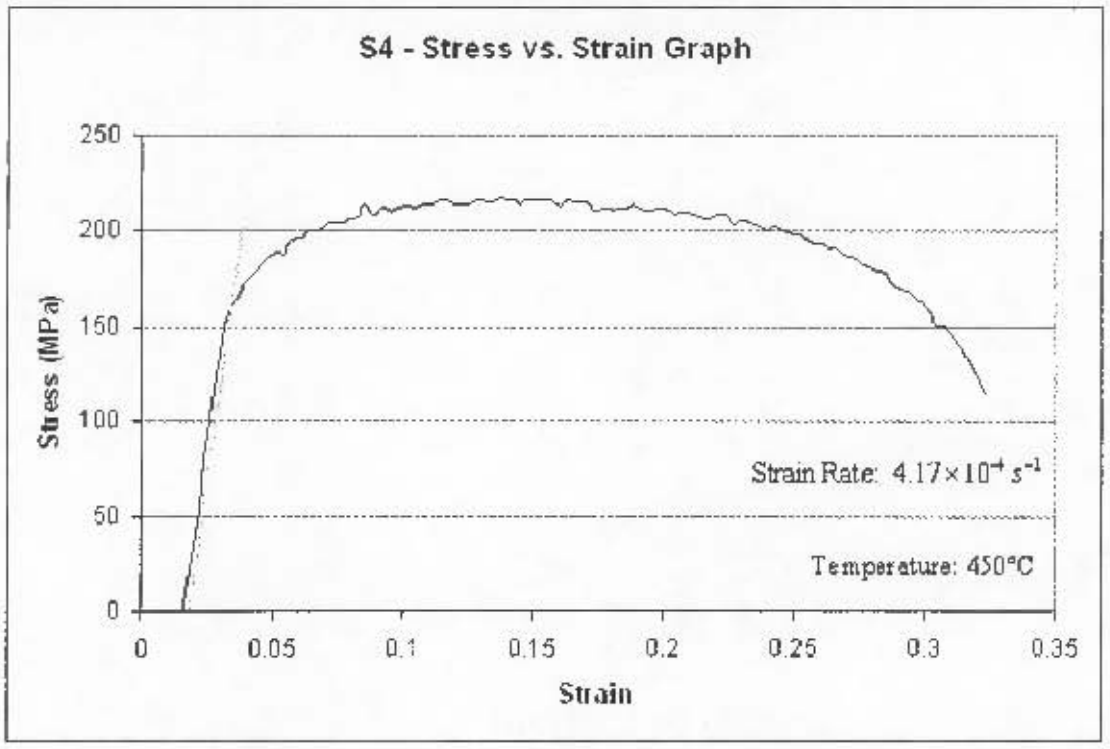

Figure A2.1.14 – Test Result for Specimen S4

Table A2.1.14 – Yield Stress and Failure Strain for Specimen S4

Yield Stress (MPa)	159.29
Ultimate Tensile Stress (MPa)	216.96
Gauge Length at Failure (mm)	77.8
Elongation of Gauge Length at Failure (mm)	17.8
Strain at failure (%)	29.67

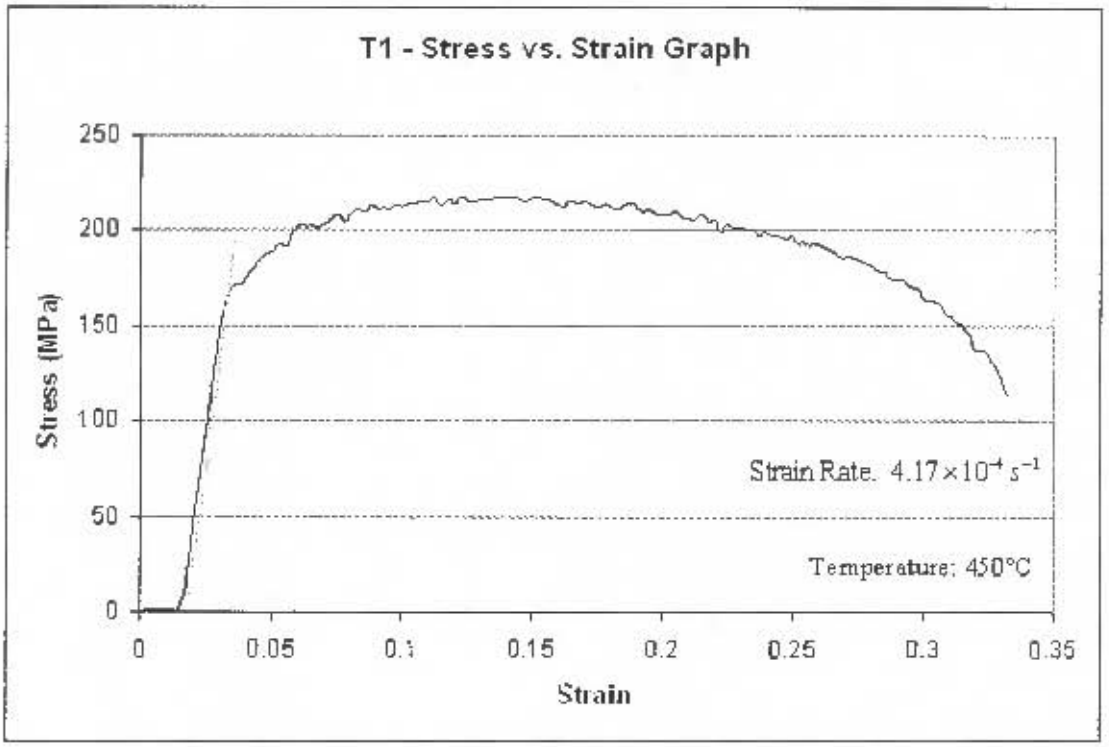

Figure A2.1.15 – Test Result for Specimen T1

Table A2.1.15 – Yield Stress and Failure Strain for Specimen T1

Yield Stress (MPa)	163.10
Ultimate Tensile Stress (MPa)	217.78
Gauge Length at Failure (mm)	78.3
Elongation of Gauge Length at Failure (mm)	18.3
Strain at failure (%)	30.50

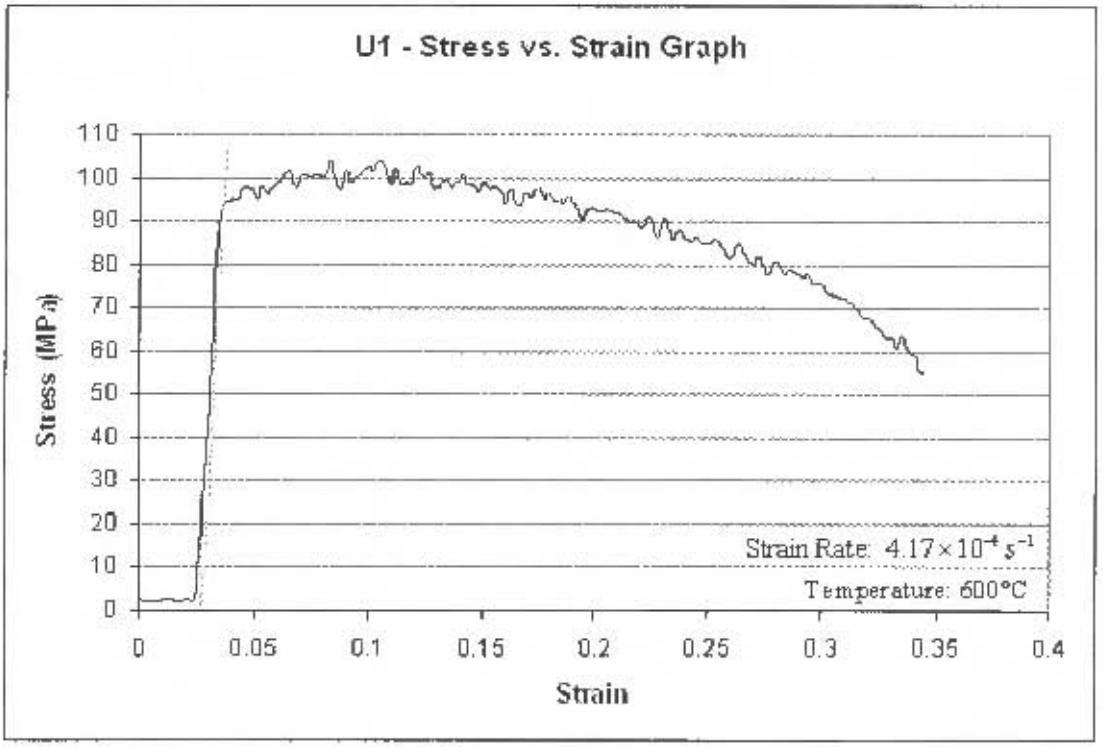

Figure A2.1.16 – Test Result for Specimen U1

Table A2.1.16 – Yield Stress and Failure Strain for Specimen U1

Yield Stress (MPa)	93.90
Ultimate Tensile Stress (MPa)	103.90
Gauge Length at Failure (mm)	79.2
Elongation of Gauge Length at Failure (mm)	19.2
Strain at failure (%)	32.00

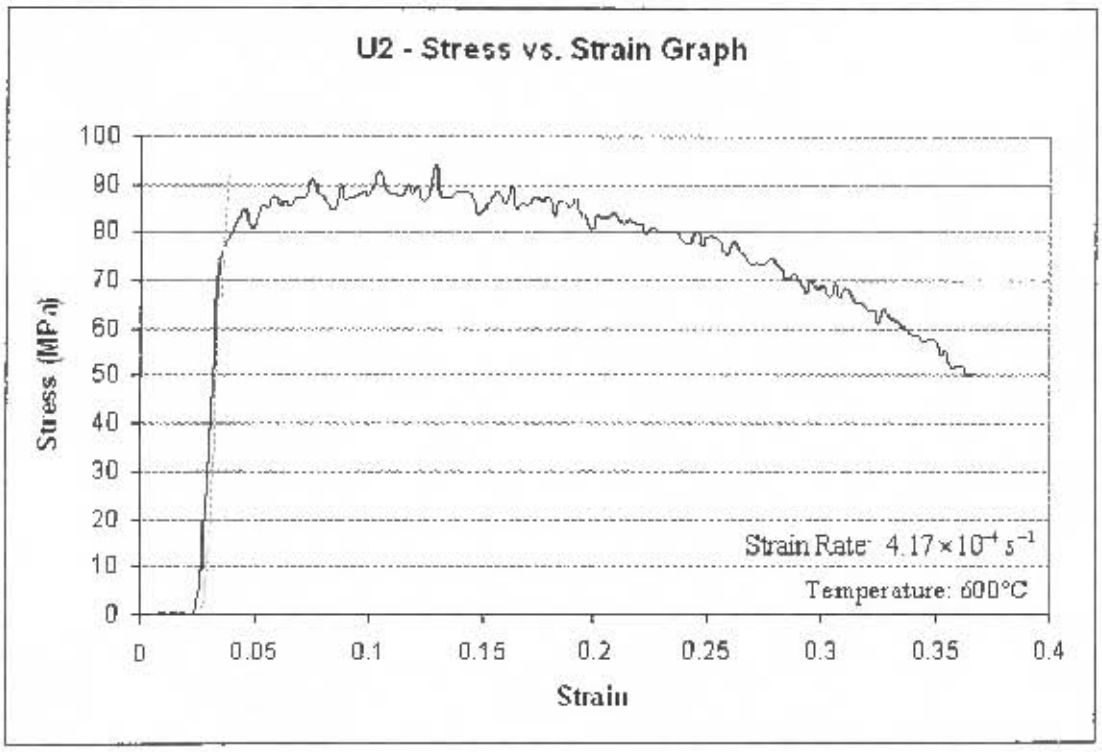

Figure A2.1.17 – Test Result for Specimen U2

Table A2.1.17 – Yield Stress and Failure Strain for Specimen U2

Yield Stress (MPa)	76.80
Ultimate Tensile Stress (MPa)	94.28
Gauge Length at Failure (mm)	81.2
Elongation of Gauge Length at Failure (mm)	21.2
Strain at failure (%)	35.33

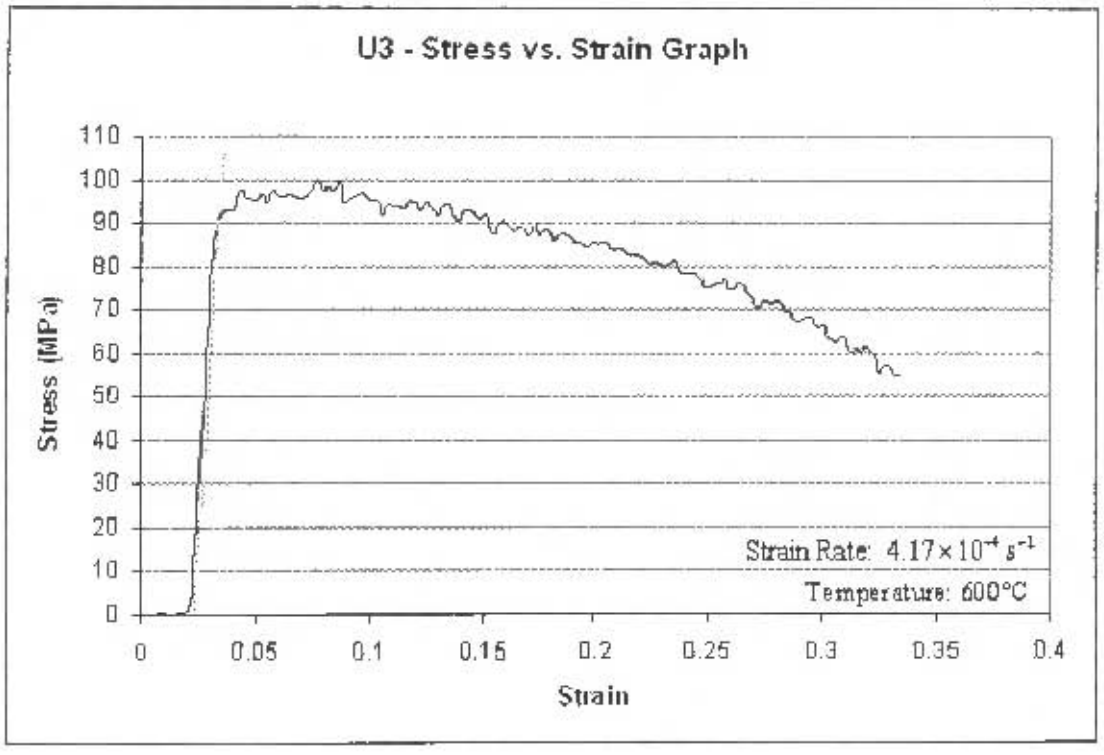

Figure A2.1.18 – Test Result for Specimen U3

Table A2.1.18 – Yield Stress and Failure Strain for Specimen U3

Yield Stress (MPa)	90.06
Ultimate Tensile Stress (MPa)	99.65
Gauge Length at Failure (mm)	80.6
Elongation of Gauge Length at Failure (mm)	20.6
Strain at failure (%)	34.33

A2.2. Test Results at a Strain Rate of: 3.33 x $10^{-3}s^{-1}$

A total of 19 tests were carried out at a strain rate of $3.33\times10^{-3}s^{-1}$. Table A2.2.1 outlines the tests carried out and the graphed results follow the table.

Table A2.2.1 Tensile Tests Carried Out at $3.33\times10^{-3}s^{-1}$

Specimen Name	Cross Section Details of Gauge Length			Temperature (°C)
	Width (mm)	Thickness (mm)	Area (mm^2)	
F1	12.48	3.00	37.44	25
F2	12.48	3.00	37.44	25
MN1	12.68	3.00	38.04	25
NB1	12.40	3.00	37.20	100
NB2	12.60	3.00	37.80	100
NB3	12.80	3.00	38.40	100
G1	12.66	3.00	37.98	200
G1NEW	12.56	3.00	37.68	200
G2	12.56	3.00	37.68	200
MN2	12.56	3.00	37.68	200
H1	12.66	3.00	37.98	300
H2	12.46	3.00	37.38	300
MN3	12.56	3.00	37.68	300
V1	12.48	3.00	37.44	450
V2	12.56	3.00	37.68	450
V3	12.46	3.00	37.38	450
W1	12.50	3.00	37.50	600
W2	12.56	3.00	37.68	600
W3	12.58	3.00	37.74	600

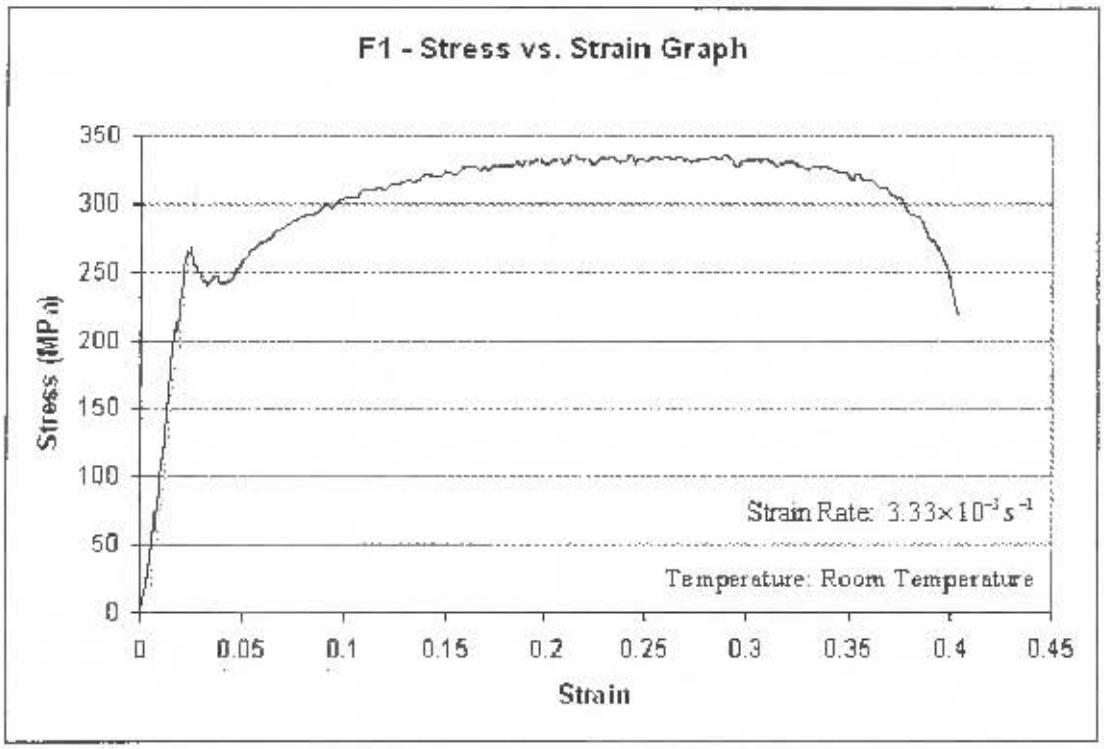

Figure A2.2.1 – Test Result for Specimen F1

Table A2.2.1 – Yield Stress and Failure Strain for Specimen F1

Yield Stress (MPa)	266.92
Ultimate Tensile Stress (MPa)	335.23
Gauge Length at Failure (mm)	81.3
Elongation of Gauge Length at Failure (mm)	21.3
Strain at failure (%)	35.50

Note: The ultimate tensile stress reported here refers to the maximum stress recorded as per the engineering stress vs. engineering strain graph. It does not refer to the true stress experienced at failure. This applies to all the test results at a strain rate of $3.33\times10^{-3}s^{-1}$.

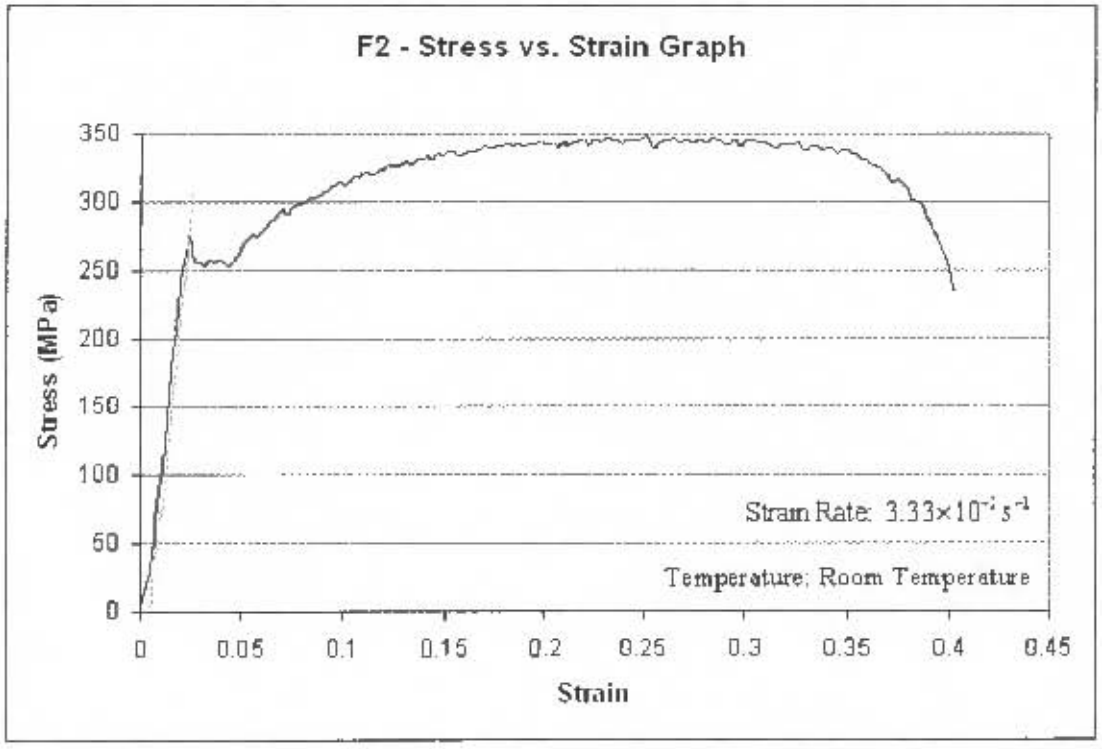

Figure A2.2.2 – Test Result for Specimen F2

Table A2.2.2 – Yield Stress and Failure Strain for Specimen F2

Yield Stress (MPa)	275.62
Ultimate Tensile Stress (MPa)	348.32
Gauge Length at Failure (mm)	81.7
Elongation of Gauge Length at Failure (mm)	21.7
Strain at failure (%)	36.17

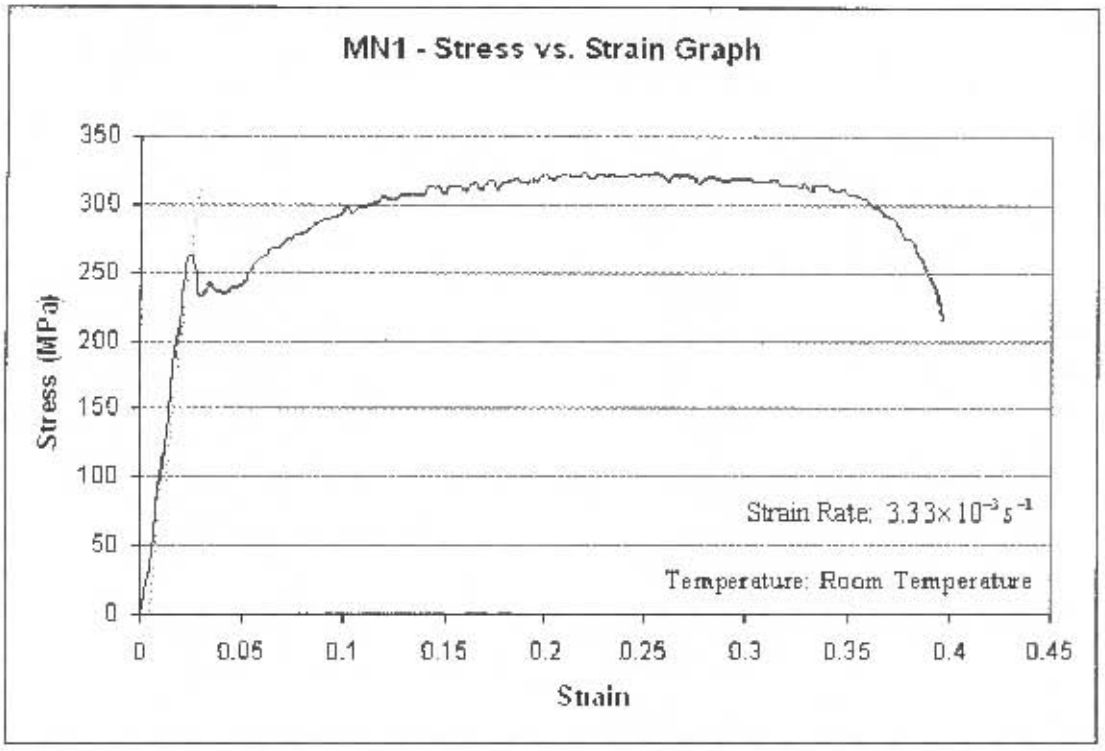

Figure A2.2.3 – Test Result for Specimen MN1

Table A2.2.3 – Yield Stress and Failure Strain for Specimen MN1

Yield Stress (MPa)	260.12
Ultimate Tensile Stress (MPa)	323.63
Gauge Length at Failure (mm)	81.8
Elongation of Gauge Length at Failure (mm)	21.8
Strain at failure (%)	36.33

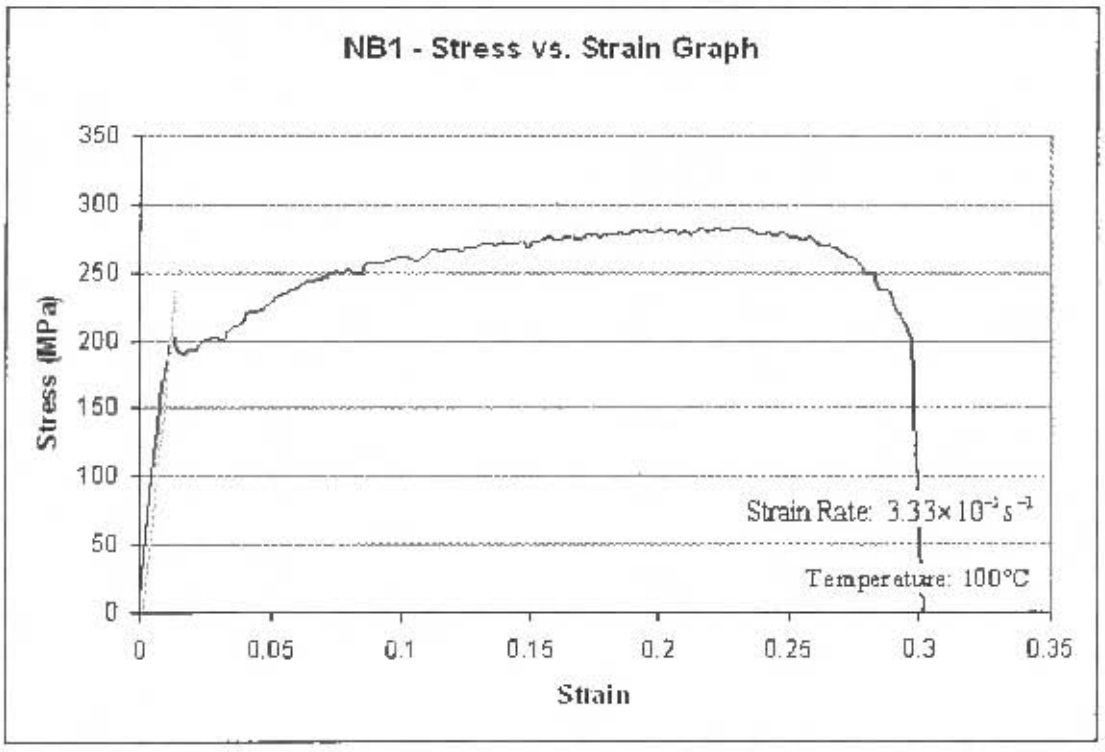

Figure A2.2.4 – Test Result for Specimen NB1

Table A2.2.4 Yield Stress and Failure Strain for Specimen NB1

Yield Stress (MPa)	199.23
Ultimate Tensile Stress (MPa)	282.72
Gauge Length at Failure (mm)	77.4
Elongation of Gauge Length at Failure (mm)	17.4
Strain at failure (%)	29.00

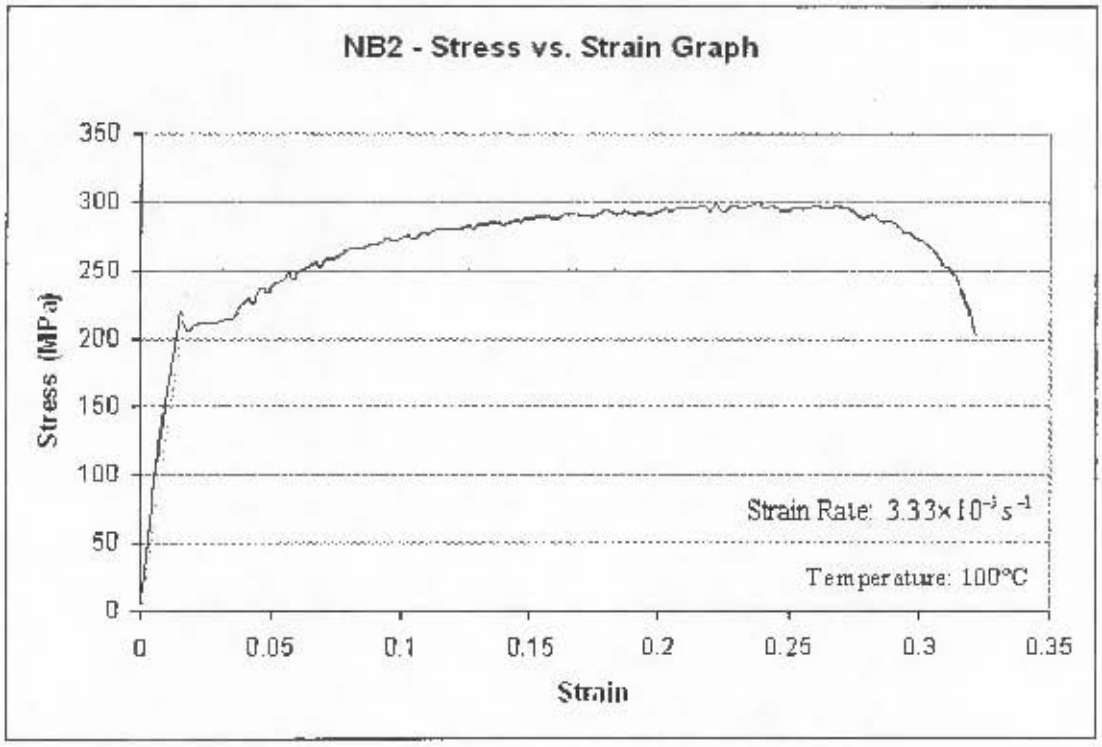

Figure A2.2.5 – Test Result for Specimen NB2

Table A2.2.5 – Yield Stress and Failure Strain for Specimen NB2

Yield Stress (MPa)	214.19
Ultimate Tensile Stress (MPa)	299.13
Gauge Length at Failure (mm)	78.4
Elongation of Gauge Length at Failure (mm)	18.4
Strain at failure (%)	30.67

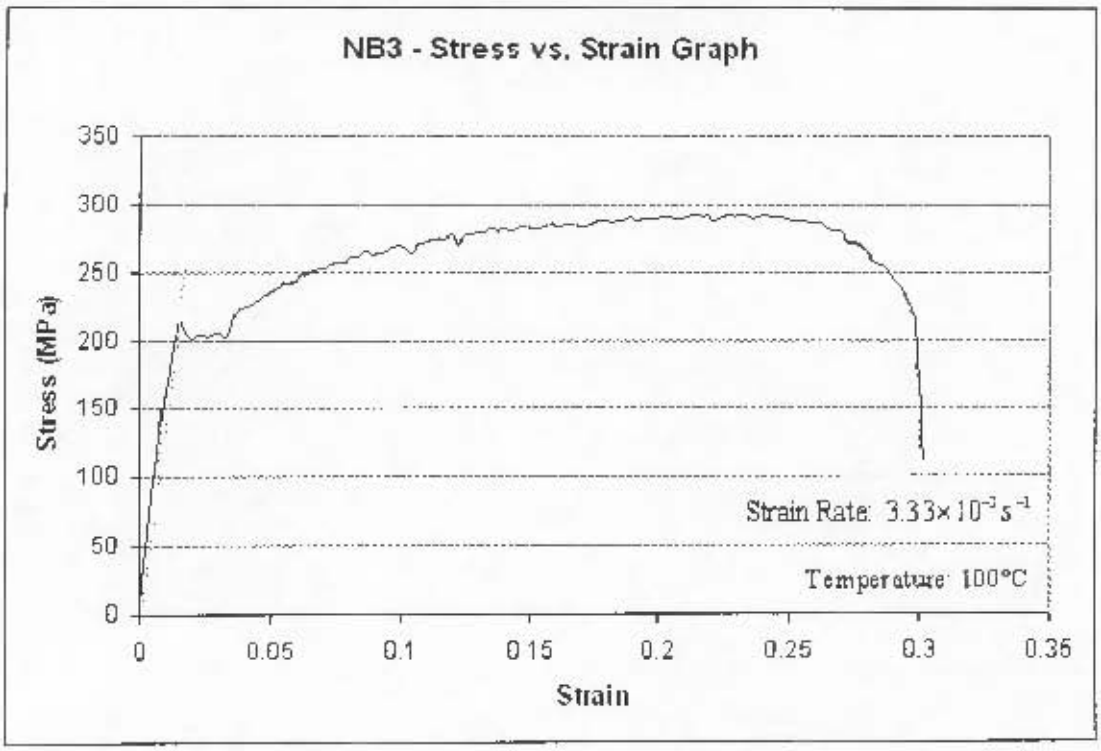

Figure A2.2.6 – Test Result for Specimen NB3

Table A2.2.6 - Yield Stress and Failure Strain for Specimen NB3

Yield Stress (MPa)	213.74
Ultimate Tensile Stress (MPa)	292.97
Gauge Length at Failure (mm)	77.1
Elongation of Gauge Length at Failure (mm)	17.1
Strain at failure (%)	28.50

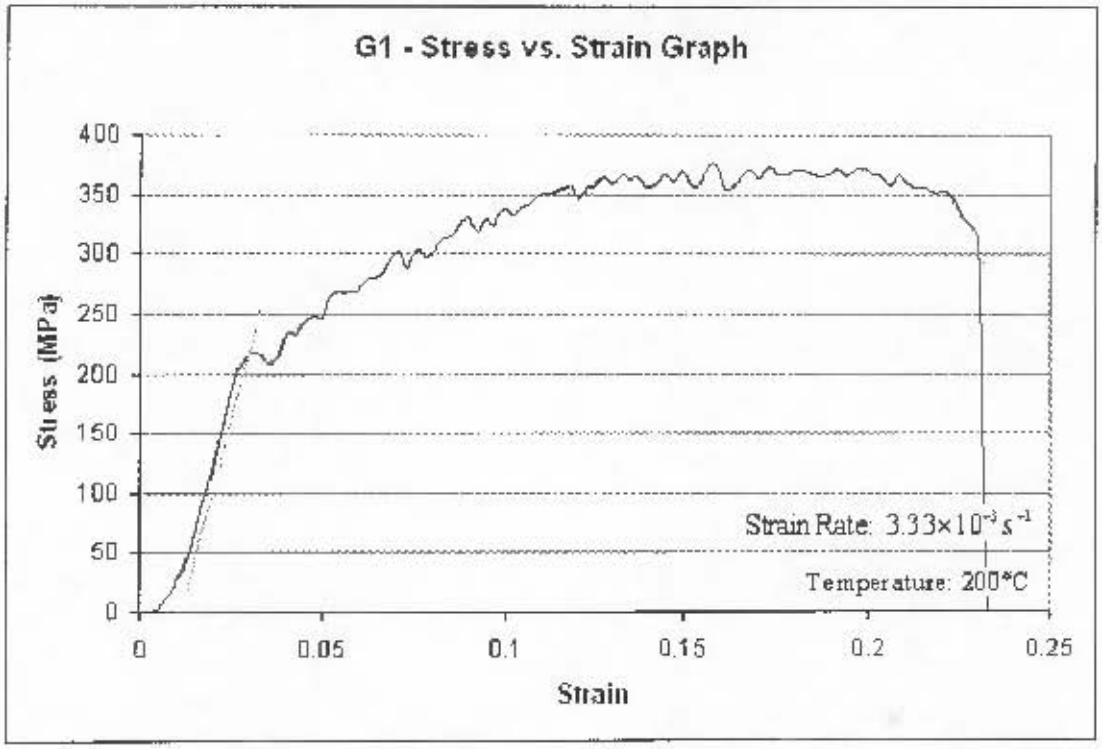

Figure A2.2.7 – Test Result for Specimen G1

Table A2.2.7 – Yield Stress and Failure Strain for Specimen G1

Yield Stress (MPa)	213.90
Ultimate Tensile Stress (MPa)	375.49
Gauge Length at Failure (mm)	70.9
Elongation of Gauge Length at Failure (mm)	10.9
Strain at failure (%)	18.17

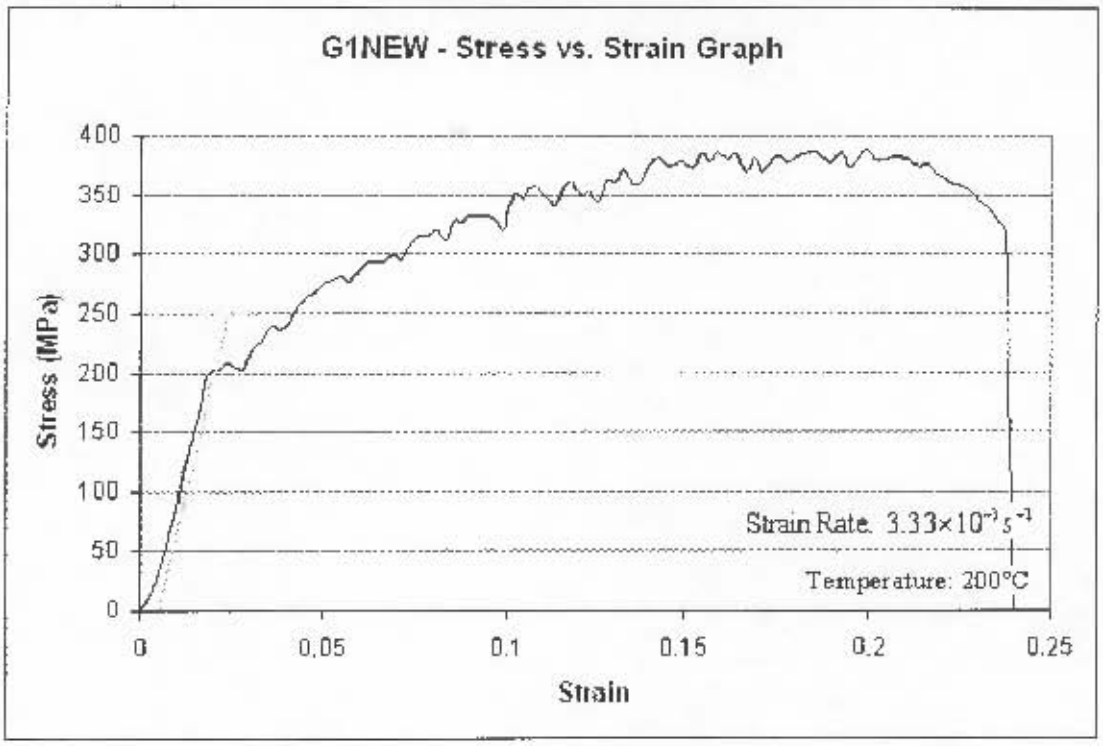

Figure A2.2.8 – Test Result for Specimen G1NEW

Table A2.2.8 – Yield Stress and Failure Strain for Specimen G1NEW

Yield Stress (MPa)	200.99
Ultimate Tensile Stress (MPa)	388.51
Gauge Length at Failure (mm)	70.7
Elongation of Gauge Length at Failure (mm)	10.7
Strain at failure (%)	17.83

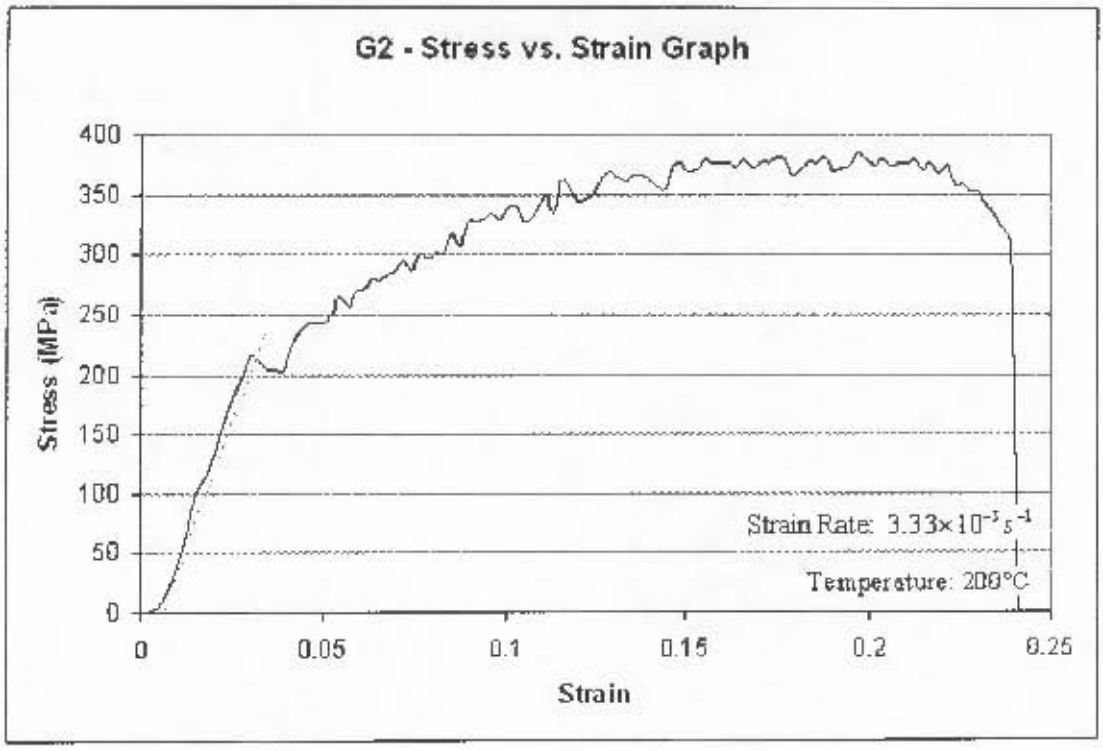

Figure A2.2.9 – Test Result for Specimen G2

Table A2.2.9 – Yield Stress and Failure Strain for Specimen G2

Yield Stress (MPa)	213.19
Ultimate Tensile Stress (MPa)	385.35
Gauge Length at Failure (mm)	71.6
Elongation of Gauge Length at Failure (mm)	11.6
Strain at failure (%)	19.33

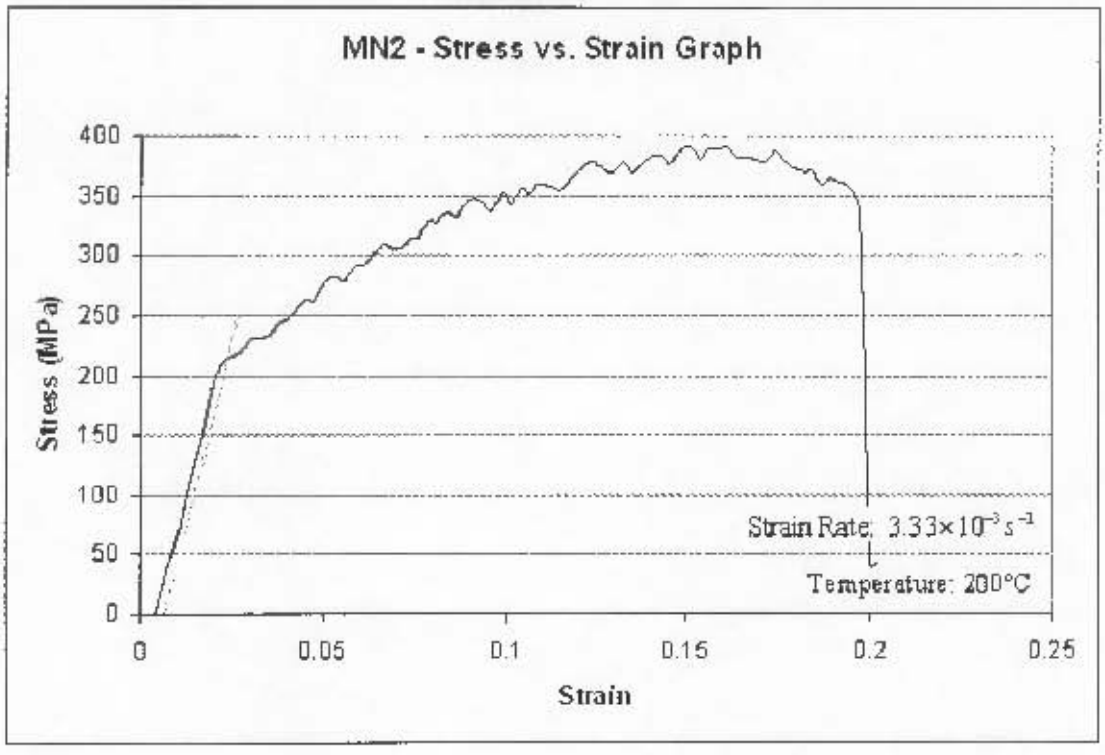

Figure A2.2.10 – Test Result for Specimen MN2

Table A2.2.10 – Yield Stress and Failure Strain for Specimen MN2

Yield Stress (MPa)	213.81
Ultimate Tensile Stress (MPa)	391.59
Gauge Length at Failure (mm)	70.0
Elongation of Gauge Length at Failure (mm)	10.0
Strain at failure (%)	16.67

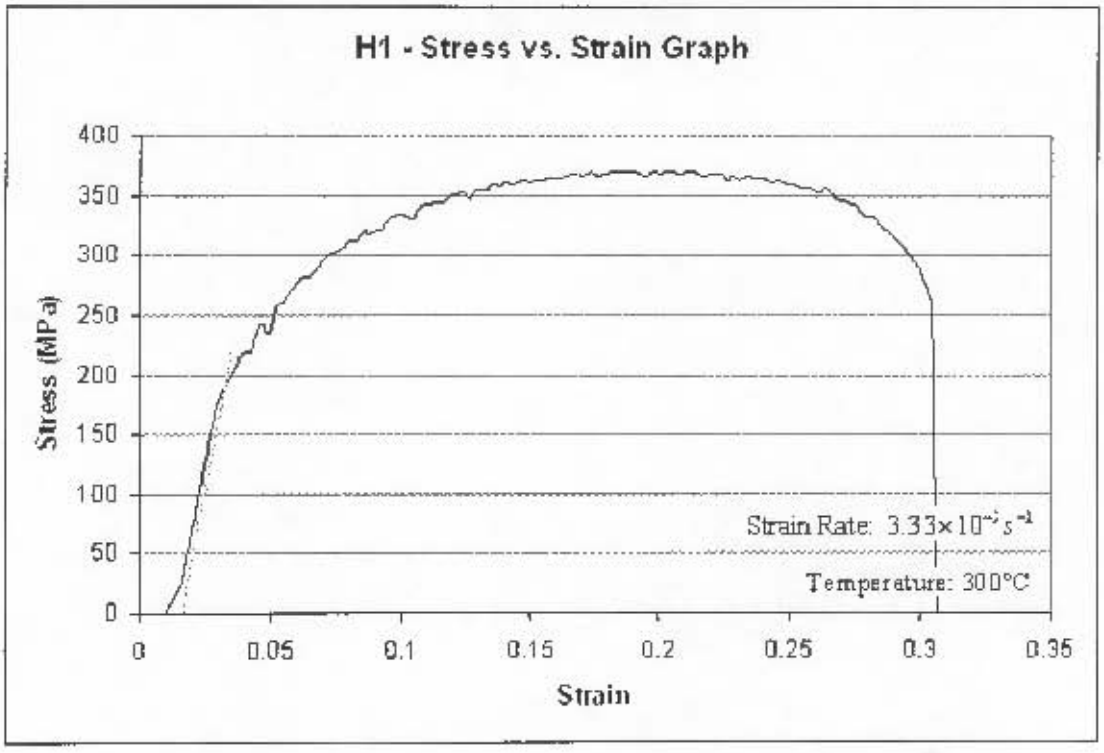

Figure A2.2.11 – Test Result for Specimen H1

Table A2.2.11 – Yield Stress and Failure Strain for Specimen H1

Yield Stress (MPa)	188.33
Ultimate Tensile Stress (MPa)	370.01
Gauge Length at Failure (mm)	75.2
Elongation of Gauge Length at Failure (mm)	15.2
Strain at failure (%)	25.33

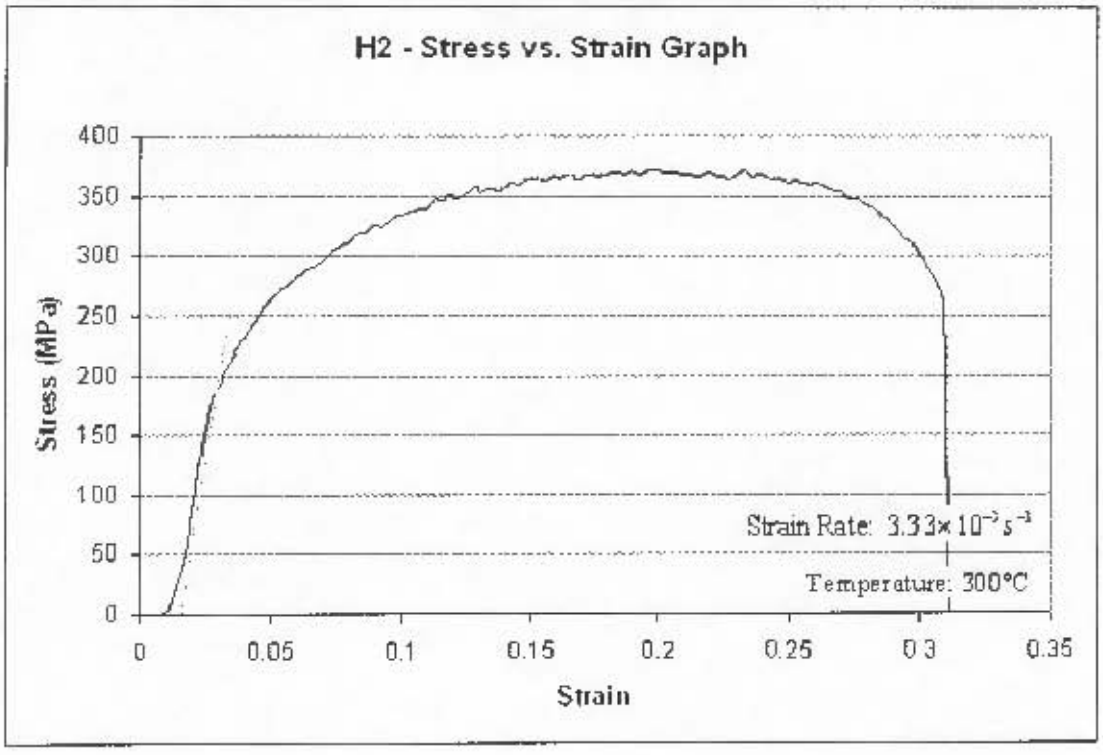

Figure A2.2.12 – Test Result for Specimen H2

Table A2.2.12 – Yield Stress and Failure Strain for Specimen H2

Yield Stress (MPa)	186.08
Ultimate Tensile Stress (MPa)	371.32
Gauge Length at Failure (mm)	75.1
Elongation of Gauge Length at Failure (mm)	15.1
Strain at failure (%)	25.17

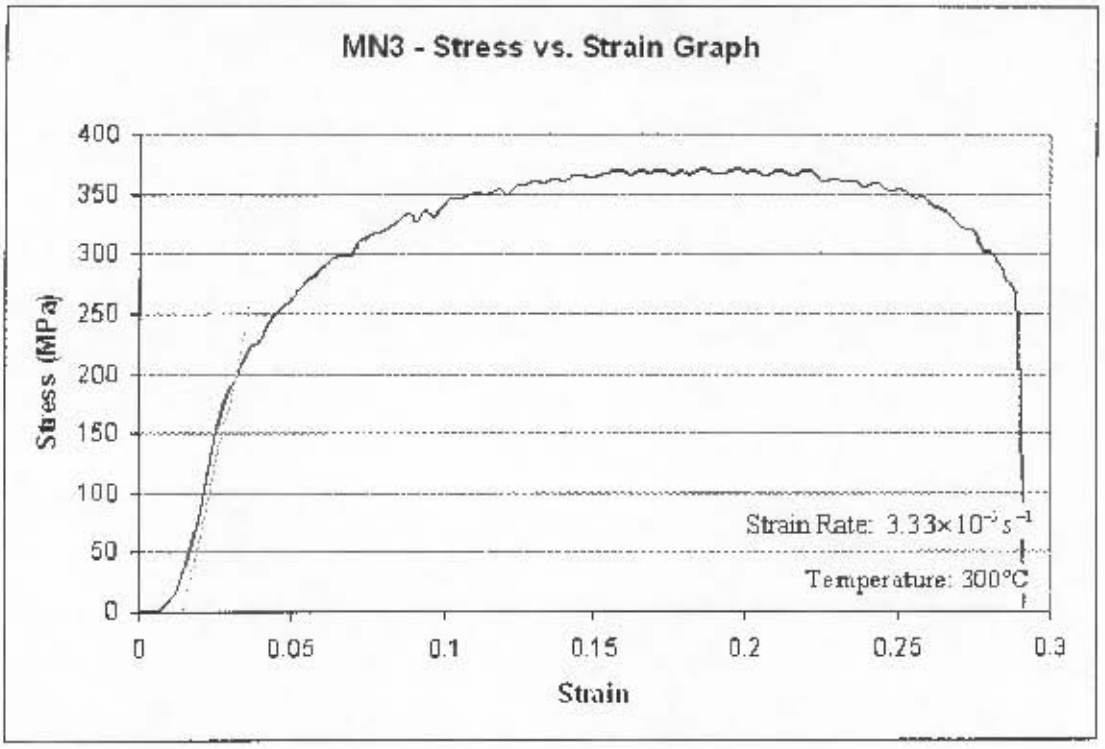

Figure A2.2.13 – Test Result for Specimen MN3

Table A2.2.13 – Yield Stress and Failure Strain for Specimen MN3

Yield Stress (MPa)	195.19
Ultimate Tensile Stress (MPa)	371.58
Gauge Length at Failure (mm)	74.5
Elongation of Gauge Length at Failure (mm)	14.5
Strain at failure (%)	24.17

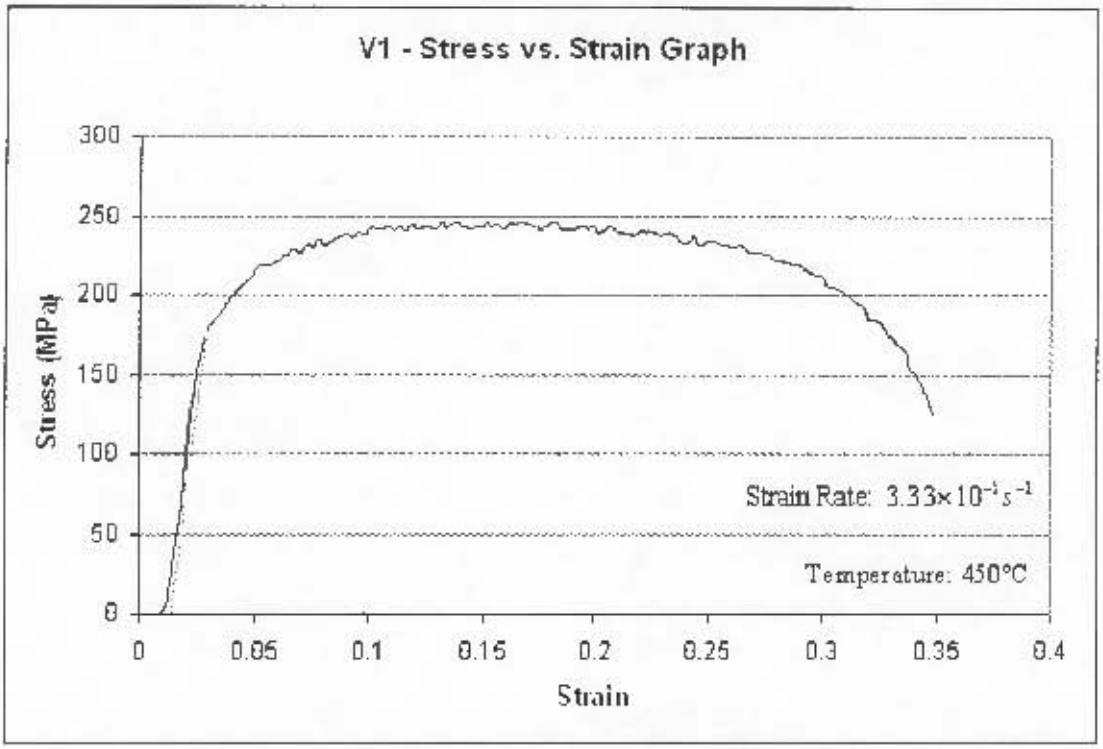

Figure A2.2.14 – Test Result for Specimen V1

Table A2.2.14 – Yield Stress and Failure Strain for Specimen V1

Yield Stress (MPa)	172.59
Ultimate Tensile Stress (MPa)	246.05
Gauge Length at Failure (mm)	79.7
Elongation of Gauge Length at Failure (mm)	19.7
Strain at failure (%)	32.83

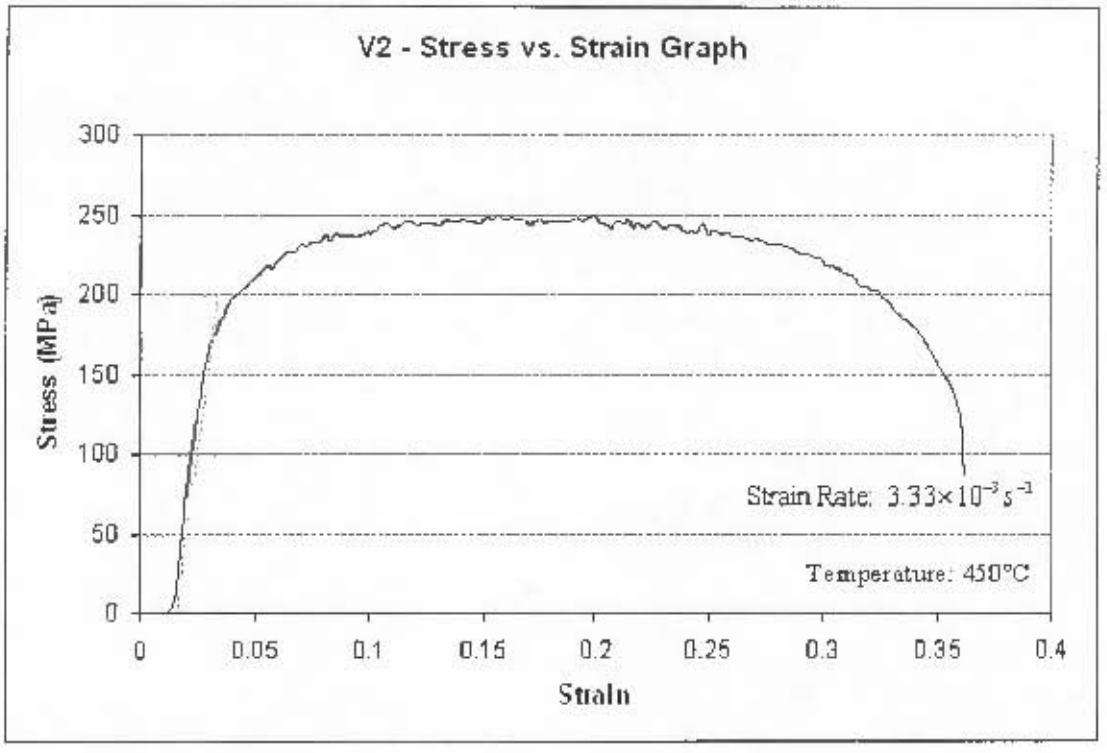

Figure A2.2.15 – Test Result for Specimen V2

Table A2.2.15 – Yield Stress and Failure Strain for Specimen V2

Yield Stress (MPa)	170.96
Ultimate Tensile Stress (MPa)	249.97
Gauge Length at Failure (mm)	80.1
Elongation of Gauge Length at Failure (mm)	20.1
Strain at failure (%)	33.50

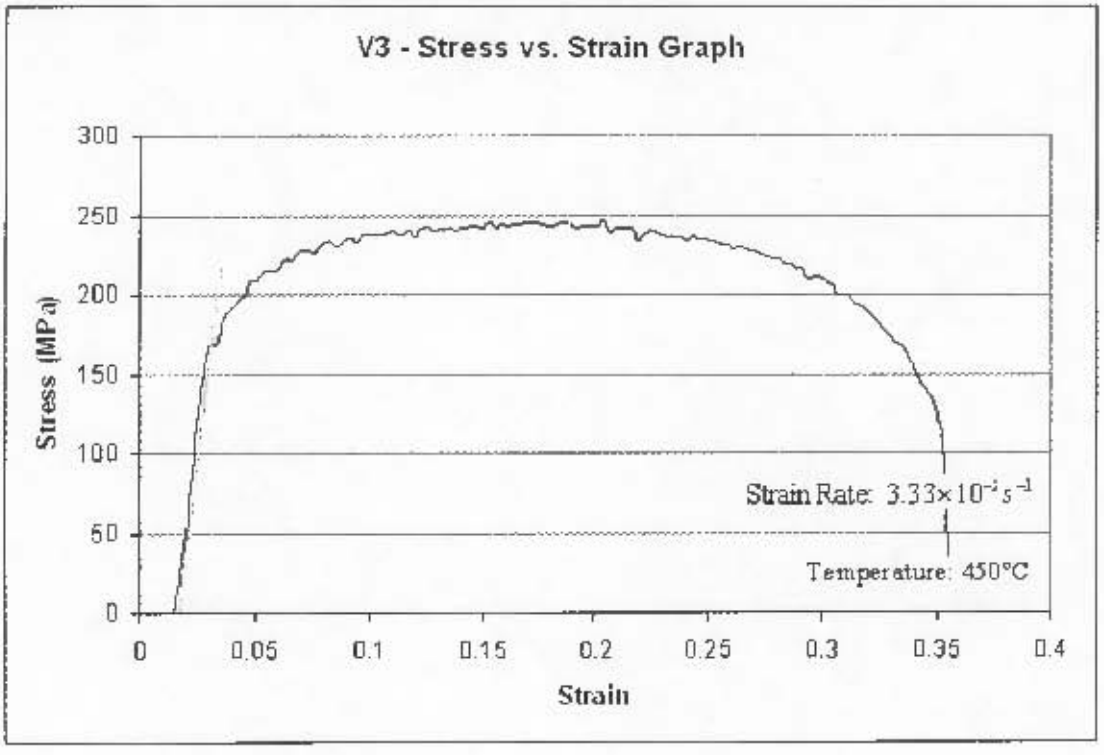

Figure A2.2.16 – Test Result for Specimen V3

Table A2.2.16 – Yield Stress and Failure Strain for Specimen V3

Yield Stress (MPa)	168.97
Ultimate Tensile Stress (MPa)	246.42
Gauge Length at Failure (mm)	79.4
Elongation of Gauge Length at Failure (mm)	19.4
Strain at failure (%)	32.33

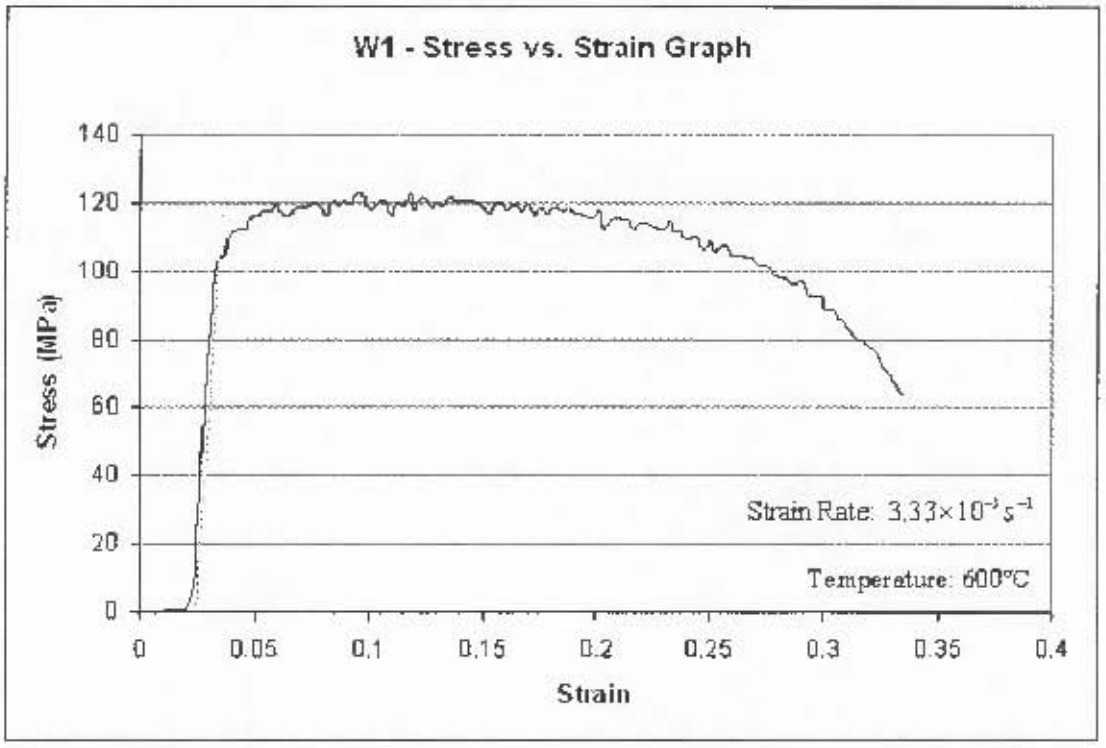

Figure A2.2.17 – Test Result for Specimen W1

Table A2.2.17 – Yield Stress and Failure Strain for Specimen W1

Yield Stress (MPa)	102.62
Ultimate Tensile Stress (MPa)	123.09
Gauge Length at Failure (mm)	79.8
Elongation of Gauge Length at Failure (mm)	19.8
Strain at failure (%)	33.00

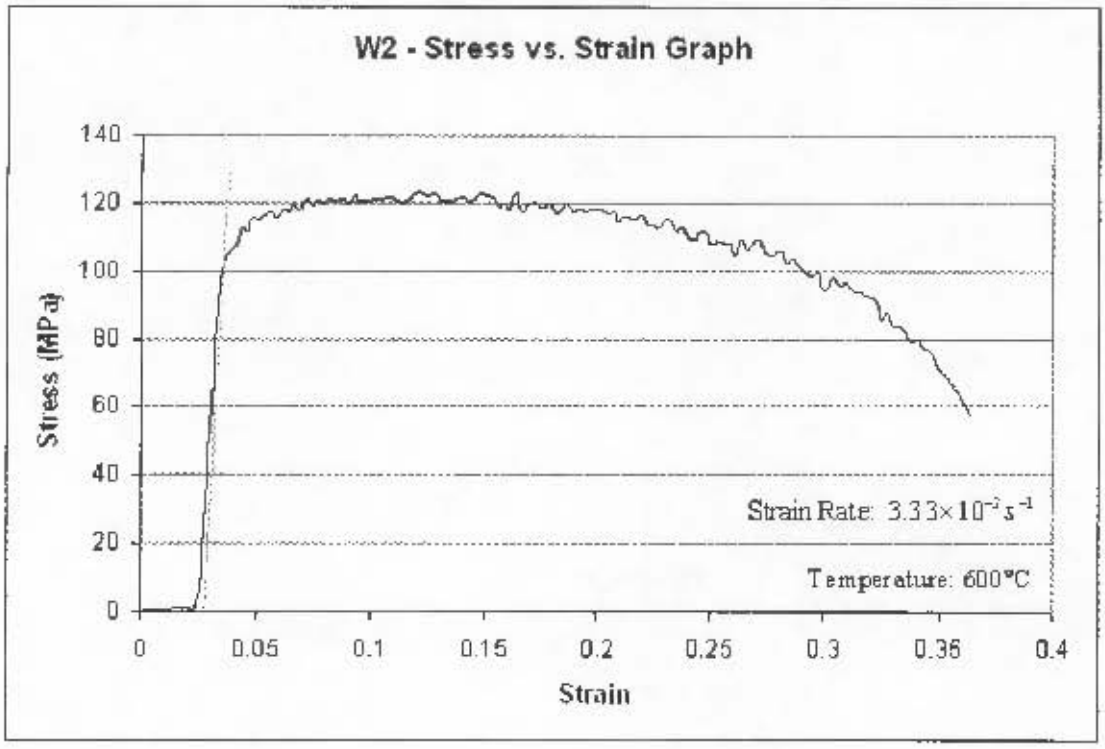

Figure A2.2.18 – Test Result for Specimen W2

Table A2.2.18 – Yield Stress and Failure Strain for Specimen W2

Yield Stress (MPa)	101.38
Ultimate Tensile Stress (MPa)	123.59
Gauge Length at Failure (mm)	80.8
Elongation of Gauge Length at Failure (mm)	20.8
Strain at failure (%)	34.67

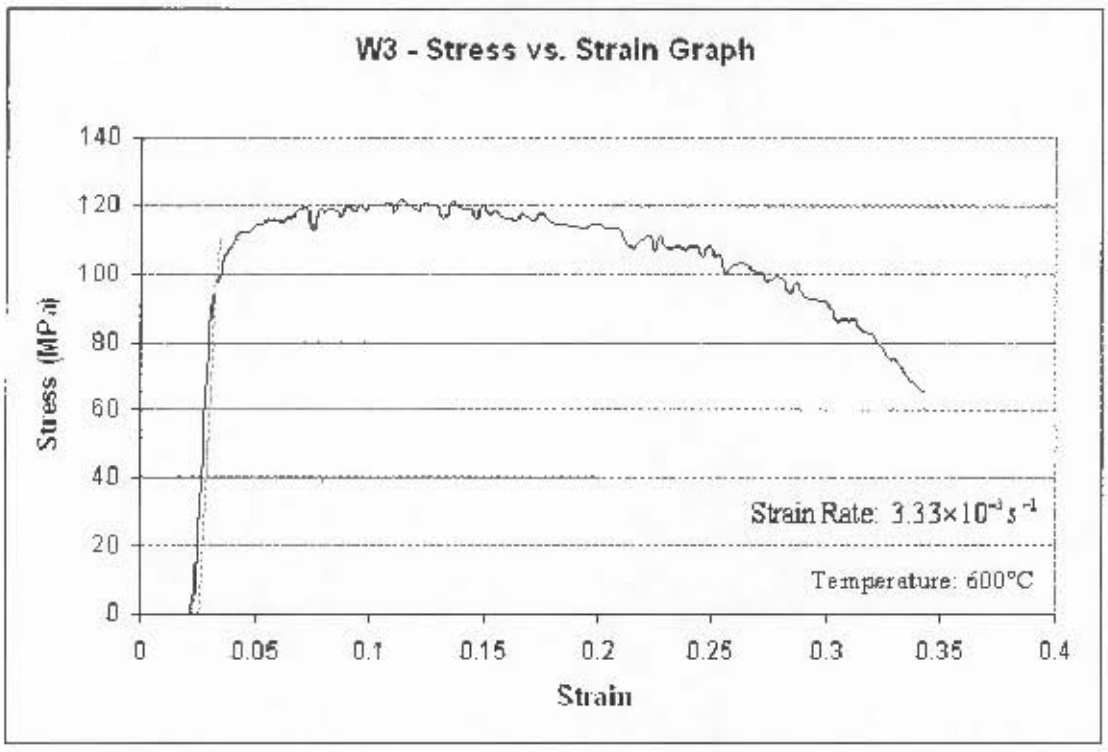

Figure A2.2.19 – Test Result for Specimen W3

Table A2.2.19 – Yield Stress and Failure Strain for Specimen W3

Yield Stress (MPa)	96.35
Ultimate Tensile Stress (MPa)	121.75
Gauge Length at Failure (mm)	79.9
Elongation of Gauge Length at Failure (mm)	19.9
Strain at failure (%)	33.17

A2.3. Test Results at a Strain Rate of: $1.67 \times 10^{-2} s^{-1}$

A total of 19 tests were carried out at a strain rate of $1.67 \times 10^{-2} s^{-1}$. Table A2.3.1 outlines the tests carried out and the graphed results follow the table.

Table A2.3.1 – Tensile Tests Carried Out at $1.67 \times 10^{-2} s^{-1}$

Specimen Name	Cross Section Details of Gauge Length			Temperature (°C)
	Width (mm)	Thickness (mm)	Area (mm^2)	
K1	12.62	3.00	37.86	25
K2	12.76	3.00	38.28	25
XZ1	12.54	3.00	37.62	25
NC1	12.80	3.00	38.40	100
NC2	12.26	3.00	36.78	100
NC3	12.70	3.00	38.10	100
L1	12.56	3.00	37.68	200
L1NEW	12.54	3.00	37.62	200
L2	12.56	3.00	37.68	200
FN2	12.52	3.00	37.56	200
M1	12.66	3.00	37.98	300
M2	12.66	3.00	37.98	300
FN3	12.66	3.00	37.98	300
X1	12.38	3.00	37.14	450
X2	12.66	3.00	37.98	450
X3	12.44	3.00	37.32	450
Y1	12.66	3.00	37.98	600
Y2	12.60	3.00	37.80	600
Y3	12.64	3.00	37.92	600

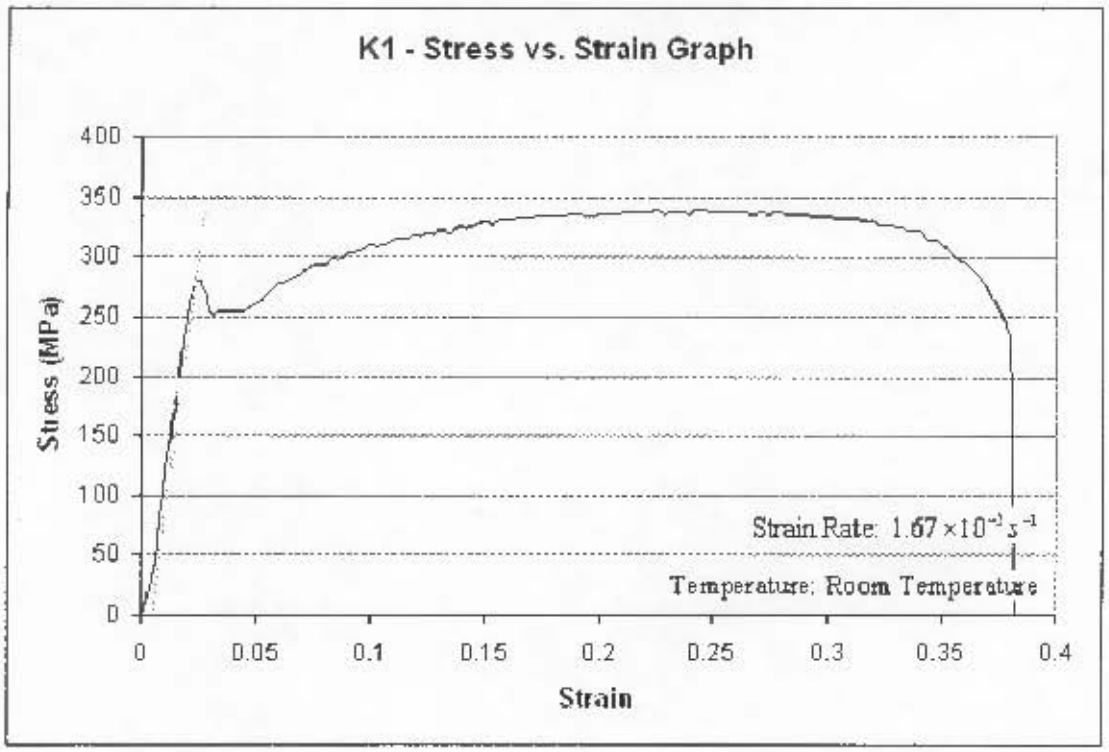

Figure A2.3.1 – Test Result for Specimen K1

Table A2.3.1 – Yield Stress and Failure Strain for Specimen K1

Yield Stress (MPa)	272.99
Ultimate Tensile Stress (MPa)	338.91
Gauge Length at Failure (mm)	80.2
Elongation of Gauge Length at Failure (mm)	20.2
Strain at failure (%)	33.67

Note: The ultimate tensile stress reported here refers to the maximum stress recorded as per the engineering stress vs. engineering strain graph. It does not refer to the true stress experienced at failure. This applies to all the test results at a strain rate of $1.67\times10^{-2}s^{-1}$.

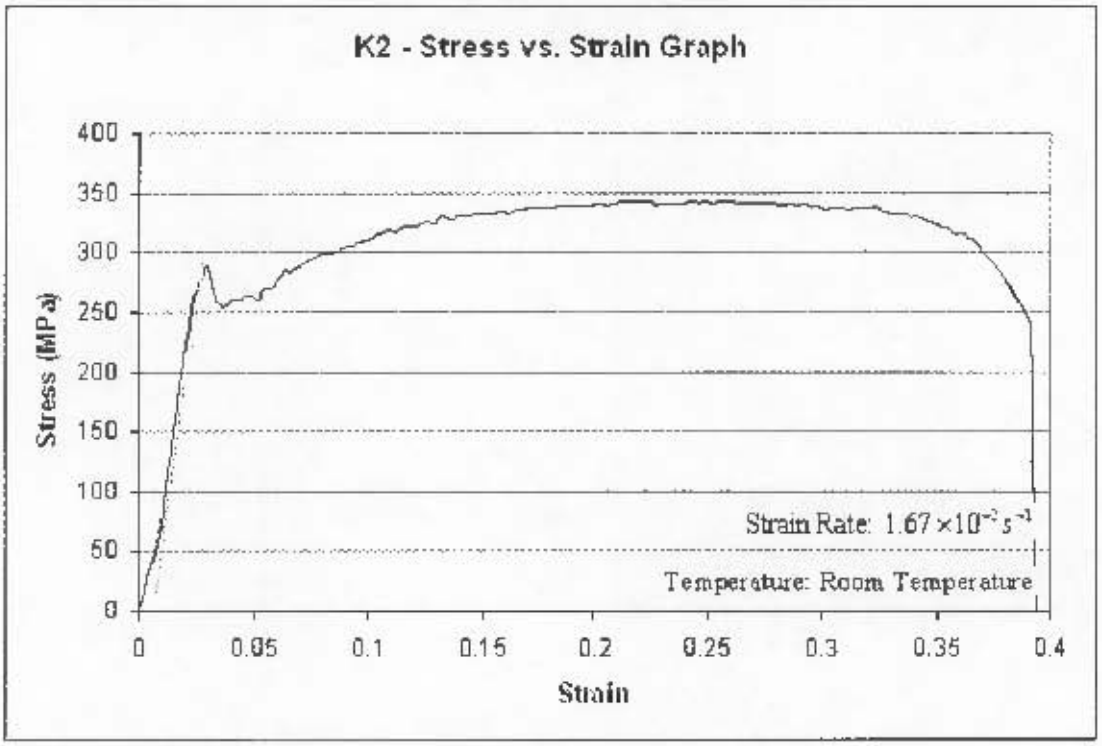

Figure A2.3.2 – Test Result for Specimen K2

Table A2.3.2 – Yield Stress and Failure Strain for Specimen K2

Yield Stress (MPa)	276.71
Ultimate Tensile Stress (MPa)	343.29
Gauge Length at Failure (mm)	81.3
Elongation of Gauge Length at Failure (mm)	21.3
Strain at failure (%)	35.50

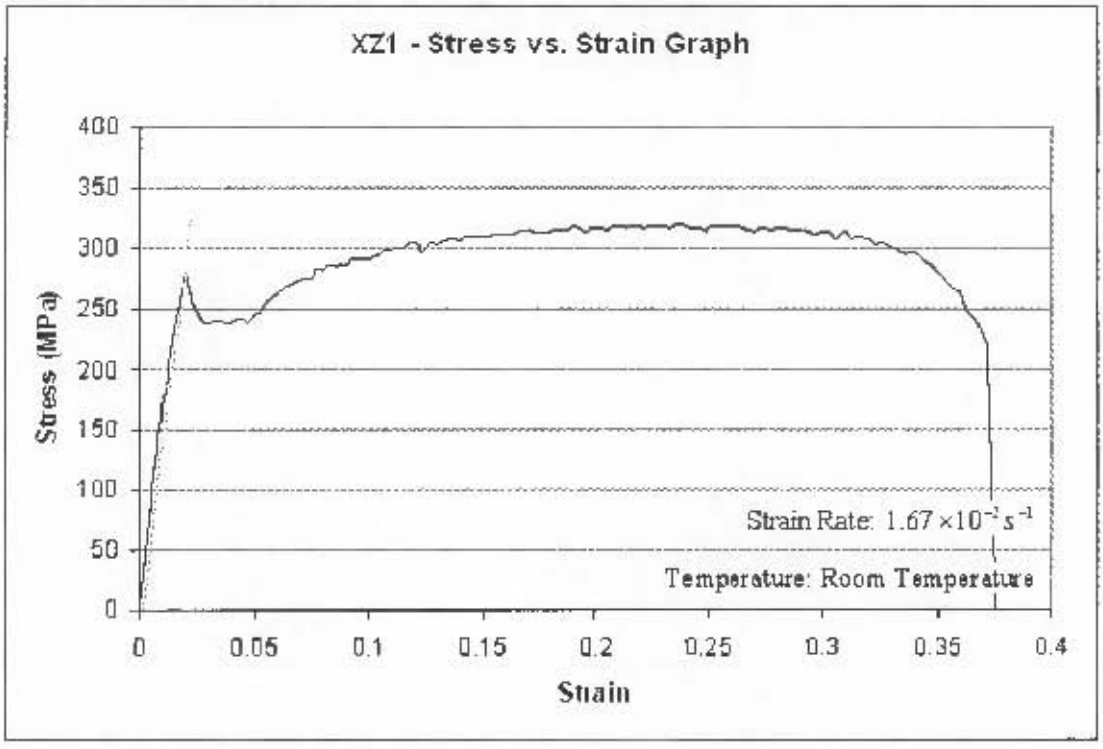

Figure A2.3.3 – Test Result for Specimen XZ1

Table A2.3.3 – Yield Stress and Failure Strain for Specimen XZ1

Yield Stress (MPa)	279.11
Ultimate Tensile Stress (MPa)	319.54
Gauge Length at Failure (mm)	80.8
Elongation of Gauge Length at Failure (mm)	20.8
Strain at failure (%)	34.67

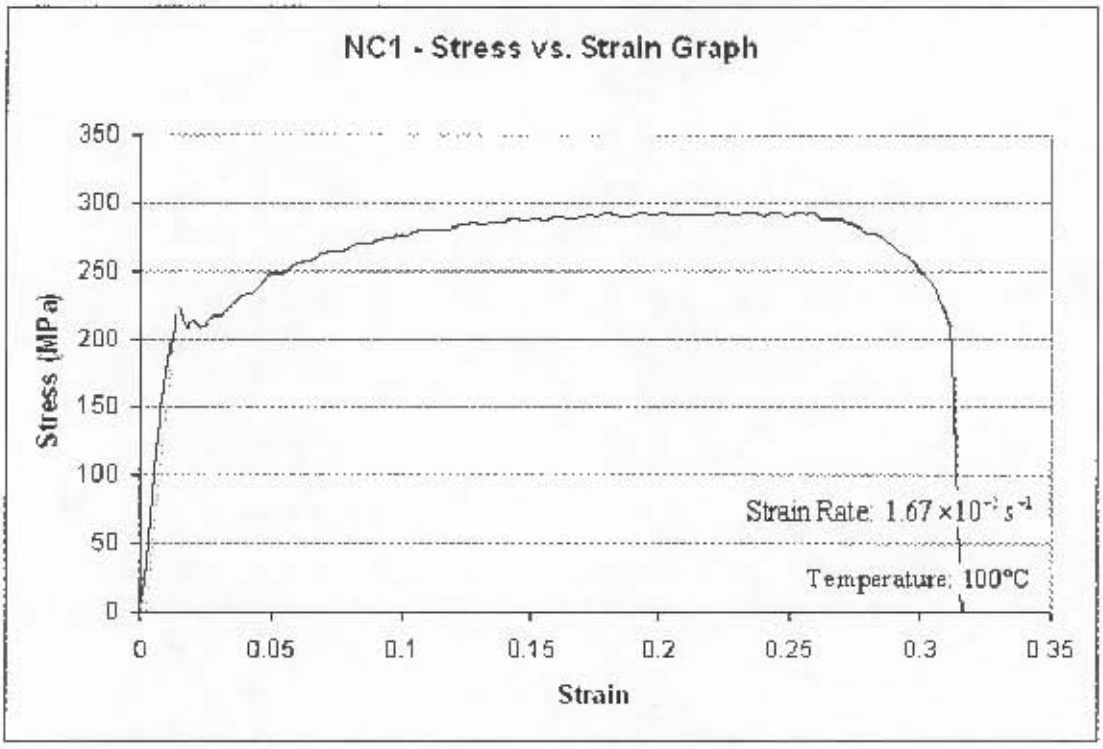

Figure A2.3.4 – Test Result for Specimen NC1

Table A2.3.4 – Yield Stress and Failure Strain for Specimen NC1

Yield Stress (MPa)	216.20
Ultimate Tensile Stress (MPa)	292.84
Gauge Length at Failure (mm)	77.5
Elongation of Gauge Length at Failure (mm)	17.5
Strain at failure (%)	29.17

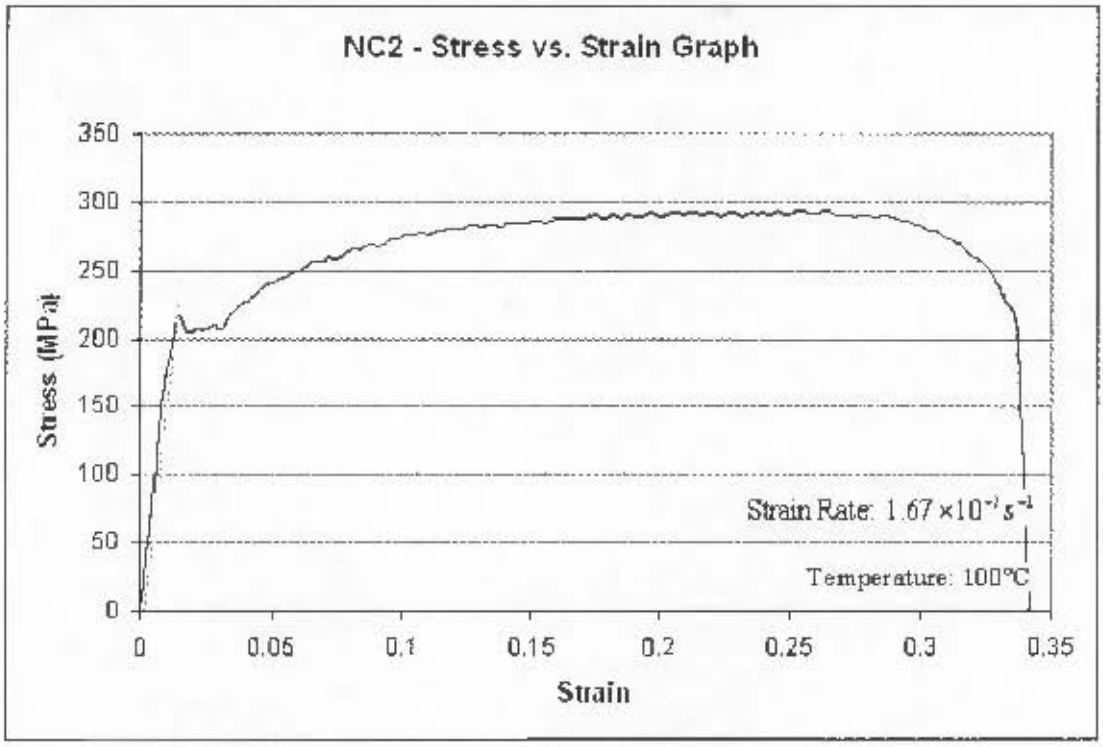

Figure A2.3.5 – Test Result for Specimen NC2

Table A2.3.5 – Yield Stress and Failure Strain for Specimen NC2

Yield Stress (MPa)	208.04
Ultimate Tensile Stress (MPa)	293.53
Gauge Length at Failure (mm)	79.5
Elongation of Gauge Length at Failure (mm)	19.5
Strain at failure (%)	32.50

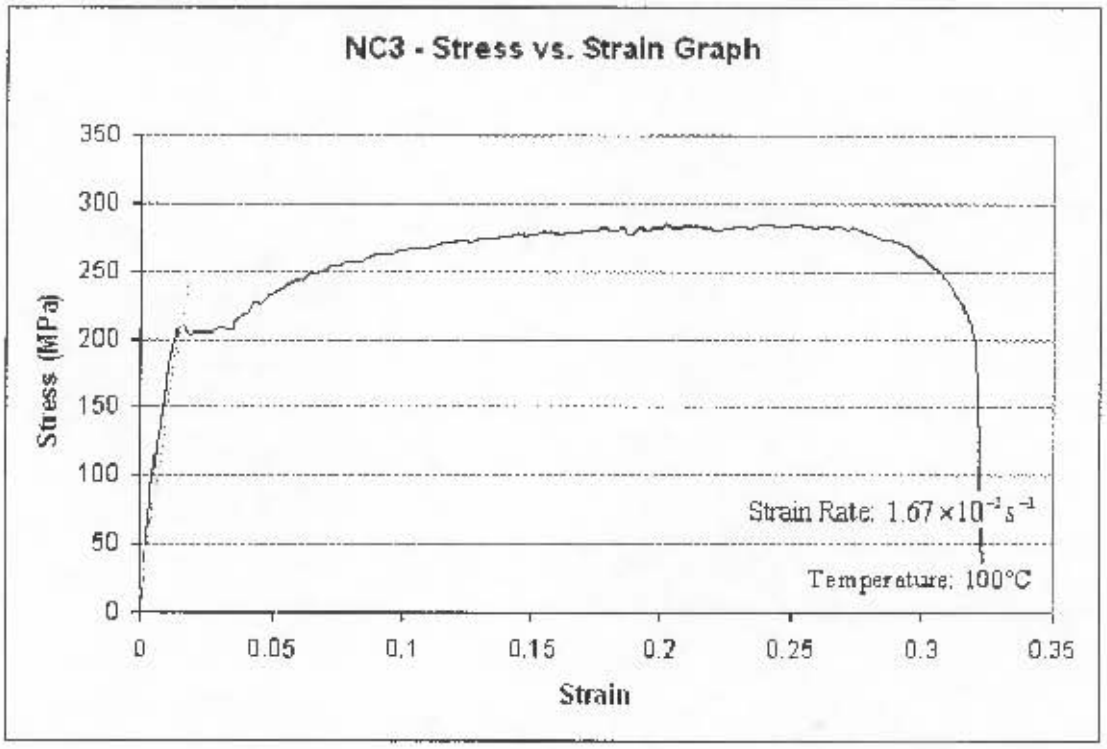

Figure A2.3.6 – Test Result for Specimen NC3

Table A2.3.6 – Yield Stress and Failure Strain for Specimen NC3

Yield Stress (MPa)	209.69
Ultimate Tensile Stress (MPa)	284.59
Gauge Length at Failure (mm)	78.3
Elongation of Gauge Length at Failure (mm)	18.3
Strain at failure (%)	30.50

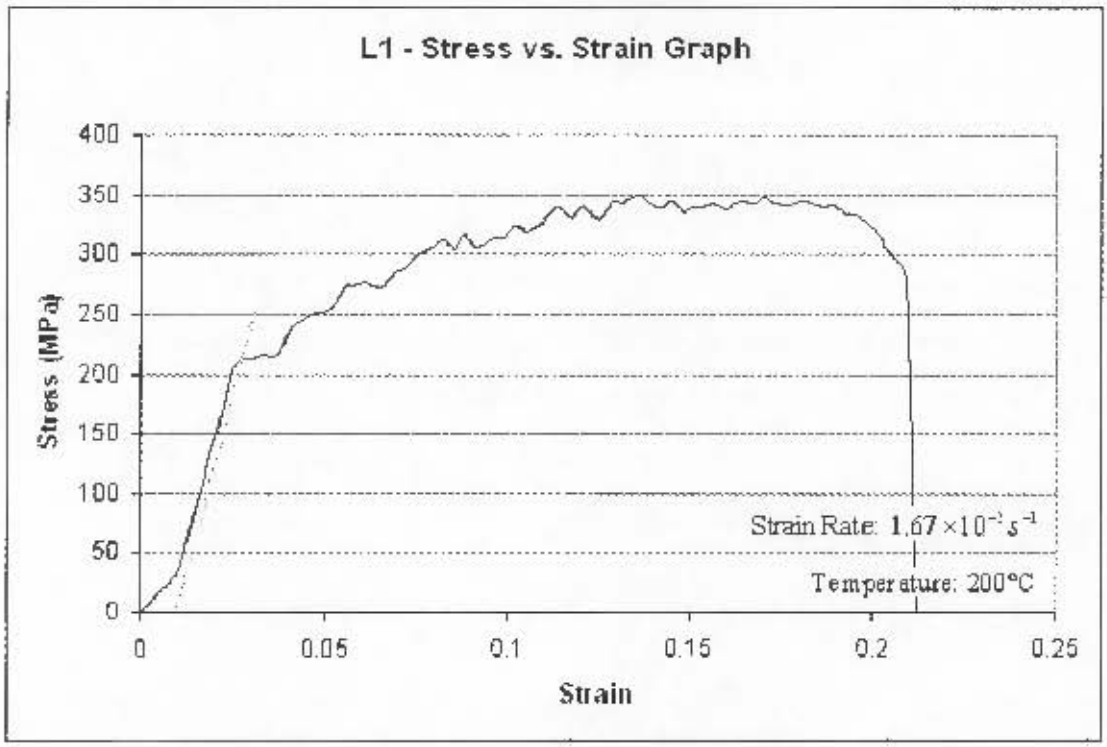

Figure A2.3.7 – Test Result for Specimen L1

Table A2.3.7 – Yield Stress and Failure Strain for Specimen L1

Yield Stress (MPa)	210.72
Ultimate Tensile Stress (MPa)	348.65
Gauge Length at Failure (mm)	70.1
Elongation of Gauge Length at Failure (mm)	10.1
Strain at failure (%)	16.83

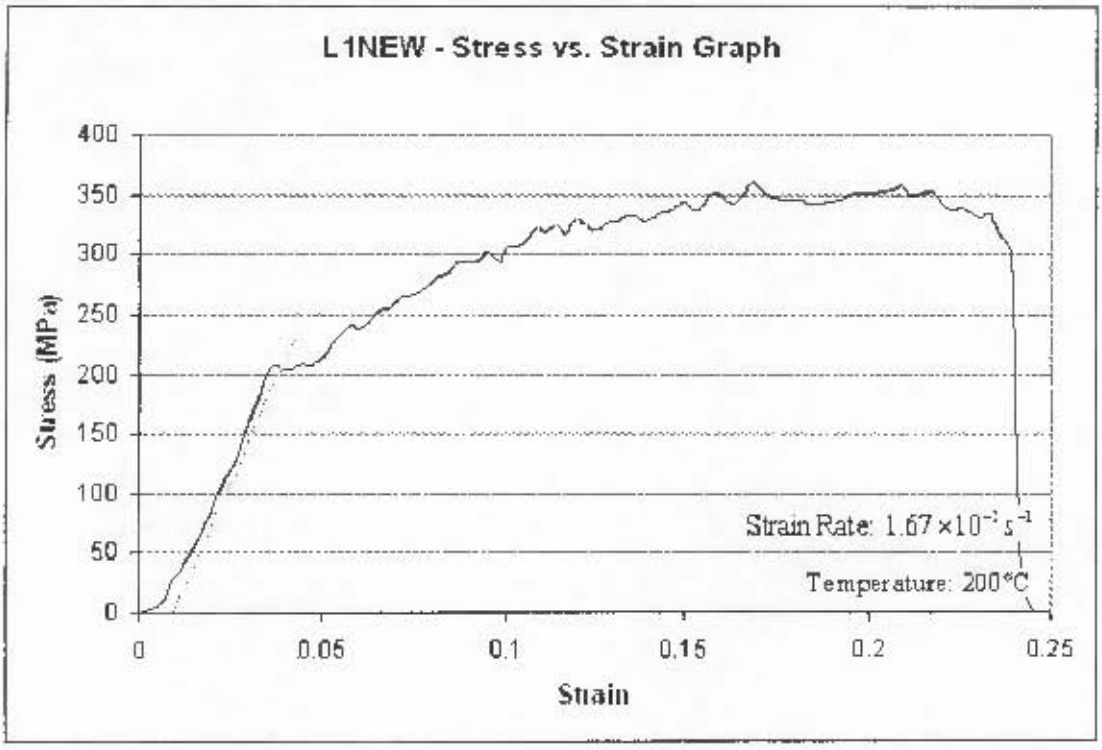

Figure A2.3.8 – Test Result for Specimen L1NEW

Table A2.3.8 - Yield Stress and Failure Strain for Specimen L1NEW

Yield Stress (MPa)	205.46
Ultimate Tensile Stress (MPa)	361.14
Gauge Length at Failure (mm)	71.2
Elongation of Gauge Length at Failure (mm)	11.2
Strain at failure (%)	18.67

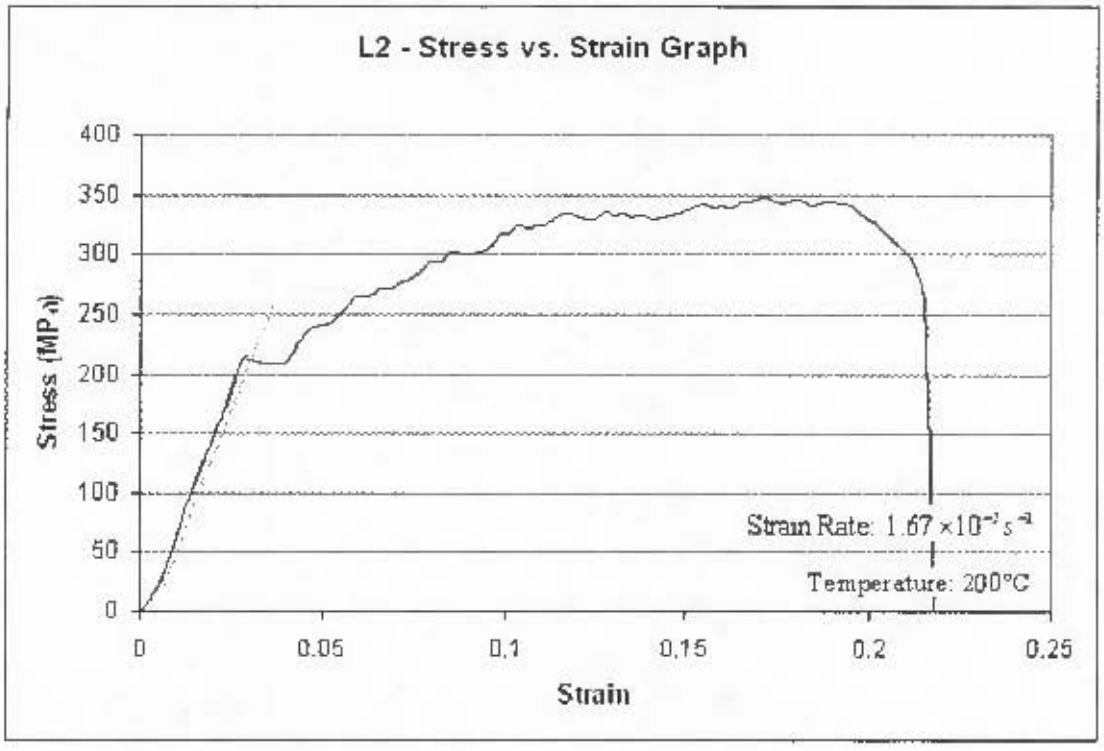

Figure A2.3.9 – Test Result for Specimen L2

Table A2.3.9 – Yield Stress and Failure Strain for Specimen L2

Yield Stress (MPa)	210.94
Ultimate Tensile Stress (MPa)	348.09
Gauge Length at Failure (mm)	69.8
Elongation of Gauge Length at Failure (mm)	9.8
Strain at failure (%)	16.33

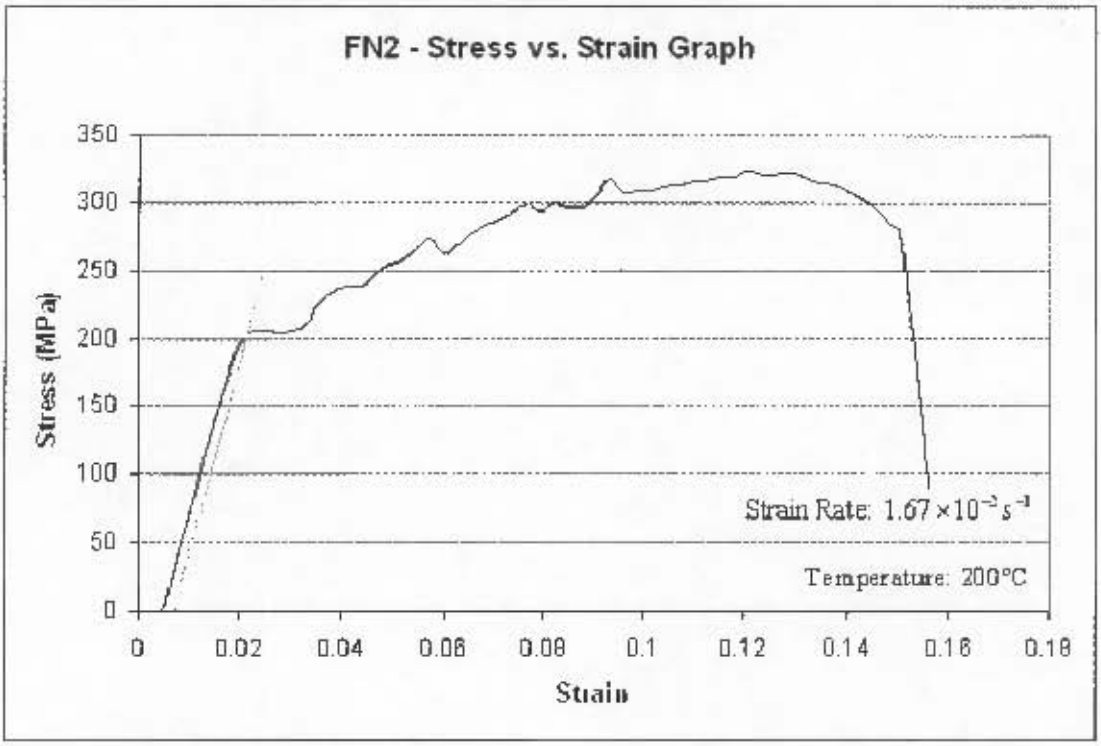

Figure A2.3.10 – Test Result for Specimen FN2

Table A2.3.10 – Yield Stress and Failure Strain for Specimen FN2

Yield Stress (MPa)	201.74
Ultimate Tensile Stress (MPa)	322.84
Gauge Length at Failure (mm)	68.4
Elongation of Gauge Length at Failure (mm)	8.4
Strain at failure (%)	14.00

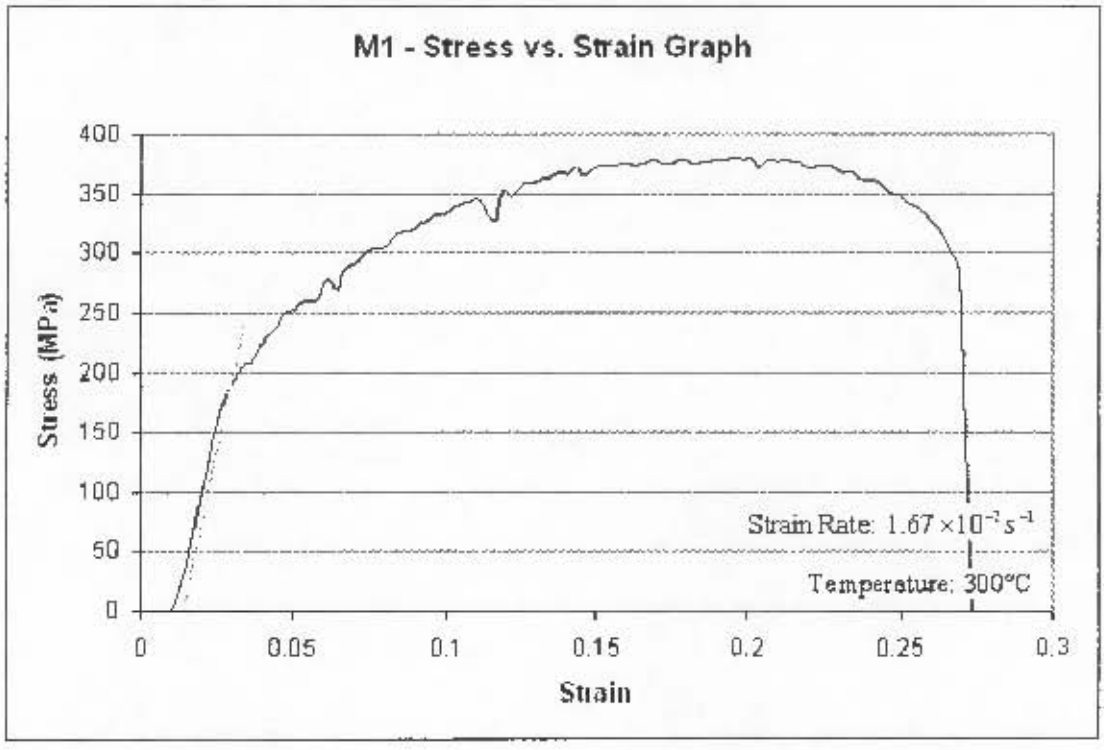

Figure A2.3.11 – Test Result for Specimen M1

Table A2.3.11 – Yield Stress and Failure Strain for Specimen M1

Yield Stress (MPa)	186.97
Ultimate Tensile Stress (MPa)	379.23
Gauge Length at Failure (mm)	73.5
Elongation of Gauge Length at Failure (mm)	13.5
Strain at failure (%)	22.50

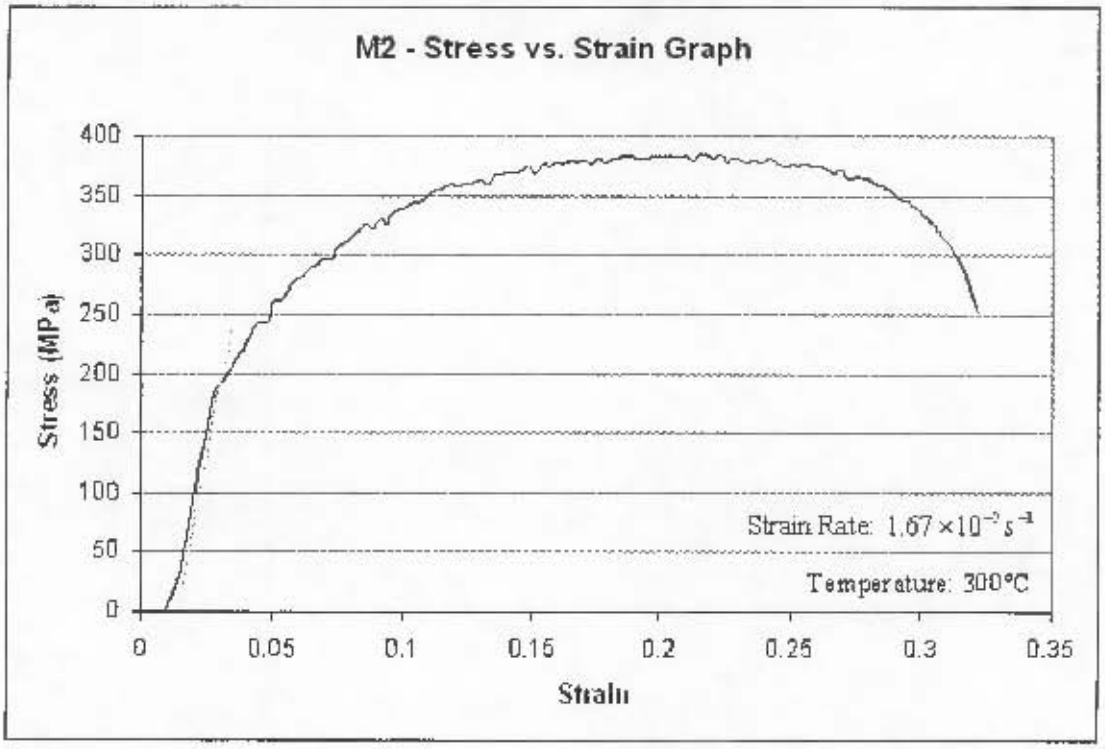

Figure A2.3.12 – Test Result for Specimen M2

Table A2.3.12 – Yield Stress and Failure Strain for Specimen M2

Yield Stress (MPa)	189.90
Ultimate Tensile Stress (MPa)	384.91
Gauge Length at Failure (mm)	75.5
Elongation of Gauge Length at Failure (mm)	15.5
Strain at failure (%)	25.83

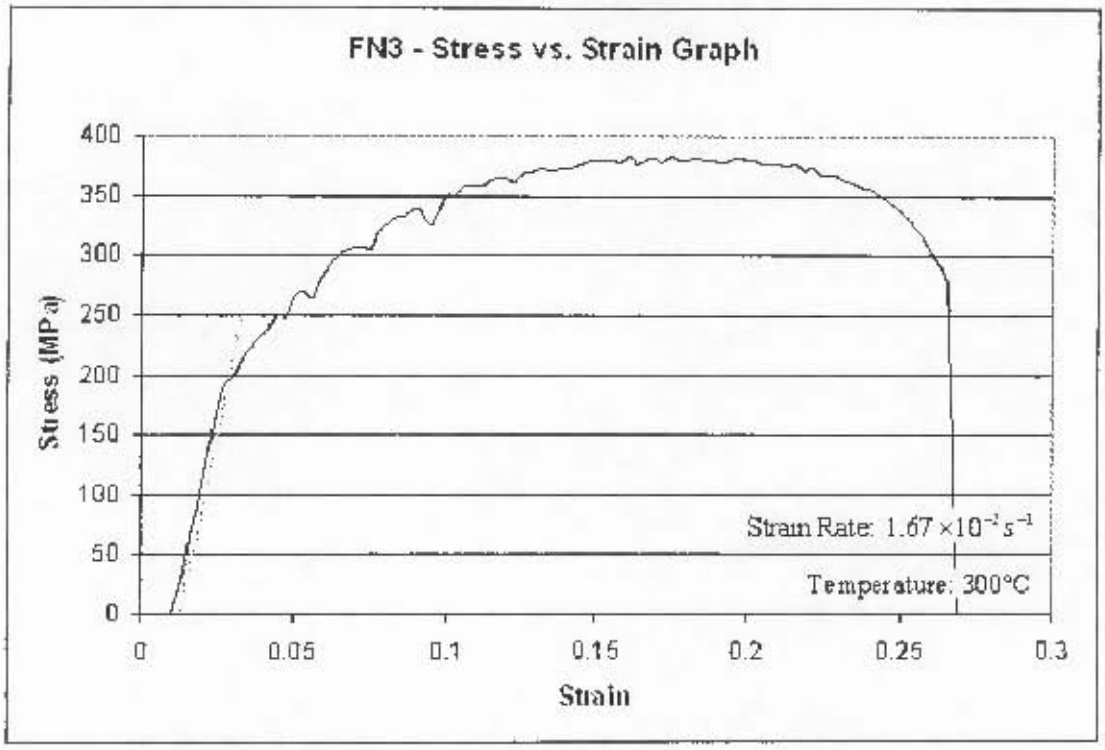

Figure A2.3.13 – Test Result for Specimen FN3

Table A2.2.13 Yield Stress and Failure Strain for Specimen FN3

Yield Stress (MPa)	194.39
Ultimate Tensile Stress (MPa)	383.07
Gauge Length at Failure (mm)	73.4
Elongation of Gauge Length at Failure (mm)	13.4
Strain at failure (%)	22.33

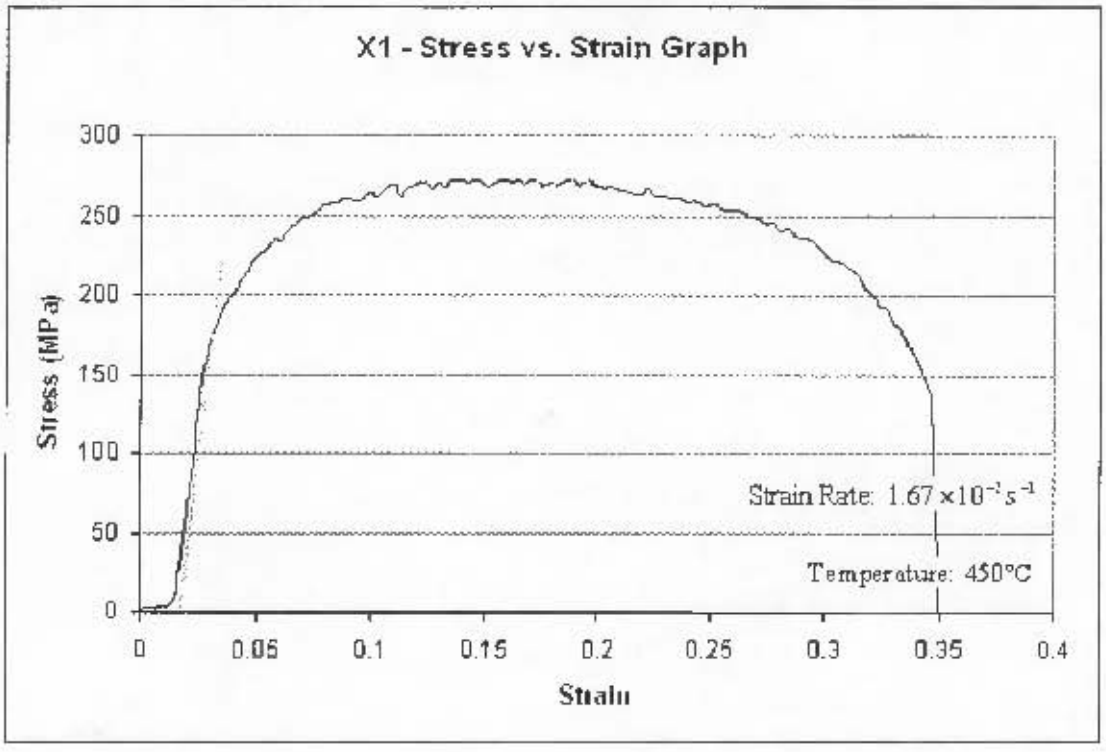

Figure A2.3.14 – Test Result for Specimen X1

Table A2.3.14 – Yield Stress and Failure Strain for Specimen X1

Yield Stress (MPa)	174.36
Ultimate Tensile Stress (MPa)	272.75
Gauge Length at Failure (mm)	78.8
Elongation of Gauge Length at Failure (mm)	18.8
Strain at failure (%)	31.33

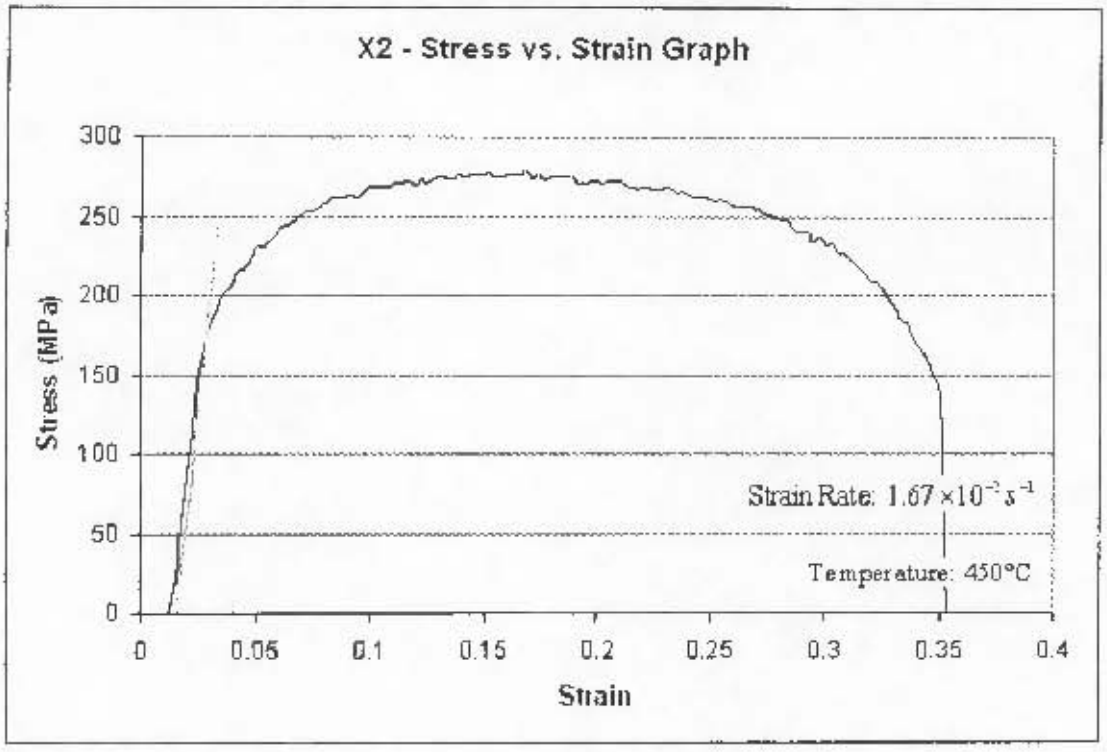

Figure A2.3.15 – Test Result for Specimen X2

Table A2.3.15 – Yield Stress and Failure Strain for Specimen X2

Yield Stress (MPa)	173.55
Ultimate Tensile Stress (MPa)	278.17
Gauge Length at Failure (mm)	79.0
Elongation of Gauge Length at Failure (mm)	19.0
Strain at failure (%)	31.67

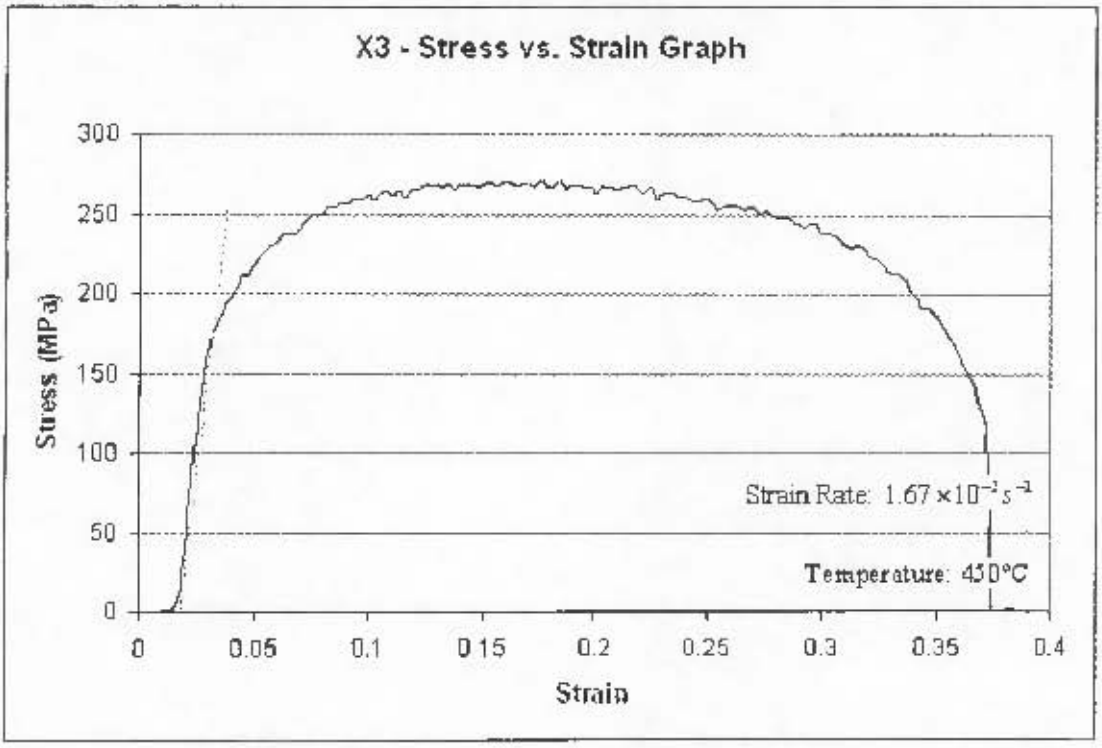

Figure A2.3.16 – Test Result for Specimen X3

Table A2.3.16 – Yield Stress and Failure Strain for Specimen X3

Yield Stress (MPa)	174.16
Ultimate Tensile Stress (MPa)	270.53
Gauge Length at Failure (mm)	79.8
Elongation of Gauge Length at Failure (mm)	19.8
Strain at failure (%)	33.00

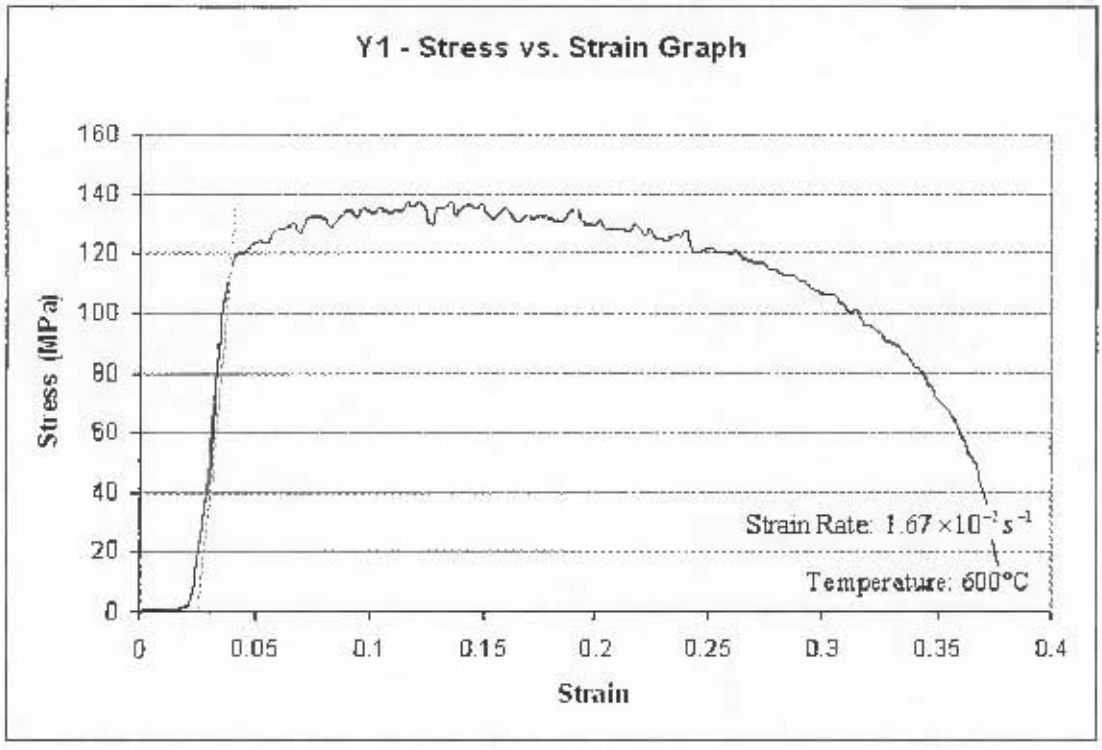

Figure A2.3.17 – Test Result for Specimen Y1

Table A2.3.17 – Yield Stress and Failure Strain for Specimen Y1

Yield Stress (MPa)	112.15
Ultimate Tensile Stress (MPa)	136.89
Gauge Length at Failure (mm)	81.5
Elongation of Gauge Length at Failure (mm)	21.5
Strain at failure (%)	35.83

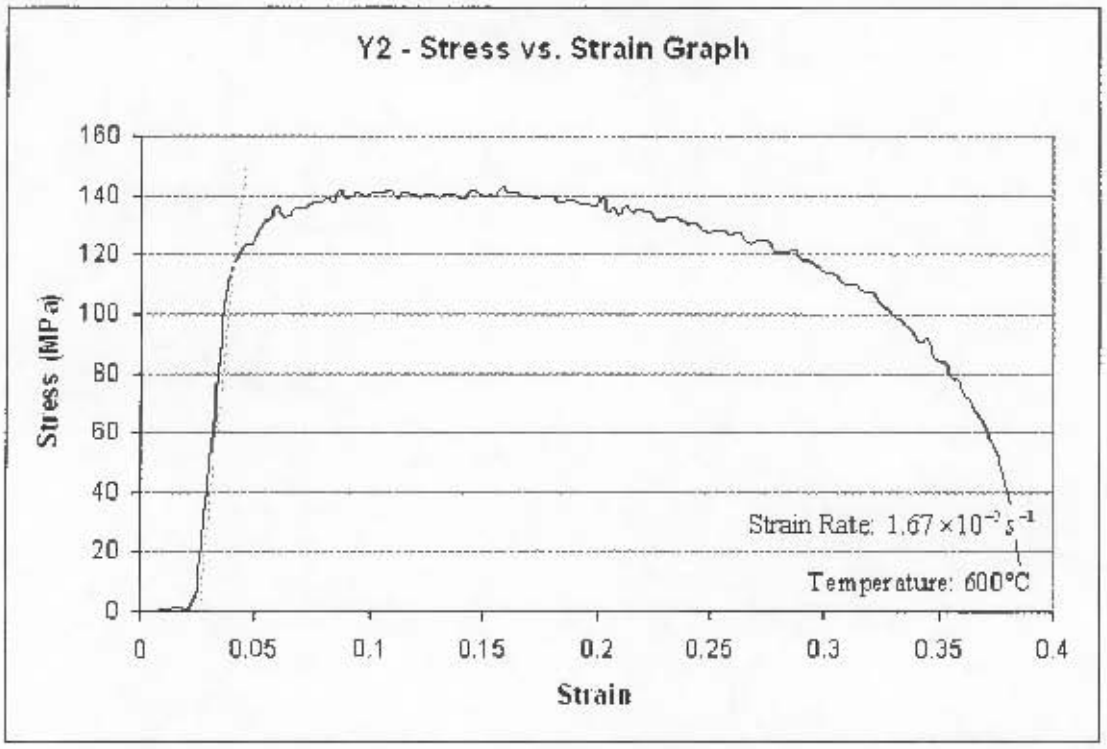

Figure A2.3.18 – Test Result for Specimen Y2

Table A2.3.18 – Yield Stress and Failure Strain for Specimen Y2

Yield Stress (MPa)	115.87
Ultimate Tensile Stress (MPa)	142.94
Gauge Length at Failure (mm)	82.0
Elongation of Gauge Length at Failure (mm)	22.0
Strain at failure (%)	36.67

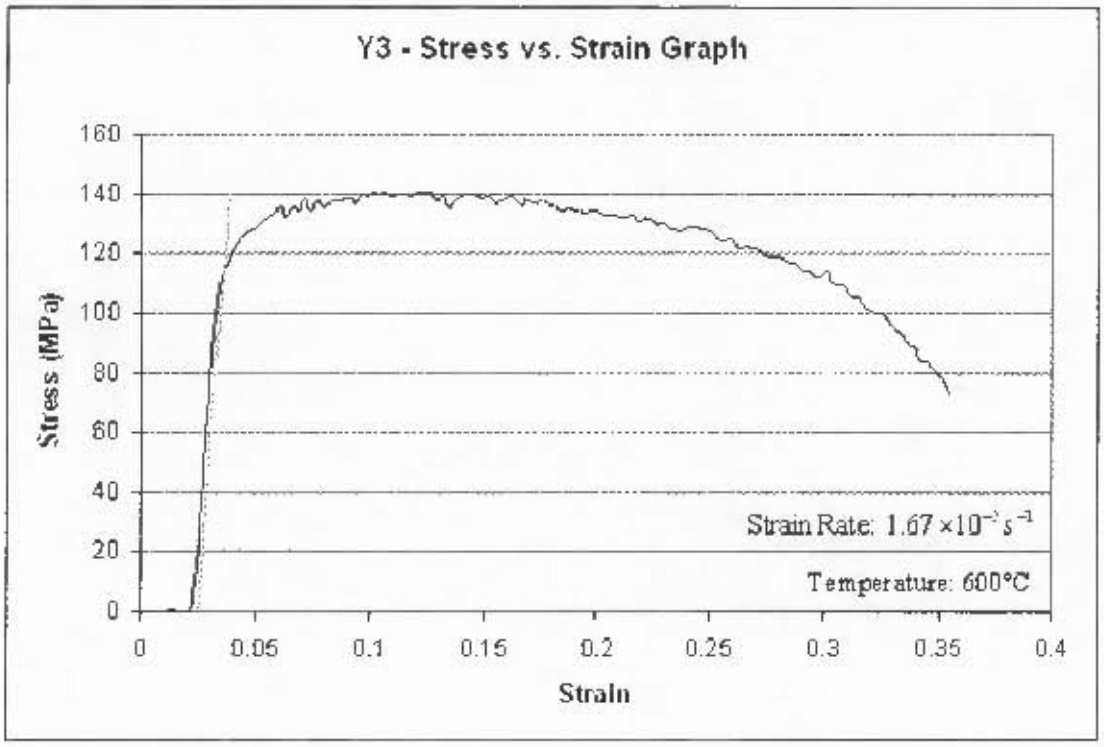

Figure A2.3.19 – Test Result for Specimen Y3

Table A2.3.19 - Yield Stress and Failure Strain for Specimen Y3

Yield Stress (MPa)	114.00
Ultimate Tensile Stress (MPa)	140.72
Gauge Length at Failure (mm)	81.7
Elongation of Gauge Length at Failure (mm)	21.7
Strain at failure (%)	36.17

A2.4. Test Results at a Strain Rate of: 1 x $10^{-1}s^{-1}$

A total of 15 tests were carried out at a strain rate of $1\times10^{-1}s^{-1}$. Table A2.4.1 outlines the tests carried out and the graphed results follow the table.

Table A2.4.1 – Tensile Tests Carried Out at $1\times10^{-1}s^{-1}$

Specimen Name	Cross Section Details of Gauge Length			Temperature (°C)
	Width (mm)	Thickness (mm)	Area (mm^2)	
SA2	12.68	3.00	38.04	25
SA6	12.56	3.00	37.68	25
SB2	12.66	3.00	37.98	100
XE2	12.62	3.00	37.86	100
FD3	12.60	3.00	37.80	100
SC1	12.64	3.00	37.92	200
SC2	12.56	3.00	37.68	200
SC3	12.64	3.00	37.92	200
SD2	12.60	3.00	37.80	300
XB2	12.66	3.00	37.98	300
SE1	12.46	3.00	37.38	450
XC1	12.58	3.00	37.74	450
XC2	12.58	3.00	37.74	450
SF3	12.40	3.00	37.20	600
XD2	12.62	3.00	37.68	600

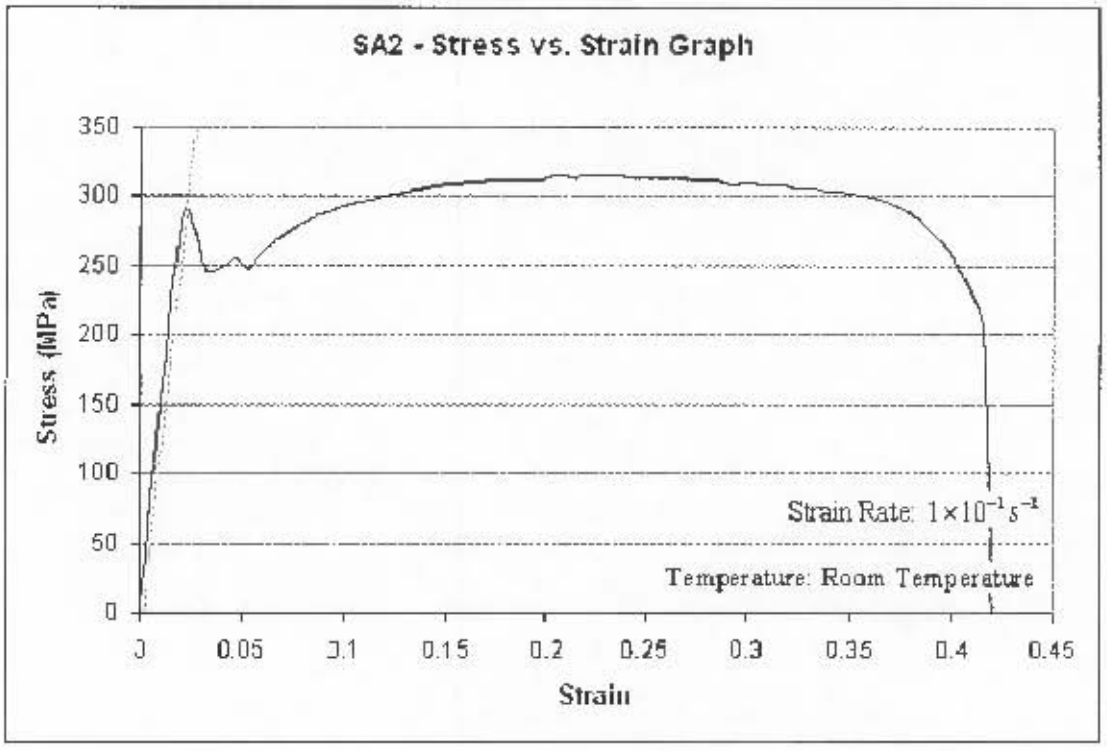

Figure A2.4.1 – Test Result for Specimen SA2

Table A2.4.1 – Yield Stress and Failure Strain for Specimen SA2

Yield Stress (MPa)	282.26
Ultimate Tensile Stress (MPa)	315.27
Gauge Length at Failure (mm)	83.3
Elongation of Gauge Length at Failure (mm)	23.3
Strain at failure (%)	38.83

Note: The ultimate tensile stress reported here refers to the maximum stress recorded as per the engineering stress vs. engineering strain graph. It does not refer to the true stress experienced at failure. This applies to all the test results at a strain rate of $1\times10^{-1}s^{-1}$.

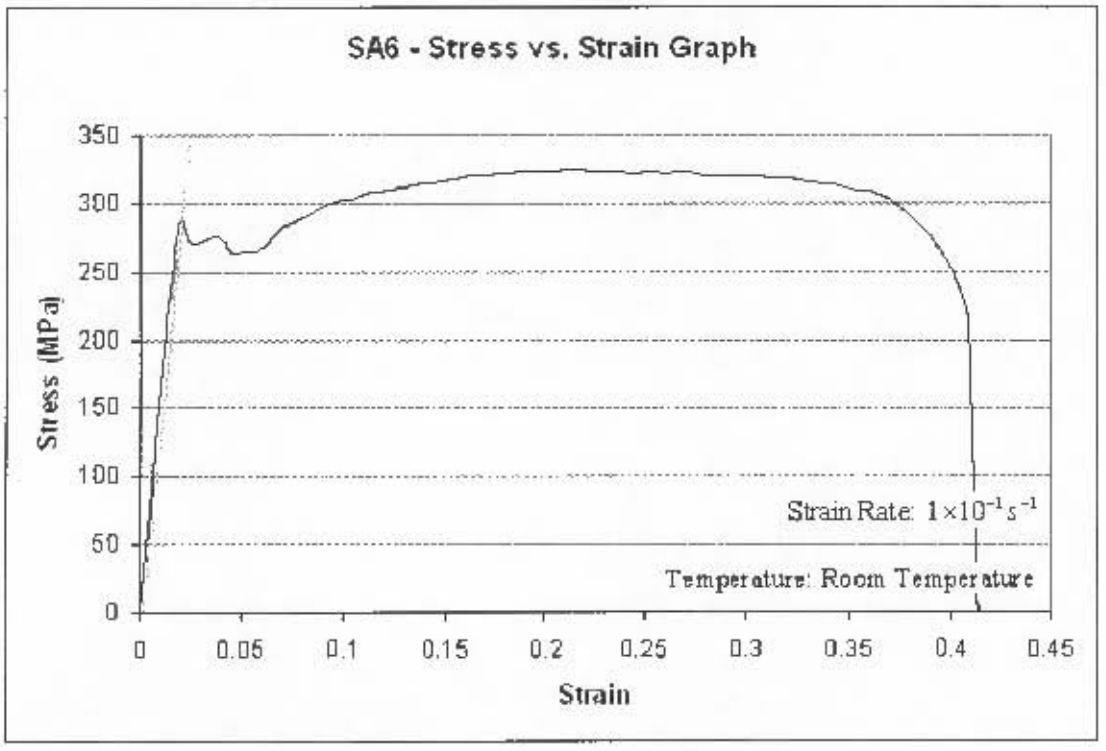

Figure A2.4.2 – Test Result for Specimen SA6

Table A2.4.2 – Yield Stress and Failure Strain for Specimen SA6

Yield Stress (MPa)	283.62
Ultimate Tensile Stress (MPa)	324.47
Gauge Length at Failure (mm)	83.1
Elongation of Gauge Length at Failure (mm)	23.1
Strain at failure (%)	38.50

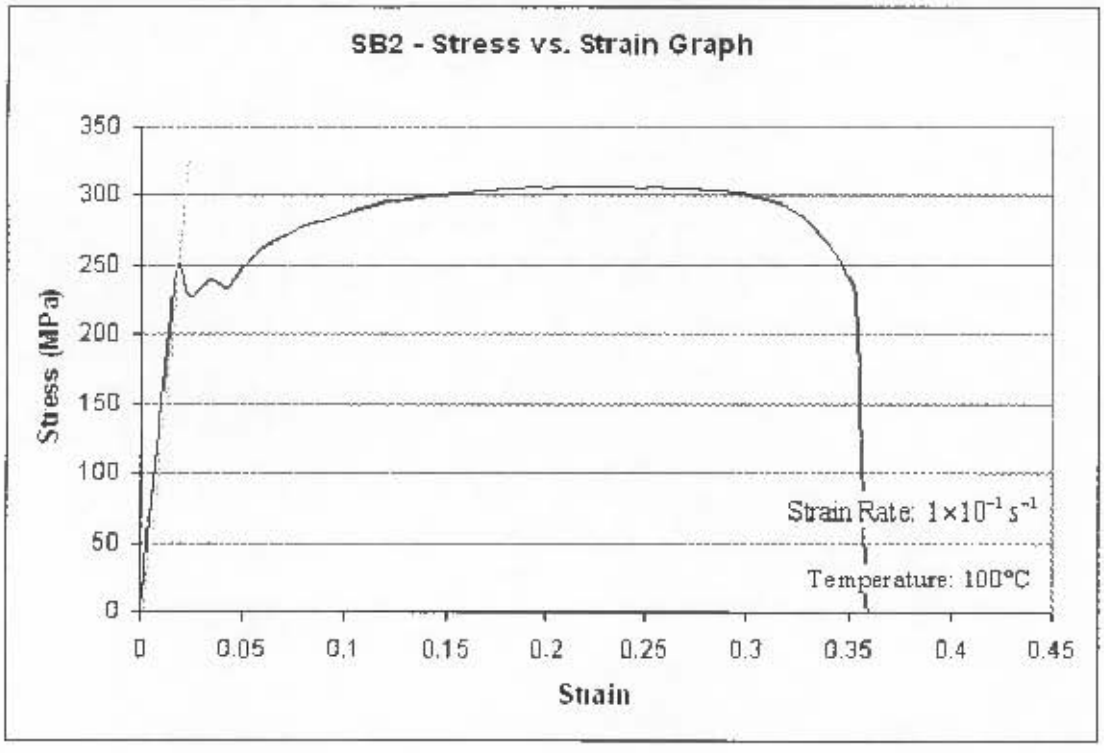

Figure A2.4.3 – Test Result for Specimen SB2

Table A2.4.3 – Yield Stress and Failure Strain for Specimen SB2

Yield Stress (MPa)	248.64
Ultimate Tensile Stress (MPa)	306.69
Gauge Length at Failure (mm)	79.7
Elongation of Gauge Length at Failure (mm)	19.7
Strain at failure (%)	32.83

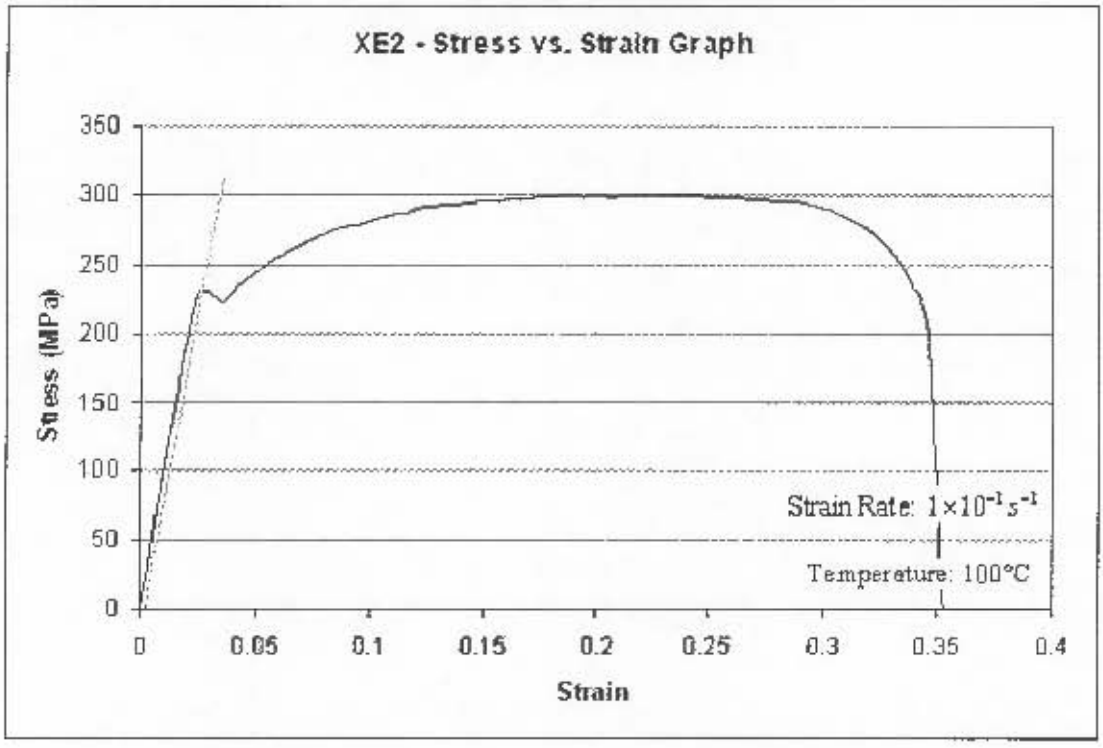

Figure A2.4.4 – Test Result for Specimen XE2

Table A2.4.4 – Yield Stress and Failure Strain for Specimen XE2

Yield Stress (MPa)	227.63
Ultimate Tensile Stress (MPa)	300.71
Gauge Length at Failure (mm)	79.3
Elongation of Gauge Length at Failure (mm)	19.3
Strain at failure (%)	32.17

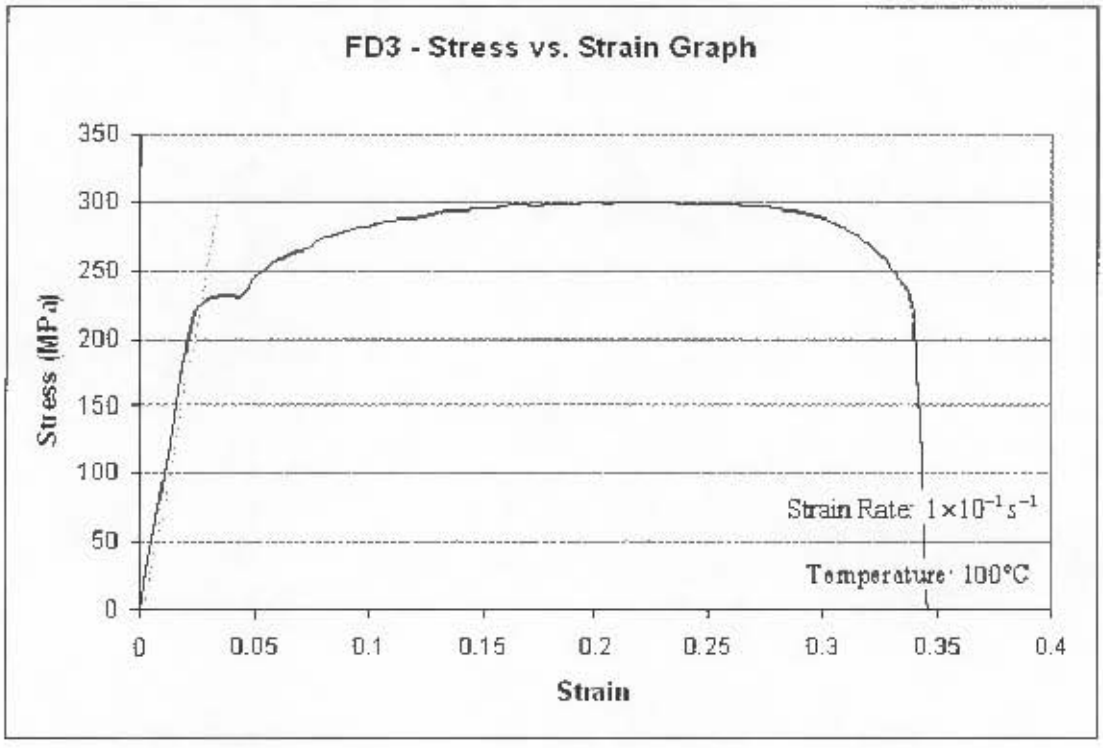

Figure A2.4.5 – Test Result for Specimen FD3

Table A2.4.5 – Yield Stress and Failure Strain for Specimen FD3

Yield Stress (MPa)	221.63
Ultimate Tensile Stress (MPa)	299.68
Gauge Length at Failure (mm)	80.0
Elongation of Gauge Length at Failure (mm)	20.0
Strain at failure (%)	33.33

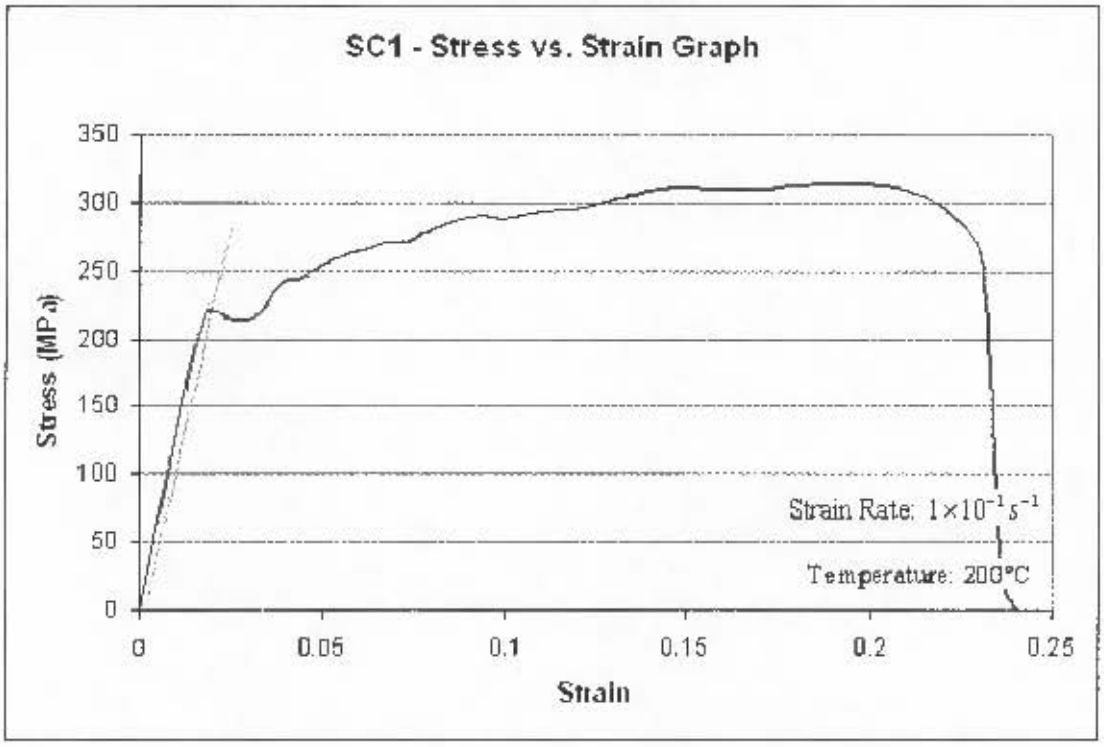

Figure A2.4.6 – Test Result for Specimen SC1

Table A2.4.6 – Yield Stress and Failure Strain for Specimen SC1

Yield Stress (MPa)	216.66
Ultimate Tensile Stress (MPa)	314.45
Gauge Length at Failure (mm)	72.8
Elongation of Gauge Length at Failure (mm)	12.8
Strain at failure (%)	21.33

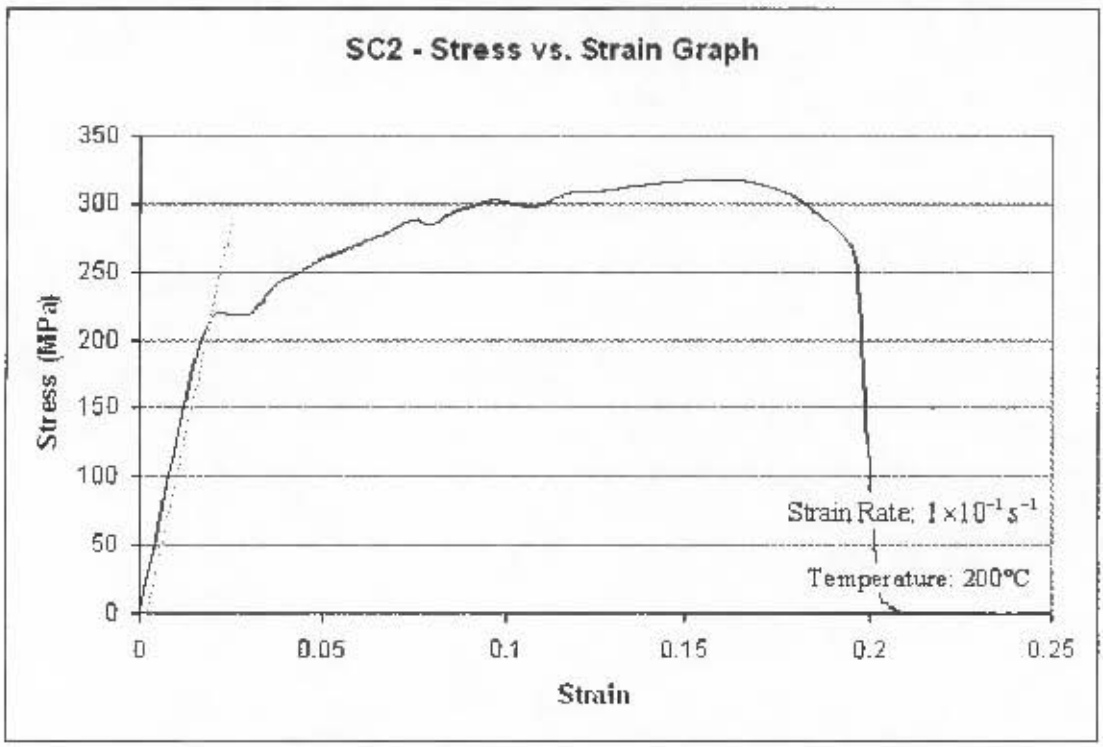

Figure A2.4.7 – Test Result for Specimen SC2

Table A2.4.7 – Yield Stress and Failure Strain for Specimen SC2

Yield Stress (MPa)	211.32
Ultimate Tensile Stress (MPa)	317.62
Gauge Length at Failure (mm)	70.4
Elongation of Gauge Length at Failure (mm)	10.4
Strain at failure (%)	17.33

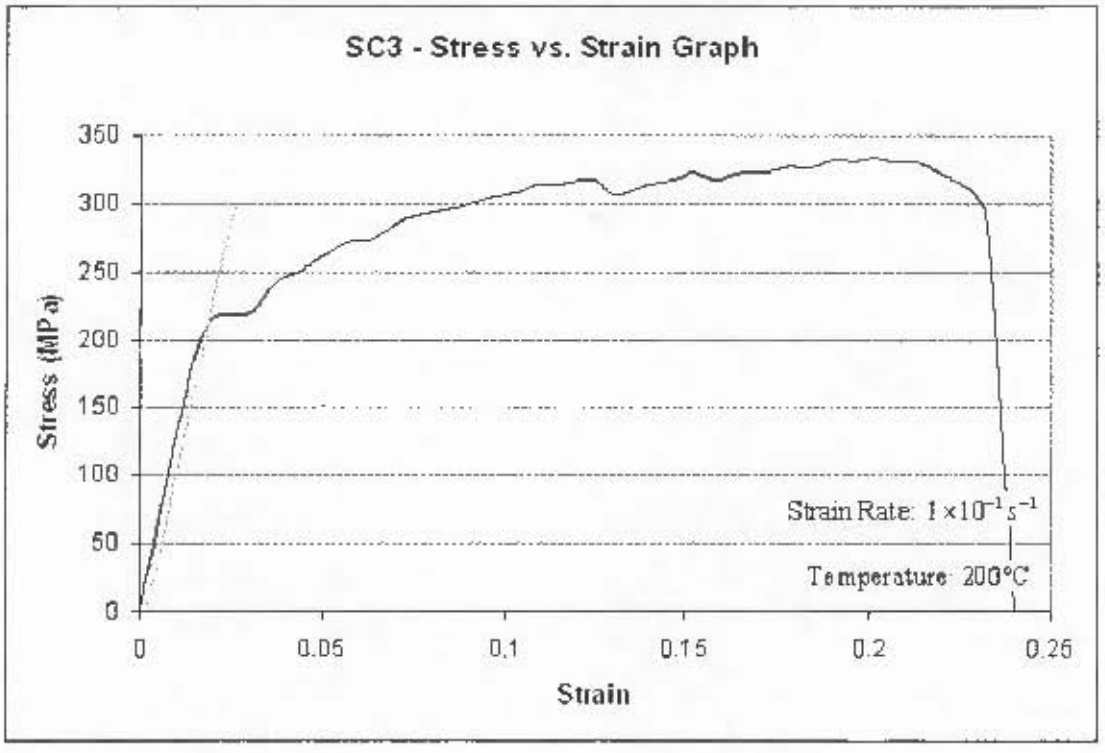

Figure A2.4.8 – Test Result for Specimen SC3

Table A2.4.8 – Yield Stress and Failure Strain for Specimen SC3

Yield Stress (MPa)	206.00
Ultimate Tensile Stress (MPa)	333.54
Gauge Length at Failure (mm)	72.9
Elongation of Gauge Length at Failure (mm)	12.9
Strain at failure (%)	21.50

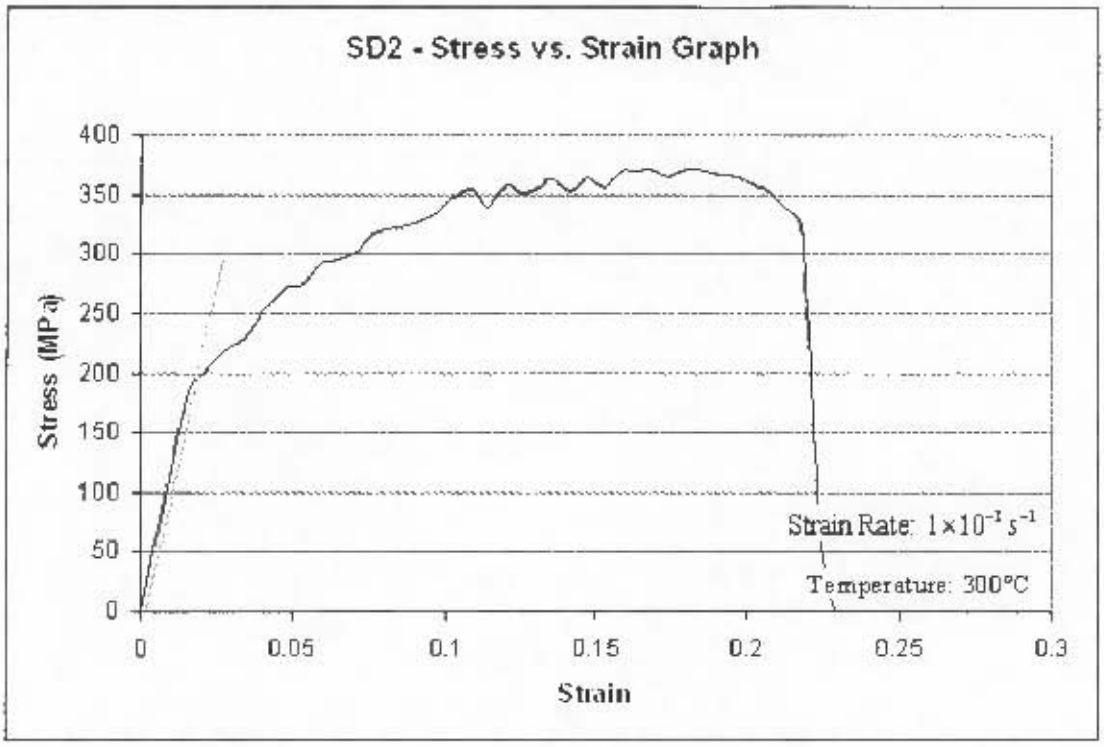

Figure A2.4.9 – Test Result for Specimen SD2

Table A2.4.9 – Yield Stress and Failure Strain for Specimen SD2

Yield Stress (MPa)	191.83
Ultimate Tensile Stress (MPa)	371.32
Gauge Length at Failure (mm)	71.8
Elongation of Gauge Length at Failure (mm)	11.8
Strain at failure (%)	19.67

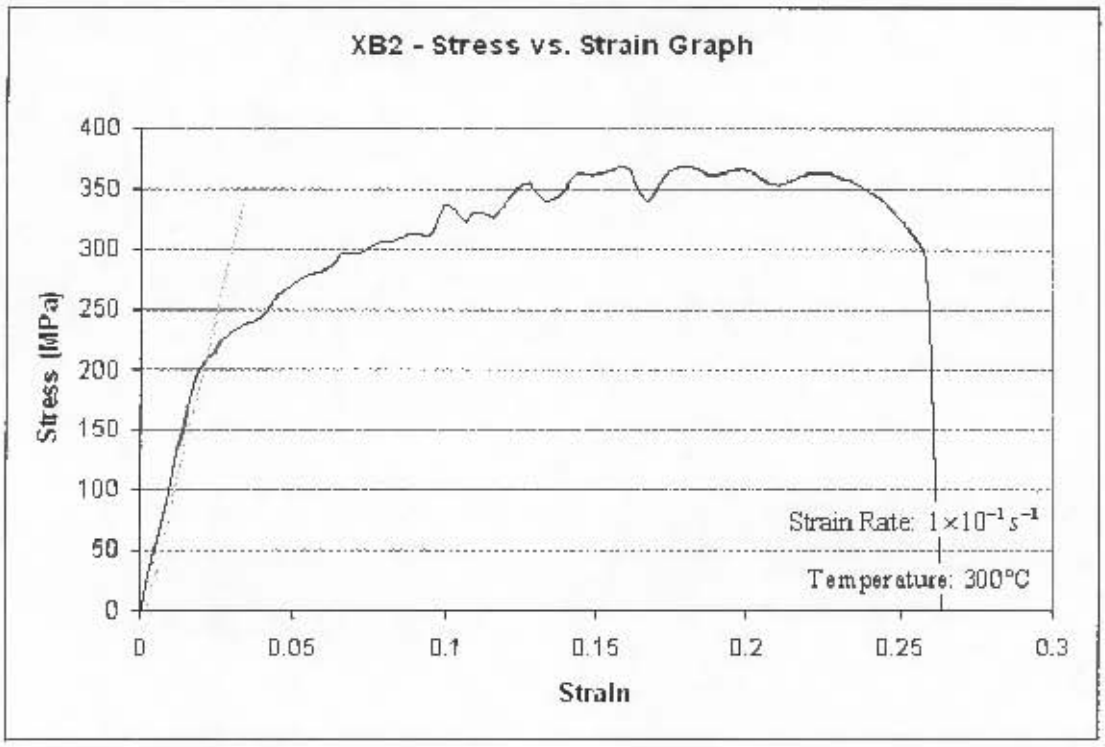

Figure A2.4.10 – Test Result for Specimen XB2

Table A2.4.10 Yield Stress and Failure Strain for Specimen XB2

Yield Stress (MPa)	202.97
Ultimate Tensile Stress (MPa)	367.80
Gauge Length at Failure (mm)	73.7
Elongation of Gauge Length at Failure (mm)	13.7
Strain at failure (%)	22.83

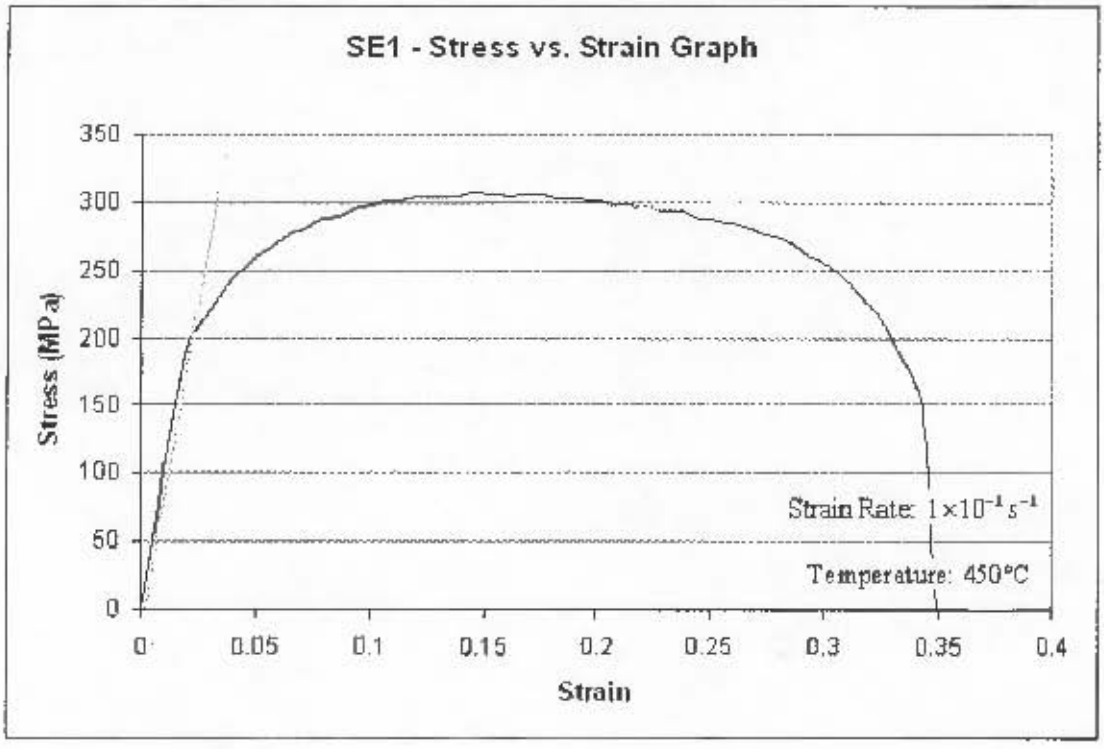

Figure A2.4.11 – Test Result for Specimen SE1

Table A2.4.11 – Yield Stress and Failure Strain for Specimen SE1

Yield Stress (MPa)	195.07
Ultimate Tensile Stress (MPa)	307.17
Gauge Length at Failure (mm)	79.8
Elongation of Gauge Length at Failure (mm)	19.8
Strain at failure (%)	33.00

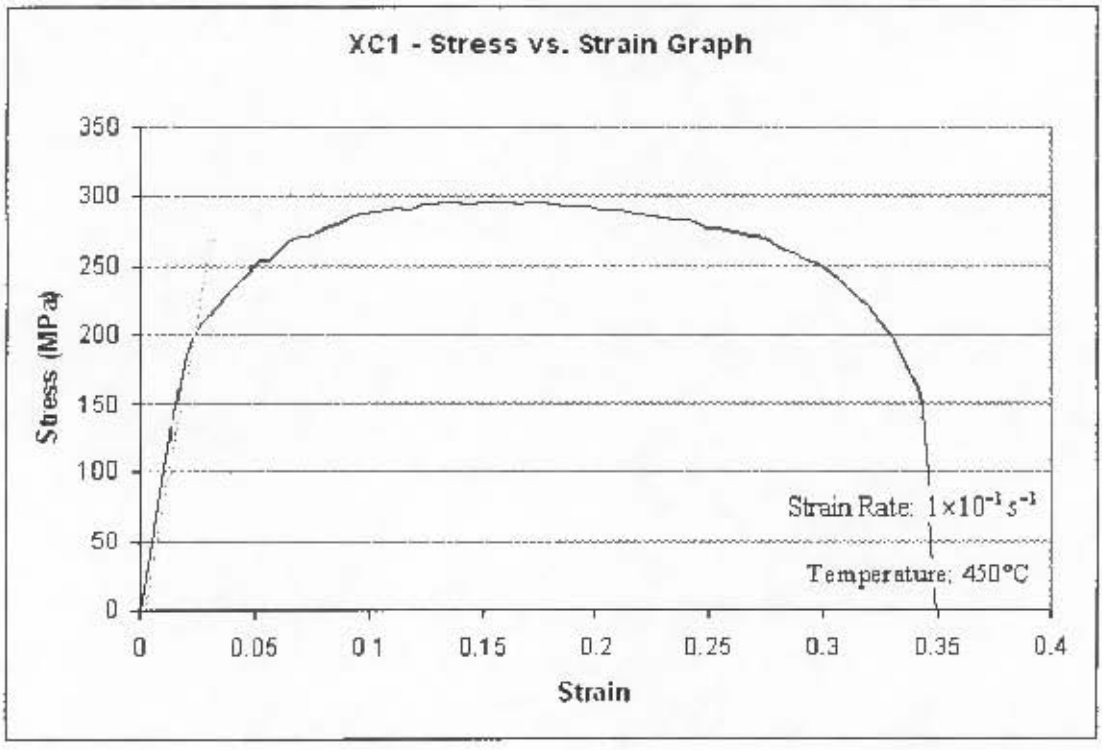

Figure A2.4.12 – Test Result for Specimen XC1

Table A2.4.12 – Yield Stress and Failure Strain for Specimen XC1

Yield Stress (MPa)	192.11
Ultimate Tensile Stress (MPa)	296.77
Gauge Length at Failure (mm)	79.6
Elongation of Gauge Length at Failure (mm)	19.6
Strain at failure (%)	32.67

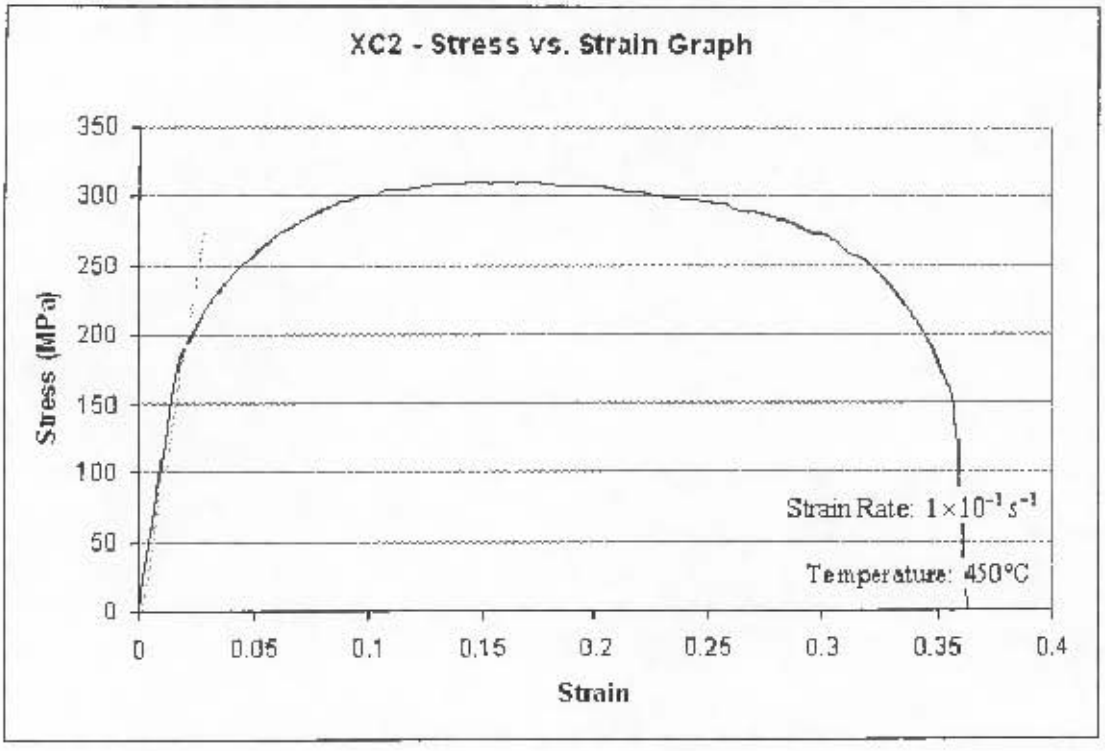

Figure A2.4.13 – Test Result for Specimen XC2

Table A2.4.13 – Yield Stress and Failure Strain for Specimen XC2

Yield Stress (MPa)	188.62
Ultimate Tensile Stress (MPa)	310.94
Gauge Length at Failure (mm)	79.9
Elongation of Gauge Length at Failure (mm)	19.9
Strain at failure (%)	33.17

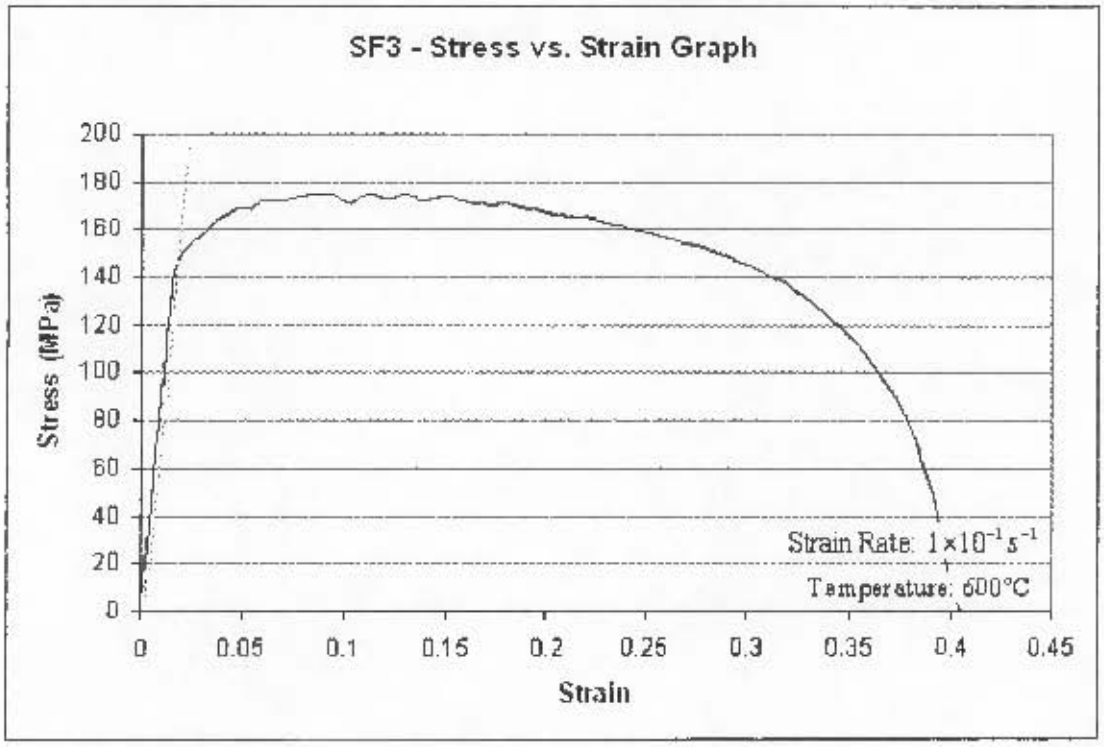

Figure A2.4.14 – Test Result for Specimen SF3

Table A2.4.14 – Yield Stress and Failure Strain for Specimen SF3

Yield Stress (MPa)	144.85
Ultimate Tensile Stress (MPa)	175.00
Gauge Length at Failure (mm)	83.8
Elongation of Gauge Length at Failure (mm)	23.8
Strain at failure (%)	39.67

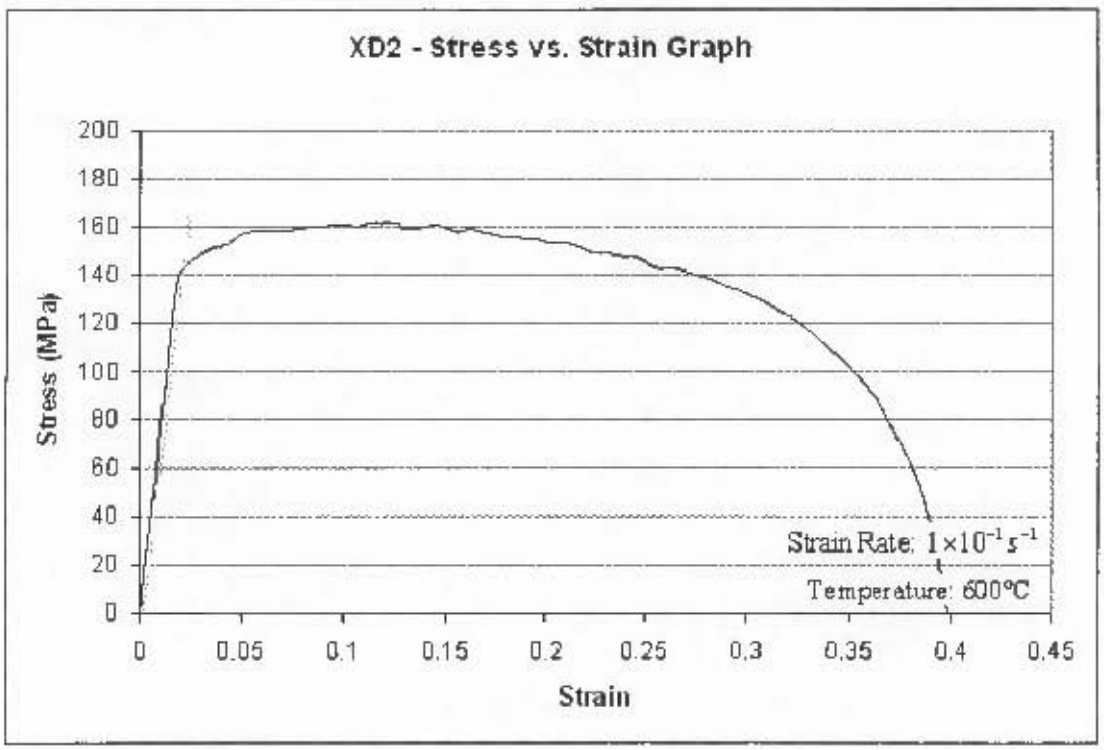

Figure A2.4.15 – Test Result for Specimen XD2

Table A2.4.15 – Yield Stress and Failure Strain for Specimen XD2

Yield Stress (MPa)	141.04
Ultimate Tensile Stress (MPa)	161.91
Gauge Length at Failure (mm)	83.6
Elongation of Gauge Length at Failure (mm)	23.6
Strain at failure (%)	39.33

A3. CHEMICAL COMPOSITION ANALYSIS REPORT

J. MULLER
LABORATORIES (PTY) LTD
ANALYTICAL CHEMISTS

P O BOX 51;
PAARDEN ILAND 7420
REP. OF SOUTH AFRICA
TELEPHONE: 27-021-5103800/2
FAX: 27-021-5103800
E-mail: jmlabs@iafrica.com

OFFICE & LABORATORIES AT:
50 MARINE DRIVE
PAARDEN ILAND 7405
REP. OF SOUTH AFRICA

Our Ref: JMS11476-U90204

Date of Issue: 13 DECEMBER 2005

Certificate of Analysis

PAGE 1 OF 1

This is to certify that the samples listed below were analysed

SUBMITTED BY: UCT
PRIVATE BAG X3
RONDEBOSCH
7701
ATTENTION: S BATHO
ORDER NO: 760043

SAMPLE TYPE: METAL

SAMPLE MARKS:
01. SPECIMEN A2
02. SPECIMEN H2
03. SPECIMEN R
04. SPECIMEN N

DATE SAMPLE RECEIVED: 29 NOVEMBER 2005
DATE ANALYSIS STARTED: 30 NOVEMBER 2005
DATE ANALYSIS COMPLETED: 12 DECEMBER 2005

Analysis relates only to the sample/s tested.
Analysis done:

		01	02	03	04
Carbon (C)	%m/m	0,07	0,06	0,06	0,07
Manganese (Mn)	%m/m	0,14	0,15	0,17	0,16
Silicon (Si)	%m/m	<0,05	<0,05	<0,05	<0,05
Phosphorous (P)	%m/m	0,006	0,003	0,007	0,007
Sulphur (S)	%m/m	0,002	0,002	0,003	0,002

Values reported as less than (<) are lower than the limit of detection for the method employed.

ANALYST
I JOHNSON

ANALYST
A BOTHA

ANALYST
S TERRY

DEPUTY LAB MANAGER
S TERRY

J. MULLER LABORATORIES (PTY) LTD DIRECTOR: I.M. JOHNSON
CONDITIONS OF ISSUE SEE OVERLEAF

Figure A3.1 – Chemical Composition Analysis Report

The specimens used for the tests carried out in this project were cut from the same sheet of steel. Samples of these specimens were then sent for an external chemical composition analysis. The samples marked as specimen A2 and specimen II2 in figure A3.1 represent the test specimens used in this project. Note that the samples marked as specimen R and specimen N were used in the tests found in reference [1] and were cut from a different sheet of steel. A summary of the chemical composition of the specimens used in this project is presented in table A3.1.

Table A3.1 – Chemical Composition of Mild Steel Tensile Specimens

Chemical	Carbon (C)	Manganese (Mn)	Silicon (Si)	Phosphorous (P)	Sulphur (S)
%m/m	0.06 ~ 0.07	0.14 ~ 0.15	<0.05	0.005 ~ 0.006	0.002

A4. MICROGRAPHS

25 samples were selected for analysis under an optical microscope. Table A4.1 indicates the selected specimens. Pieces were cut from one of the fractured ends of the tested specimens and mounted in polymer resin as shown in figure A4.1; micrographs were taken from the regions within the green circles. The micrographs, taken at $\times 500$ magnification, follow figure A4.1.

Table A4.1 – Microstructure Analysis Samples

Specimens	Test Temperatures and Strain Rate
Untested	N/A
A1, NA1, B1NEW, C1, D1 and U2	25°C to 600°C respectively; $4.17\times10^{-4}\,s^{-1}$
F1, NB3, G1, H2, V2 and W2	25°C to 600°C respectively; $3.33\times10^{-3}\,s^{-1}$
K2, NC3, L2, M1, X2 and Y1	25°C to 600°C respectively; $1.67\times10^{-2}\,s^{-1}$
SA2, SB2, SC1, XB2, SE1 and SF3	25°C to 600°C respectively; $1\times10^{-1}\,s^{-1}$

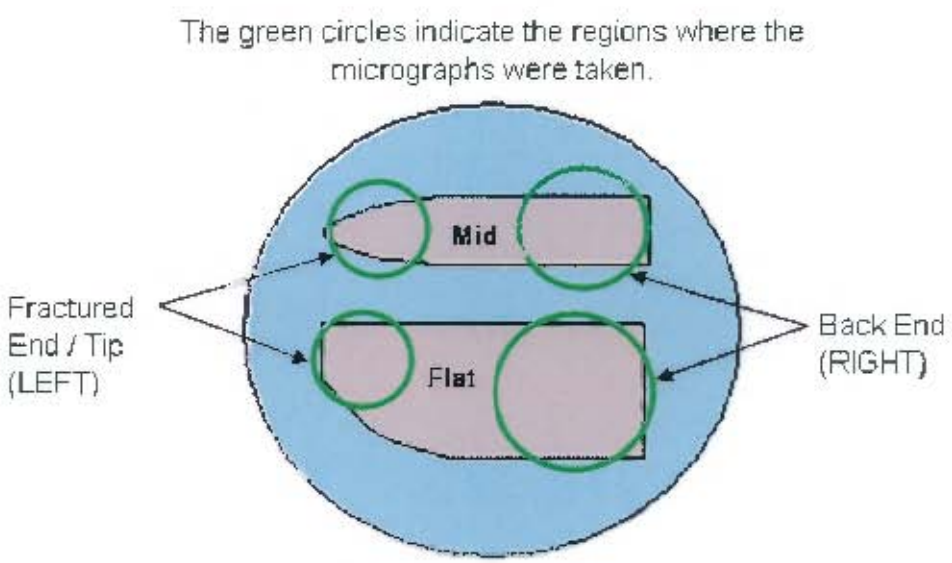

Figure A4.1 – Micrograph Regions

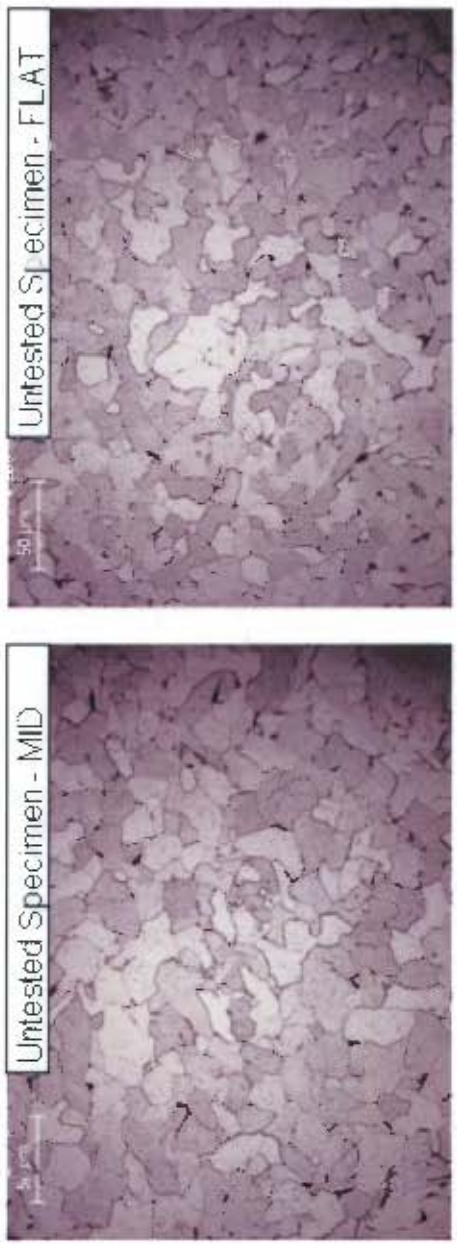

Figure A4.2 – Micrographs of an Untested Specimen along its Gauge Length

Note: In all micrographs of the tested specimens, the fractured end is located on the left.

Figure A4.3 – Micrographs of Specimen A1 (Tested at 25°C and 4.17 x $10^{-4}s^{-1}$)

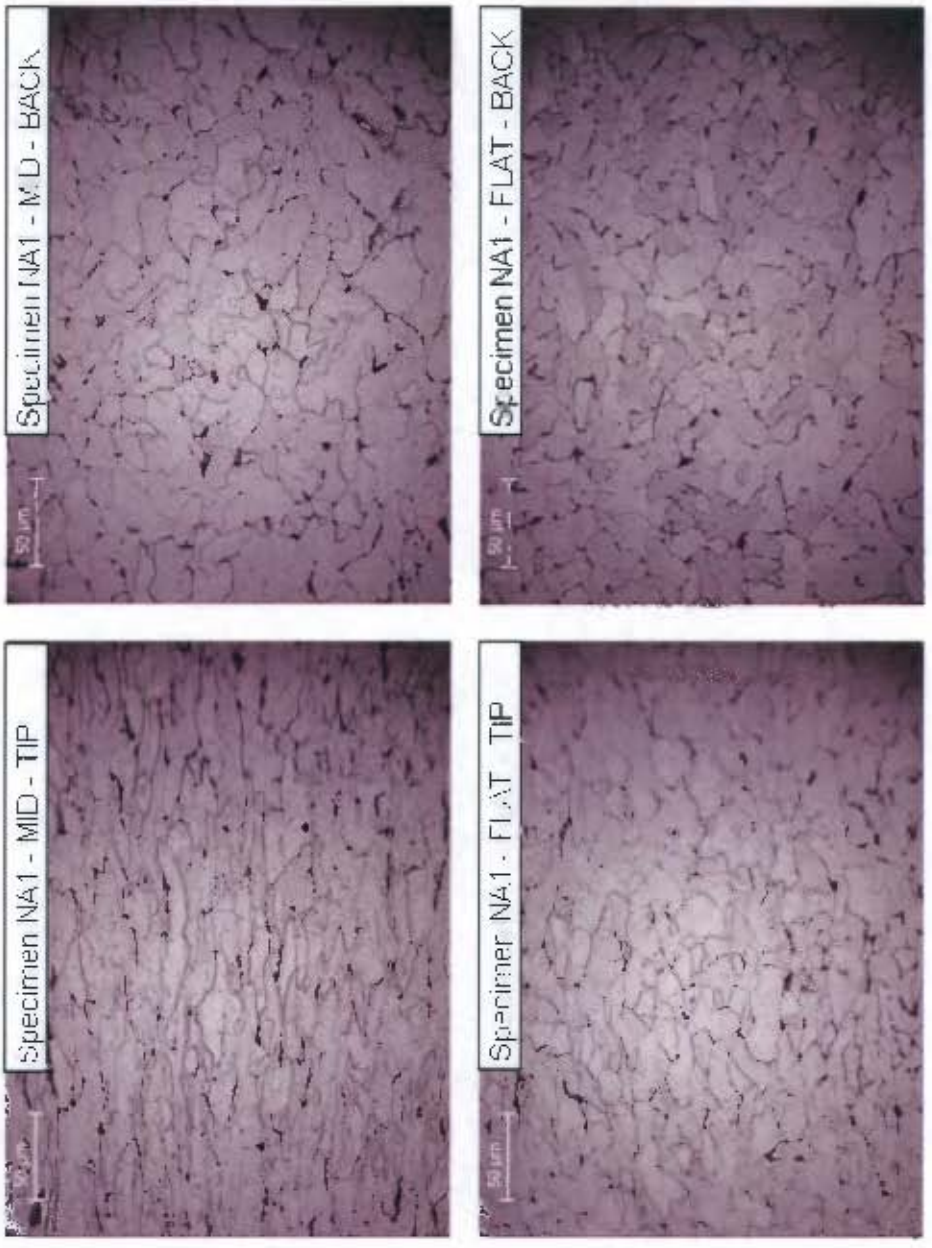

Figure A4.4 – Micrographs of Specimen NA1 (Tested at 100°C and 4.17 x $10^{-1}s^{-1}$)

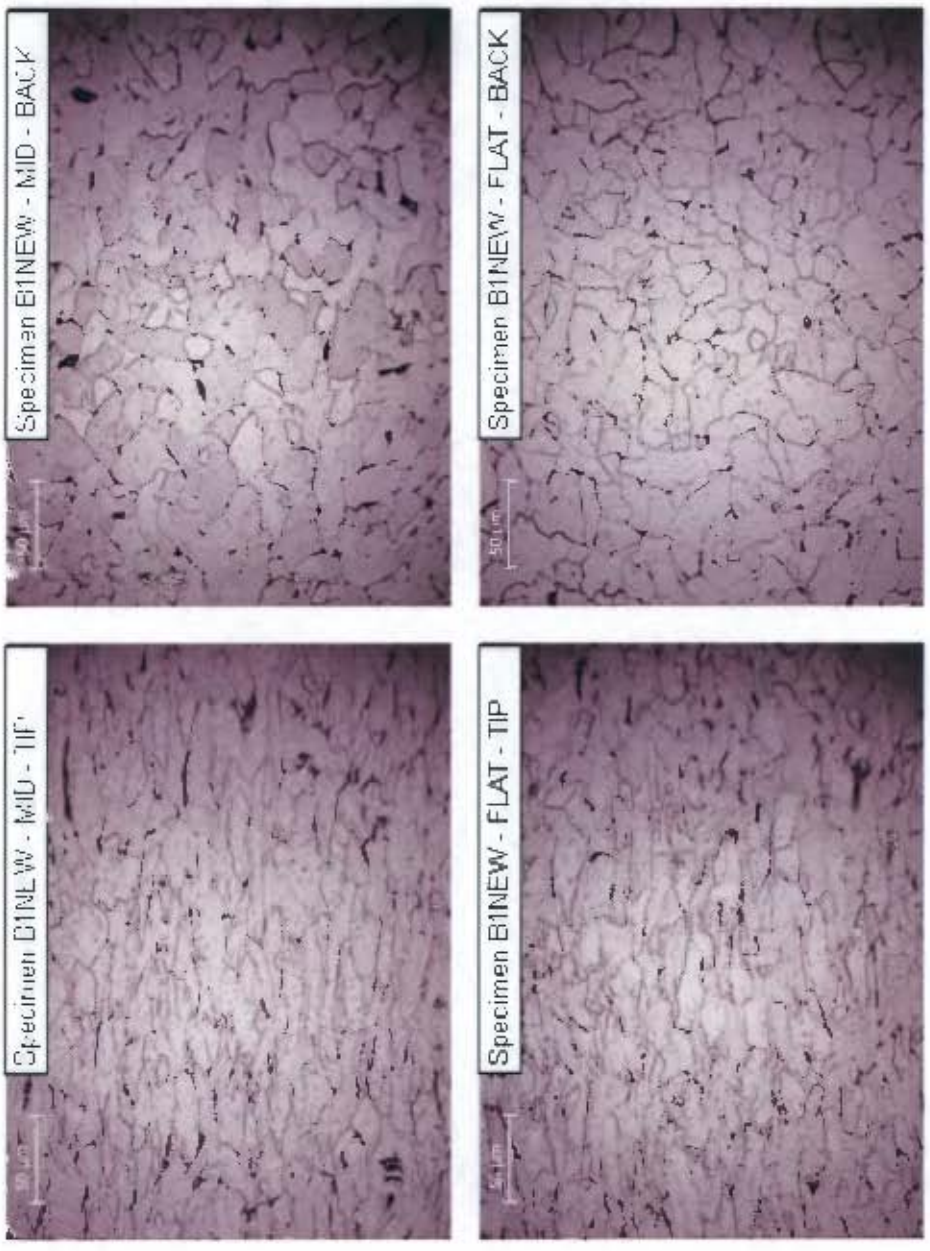

Figure A4.5 - Micrographs of Specimen B1NEW (Tested at 200°C and 4.17 x $10^{-4}s^{-1}$)

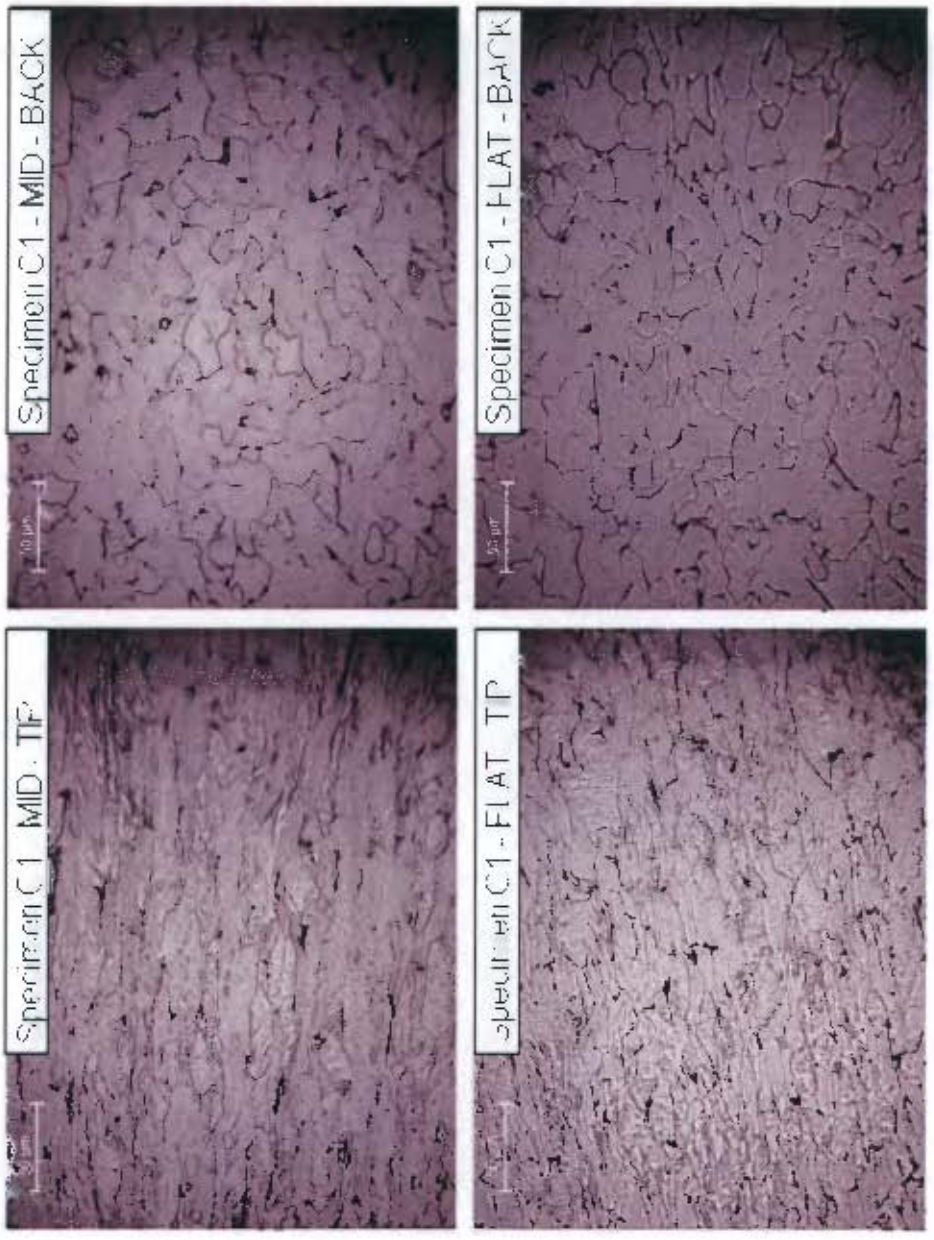

Figure A4.6 – Micrographs of Specimen C1 (Tested at 300°C and 4.17 x $10^{-4}s^{-1}$)

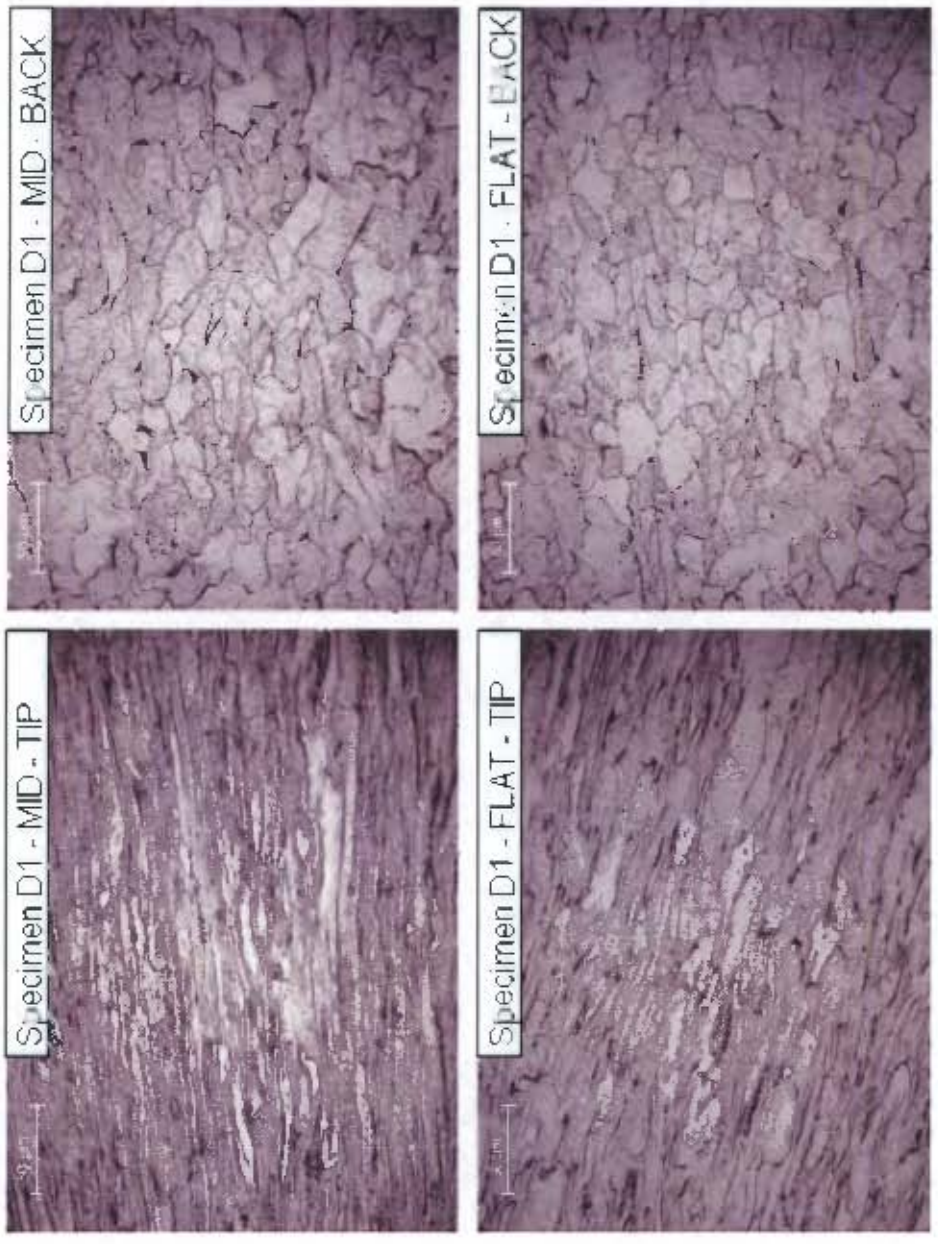

Figure A4.7 – Micrographs of Specimen D1 (Tested at 450°C and 4.17 x $10^{-4}s^{-1}$)

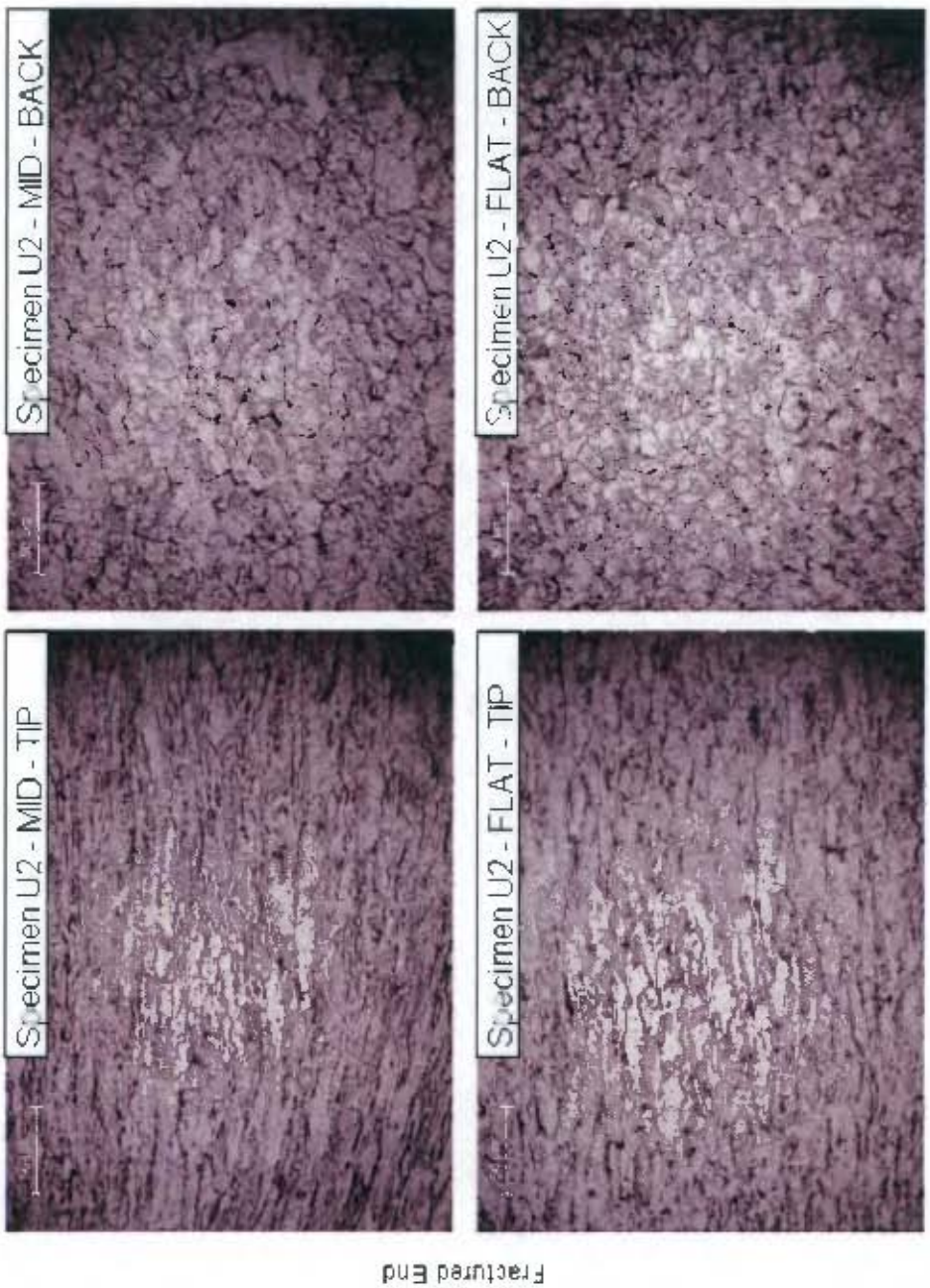

Figure A4.8 – Micrographs of Specimen U2 (Tested at 600°C and 4.17 x $10^{-4}s^{-1}$)

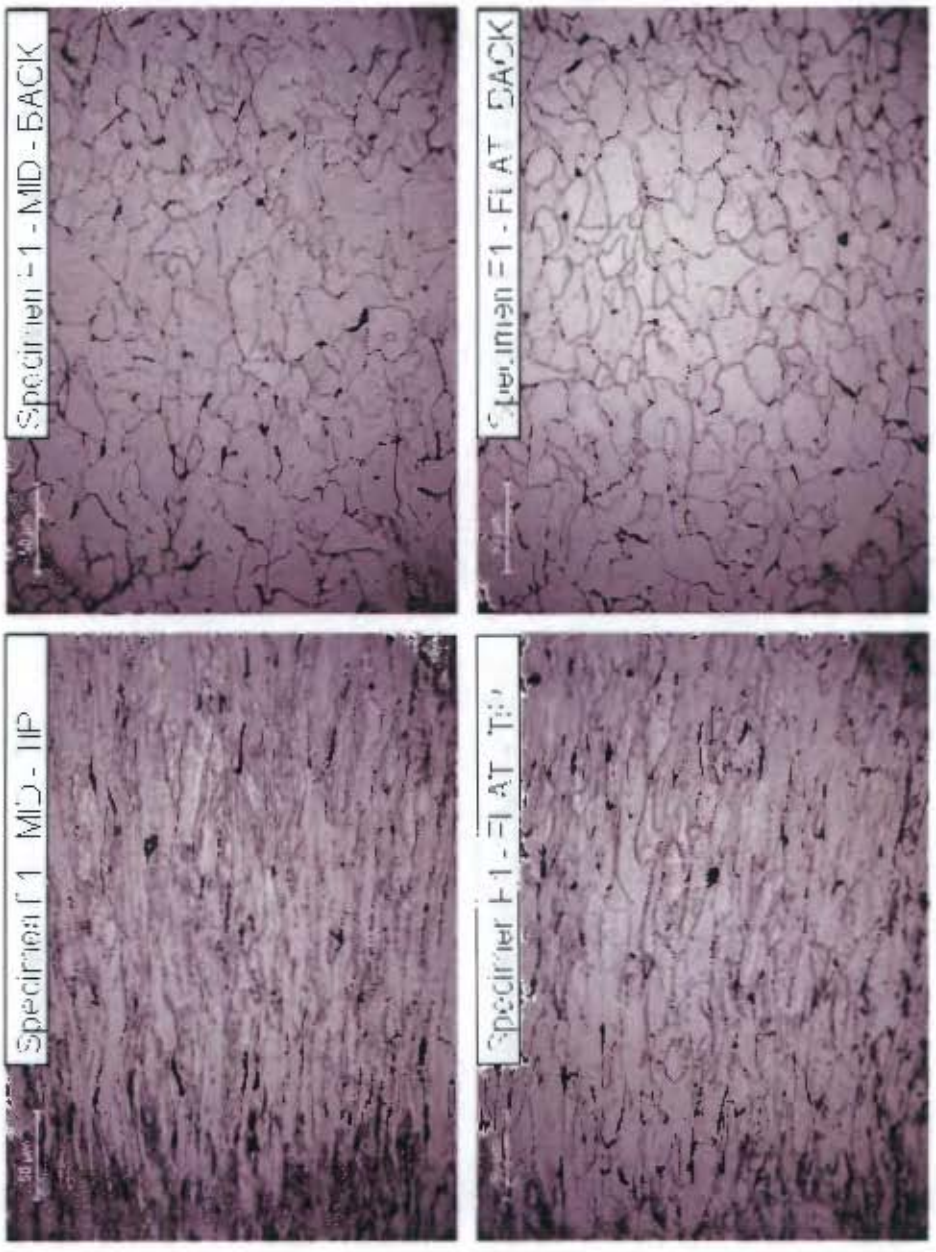

Figure A4.9 – Micrographs of Specimen F1 (Tested at 25°C and 3.33 x $10^{-3}s^{-1}$)

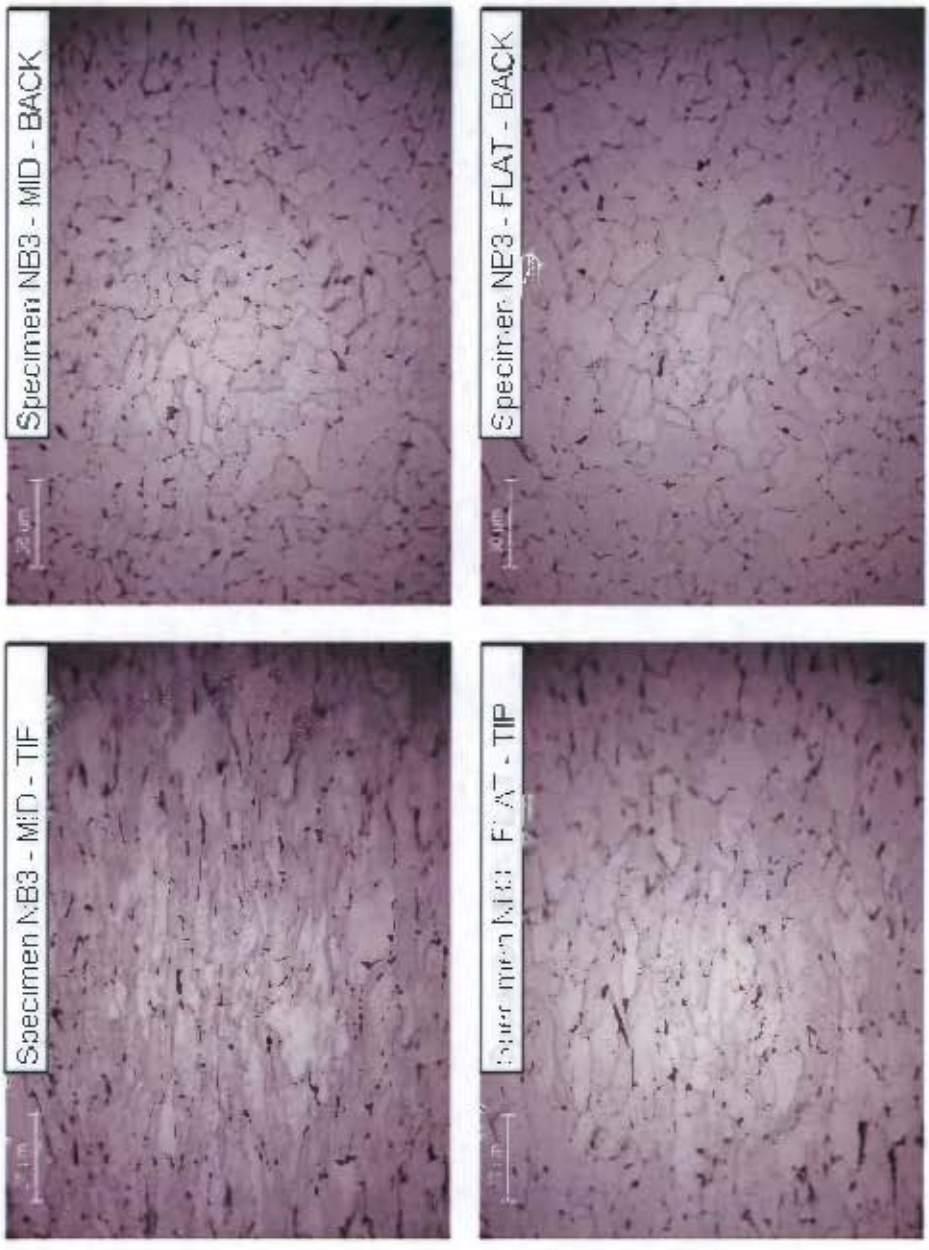

Figure A4.10 – Micrographs of Specimen NB3 (Tested at 100°C and 3.33 x $10^{-3}s^{-1}$)

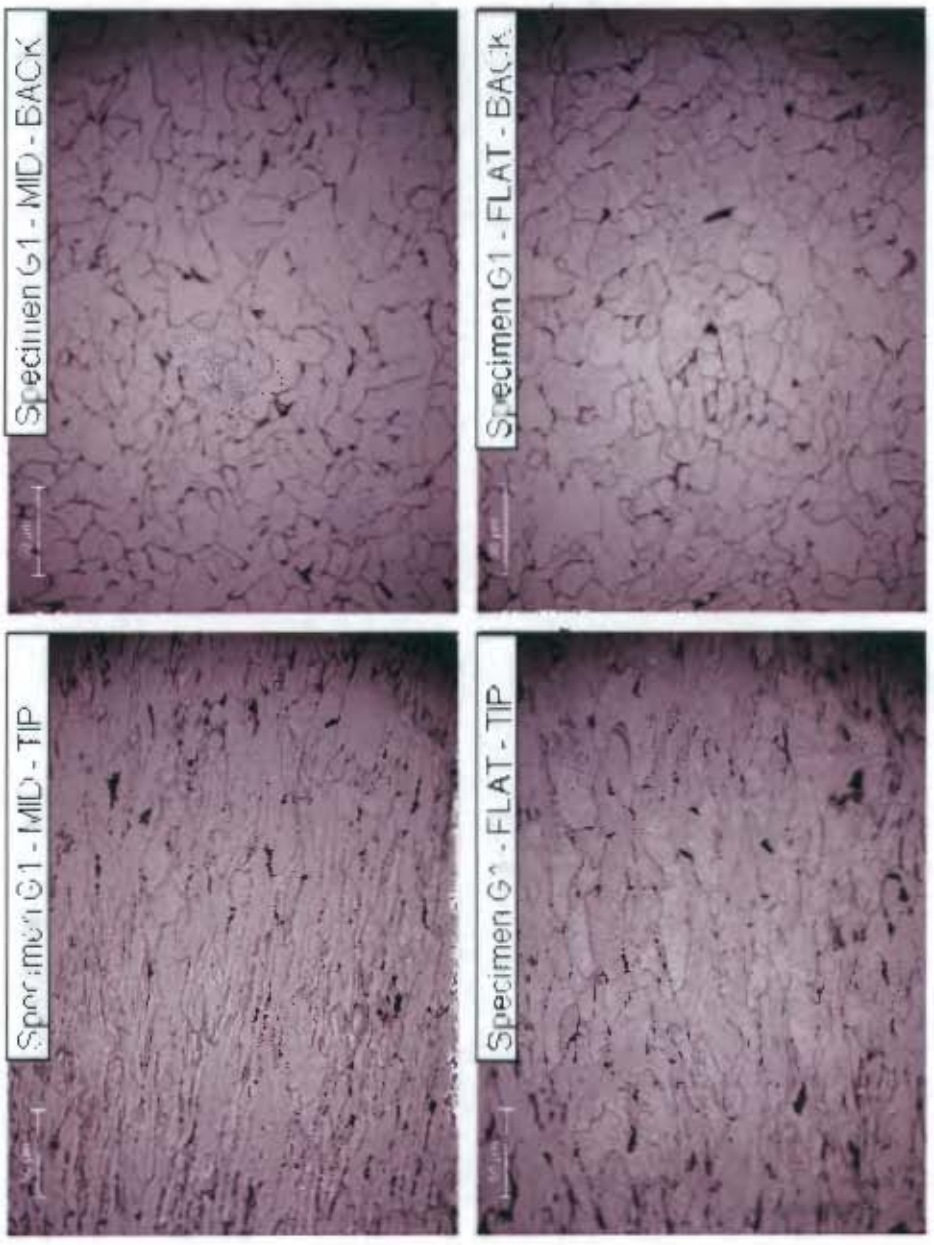

Figure A4.11 – Micrographs of Specimen G1 (Tested at $3.33 \times 10^{-1} s^{-1}$)

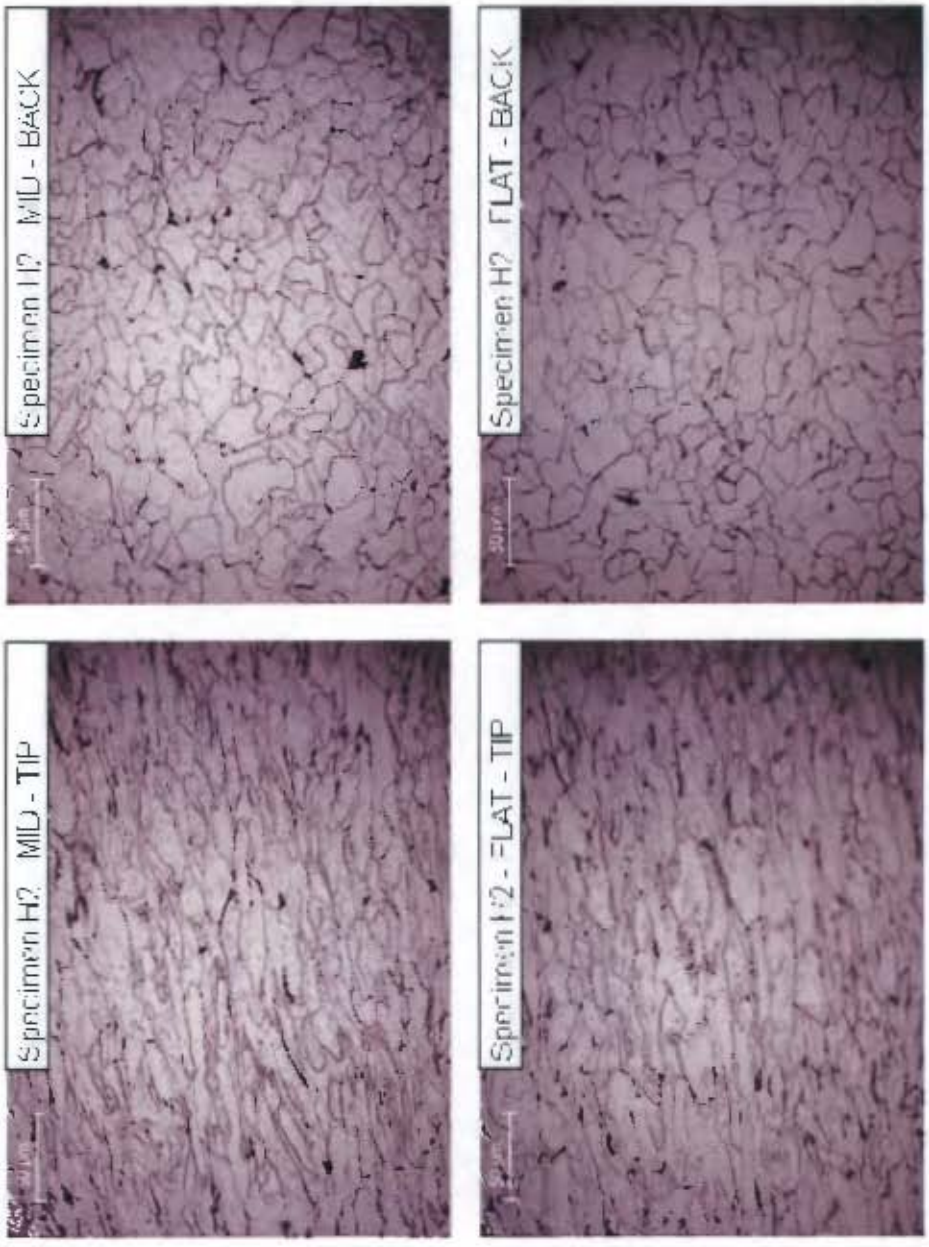

Figure A4.12 – Micrographs of Specimen H2 (Tested at 300°C and 3.33 x $10^{-3}s^{-1}$)

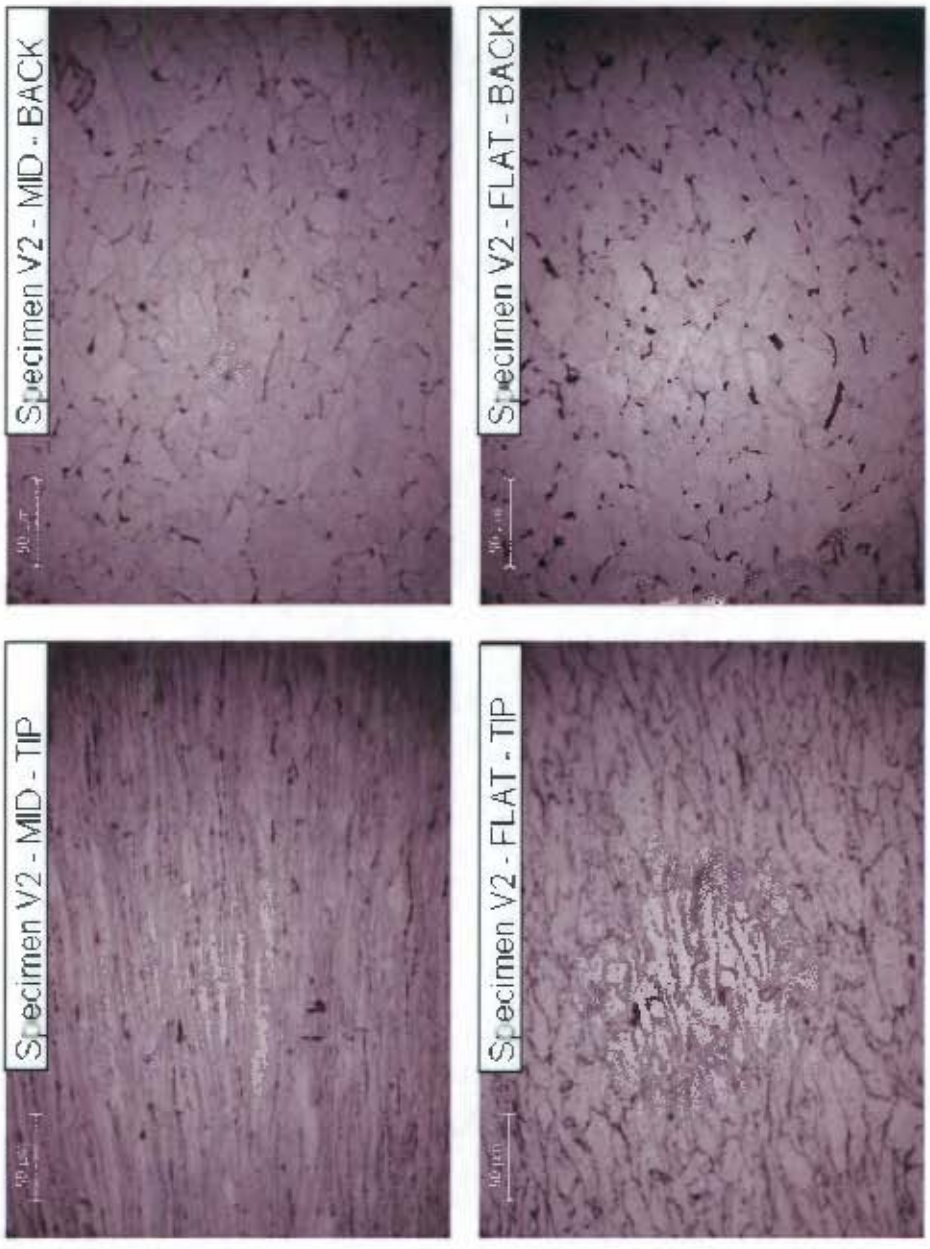

Figure A4.13 – Micrographs of Specimen V2 (Tested at 450°C and 3.33 x $10^{-3}s^{-1}$)

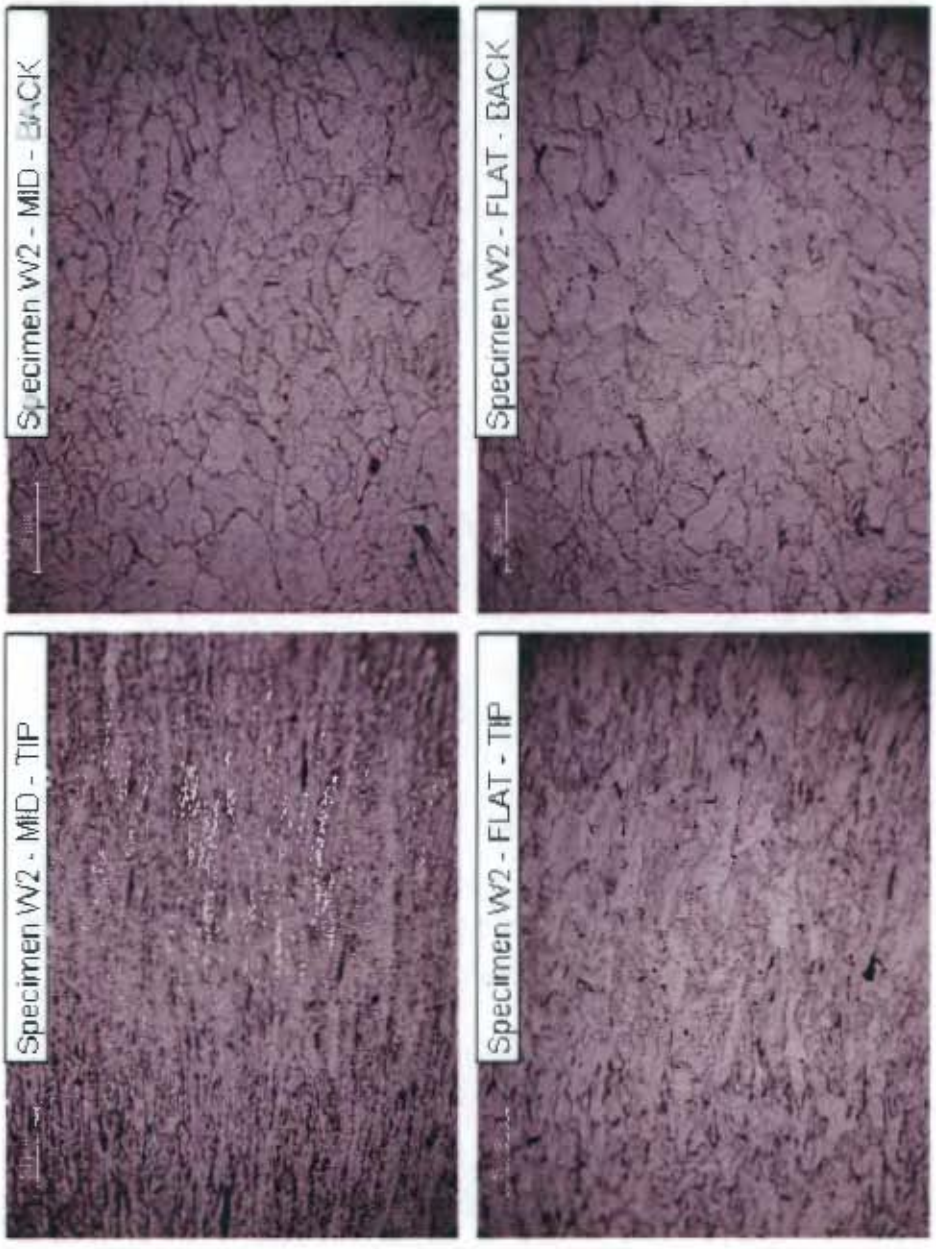

Figure A4.14 – Micrographs of Specimen W2 (Tested at 600° and 3.33 x $10^{-3}s^{-1}$)

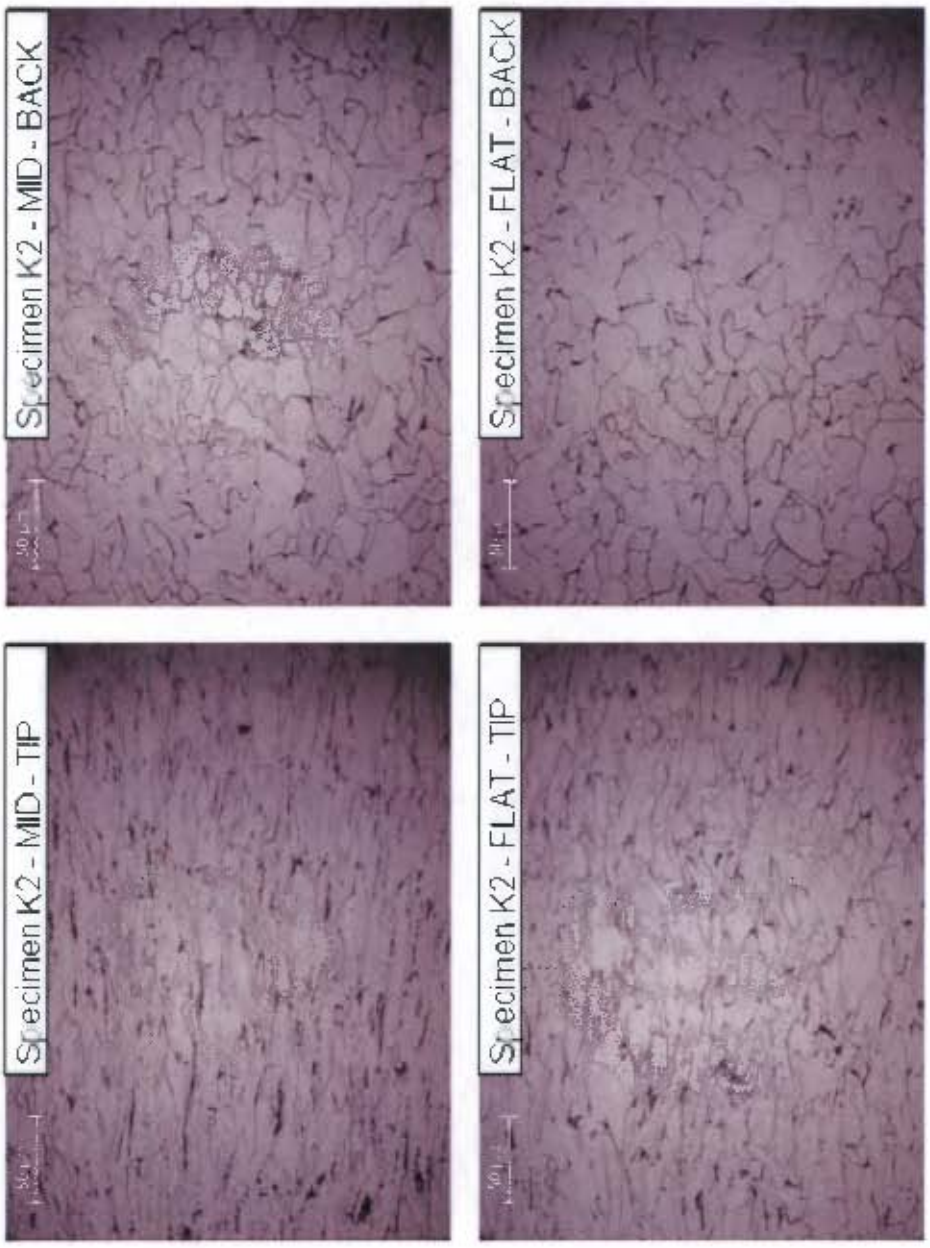

Figure A4.15 – Micrographs of Specimen K2 (Tested at 25°C and 1.67 x $10^{-2}s^{-1}$)

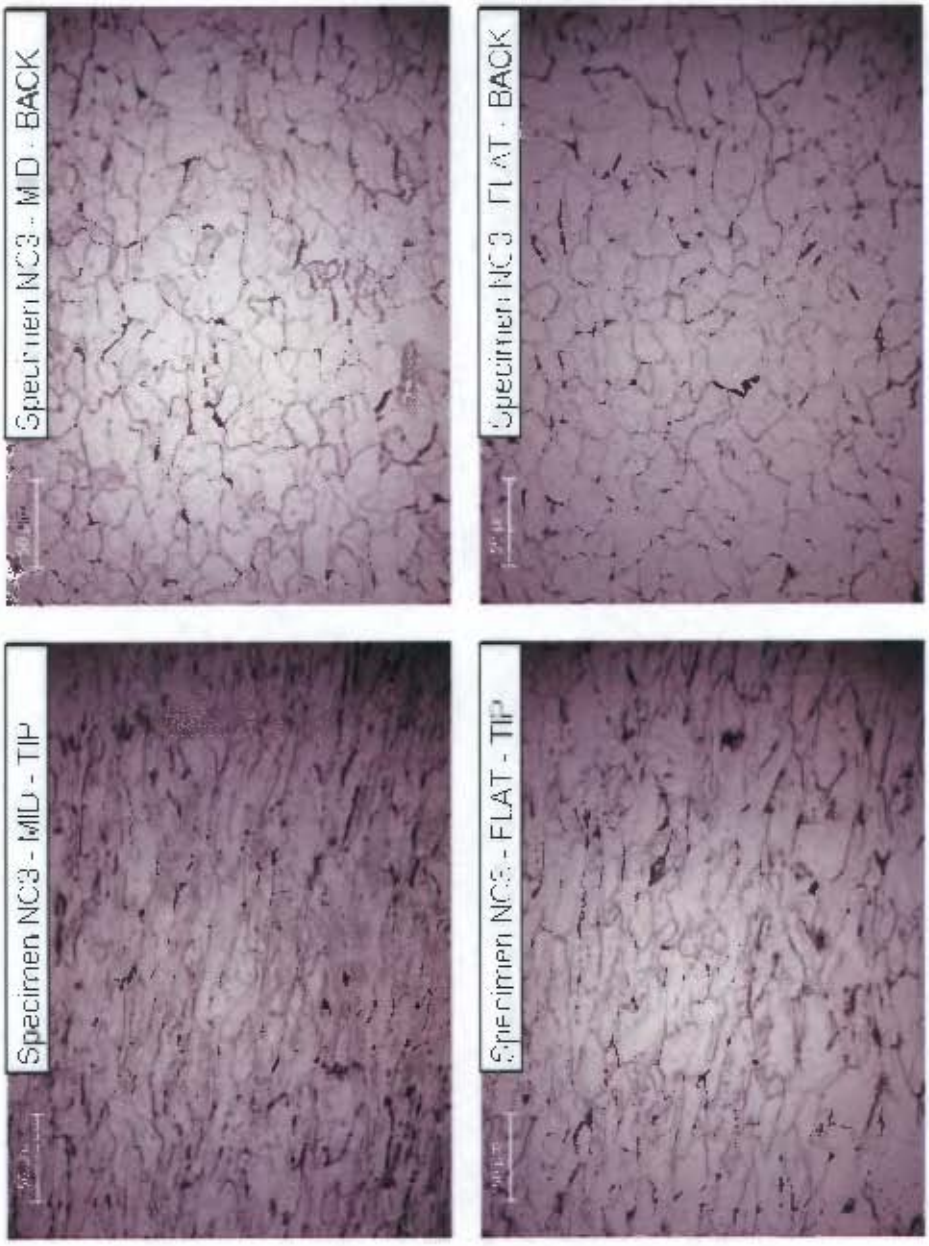

Figure A4.16 – Micrographs of Specimen NC3 (Tested at 100°C and 1.67 x $10^{-2}s^{-1}$)

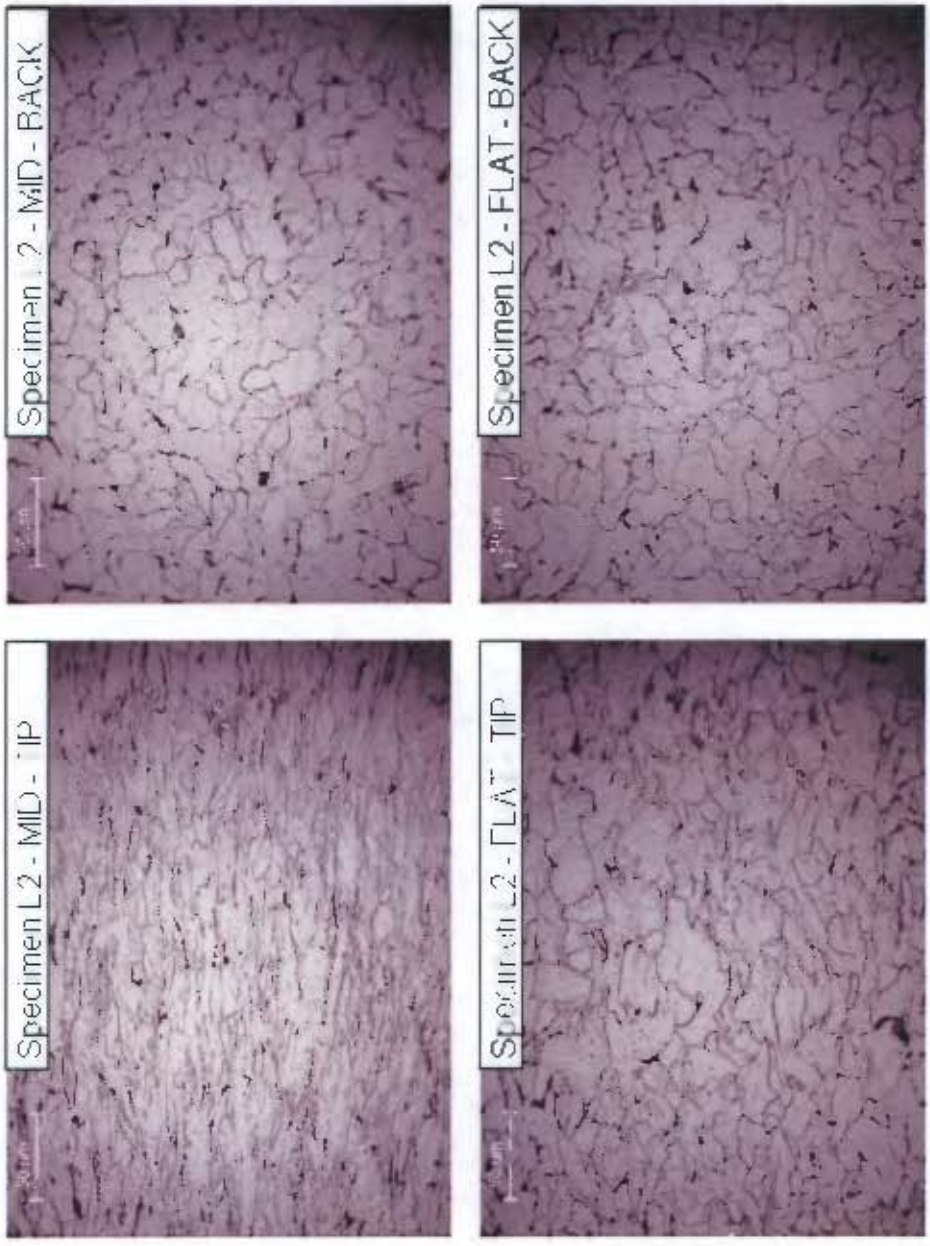

Figure A4.17 – Micrographs of Specimen L2 (Tested at 200°C and 1.67 x $10^{-2}s^{-1}$)

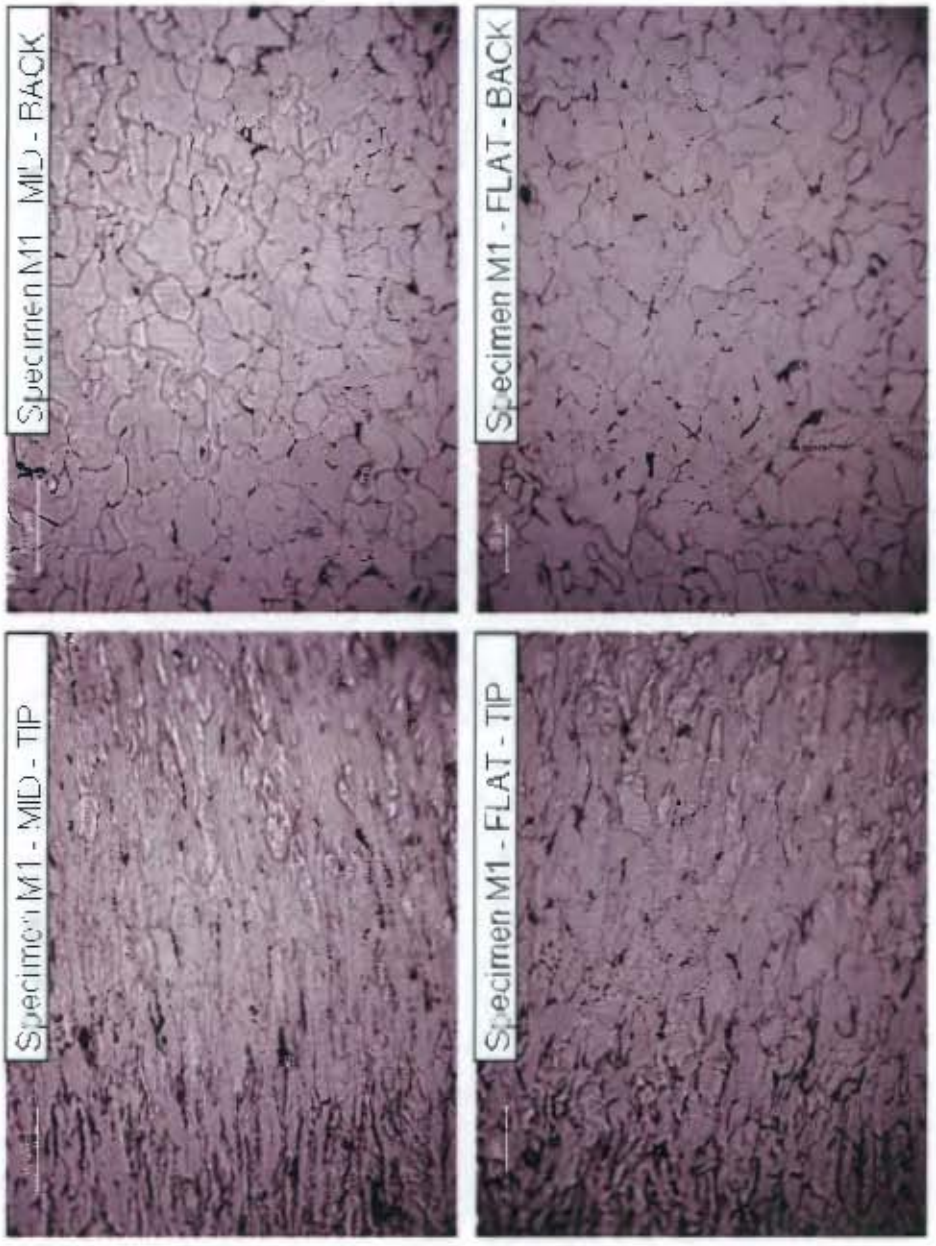

Figure A4.18 – Micrographs of Specimen M1 (Tested at 300°C and 1.67 x $10^{-2}s^{-1}$)

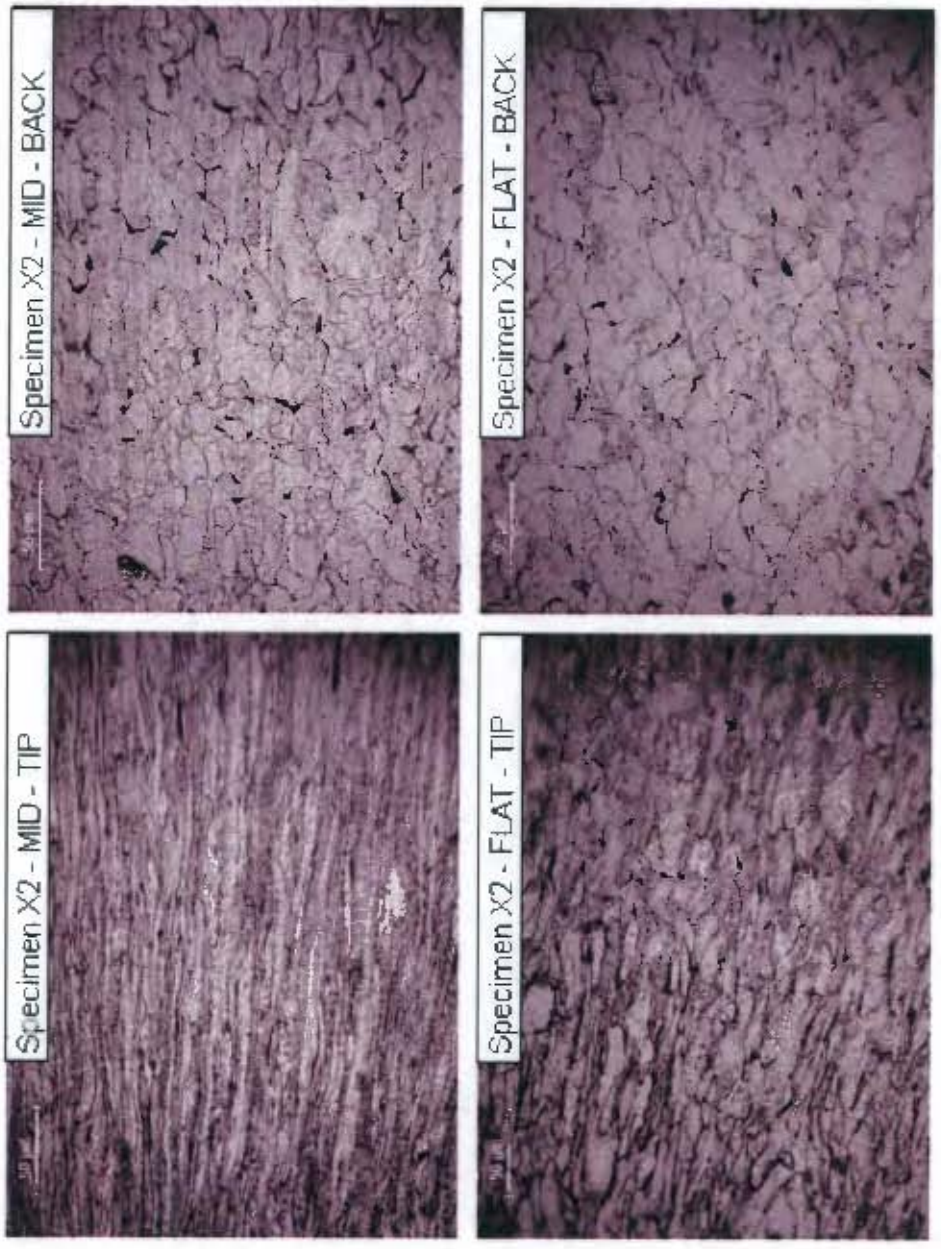

Figure A4.19 – Micrographs of Specimen X2 (Tested at 450°C and 1.67 x $10^{-2}s^{-1}$)

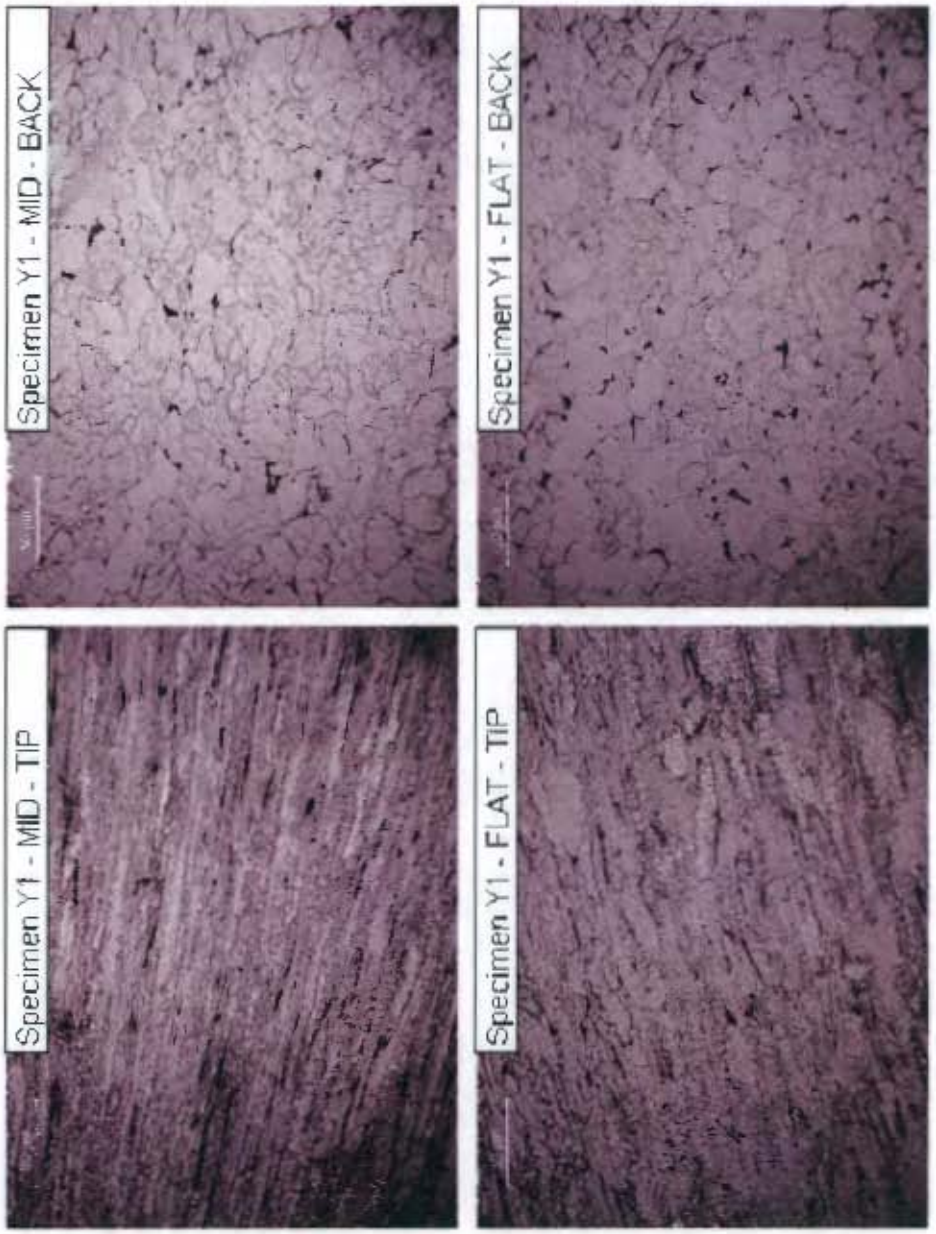

Figure A4.20 – Micrographs of Specimen **Y1** (Tested at 600°C and 1.67 x $10^{-2}s^{-1}$)

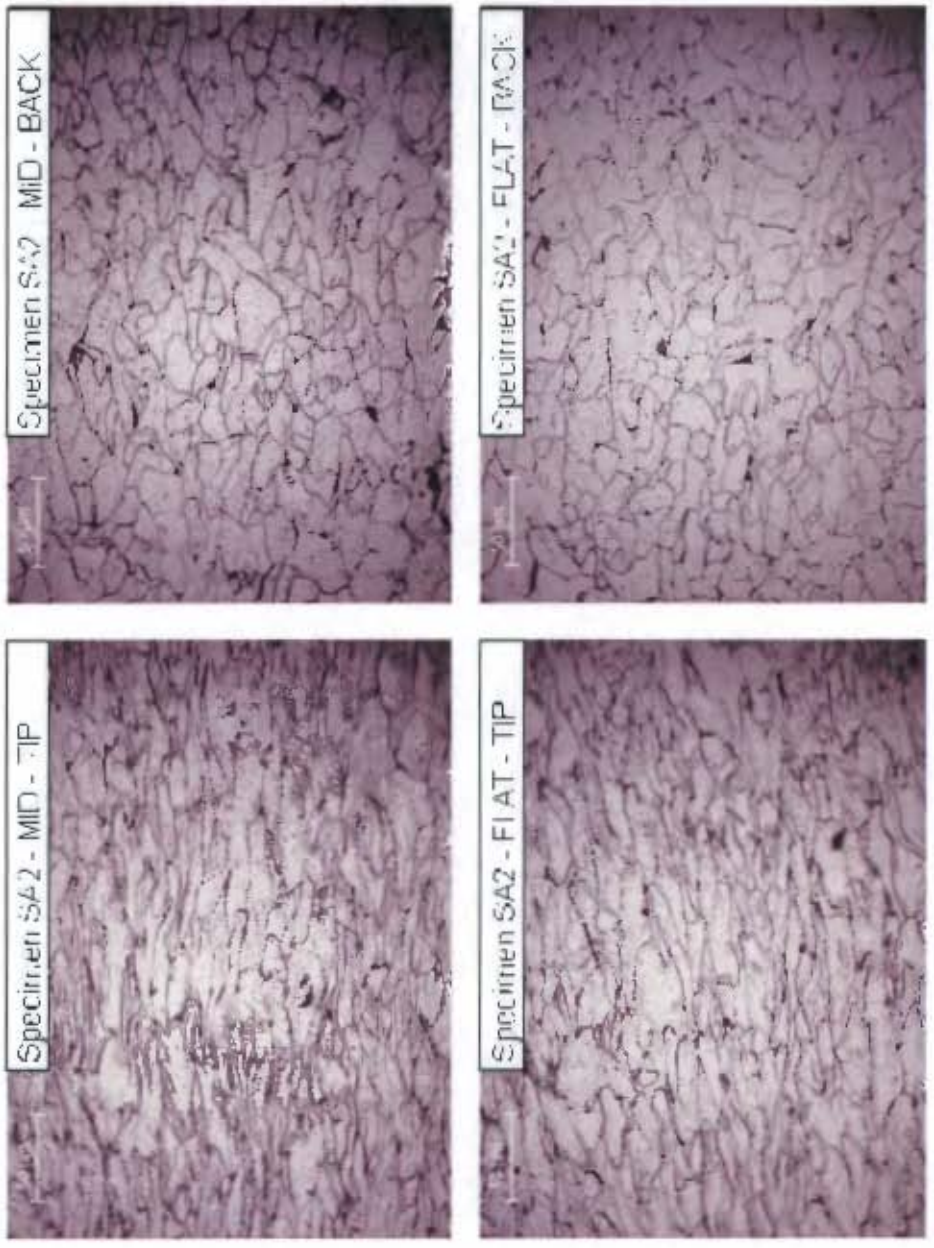

Figure A4.21 – Micrographs of Specimen SA2 (Tested at 25°C and 1 x $10^{-1}s^{-1}$)

Figure A4.22 – Micrographs of Specimen SB2 (Tested at 100°C and 1 x 10^{-1} s^{-1})

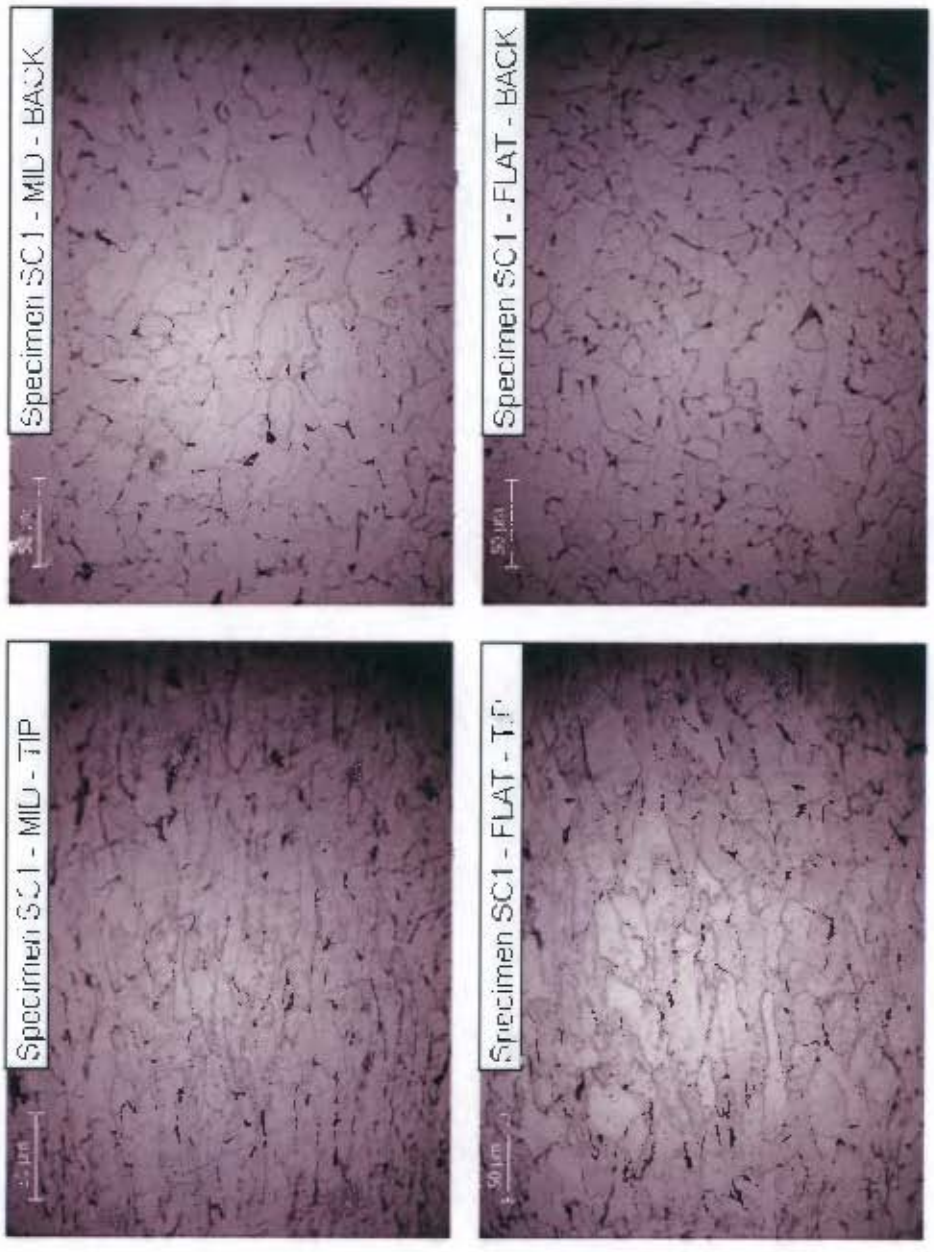

Figure A4.23 Micrographs of Specimen SC1 (Tested at 200°C and 1 x 10^{1}s^{-1})

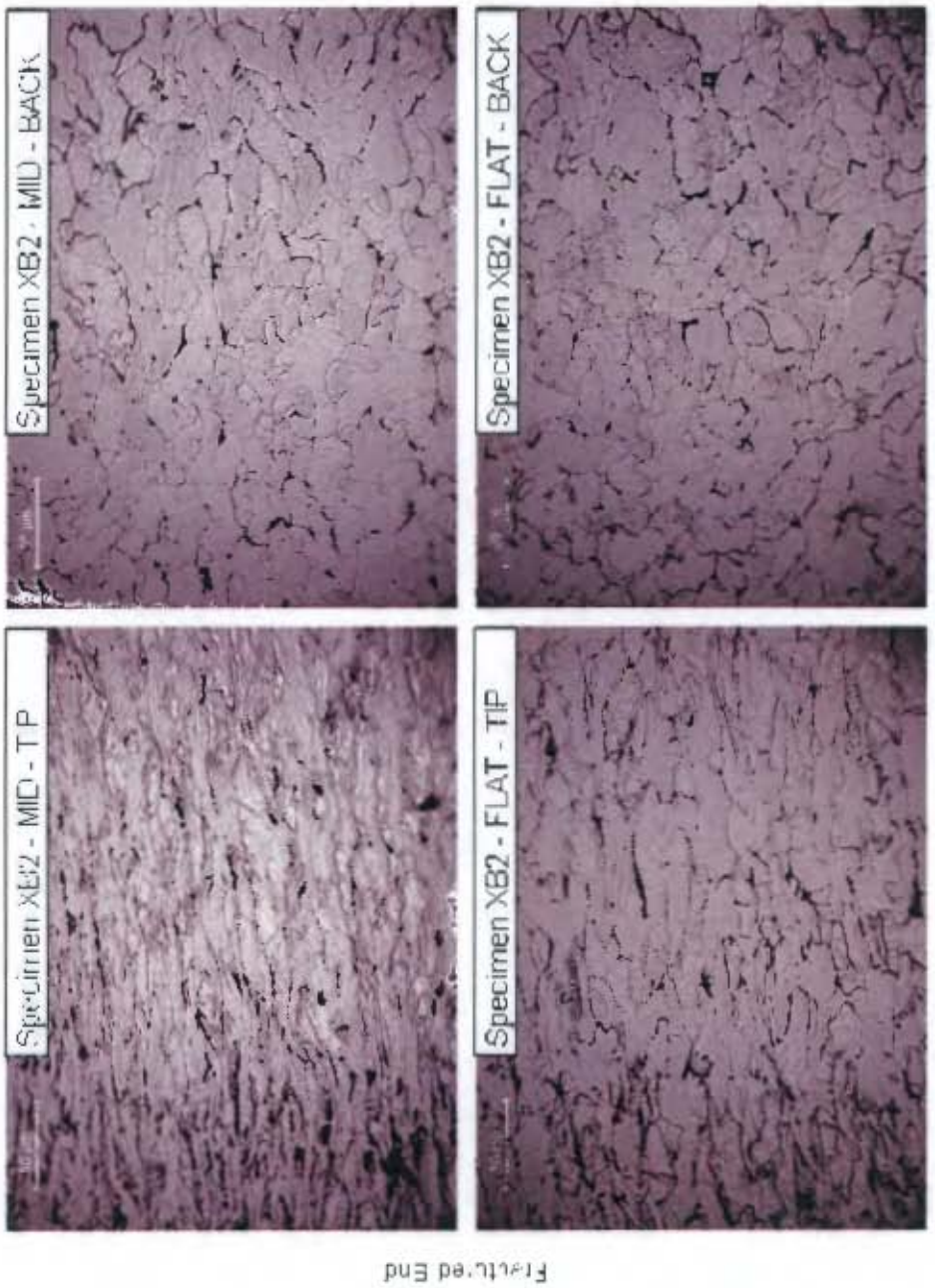

Figure A4.24 – Micrographs of Specimen XB2 (Tested at 300°C and 1 x $10^{-1}s^{-1}$)

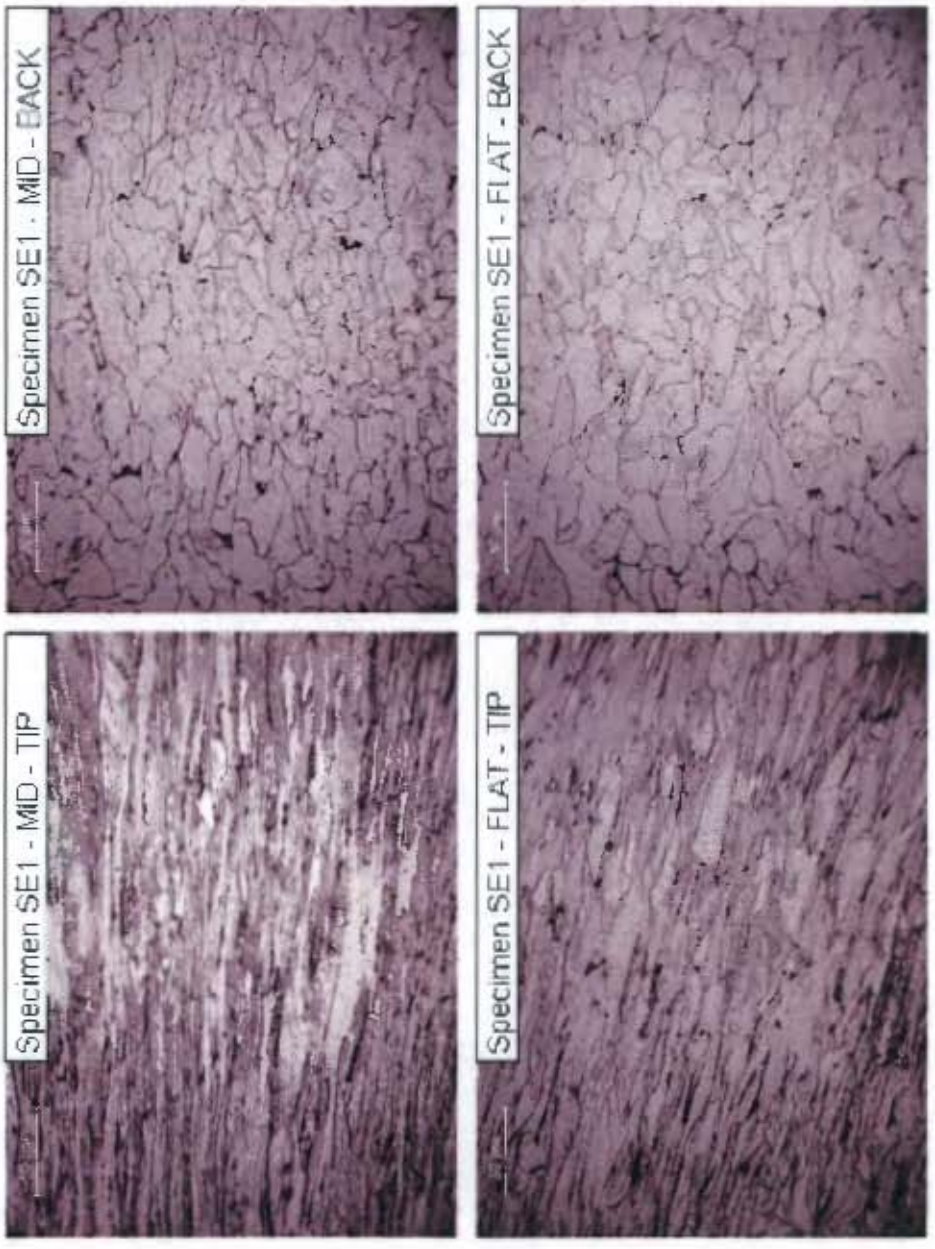

Figure A4.25 – Micrographs of Specimen SE1 (Tested at 450°C and 1 x $10^{-1}s^{-1}$)

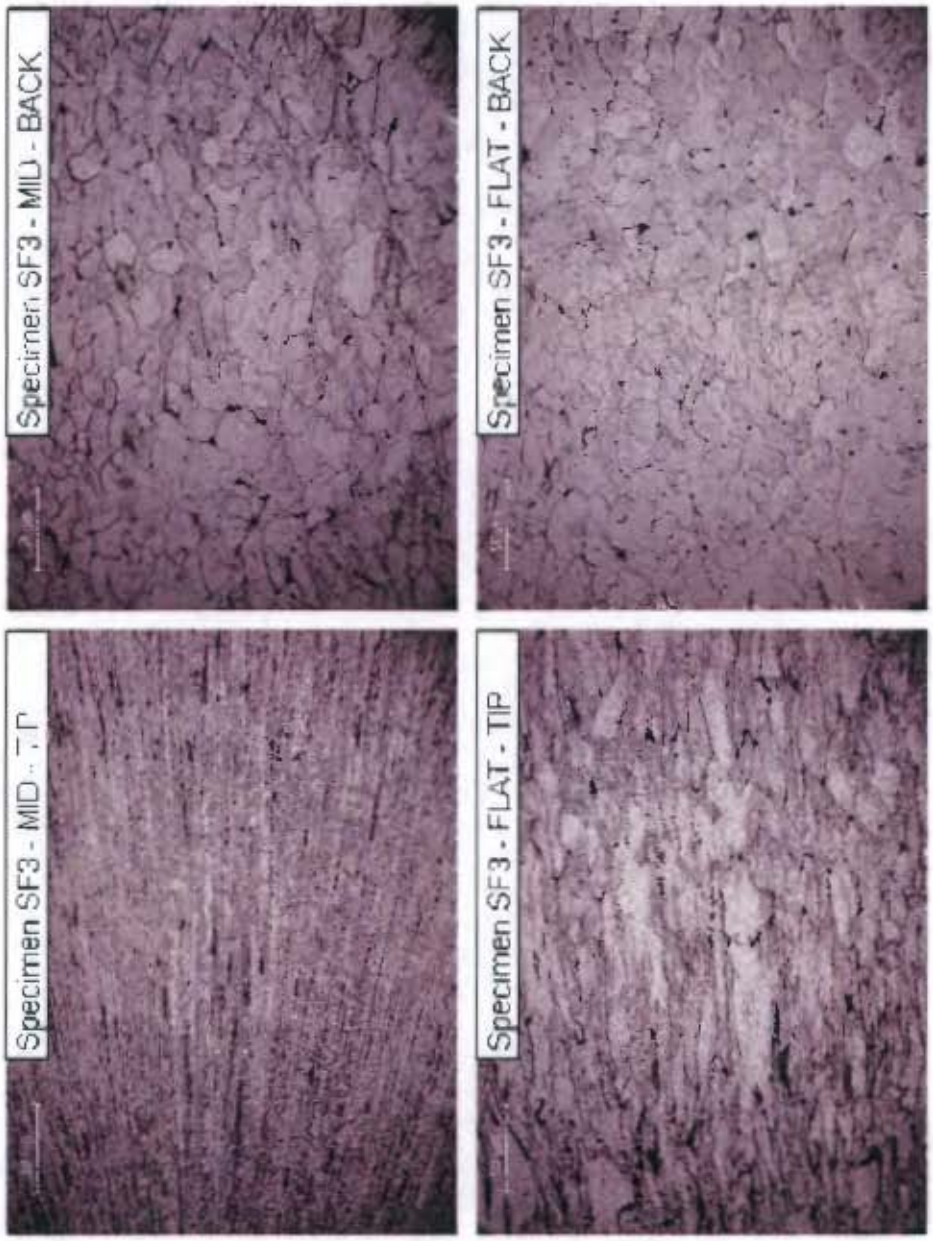

Figure A4.26 – Micrographs of Specimen SF3 (Tested at 600°C and 1 x $10^{-1}s^{-1}$)

A5. REFERENCES

[1] VARA, AR. "Determination of material properties at different temperatures and strain rates." Unpublished undergraduate thesis, University of Cape Town, Department of Mechanical Engineering, October 2004.